BROADSIDE AND ENDFIRE ANTENNAS ASSOCIATED WITH DIFFRACTING PARTITIONS IN NAVIGATION

by

VAN NGUYEN TRAN
B.Sc. and B.E. Hons.

Thesis submitted for the degree of

DOCTOR OF PHILOSOPHY

Department of Electrical Engineering

University of Adelaide

May, 1973.

STATEMENT

This thesis does not contain any material which has been accepted for the award of any other degree or diploma in any University and to the best of the author's knowledge and belief it contains no material previously published or written by another person, except when due reference has been made in the text.

Van Nguyen Tran.

ACKNOWLEDGEMENTS

The author wishes:

To thank Professor E.O. Willoughby, Department of Electrical Engineering, University of Adelaide for his supervision and patient guidance.

To thank the University of Adelaide for the financial support.

To thank the Director of The Weapons Research Establishment for his generosity in making the antenna test field available to the author and also Mr. G.E. Mawer for his keen assistance.

And finally to thank all those who have helped to make the completion of this thesis possible.

SUMMARY

This thesis presents the solution to the diffraction off the edge of a partition by using the theory of geometrical diffraction. The partition is placed along the medial plane of symmetry of a distributed radiating system in order to produce navigational patterns free of false courses. The solution has been obtained for the general case of two line sources and two apertures with a propagation normal to or at an oblique angle with the edge of the partition.

Three experimental models have been used to verify the diffraction solution. They are: two slot dipoles, two travelling wave slot lines and two parabolic cylinders having each a slot line at its focal line. The slot line is a new type of leaky wave slot antenna whose characteristics have been analysed by solving its transverse resonance equation. The new slot line has been shown to possess some interesting properties viz. low characteristic impedance, beam shaping and sidelobe suppression.

The theoretical and experimental results have been found to agree reasonably well. Navigational patterns free of false courses can be produced when the partition is sufficiently high.

TABLE OF CONTENTS

INTRODUCTION

The work presented in this thesis consists of three major parts:

(a) The solution for the diffraction off the edge of an E plane or H plane partition in the plane of symmetry of two identical source distributions.

(b) The analysis for a new type of a slot antenna which can be used as a ground based antenna or a feed for a parabolic cylinder.

(c) The experimental verification of the diffraction solution using the slot antenna as a suitable line source and a parabolic cylinder as a suitable aperture.

The idea of using a partition in a system of two identical source distributions has been investigated in an effort to produce navigational patterns free of false courses. The basic idea underlying the principle of navigation without false courses is to arrange for the nulls and sidelobes of the sum and difference patterns to line up one by one. In such an arrangement the product of the sum and difference patterns will have the same sign everywhere on either sides of the main null of the difference pattern, thus the instructio for an aircraft to go right or to go left according to the sign of th

product is not ambiguous and no possible false courses could result. Since any horizontally polarized source will have a positive image in an H plane partition, such a partition has no effect on the sum pattern but could create a sharp null in the difference pattern with the sidelobes exactly the same as those of the sum pattern.

Diffraction off the edge of the partition has no effect on the sum pattern but is a deciding factor in the difference pattern since i has been found that an electromagnetic wave polarized at right angles to the partition'bends round the corner' much more than a wave polarized parallel to the partition. The solution for this diffraction problem has been obtained using the extended cylindrical wave formulation of the geometrical theory of diffraction. The two dimensional and three dimensional cases of two line sources and two apertures hav been treated in detail for normal as well as oblique incidence to an H plane partition. The advantages of the geometrical theory of diffraction are the fact that rays are easier to visualize and the expressions for the diffracted field are given in terms of well tabulated functions which could be programmed on a digital computer. The diffracted field is found to consist of the incident and reflecte components. These components are dominant along the corresponding shadow boundaries and thus help removing the discontinuities left by the incident and reflected field.

A suitable line source which could be used to verify the above solution is a new type of slot antenna. It is virtually a strip line backed by a cavity. This slot antenna has a velocity of propagation very close to that of light. Its characteristics have been analysed using the technique of transverse resonance. Sidelobe suppression, beam shaping, low characteristics impedance, wide bandwidth if used as a travelling wave antenna and multimode operation are among its interesting potentialities. The problem of a parabolic cylinder using such a slot line as a feed at its focal length has also been carefully studied. The conical wavefront around the slot line can be assumed at a distance as close as 0.3λ from the source without any serious errors. The behaviour of a parabolic cylinder has been shown experimentally not to differ much from an approximate corner reflector. This is a very useful property in the construction of such an antenna system.

The diffraction solution has been put to test by using two slot dipoles, two slot lines and two apertures. The experimental results tend to show reasonably good agreement in all three cases. It appears from the theoretical and experimental results that the partition will be prohibitively high for present aircraft navigational systems however the study may have some useful application in future microwave

systems. Some efforts have also been made to suppress the edge diffraction in the difference pattern and the idea of using a slot in the partition seems to give some suppression in the difference pattern and at the same time leaving the sum pattern unchanged.

The presentation of the thesis is as follows:

The diffraction problem which arises out of the study of navigational patterns free of false courses is presented and its physical implication is described in chapter one. The possible methods of solution are also discussed here.

The solution to the diffraction problem using the geometrical theory of diffraction is given in chapter two with a special emphasis on the H plane partition because of its potential application in aircraft navigational systems.

The line source and aperture have been studied in chapter three as materials for verifying the solution for the diffraction problem. Extensive studies have been made to the new slot antenna as well as the parabolic cylinder.

The experimental verification is given in chapter four. The three models are described and the technique of measurement is discussed. The theoretical results are plotted against the experimental

ones to verify the solution for the diffraction problem.

The conclusion includes a brief discussion on the diffraction solution, the slot antenna, and its broadband feeding, the suppression of the edge diffraction and the potential application of this work.

CHAPTER ONE

THE PROBLEM

The problem of diffraction off the edge of a partition separating two identical antenna systems arises out of the study of a navigational system free of false courses. In this chapter, the principle of navigation free of false courses [1] is briefly explained together with some of its areas of application. The diffraction problem and its methods of solution are presented in general terms here to act as a prelude to the detailed solution later.

1. NAVIGATION FREE OF FALSE COURSES

To provide successful lateral guidance for a flying aircraft, a localizer should have an antenna system with a hybrid feed arrangement the basic unit of which is shown in Fig. 1. The LHS antennas are fed by the carrier plus the difference of the two sidebands and the RHS antennas are fed by the carrier minus the difference of the two sidebands. The sum pattern is the sum of the LHS and RHS antennas, i.e. the radiation pattern of the carrier frequency. The difference pattern is the difference of the LHS and RHS antennas i.e. the radiation pattern of the difference of the two sidebands. A

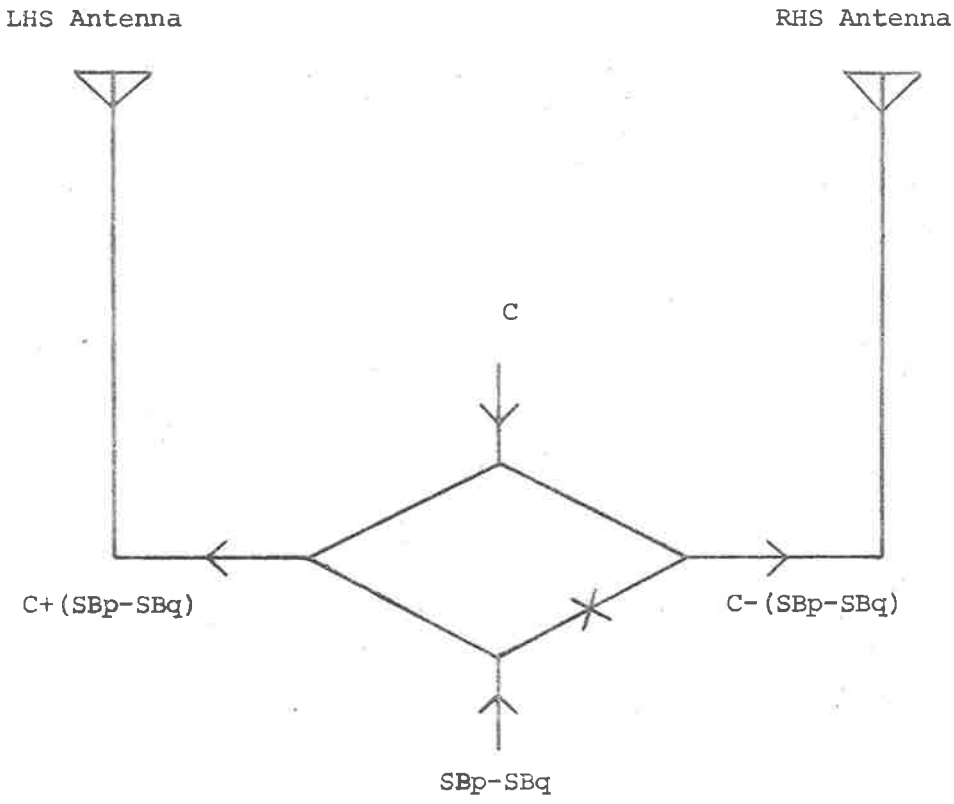

Fig. 1. Hybrid feed arrangement

C : Carrier
SBp : First sideband
SBq : Second sideband

localizer should have the following major characteristics:

(a) A sharp null in the difference pattern.

(b) Very low sidelobe levels in both of the sum and difference patterns.

(c) The nulls of the sum and difference patterns should coincide.

Information on whether to go left or to go right on board an aircraft is obtained by using an AVC receiver to detect the sign of the product of the carrier and sideband signals from a localizer. Requirement (a) is necessary to clearly define the localizer plane and when associated with a strong carrier signal, to minimize the effect of tall structures such as buildings, towers or mountain sides etc. Requirement (b) is to reduce stray reflection from sidelobes which could interfere with the true course. When the requirement (c) is not met, the aircraft may be steered further away instead of towards the null plane, by the combined effect of AVC, the sum carrier signal and the corresponding difference signal. Considering the situation illustrated in Fig. 2(a), apart from the true course in the middle, there are two other courses, one on each side, these are false courses. Any one of these false courses could lead an aircraft astray and the consequence could be disastrous!

The above stated requirements of a sharp null and very low

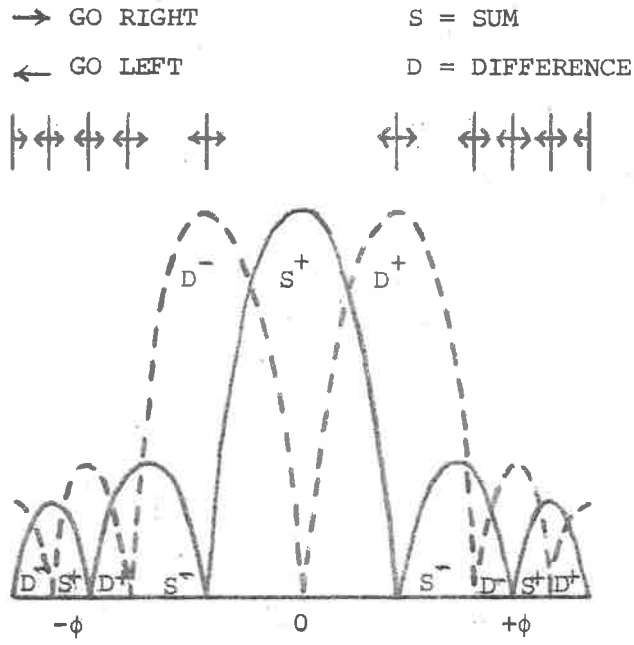

Fig. 2(a). Sum and difference patterns with many possible false courses

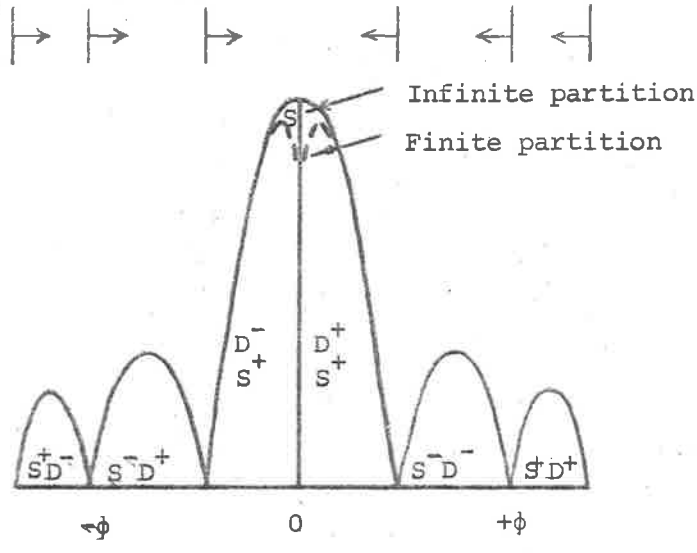

Fig. 2(b). The partition removes all the possible false courses

sidelobe levels could be realised in practice at great expense by employing arrays of antennas consisting of many elements with wide spacing and elaborate field strength distribution. These are far too complicated and expensive for many a small airport and moreover require very large clear areas. It is in an effort to look for simpler antenna systems for use as a localizer on small aerodromes that the idea of using a plane partition to control the polar diagrams of a distributed antenna system has been closely studied. There are two types of partition which need be considered here: the electric plane partition made of a perfect conducting material and the magnetic plane partition made of a perfect magnetic material. From practical consideration and also from the symmetry in Maxwell's equations, only the former type of partition needs be considered. An electric plane partition when placed along the plane of symmetry of two dipoles will have no effect on the resulting field if the dipoles are at right angles to the partition and fed in phase or parallel to the partition and fed in opposite phase. The partition in the former set up is in fact in the H plane of symmetry and in the latter set up in the E plane of symmetry of the two dipoles. Thus by using a symmetrical H plane partition in a distributed radiating system, the sum pattern is not going to be affected by the partition but the difference pattern will have a sharp null in the regions where the two sides 'see' each other and sidelobes more or less in the same positions as those of the sum pattern in the regions

where the two sides do not 'see' each other. This is the basis for the principle of navigation free of false courses.

To clarify the above point, considering a specific example of a system of two colinear dipoles or two parallel slot dipoles which when fed in phase will have a radiation pattern in the E plane as shown in Fig. 2(b). Such a radiation pattern will not be affected by introducing an electric partition of infinite height along the H plane of symmetry with the electric field being at right angles to it. Since the dipoles are fed in phase, the above radiation pattern is the sum pattern. Now with the same infinite electric partition but the dipoles are fed in phase opposition, the resulting radiation pattern instead of resembling its counterpart in Fig. 2(a), remains the same as the sum pattern but each half has a different sign due to the opposite phase feeding of the two dipoles. No cancellation from the two dipoles occurs because they never 'see' each other. The difference pattern does have a very sharp null in the middle and its sidelobes line up beautifully with those of the sum pattern. This is the situation in which, even with high sidelobe levels as seen in Fig. 2(b), no false courses exist. Thus by using an infinite electric partition, the requirement (b) above of very low sidelobe levels could be relaxed while the requirement (a) could be easily met very successfully.

Unfortunately, in practice the idea of using an infinite partition is not realizable. The electric plane partition has to be finite in height, which poses the question of diffraction off the edge of the partition by the electromagnetic waves from the sources on either sides of the partition. The solution for this diffraction problem and its experimental verification will constitute the major part of this thesis. It should be noted that as far as the sum pattern is concerned, a symmetrical H plane partition of any height will not affect it at all. It will be seen later that the diffraction in the sum pattern cancels each other out. However, for a difference pattern, a finite partition will prevent the two sides from 'seeing' each other. Thus addition will take place because of the positive image up to the height of the partition then cancellation will begin because of the opposite phase feeding giving rise to a sharp null. The diffraction off the edge of the partition from the two sides will add because the radiating system is no longer balanced and resulting field is affected throughout. As the partition height tends to infinity, the diffraction contribution tends to zero due to spatial attenuation of the electromagnetic waves and the difference pattern will become coincident with the sum pattern.

The areas of application of an electric partition in many distributed radiating systems are along the symmetrical E plane or

H plane depending on whether it is the difference or the sum pattern which needs be preserved. For localizer application, the sum pattern could remain the same whereas the difference pattern has to have a sharp null and the same sidelobe positions as the sum pattern. This is the case for using an electric partition along the H plane of symmetry. Some of the arrays of antennas which could be used to generate the sum and difference patterns for a localizing system are:

- An array of two or a multiple of two colinear antennas (such as dipoles, yagis....)
- An array of two or a multiple of two slot dipoles or slot lines
- An array of two or a multiple of two apertures (such as corner reflectors, horns, paraloidal reflectors, parabolic cylinders...).

2. POSSIBLE METHODS OF SOLUTION

There are at least three ways of obtaining a solution for the above problem of diffraction off the edge of the partition:

(a) The boundary value solution

(b) The induced current approximation

(c) The geometrical theory of diffraction.

In many antenna problems of this type, only a principal polarization is involved therefore the vector formulation for the diffraction theory could be approximated by using the scalar diffraction theory. This sort of approximation does not cause much error as far as far field patterns are concerned and will be adopted here to solve the diffraction problem presented above. The following is a brief outline of the above-mentioned three methods of solutions.

(a) The boundary value method of solution.

Using the famous solution of the diffraction of a plane wave by a half plane by Sommerfeld as the starting point, in principle, the solution of the diffraction problem for any source distribution can be built up from the solutions for the individual plane waves because a field radiated by any source distribution can be represented by a spectrum of plane waves. Based on this approach Born and Wolf [2] give the solutions for the diffraction of an infinite line source and a point source by an edge. From these solutions and by using the principle of supposition, the solution for the present diffraction problem could be obtained at least for the infinite line source and point source cases. These cases are involved but nevertheless quite tractable. Things begin to get difficult when the diffraction of an aperture or a finite line

source is needed as is often the case in practice. The expressions for the plane wave spectrum are just simply too formidable to tackle. It is a method of solution which could not be adopted here.

(b) The induced current method of solution.

The current induced on the partition by a source could be approximated by using the geometrical optics current for points away from the edge. There is a narrow strip along the edge where the geometrical optics current approximation breaks down. The discontinuity at the edge can be taken into account by assuming the existence of an equivalent line source whose far field is not uniform all round and can be assumed to have the distribution of the far field pattern of the Sommerfeld's solution for a half plane. Since the diffraction of a point source by a half plane is known, the solution for the diffraction of a distributed source can be obtained by integrating the contributions of all points over the source and using the principle of superposition to obtain the solution for the diffraction off the edge of a partition separating two such sources. Most distributed systems tend to have a principal polarization in such a way that the systems could be treated as an aggregation of either electric or magnetic line sources.

In such cases the formulation of the solution of the present problem of diffraction using the solution for the diffraction of a line source by a half plane is attractive. Plonsey [3] and Moullin [4] are the champions in the study of diffraction by an edge using the induced current method. This method is suited to the needs of the engineer since it tells him the area where there is a large current so that he can take the appropriate measure to improve the conductivity at that area in order to reduce the loss,and the area where there is very small current,so that he can either ignore it or does not bother much about good conductivity. It is conceptually more or less the same as that of the geometrical theory of diffraction.

(c) The geometrical theory of diffraction method of solution.

The geometrical theory of diffraction was developed by Keller [5] and extended by Rudduck [6] to the antenna theory. It is an asymptotic approximation of the exact theory. When the partition is plane, the expression for Sommerfeld's diffraction function can be written in terms of the Fresnel integrals and is exact so the solution to the present problem of diffraction inclines more towards the exact method of solution.

The geometrical theory of diffraction method of solution offers two main advantages: (a) it is much easier to visualize physically in terms of rays and (b) it contains expressions of well tabulated functions which can be easily programmed on a digital computer. The solutions for the normal as well as oblique incidence of the diffraction of a plane wave and cylindrical wave by a wedge of $(2-n)\pi$ included angle have been obtained. But again they are the solutions for the two dimensional case and therefore cannot be readily applied to any three dimensional cases of finite length. For such cases, the diffraction in the direction at right angles to the edge is taken to be the same as that of the two dimensional case above and the diffraction in the dimension in which the rays are parallel is assumed to be the same as the radiation pattern of a line source of finite length. The results obtained so far do confirm the above assumption. This method of solution using the geometrical theory of diffraction will be adopted to obtain the solution for the present problem.

In the next chapter, the solutions for the problem of diffraction off the edge of the partition will be given in details for the following two cases:

(a) The case of a partition separating two lines and two apertures infinite in length.

(b) The case of a partition separating to lines and two apertures finite in length.

The solutions will be given for both of the normal and oblique incidence.

CHAPTER TWO

THE SOLUTION

In this chapter, the solution to the problem of diffraction off the edge of a partition described in the previous chapter is presented The general case of two lines and two apertures of finite and infinite lengths will be considered. The incidence to the partition can be normal or oblique. In all cases, the partition is assumed to have a finite height and an infinite length. The case of a finite partition thickness can be extended and the case of a wedge partition of arbitrary included angle $(2-n)\pi$, where n is an integer is implicitly covered as seen in the survey of the wedge diffraction theory.

The problem of the diffraction of an electromagnetic wave by a wedge is a difficult boundary value problem. Its solution began with the well known Sommerfeld's solution for a plane wave. When applied to a half plane, Sommerfeld's solution leads to the familiar Fresnel diffraction by an edge. However for a general wedge, the solution cannot be expressed in closed form using Fresnel integrals. Some thirty years later, Pauli [7] developed a rapidly converging series representation for the solution of a general wedge. Pauli's series is applicable to a situation where the distance from the source to the wedge is large and for points of observation well away from the

shadow boundaries only. When the distance is not large enough, higher order terms have to be included and these are unwieldy and not very well formulated. When a point of observation is on a shadow boundary, Pauli's series breaks down due to a singularity there except the half plane case. The plane wave solution is a big step forward but it has limited areas of application in the antenna theory. Russo et al. [7a] has pointed out some of the shortcomings of Sommerfeld's plane wave solution when it is applied to the calculation of the E-plane patterns of a horn. Rudduck [6] makes use of the reciprocity theorem together with Pauli's series representation to obtain the far field of a line source placed at a finite distance from a wedge. This is the cylindrical wave formulation.

Due to the finite distance between the sources and the edge of a partition, Rudduck's cylindrical wave formulation has been used here to obtain the solution for the diffraction problem described in Chapter one. Before presenting it in details, a survey of the wedge diffraction is given first.

1. A SURVEY OF WEDGE DIFFRACTION THEORY

There are three formulations for the problem of wedge diffraction, viz:

- The plane wave formulation
- The cylindrical wave function formulation
- The cylindrical wave formulation

The material presented in this survey is based on an interesting report on 'the application of wedge diffraction to antenna' by Rudduck [6] and a paper by Pauli [7].

(a) Plane Wave Diffraction Formulation

It was Sommerfeld who gave the solution to the problem of diffraction of a plane electromagnetic wave incident normally to a wedge of included angle $(2-n)\pi$ as shown in Fig. 1.

When the wedge coincides with the z-axis of the cylindrical coordinates (r,ψ,z), the diffraction problem becomes independent of z and thus scalar in nature. The field $u(r,\psi)$ is a solution of the two dimensional scalar wave equation $\nabla^2 u + k^2 u = 0$ satisfying the boundary conditions $u = 0$ or $\frac{\partial u}{\partial n} = 0$ depending on whether the electric polarization is parallel or normal to the wedge. The total field $u(r,\psi)$ can be separated into the incident and reflected wave by putting

$$u(r,\psi) = v(r,\psi-\psi_0) \pm v(r,\psi+\psi_0) \qquad \ldots(1)$$

where $v(r,\phi)$ is the Sommerfeld's function, a solution of the wave equation. The minus sign applies to the boundary condition $u = 0$ i.e.

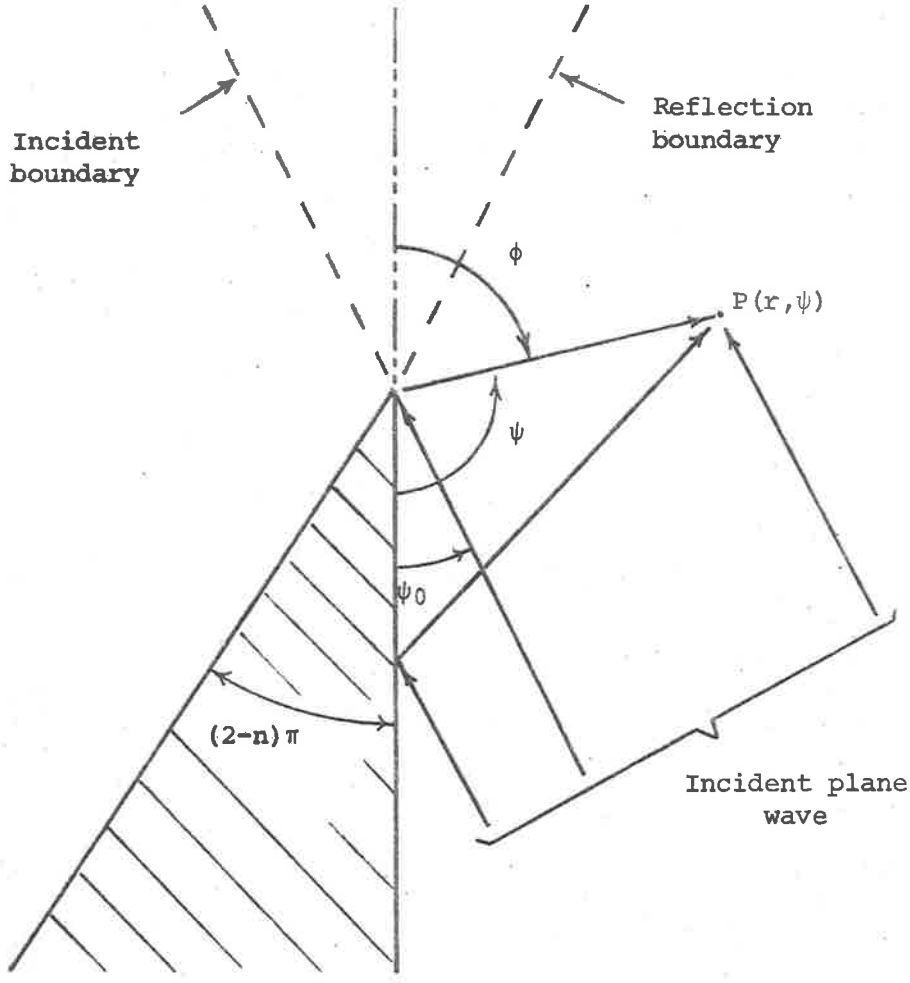

Fig. 1. Diffraction of a plane wave by a conducting wedge

when the electric field is parallel to the wedge and the plus sign applies to the boundary condition $\frac{\partial u}{\partial n} = 0$ i.e. when the electric field is normal to the wedge.

The function $v(r,\phi)$ has the period $2\pi n$ in ϕ and is a one valued function of the variable $\cos\phi/n$ i.e.

$$v(r,\phi + 2\pi n) = v(r,\phi) \qquad \ldots(2)$$

$$v(r,\phi) = v(r,-\phi) \qquad \ldots(3)$$

$v(r,\phi)$ can be separated into components:

$$v(r,\phi) = v^*(r,\phi) + v_B(r,\phi) \qquad \ldots(4)$$

where v^* is the geometrical optics field and v_B is the diffracted field. v^* is given by

$$v^*(r,\phi) = \begin{cases} \exp(jkr\cos(\phi+2\pi nN)) & -\pi < \phi + 2\pi nN < \pi \\ & \text{and } N = 0, \pm 1, \pm 2, \\ 0 & \text{otherwise} \end{cases} \qquad \ldots(5)$$

$v^*(r,\phi)$ represents the incident field when $\phi = \psi - \psi_0$ and the reflected field when $\phi = \psi + \psi_0$. From (5), it is clear that the incident field consists of the incident plane wave in the illuminated region $(0 < \psi < \pi + \psi_0)$ and zero in the shadow region $(\pi + \psi_0 < \psi < \pi n)$; the two regions are separated by the incident shadow boundary at $\psi = \pi + \psi_0$ as shown in Fig. 1. Similarly, the reflected field consists

of the reflected plane wave in the illuminated region ($0<\psi<\pi - \psi_0$) and zero in the shadow region ($\pi - \psi_0 < \psi < \pi n$); the two regions are separated by the reflected shadow boundary at $\psi = \pi - \psi_0$.

v_B is given by:

$$v_B(r,\phi) = \frac{1}{2\pi n} \int_C \frac{\exp(jkr\cos\beta)}{1-\exp(-j(\beta+\phi)/n)}\, d\beta \qquad \ldots(6)$$

where C is the appropriate path in the plane of the complex variable. The associated diffracted fields combime with the incident and reflected field to eliminate the discontinuity at the appropriate shadow boundary. Using the method of steepest descent, Sommerfeld obtained an asymptotic expression for equation (6) as:

$$v_B(r,\phi) \approx \frac{1}{\sqrt{2\pi kr}} \exp(-j(kr+\pi/4)) \frac{\sin \pi/n}{n(\cos\pi/n-\cos\phi/n)} \qquad \ldots(7)$$

This leads to the interpretation that the diffracted field can be thought of as a cylindrical wave radiating from the wedge and having a ψ dependent amplitude. (7) is valid only when

$$kr(\cos\pi/n - \cos\phi/n)^2 >> 1$$

and becomes infinitely large in the neighbourhood of the shadow boundaries, where $\cos \pi/n = \cos \phi/n$. Sommerfeld tried, without much success, to obtain an asymptotic representation of (5) which would

also be valid in the vicinity of the shadow boundaries.

It should be pointed out here that in the special case of n = 2 i.e. the half plane problem, the diffracted field can be expressed in terms of the Fresnel integral as:

$$v_B(r,\phi) = -\exp(j\pi/4)\left(\frac{2}{\pi kr}\right)^{1/2} \exp(jkr\cos\phi)\cdot\left|\cos\phi/2\right|\cdot\int_Z^\infty \exp(-j\tau^2)d\tau \qquad \ldots(8)$$

where $Z = (kr(1+\cos\phi))^{1/2}$

and the total field becomes:

$$v_B(r,\phi) = \frac{e^{j(\pi/4)}}{\sqrt{\pi}}\, e^{jkr\cos\phi}\int_{-\infty}^{Z} e^{-j\tau^2}\, d\tau \qquad \ldots(9)$$

where Z can be simplified to $(2kr)^{1/2}\cos\phi/2$. The expression (9) is regular at $\phi = \pi$.

Pauli took the hint from the above special case to develop a series asymptotic representation for (6). He transformed the integrand of (5) without changing the path of integration to develop a rapidly coverging series for v_B which is also valid near the shadow boundaries $\phi = \pi$ but infinite at other shadow boundaries $\phi = \pi+2\pi nN$, $(N\neq 0)$. Pauli expressed v_B as:

$$v_B(r,\phi) = \frac{2e^{j\pi/4}}{\sqrt{\pi}}\,\frac{\sin\pi/n\left|\cos\phi/2\right|}{n(\cos\pi/n-\cos\phi/n)}\cdot e^{jkr\cos\phi}\int_Z^\infty e^{-j\tau^2}d\tau + [\text{Higher order terms}] \qquad \ldots(10)$$

where $Z = (kr(1 + \cos\phi))^{1/2}$ and all the higher order terms may be neglected for large kr. It is worth noting that when n = 2, all the higher order terms become zero and (10) becomes (8).

The value of the diffracted field on the shadow boundaries can be approximated by:

$$v_B(r,\pi) = \begin{matrix} - \\ + \end{matrix} \frac{1}{2} e^{-jkr} + [O(r^{-1/2})] \begin{cases} - \text{ for } \phi = \pi^- \\ \\ + \text{ for } \phi = \pi^+ \end{cases} \quad \ldots(11)$$

and the value of the total field on the boundaries is

$$v(r,\pi) = v^*(r,\pi) + v_B(r,\pi) = \frac{1}{2} e^{-jkr} + [O(r^{-1/2})]$$

which will converge to one half the incident field on the illuminated side of the shadow boundary for large r.

$v(r,\phi)$ is periodic in ϕ with a period $2\pi n$ but $v_B(r,\phi)$ is not. Since $v_B(r,\phi)$ is only regular in the vicinity of $\phi = \pi$, if $v_B(r,\phi)$ is to be evaluated near $2\pi n - \pi$, a substitution of $v_B(r,\phi)$ for $v_B(r,\phi-2\pi n$ will give a rapidly converging answer for $v_B(r,\phi-2\pi n)$ near the shadow boundaries $2\pi n - \pi$.

Keller [5] used the asymptotic expression given in (10) for large values of $kr(1 + \cos\phi)$ to develop his geometrical theory of diffractio by plane waves:

$$v_B(r,\phi) = \frac{e^{-j(kr+\pi/4)}}{\sqrt{2\pi kr}} \cdot \frac{1/n \sin\pi/n}{\cos\pi/n - \cos\phi/n}$$

$$= D(\phi) \cdot \frac{e^{-jkr}}{\sqrt{r}} \qquad \ldots(12)$$

Due to its approximate nature, the theory can only be applied successfully to those problems of waves which are either plane or approximately so. Russo et al. [7a] has pointed out the shortcomings of the plane wave diffraction formulation when it is applied to the calculation of the E-plane radiation patterns of a horn. It was demonstrated clearly in the article that a cylindrical wave diffraction formulation gives a better agreement than the plane wave diffraction formulation. To summarize, the total field of a plane wave incident on a perfectly conducting wedge is given (1):

$$u(r,\psi) = \begin{pmatrix} \exp(jkr\cos(\psi-\psi_0)) \\ \\ \\ \\ 0 \end{pmatrix} \pm \begin{pmatrix} \exp(jkr\cos(\psi+\psi_0)) \\ \\ \\ \\ 0 \end{pmatrix}$$

$$+ v_B(r,\psi-\psi_0) \pm v_B(r,\psi+\psi_0) \qquad \ldots(13)$$

where the proper choice of terms in the brackets has been discussed in (5) and the choice of sign ($\pm$) is determined by the polarisation as mentioned in (1).

For grazing incidence ($\psi_0 = 0$), (13) reduces to

$$u(r,\phi) = \begin{pmatrix} \exp(jkr\cos(\psi-\psi_0)) \\ \\ 0 \end{pmatrix} + v_B(r,\psi-\psi_0) \qquad \ldots(14)$$

thus only the incident field is involved.

(b) Cylindrical Wave Functions Formulation

As mentioned earlier, when $n = 2$, all the higher order terms in the series representation of $v_B(r,\phi)$ are zero and so (10) can be used to obtain the field for any point at any distance away from the edge. However, when $n \neq 2$, the higher order terms are not zero and cannot usually be neglected for distance which is small compared to the wavelength. One way of obtaining the field at such a distance is to use the cylindrical wave function formulation given by Wait [8] and Harrington [9]:

$$v_B(r,\phi) = 1/n \sum_{m=0,1}^{\infty} \varepsilon_{m/n}\, j^{m/n}\, J_{m/n}(kr)\cos m/n\phi - v^*(r,\phi) \qquad \ldots(15)$$

where $v^*(r,\phi)$ is the geometrical optics incident or reflected field.

$$\varepsilon_{m/n} = 1 \text{ for } m/n = 0$$

$$\varepsilon_{m/n} = 2 \text{ for } m/n > 0$$

$v_B(r,\phi)$ is pretty accurately represented for $r < \lambda$ when $m/n \leq 15$, accurate values for $v_B(r,\phi)$ can also be achieved for $r \gtrsim \lambda$ by including more terms.

(c) Cylindrical Wave Formulation

The solution for a cylindrical wave diffraction can be determined in several ways. The usual way is to represent the cylindrical wave by a spectrum of plane waves. In fact, in principle, the proble of diffraction of any source distribution can be built up from the individual plane wave in the spectrum. However when far field patterns only are of interest, there is a simpler way of determining the diffracted wave by using the principle of reciprocity together with the solution for plane wave diffraction by Pauli [7].

When a wedge is illuminated by a plane wave, the total field $u_a(r_0,\psi_0)$ in Fig. 2a is given by (13). If the wedge is now illuminated by a cylindrical wave u_b with its source at $P(r_0,\psi_0)$ in Fig. 2b, the field at infinity is a plane wave. Thus this is a situation wher the point of observation and the source are interchanged i.e. the principle of reciprocity applies. Since:

$$u_a(r_0,\psi_0) = v(r_0,\psi_0-\psi) \pm v(r_0,\psi_0+\psi) \qquad \ldots(16)$$

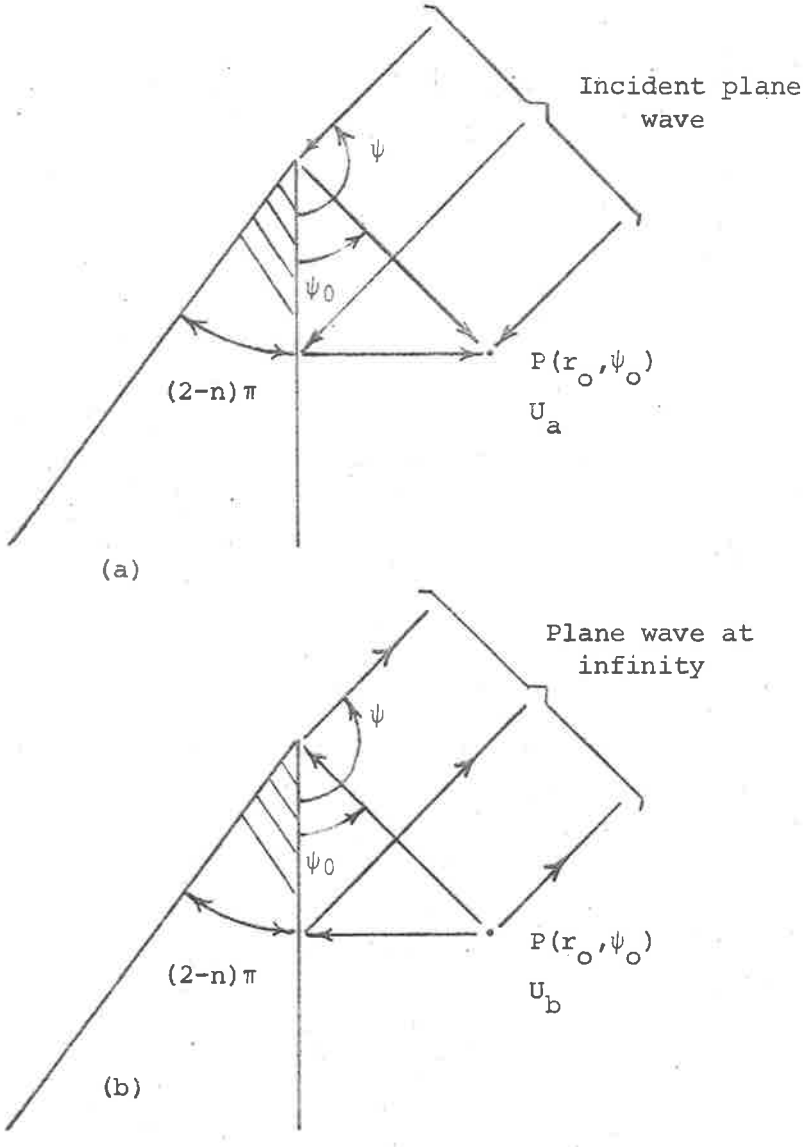

Fig. 2. Reciprocity and cylindrical wave formulation

upon using $v(r,\phi) = v(r,-\phi)$, $u_b(r_0,\psi)$ becomes:

$$u_b(r_0,\psi) = v(r_0,\psi-\psi_0) \pm v(r_0,\psi+\psi_0) \qquad \ldots(17)$$

(17) is the solution for the diffraction of a cylindrical wave by a wedge. The radial distribution of the line source must be included, thus:

$$u(r,\psi) = \frac{e^{-jkr}}{\sqrt{r}} \left[\begin{bmatrix} \exp(jkr_0\cos(\psi-\psi_0)) \\ 0 \end{bmatrix} \pm \begin{bmatrix} \exp(jkr_0\cos(\psi+\psi_0)) \\ 0 \end{bmatrix} + v_B(r_0,\psi-\psi_0) \pm v_B(r_0,\psi+\psi_0) \right] \qquad \ldots(18)$$

where (r_0,ψ_0) is the coordinates of the source and (r,ψ) is that of a point of observation. The exponential terms arise because the phase centre is assumed to be at the wedge. Plane wave diffraction is a special case of (18) when the line source recedes to infinity. The diffraction for a cylindrical wave incidence in regions sufficiently removed from any shadow boundary is virtually the same as that of a plane wave incidence. The region about the shadow boundary where the two are significantly different depends on the distance r_0 to the line source.

A general line source has a pattern $F(\psi) \neq 1$, thus (18) should be written as:

$$u = \frac{e^{-jkr}}{\sqrt{r}} \left[F(\psi) \begin{bmatrix} \exp(jkr_0\cos(\psi-\psi_0)) \\ 0 \end{bmatrix} \pm \begin{bmatrix} \exp(jkr_0\cos(\psi+\psi_0)) \\ 0 \end{bmatrix} F(2\pi-\psi) \right.$$

$$\left. + F(\pi+\psi_0) \left[v_B(r_0,\psi-\psi_0) \pm v_B(r_0,\psi+\psi_0) \right] \right] \quad \ldots(19)$$

(19) is valid for $r >> r_0$.

For distance r from the wedge comparable to that of the source, some modification to (19) should be carried out along the line suggested by Ohba [10] and Rudduck [6].

The cylindrical wave formulation of edge diffraction together with the principle of superposition have been used successfully in the treatment of quite a number of two dimensional antennas and scattering bodies such as parallel plate waveguides, walls of finite thickness principal plane cross sections of pyramid horn antennas and polygonal cylinders etc...[6].

It can be seen clearly that the diffraction problem arising out of the study of navigational system free of false courses involves the use of line sources or an aggregation of line sources at finite distances from the edge of a partition, the cylindrical wave diffraction formulation seems the most appropriate choice. Before discussing the solution by the cylindrical wave formulation, it is worth mentioning the interesting properties of the diffracted field function.

2. PROPERTIES OF THE DIFFRACTED FIELD FUNCTION

To illustrate the properties of the diffracted field function only the plane partition case is considered here. Other cases such as a thick partition or a wedge partition could be extended by making use of (10) and its line source characteristics.

When the partition is plane i.e. n = 2, the diffracted field function given by (8) can be re-written as

$$v_B(r,\phi) = \pm (1+j)/2 \exp(jkr\cos\phi) \int_Z^\infty \frac{e^{-jt}}{\sqrt{2\pi t}}\, dt \qquad \ldots(20)$$

where $\phi = \psi - \psi_0$,

$Z = kr(1+\cos\phi)$ and $v_B(r,\phi)$ takes the + sign when $\phi < \pi$ and - sign when $\phi > \pi$ i.e. $v_B(r,\phi)$ changes sign everytime a shadow boundary is passed.

The integral in (20) can be written in terms of the standard Fresnel integrals:

$$v_B(r,\phi) = \pm (1+j)/2 \exp(jkr\cos\phi)\left[\left(C(Z)-\frac{1}{2}\right)-j\left(S(Z)-\frac{1}{2}\right)\right] \ldots(21)$$

where

$$C(Z) = \int_0^Z \frac{\cos(t)}{\sqrt{2\pi t}}\, dt \text{ and } S(Z) = \int_0^Z \frac{\sin(t)}{\sqrt{2\pi t}}\, dt \qquad \ldots(22)$$

The total diffracted field by the partition due to one of the two sources is:

$$V_B(r,\psi) = v_B(r,\psi-\psi_0) \pm v_B(r,\psi+\psi_0) \quad \ldots(23)$$

When the partition lies in the H plane (23) takes the + sign and when it lies in the E plane, the - sign. It is more convenient to use the coordinates (r,ϕ) instead of (r,ψ) as shown in Fig. 3a, thus:

$$V_B(r,\phi) = v_B(r,\pi-\phi-\psi_0) \pm v_B(r,\pi-\phi+\psi_0) \quad \ldots(24)$$

By using (24) and the fact that every time a shadow boundary is passed $v_B(r,\phi)$ changes sign as mentioned in (20), $V_B(r,\phi)$ can be shown to have the following characteristics:

$$V_B(r,\phi) = - V_B(r,-\phi) \text{ for H plane partition} \quad \ldots(25)$$

and $$V_B(r,\phi) = V_B(r,-\phi) \text{ for E plane partition,} \quad \ldots(26)$$

It is obvious that:

(a) From (25) total diffraction due to a H plane partition of two identical sources having symmetrical field patterns $F(\phi)$ fed in phase is zero, i.e. the partition has no effect on the resulting sum pattern of the two sources. On the other hand, the total diffraction contribution when the sources are fed 180° out of phase is not zero but equal to twice $V_B(r,\phi)$ in (25).

(b) Similarly, from (26) the total diffraction due to an E plane partition of two identical sources having symmetrical field patterns $F(\phi)$ fed 180° out of phase is also zero i.e. the partition has no effect on the resulting difference pattern of the two sources. But when the sources are fed in phase, the total diffraction is different from zero and equal to twice $V_B(r,\phi)$ in (26).

It has been mentioned earlier on that the associated diffracted fields combine with the incident and reflected field to eliminate the discontinuity at the appropriate shadow boundary. This is clearly so when $v_B(r,\phi)$ given by (21) is computed, each diffracted field component, i.e. incident or reflected, takes the dominance over its own shadow boundary. The amplitude of total diffracted field $V_B(r,\phi)$ is plotted for a typical case of $r = 3\sqrt{2}\lambda$ and $\psi_0 = \pi/4$ in Fig. 3(b) and 3(c). When phase is taken into account $V_B(r,\phi)$ is antisymmetrical for the H plane diffraction and symmetrical for the E plane diffraction with respect to $\phi = 0$.

In the following sections, the total diffracted field contribution given by (23) will be used together with (25), (26), (21) and (22) and the principle of superposition to obtain a solution for the diffraction off the edge of a finite height partition separating two identical sources. Only the case of a H plane partition is presented

Fig. 3. Variation of the diffracted field function

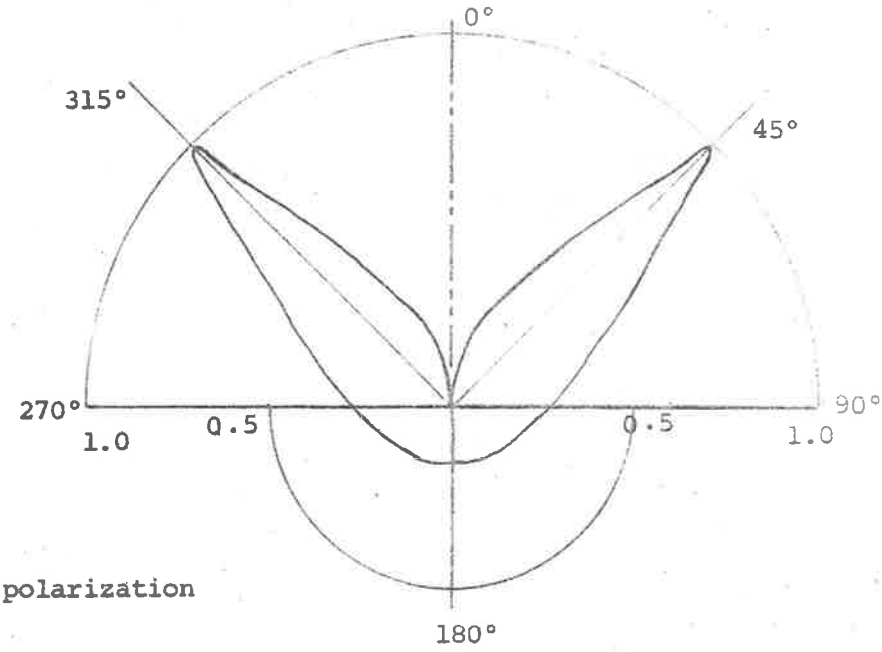

(a) H plane polarization

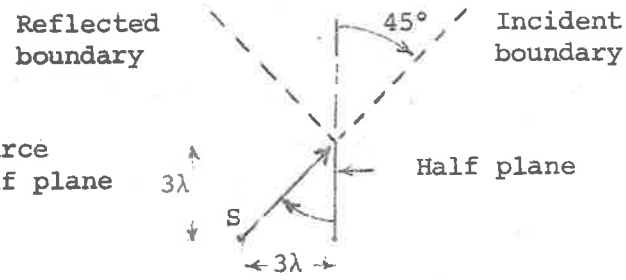

(b) Position of source relative to half plane

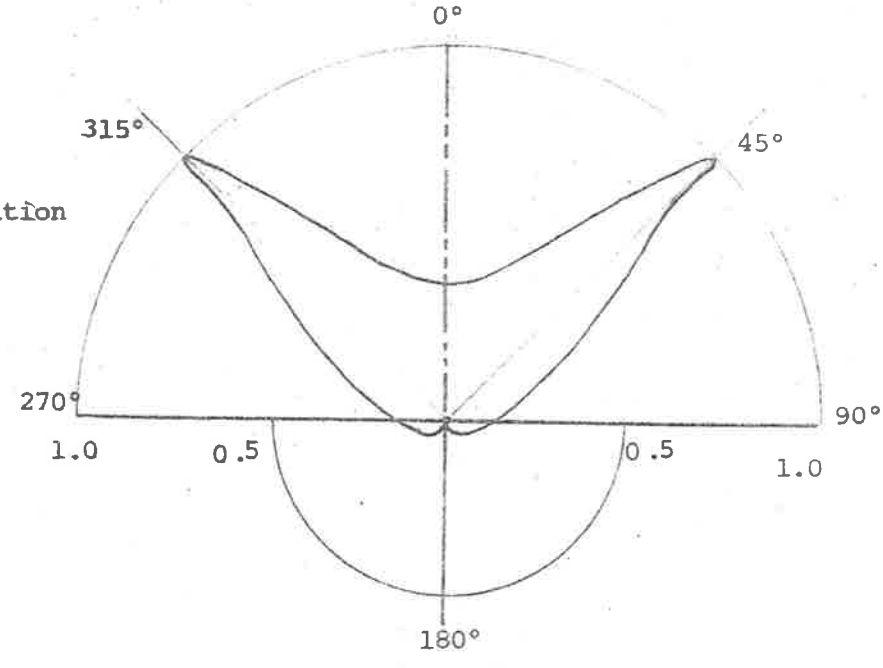

(c) E plane polarization

in detail here because of its immediate potential application to the design of a localizer without false courses and also because of the fact that the case of an E plane partition is implicit in the former case and can be readily extended with only a few changes in sign. The diffraction contribution will be added to that of the geometrical optics to give the resulting radiation pattern of the whole antenna system.

3. RADIATION PATTERNS FOR TWO SOURCES SEPARATED BY A PARTITION

Expressions for the radiation patterns of two line sources and two apertures of infinite and finite length will be derived. The partition will have a finite height but an infinite length and will lie along the H plane of symmetry of the two identical sources having symmetrical field patterns $F(\phi)$. When the field patterns $F(\phi)$ are not symmetrical, the total diffracted contribution will not be zero in the sum pattern involving an H plane partition and in the difference pattern involving an E plane partition. The case of a partition of a finite length will be briefly discussed.

A. TWO DIMENSIONAL CASE

Using a cylindrical coordinates system (r,ϕ,z), when a line source or an aperture source is infinite in length in the z direction

say, its radiation pattern will be two dimensional if there is no variation along z or a variation of the form $\exp(-jk_z z)$, where k_z is the propagation constant. The former case corresponds to a normal incidence whereas the latter corresponds to an oblique incidence. Normal incidence will be considered first.

a. Normal Incidence

(i) Two Line Sources.

The first case to be considered here is that of two infinite line sources separated by a half plane placed in the H plane of symmetry of the sources. As shown on Fig. 4(a), y_o is the distance from 0 to a source and x_o is the distance from 0 to the edge of the partition. Let 0 be the phase centre of the whole system.

Since the partition lies in the H plane of symmetry of the two sources having symmetrical field patterns $F(\phi)$, the resulting diffracted field is zero for the sum pattern. The sum pattern is given by:

$$E^{+}(\phi) = 2 \cos(ky_o \sin\phi)\ F(\phi) \qquad \ldots(27)$$

with $e^{-jkr}/\sqrt{r}$ being suppressed throughout. Where $k = 2\pi/\lambda$ and $F(\phi)$ is the ϕ variation.

When the line sources are fed 180° out of phase, the diffracted

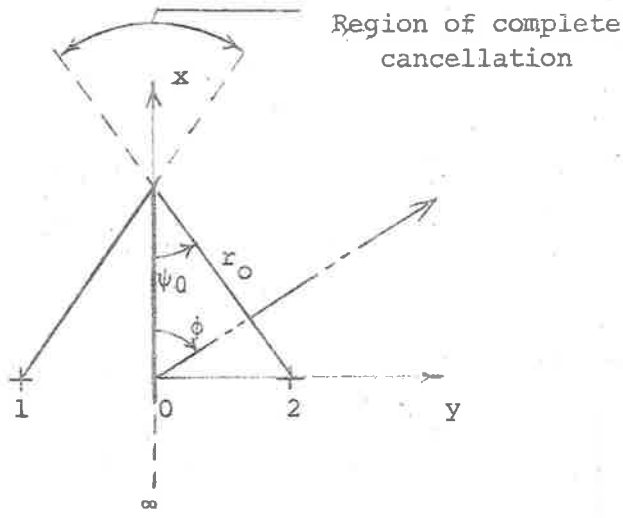

Fig. 4(a). Two line sources and half plane partition

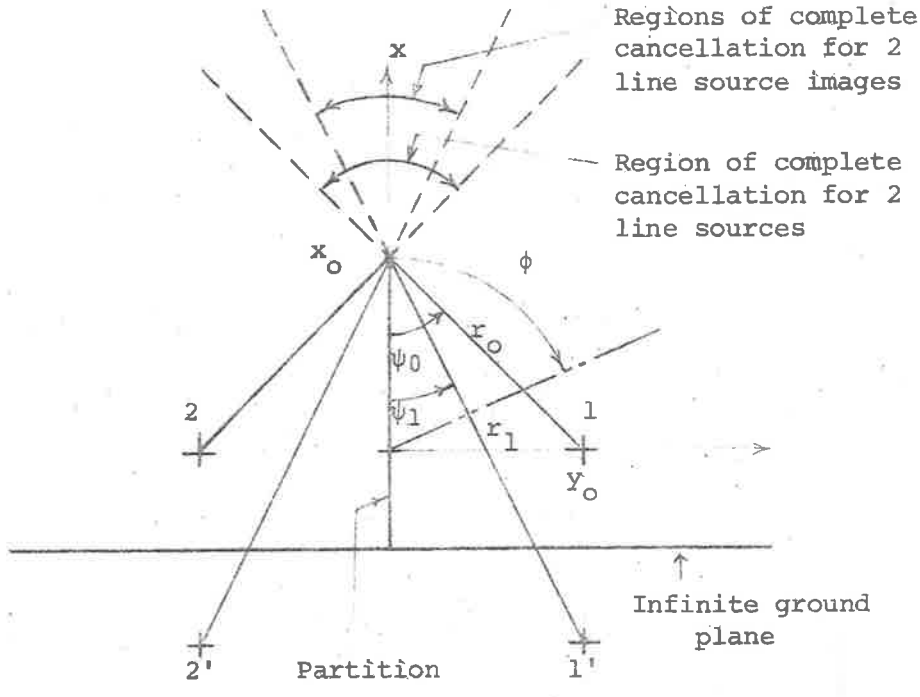

Fig. 4(b). Two line sources and partition over an infinite ground plane

field is not zero but equal to:

$$E^D(\phi) = 2[v_B(r_o,\pi-\phi-\phi_o) + v_B(r_o,\pi-\phi+\phi_o)].F(-\phi_o).\exp(jkx_o\cos\phi) \quad \ldots(28)$$

where $v_B(r,\phi)$ is given by (21) and the exponential term arises because the phase of $v_B(r,\phi)$ is referred to the edge. Proper sign must be used for $v_B(r,\phi)$ on each side of a shadow boundary as mentioned in (20). Thus the difference pattern is given by:

For $\phi < \phi_o$:

$$E^-(\phi) = 2j\sin(ky_o\sin\phi)F(\phi) + E^D(\phi) \quad \ldots(29a)$$

For $\phi > \phi_o$:

$$E^-(\phi) = 2\cos(ky_o\sin\phi)F(\phi) + E^D(\phi) \quad \ldots(29b)$$

There is no second order diffraction in this case.

When the line sources and the H plane partition are placed above an infinite ground plane as seen in Fig. 4(b), the image fields should be added and ϕ varies in the region $-\pi/2 \leq \phi \leq \pi/2$.

For the sum pattern:

$$E^+(\phi) = [F(\phi) + F(\pi-\phi)\exp(-j2kx_1\cos\phi)].2.\cos(ky_o\sin\phi) \quad \ldots(30)$$

For the diffracted field

$$E^D(\phi) = E_o^D(\phi) + E_1^E(\phi) \qquad \ldots(31)$$

where

$$E_o^D(\phi) = 2[v_B(r_o,\pi-\phi-\psi_o)+v_B(r_o,\pi-\phi+\psi_o)]F(-\phi_o)\exp(jkx_o\cos\phi) \qquad \ldots(31a)$$

$$E_1^D(\phi) = 2[v_B(r_1,\pi-\phi-\psi_1)+v_B(r_1,\pi-\phi+\psi_1)]F(-\pi+\phi_1)\exp(jkx_o\cos\phi) \qquad \ldots(31b)$$

The diffracted field is also reflected by the infinite ground plane, thus one has:

$$E_R^D(\phi) = E_{oR}^D(\phi) + E_{1R}^D(\phi) \qquad \ldots(31A)$$

where

$$E_{oR}^D(\phi) = E_o^D(\phi)\ \exp(-j2k(x_o+2x_1)\cos\phi) \qquad \ldots(31c)$$

$$E_{1R}^D(\phi) = E_o^D(\phi)\ \exp(-j2k(x_o+2x_1)\cos\phi) \qquad \ldots(31d)$$

For the difference pattern:

when $\phi < \phi_1$:

$$E^-(\phi) = [F(\phi)+F(\pi-\phi)\exp(-j2kx_1\cos\phi)].2j\sin(ky_o\sin\phi)+E^D(\phi)+E_R^D(\phi) \qquad \ldots(32a)$$

when $\phi_1 < \phi < \phi_0$:

$$E^-(\phi) = F(\phi).2j\sin(ky_o\sin\phi)+F(\pi-\phi)\exp(-j2kx_1\cos\phi).2\cos(ky_o\sin\phi)+E^D(\phi) + E_R^D(\phi) \qquad \ldots(32b)$$

and when $\phi > \phi_0$:

$$E^{-}(\phi) = [F(\phi)+F(\pi-\phi)\exp(-j2kx_1\cos\phi)]2\cos(ky_o\sin\phi)+E^{D}(\phi)+E_R^{D}(\phi) \quad \ldots(32c)$$

Once again there is no second order diffraction.

The most important case is when the ground plane is finite. This is a situation which is often encountered in practice. The diffraction due to the edge of the finite ground plane should be taken into account. Source (1) and its image at source (2) will have rays diffracted by edge R and similarly source (2) and its image at source (1) will have rays diffracted by edge L. The diffraction at R and L will present two more 'line' sources and the sum and difference patterns will be affected. Second order diffraction does exist in this case. Rays from the 'line' sources at R and L will be diffracted by edge C and rays from the 'line' source at C will be diffracted by edges R and L. Higher order diffraction terms can be included if necessary but in general all higher order terms could be ignored for large distance from an edge and for angular direction well away from a shadow boundary.

Diffracted fields due to edge R by source (1) and its image at (2) are:

$$E_2^{D}(\phi) = F(\pi/2+\psi_2)\ [v_B(r_2,\pi/2+\phi-\psi_2)+v_B(r_2,\pi/2+\phi+\psi_2)]$$
$$\exp(jky_1\sin\phi)\ \exp(-jkx_1\cos\phi) \quad \ldots(33a)$$

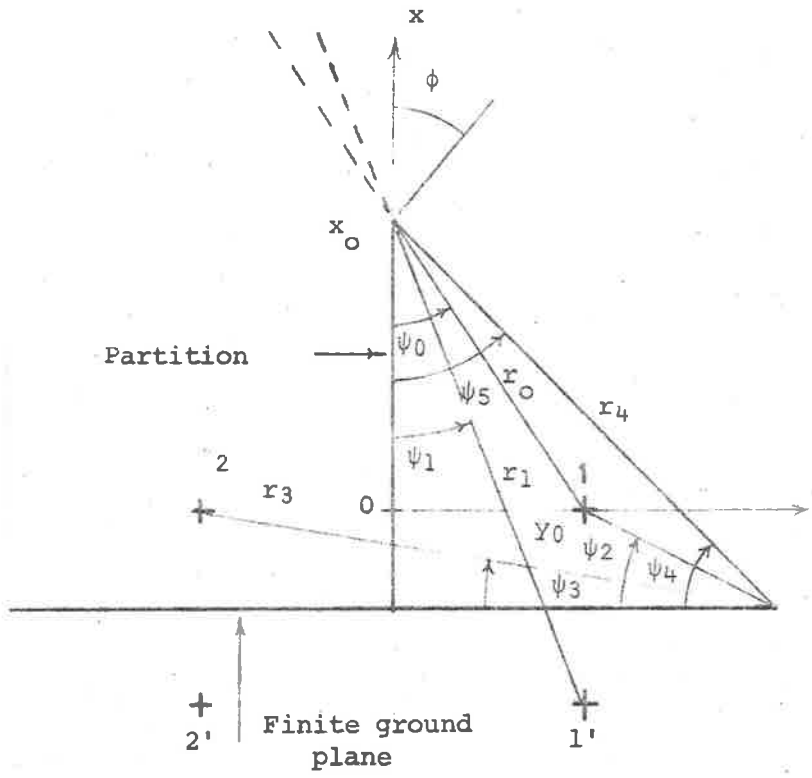

Fig. 4(c). Two line sources and partition above a finite ground plane

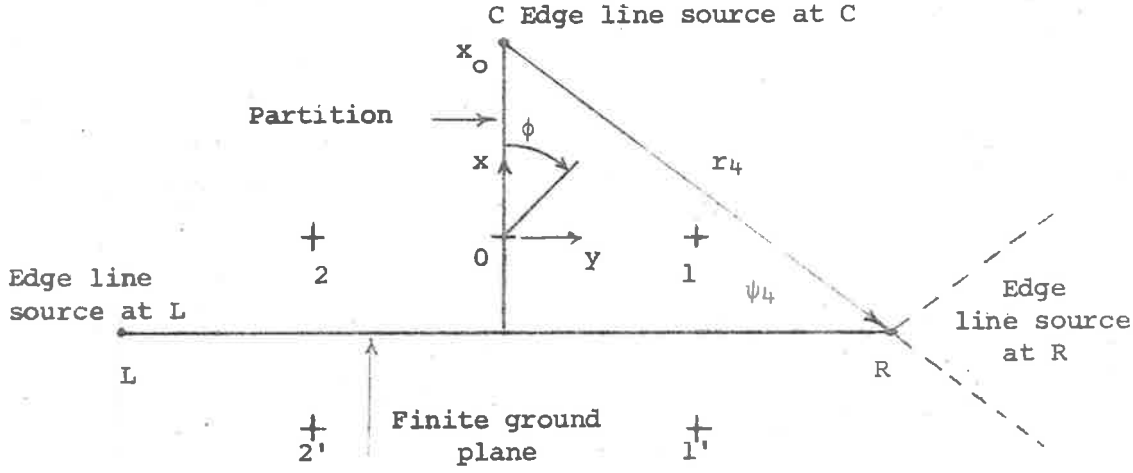

Fig. 4(d). Second order diffraction due to the finite ground plane.

$$E_3^D(\phi) = F(-(\pi/2+\psi_3))\ [v_B(r_3,\pi/2+\phi-\psi_3) + v_B(r_3,\pi/2+\phi+\psi_3)]$$

$$\exp(jky_1\sin\phi)\ \exp(-jkx_1\cos\phi) \qquad \ldots(33b)$$

Similarly, diffracted fields due to edge L by source (2) and its image at (1) are

$$E_4^D(\phi) = F(-(\pi/2+\psi_2))\ [v_B(r_2,\pi/2-\phi-\psi_2) + v_B(r_2,\pi/2-\phi+\psi_2)].$$

$$\exp(-jky_1\sin\phi)\ \exp(-jkx_1\cos\phi) \qquad \ldots(34a)$$

$$E_5^D(\phi) = F(\pi/2+\psi_3)\ [v_B(r_3,\pi/2-\phi-\psi_3) + v_B(r_c,\pi/2-\phi+\psi_3)].$$

$$\exp(-jky_1\sin\phi)\ \exp(-jkx_1\cos\phi) \qquad \ldots(34b)$$

It should be noted that E_2^D and E_4^D, E_3^D and E_5^D are not equal as indicated by the expression for the diffracted field function $v_B(r,\phi)$.

The sum pattern in this case is the sum pattern of 4 line sources at (1), (2), R and L which can be obtained for the various regions as follows, assuming $\psi_1 < \psi_3 < \psi_2 < \psi_0$ and considering the first quadrant only:

when $\phi \leq \pi/2 - \psi_2$:

$$E^+(\phi) = [F(\phi)+F(\pi-\phi)\ \exp(-j2kx_1\cos\phi)]\ 2\cos(ky_o\sin\phi).$$

$$+ E_2^D + E_3^D + E_4^D + E_5^D \qquad \ldots(35a)$$

when $\pi/2 - \psi_2 < \phi \leq \pi/2 - \psi_3$:

$$E^+(\phi) = F(\phi)2\cos(ky_o\sin\phi)+F(\pi-\phi)\exp[-j(2kx_1\cos\phi + ky_o\sin\phi)] + E_2^D + E_3^D + E_4^D + E_5^D \quad \ldots(35b)$$

when $\pi/2 - \psi_3 \leq \phi < \pi/2$:

$$E^+(\phi) = F(\phi)2\cos(ky_o\sin\phi) + E_2^D + E_3^D + E_4^D + E_5^D \quad \ldots(35c)$$

Expressions for the difference pattern is more involved than the sum pattern because of the existence of higher order diffraction terms.

Before attempting to present expressions for second order diffraction terms, the following convention should be adopted to designate the doubly diffracted field: if a first order diffracted ray comes from a 'line' source, at C say, and is diffracted again by an edge, R say, then the resulting doubly diffracted field will be denoted by $E_{CR}^D(\phi)$. Thus the first subscript designates the source and the second subscript designates the edge. A similar convention will be adopted for higher order diffraction terms if they need be taken into account.

All the second order diffraction terms can now be given as follows:

$$E^D_{CR}(\phi) = [v_B(r_4, \pi/2+\phi-\psi_4) + v_B(r_4, \pi/2+\phi+\psi_4)] .$$

$$E^D(\pi/2+\psi_4)\ \exp(jky_1\sin\phi) .\ \exp(-jkx_1\cos\phi) \qquad ...(33a)$$

$$E^D_{CL}(\phi) = [v_B(r_4, \pi/2-\phi-\psi_4) + v_B(r_4, \pi/2-\phi+\psi_4)] .$$

$$E^D(\pi/2+\psi_4)\exp(jky_1\sin\phi).\exp(-jkx_1\cos\phi) \qquad ...(33b)$$

$$E^D_{RC}(\phi) = [v_B(r_4, \pi-\phi-\psi_5) + v_B(r_4, \pi-\phi+\psi_5)] .$$

$$[E^D_2(\psi_4)+E^D_3(\psi_4)\ \exp(jkx_o\cos\phi) \qquad ...(33c)$$

$$E^D_{LC}(\phi) = -E^D_{RC}(\phi) \text{ from (25)} \qquad ...(33d)$$

It is quite obvious that there is no second order diffraction contribution to the sum pattern because the contribution given by (33a) and (33b) is zero due to $E^D(\phi) = 0$, and that given by (33c) and (33d) cancel each other out. This situation is only true when the field patterns $F(\phi)$ of the sources are symmetrical with respect to the plane partition.

Assuming $\psi_1 < \psi_3 < \psi_2 < \psi_0 < \psi_5 < \psi_4$, expressions for the difference pattern can be obtained for the various regions in the first quadrant, bearing in mind that two corresponding terms from

either side of the partition will subtract if they 'see' each other and will add if they do not.

For $\phi \leq \psi_1$:

$$\bar{E}(\phi) = [F(\phi)+F(\pi-\phi)\ \exp(-j2kx_1\cos\phi)]\ 2j\sin(ky_o\sin\phi)$$

$$E^D + E_R^D + E_2^D + E_3^D - (E_4^D + E_5^D) + 2E_{RC}^D + E_{CR}^D + E_{CL}^D \quad \ldots(34)$$

For $\psi_1 < \phi \leq \psi_0$:

$$\bar{E}(\phi) = [F(\phi)2j\sin(ky_o\sin\phi)+F(\pi-\phi)\exp(-j2kx_1\cos\phi)2\cos(ky_o\sin\phi)]$$

$$E^D + E_R^D + E_2^D + E_3^D - (E_4^D+E_5^D) + 2E_{RC}^D + E_{CR}^D + E_{CL}^D \quad \ldots(35)$$

For $\psi_0 < \phi \leq \psi_5$:

$$\bar{E}(\phi) = [F(\phi)+F(\pi-\phi)\exp(-j2kx_1\cos\phi)]\ 2\cos(ky_o\sin\phi)$$

$$E^D + E_R^D + E_2^D + E_3^D - (E_4^D + E_5^D) + 2E_{RC}^D + E_{CR}^D + E_{CL}^D \quad \ldots(36)$$

For $\psi_5 < \phi \leq \pi/2 - \psi_2$:

$$\bar{E}(\phi) = [F(\phi)+F(\pi-\phi)\ \exp(-j2kx_1\cos\phi)]\ 2\cos(ky_o\sin\phi)$$

$$+ E^D + E_2^D + E_3^D + E_4^D + E_5^D + 2E_{RC}^D + E_{CR}^D + E_{CL}^D \quad \ldots(37)$$

For $\pi/2 - \psi_2 < \phi \leq \pi/2 - \psi_3$:

$$E^{-}(\phi) = [F(\phi)2\cos(ky_o\sin\phi)+F(\pi-\phi)\exp(-j2kx_1\cos\phi).\exp(jky_o\sin\phi)]$$

$$E^D + E_2^D + E_3^D + E_4^D + E_5^D + 2E_{RC}^D + E_{CR}^D + E_{CL}^D \quad \ldots(38)$$

For $\pi/2 - \psi_3 < \phi \leq \pi/2$:

$$E^{-}(\phi) = F(\phi)2\cos(ky_o\sin\phi)+ E^D + E_2^D + E_3^D + E_4^D + E_5^D + 2E_{RC}^D + E_{CR}^D + E_{CL}^D \quad \ldots(39)$$

The procedure can be readily extended to the back region i.e. $\pi/2 < \phi < \pi$ of the ground plane. It is omitted here to preserve the clarity of the presentation.

When the line sources lie in the finite ground plane the above expressions have to be modified for grazing incidence along the line suggested by (14).

(ii) Two Apertures.

Assuming there exists the same arrangement as above but now the two line sources are replaced by two infinite apertures whose cross section is given in Fig. 5(a). Let a uniform plane wave travel in the x direction.

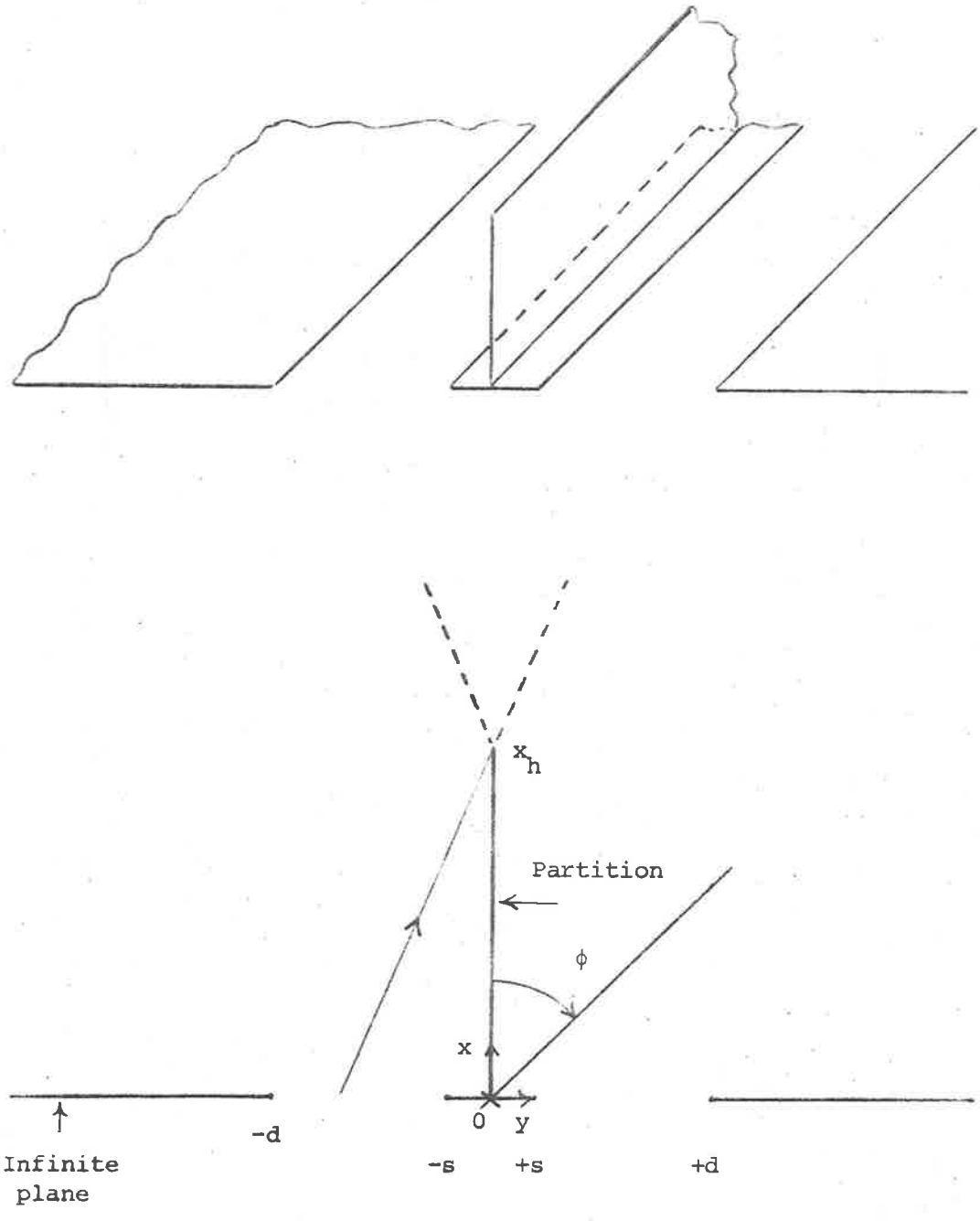

Fig. 5(a). Two apertures and partition

The field variation across each aperture in general is given by $E(y) = A(y) \exp(jf(y))$ where $A(y)$ is the amplitude distribution and $f(y)$ is the phase variation, the corresponding radiation pattern in the x-y plane, Fig. 5(b), is:

$$E^{A}(\phi) = \int_{d}^{d} E(y)\exp(jky\sin\phi)dy \qquad \ldots(40)$$

where $\exp(-jkr)/\sqrt{r}$ will be suppressed throughout. Since an aperture is supposed to be bounded by an infinite ground plane, if the field variation $E(y)$ is symmetrical with respect to the H plane partition, the sum pattern is not affected by the presence of the partition. Thus the sum pattern is given by the radiation pattern of the two apertures separated by a distance 2s i.e.

$$E^{+}(\phi) = \int_{-d}^{d} E(y)\exp(jky\sin\phi)dy \qquad \ldots(41)$$

where d is defined as in Fig. 5(a).

The integration can be broken down into:

$$\int_{-d}^{d} = \int_{-d}^{-s} \int_{s}^{d} \qquad \ldots(41a)$$

For a plane wave, $f(y) = 0$ i.e. $E(y) = A(y)$, (4) can be further simplified to:

$$E^{+}(\phi) = \int_{s}^{d} E(y)2\cos(ky\sin\phi)dy \qquad \ldots(42)$$

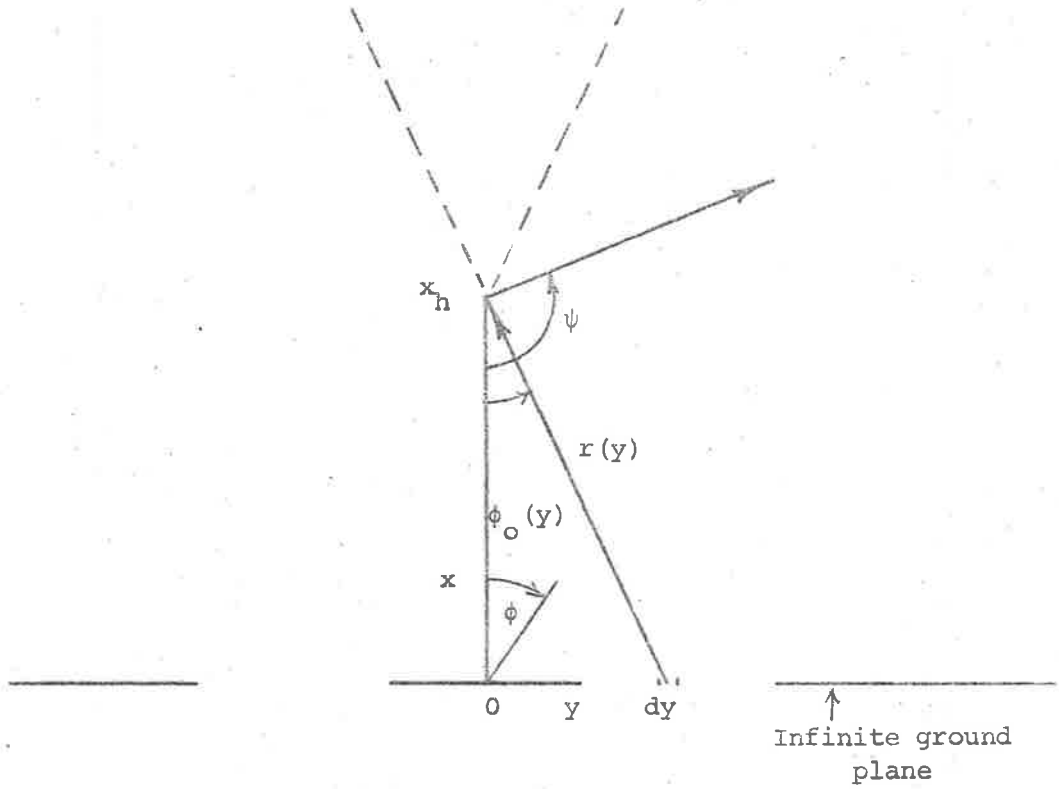

Fig. 5(b). Diffraction by each element dy.

The difference pattern of the two apertures when there is no partition is given by:

$$E^{-}(\phi) = \int_{s}^{d} E(y)\,2j\sin(ky\sin\phi)\,dy \qquad \ldots(43)$$

Since the image of an aperture in the H plane partition is positive, which is the same for a line source the incident and reflected fields will add. The geometrical optics difference pattern of the two apertures separated by a partition can be divided into three regions:

- The region where the two apertures can 'see' each other completely, the difference pattern is given by (43).

- The region where the two apertures do not 'see' each other at all i.e. they are completely separated by the partition, the difference pattern is actually the sum pattern given by (42).

- The region where the two apertures can partially 'see' each other, the difference pattern is given by the combination of (43) and (42), i.e.

$$E^{-}(\phi) = \int_{s}^{x_h \tan\phi} E(y)\,2\cos(ky\sin\phi)\,dy + \int_{x_h \tan\phi}^{d} E(y)\,2j\sin(ky\sin\phi)\,dy \qquad \ldots(44)$$

The diffracted field contribution should be added to the above

geometrical optics terms to give the resulting difference pattern for the two apertures separated by an H plane partition in their plane of symmetry.

The diffracted field contribution can be approximated by assuming that each element dy acts as a line source. The diffraction off the edge of a partition by two line sources has been presented above in Section a(i) and can be put into use here. By integrating the diffracted field contribution of all elemental line sources dy across each aperture in a particular direction the total diffracted field contribution due to the partition in that direction will be obtained.

If $E^D(y)$ is the diffracted field in the direction ϕ due to an element dy of unit amplitude, it can be written as:

$$E^D(y) = [v_B(r(y),\ \pi-\phi-\phi_o(y)) + v_B(r(y),\ \pi-\phi+\phi_o(y)]$$

$$\exp(jkx_h\sin\phi) \qquad \ldots(45)$$

where $v_B(r,\phi)$ is given by (20) and the phase centre is at 0.

The total diffracted field is:

$$E_t^D(\phi) = \int_s^d E(y)\ E^D(y)\ dy \qquad \ldots(46)$$

The sign of $v_B(r,\phi)$ should be correctly observed when each shadow

boundary is crossed as mentioned in (20).

Referring to Fig. 5(c), the difference pattern for two apertures separated by a partition can now be given as:

For $\phi \leq \phi_s$ i.e. the apertures 'see' each other:

$$E^{-}(\phi) = \int_s^d E(y)\,2j\sin(ky\sin\phi)\,dy + E_t^D(\phi) \qquad \ldots(47)$$

For $\phi_s < \phi \leq \phi_d$ i.e. the apertures 'see' each other only partially:

$$E^{-}(\phi) = \int_s^{x_h\tan\phi} E(y)\,2\cos(ky\sin\phi)\,dy + \int_{x_h\tan\phi}^d E(y)\,2j\sin(ky\sin\phi)\,dy + E_t^D(\phi) \qquad \ldots(48)$$

For $\phi_d < \phi$ i.e. the apertures do not 'see' each other:

$$E^{-}(\phi) = \int_s^d E(y)\,2\cos(ky\sin\phi)\,dy + E_t^D(\phi) \qquad \ldots(49)$$

Where $E_t^D(\phi)$ is given by (45).

It should be noted that $e^{-jkr}/\sqrt{r}$ has been suppressed throughout.

b. Oblique Incidence

The above results obtained for normal incidence can be extended to oblique incidence. For an obliquely incident plane wave:

$$e^{-jks} = e^{-jk(r\sin\theta + z\cos\theta)} \qquad \ldots(50)$$

Fig. 5(c). Three geometrical optic regions determined by the partition

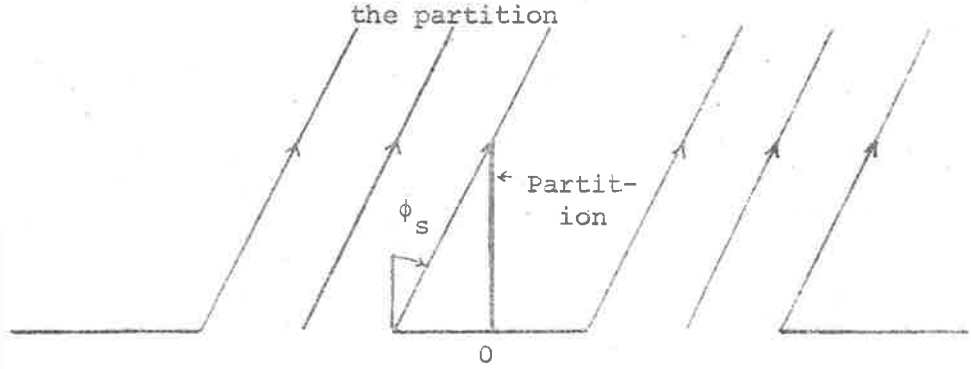

when $\phi < \phi_s$: Both sides 'see' each other

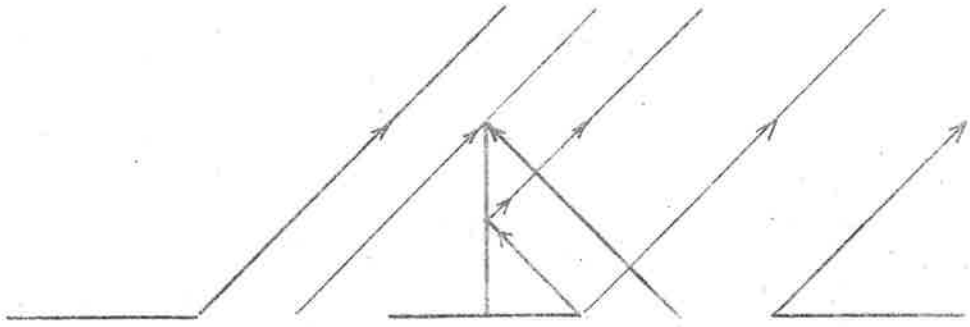

when $\phi_s < \phi < \phi_d$: Partial blockage

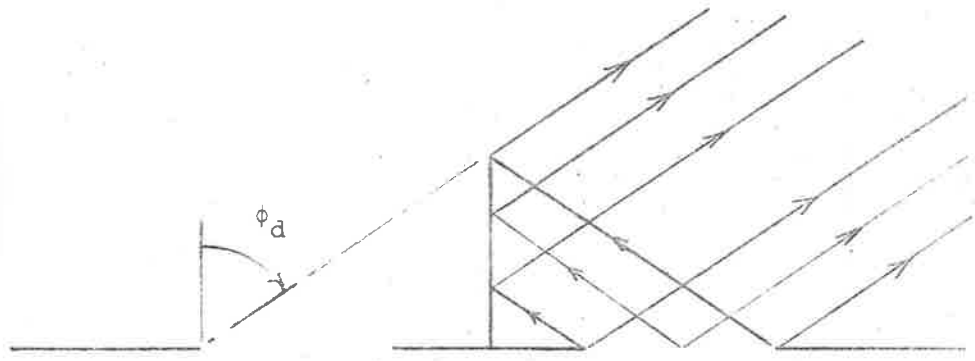

when $\phi_d < \phi$: Complete blockage

where θ is the angle of incidence i.e. the angle each ray makes with the z axis. The wave equation $\nabla^2 V + k^2 V = 0$ reduces to:

$$\nabla^2 V_r + k_r^2 V_r = 0 \qquad \ldots(51)$$

by making the substitution $V = V_r e^{-jk\cos\theta z}$ where $k_r = k\sin\theta$, the transverse wave number and V_r is the transverse scalar field.

From (51), it is quite clear that the expressions for the two dimensional oblique incidence can be deduced from those of the normal incidence by simply replacing k for its transverse component $k_r = k\sin\theta$ and multiplying throughout by $\exp(-jk\cos\theta z)$. r in $v_B(r,\phi)$ is still the distance from the source to the edge.

B. THREE DIMENSIONAL CASE

This is the most useful solution since it is a solution for a practical situation. The partition is again assumed to be infinite in length first and a discussion on a partition of finite length will be given later.

When a line source or an aperture has a finite length, it is considered as a point source for points beyond the Fraunhoffer's boundary. Thus spherical coordinates should be employed to describe the far field radiation patterns. However cylindrical wave formulatio

can still be used for the treatment of diffraction off the edge of a partition since it is normally placed in the vicinity of a source.

It has been pointed out in chapter one that the basic assumption in a three dimensional case is that the diffraction in the direction normal to the partition is given by the appropriate two dimensional case whereas the diffraction in the direction parallel to the partition is given by the radiation pattern of a finite line source [6]. Again two cases of incidence will be considered here and the normal incidence treatment will be given first.

a. Normal Incidence

(i) Two Line Sources

Assuming the line sources have a length L the radiation patterns can be deduced from the two dimensional expressions for two line sources with some slight modification.

(1) $e^{-jkr}/\sqrt{r}$ is replaced by $je^{-jkr}/2\lambda r$ which will be suppressed throughout.

(2) k is replaced by $k\sin\theta$ for the phase terms in the y and x directions.

(3) All expressions for the radiation patterns should be multiplied by:

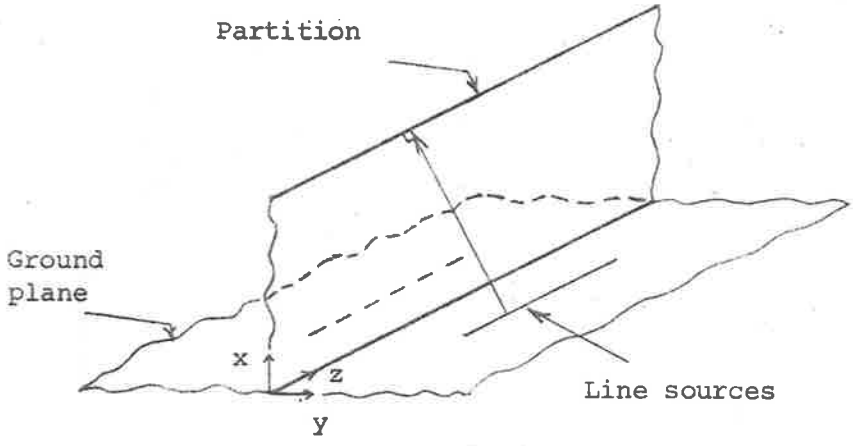

(a) Two finite length line sources

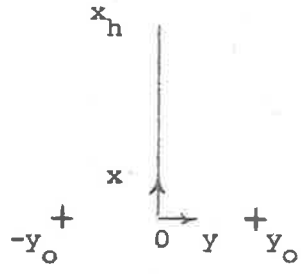

(b) Cross section

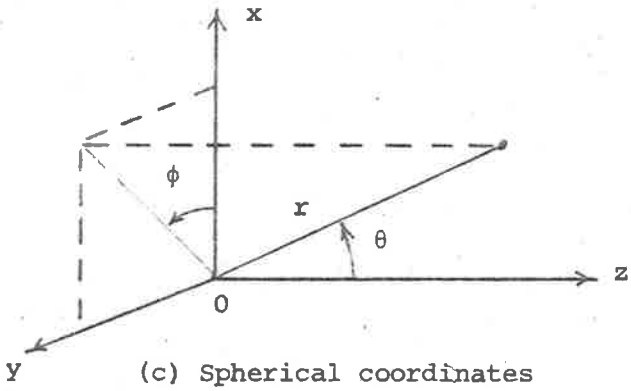

(c) Spherical coordinates

Fig. 9. Diffraction by two finite length line sources (normal incidence)

$$\sin\theta \int_{z_1}^{z_2} E(z)e^{jk\cos\theta z}\, dz$$

where $z_1 = z_o - L/2$ and $z_2 = z_o + L/2$, $E(z)$ is the field variation along z and the line source centres are $(0,y_o,z_o)$ and $(0,-y_o,z_o)$.

The sum pattern in the direction (ϕ,θ) is now given by:

$$E^{+}(\phi,\theta) = 2\cos(ky_o\sin\theta\sin\phi).F(\phi).\sin\theta\int_{z_1}^{z_2}E(z)e^{jk\cos\theta z}dz \quad ...(52)$$

The diffracted field is:

$$E^{D}(\phi,\theta) = 2[v_B(r_o,\pi-\phi-\phi_o) + v_B(r_o,\pi-\phi+\phi_o)].F(-\phi_o)$$

$$\exp(jkx_o\sin\theta\cos\phi)\sin\theta\int_{z_1}^{z_2}E(z)e^{jk\cos\theta z}dz \quad ...(53)$$

The difference pattern is:

For $\phi \leq \phi_o$:

$$E^{-}(\phi,\theta) = 2j\sin(ky_o\sin\theta\sin\phi).\ F(\phi)\cdot$$

$$\sin\theta \int_{z_1}^{z_2} E(z)e^{jk\cos\theta z}\, dz + E^{D}(\phi,\theta) \quad ...(53a)$$

For $\phi > \phi_0$:

$$\bar{E}(\phi,\theta) = 2\cos(ky_o \sin\theta\sin\phi) \cdot F(\phi) \cdot$$

$$\sin\theta \int_{z_1}^{z_2} E(z) e^{jk\cos\theta z}\, dz + E^D(\phi,\theta) \qquad \ldots(53b)$$

(ii) Two Apertures.

From Appendix D, the radiation pattern for an aperture with normal incidence is given by D(33):

$$E(\phi,\theta) = \frac{j}{2\lambda r} E_o e^{-jkr} (\sin\theta + \cos\phi) \int_{-d/2}^{d/2} \int_{-L/2}^{L/2} \exp[jk(y\sin\theta\sin\phi + z\cos\theta)]\, dydz \qquad \ldots(54)$$

The modification of the expressions for the radiation patterns of the two dimensional case involves:

(1) $e^{-jkr}/\sqrt{r}$ is replaced by $je^{-jkr}/2\lambda r$ which will be suppressed throughout.

(2) k is replaced by $k\sin\theta$ for the phase terms in the y and z directions.

(3) All expressions for the radiation patterns should be multiplied by:

$$(\sin\theta + \cos\phi) \int_{z_1}^{z_2} E(z) e^{jk\cos\theta z}\, dz$$

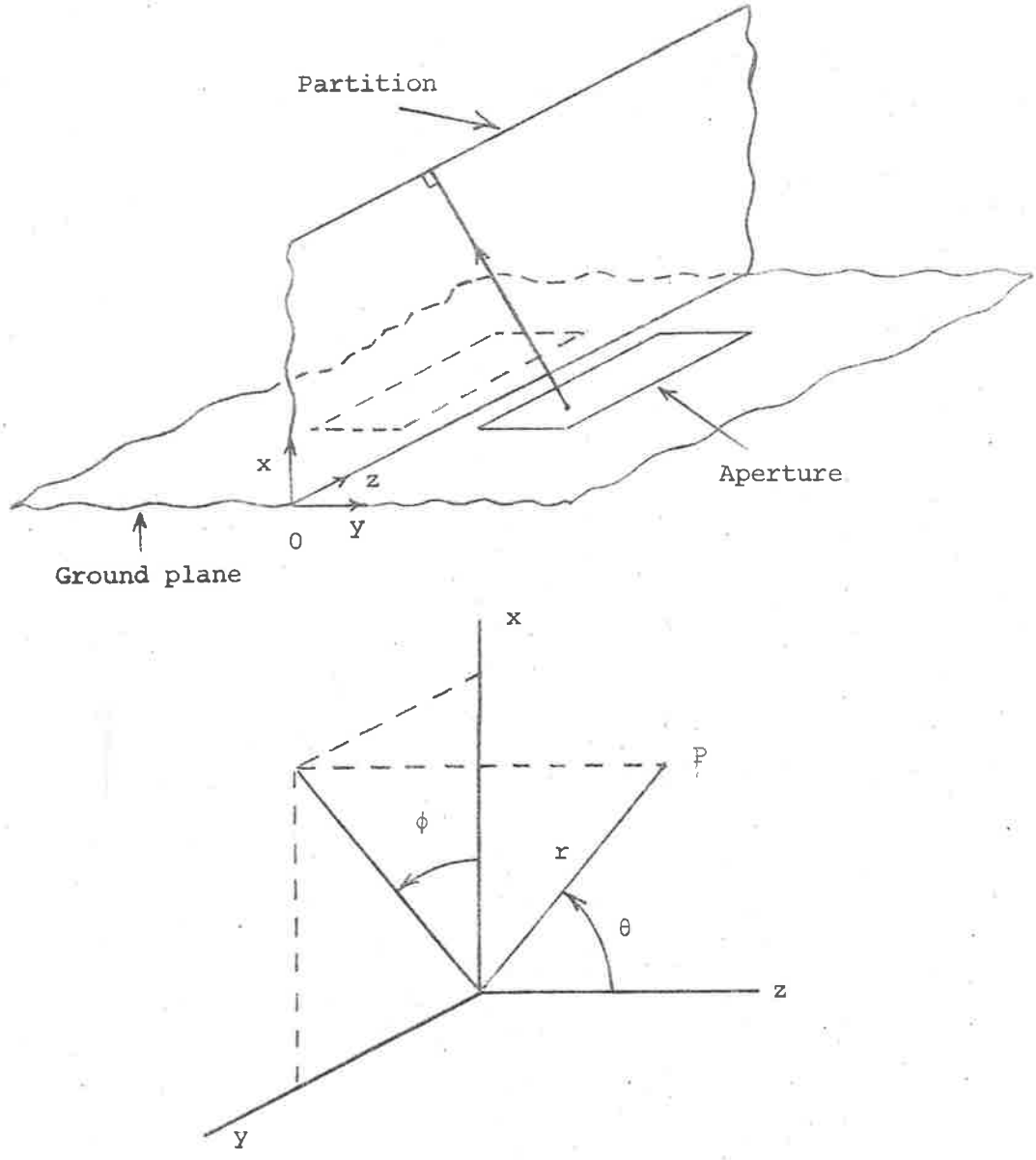

Fig. 6. Diffraction by two finite length apertures (Normal incidence)

Because of normal incidence, k in the expression for $v_B(r,\phi)$ in the line source as well as aperture case remains the same.

b. Oblique Incidence

In a three dimensional case of oblique incidence, the radiation pattern of interest is no longer the azimuth pattern as in the normal incidence case but an azimuth on elevation pattern especially when the angle of elevation is that of maximum radiation. Such a radiation form a cone of revolution of half angle $\pi/2 - \theta$ where θ is the angle of elevation. The line sources and apertures will be assumed to have a length L. Let $k_r = k\sin\theta_o$ and $k_z = k\cos\theta_o$ where θ_o is the angle an incident ray makes with the edge. Expressions for the radiation patterns can be derived by modifying those of the three dimensional normal incidence.

(i) Two Line Sources.

Referring to Fig. 7, the following modification needs be carried out.

(1) $je^{-jkr}/2\lambda r$ will be suppressed throughout as in the normal incidence.

(2) k is replaced by $k\sin\theta$ for the phase terms in the y and z directions.

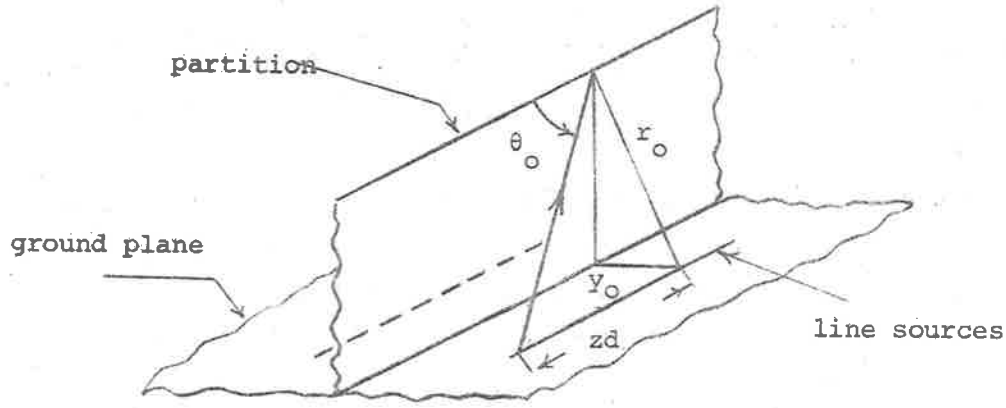

(a) Two travelling wave line sources

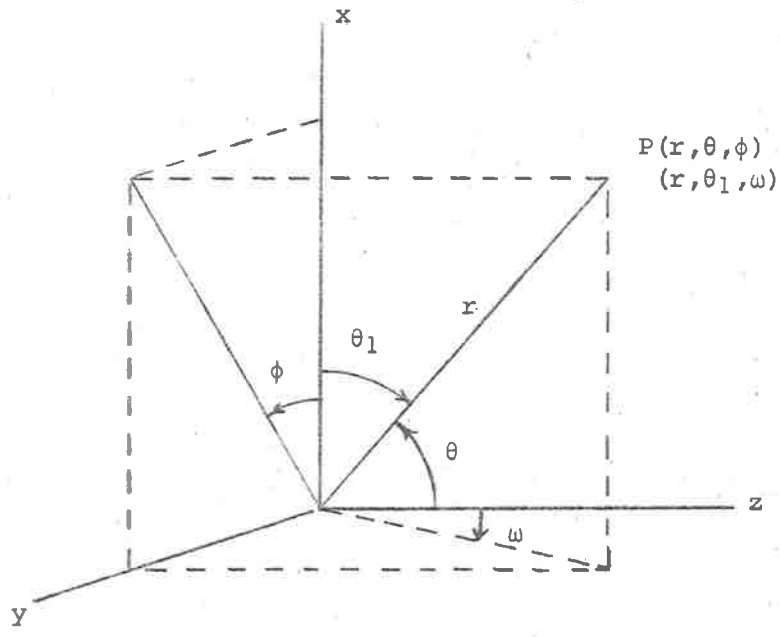

(b) Spherical coordinates

Fig. 7. Diffraction by two finite length line source (oblique incidence).

(3) From the azimuth on elevation radiation pattern given in Appendix D on the radiation pattern of an aperture with oblique incidence, all expressions for the normal incidence radiation patterns should be multiplied by:

$$\cos\theta_1\cos\omega \int_{z_1}^{z_2} E(z)e^{j(k\cos\theta - k_z)z}\, dz$$

to give the far fields in direction (ω,θ).

For a line source and its image:

$$z_1 = z_o - L/2 \text{ and } z_2 = z_o + L/2$$

For an edge diffraction 'line' and its image:

$$z_1 = z_d + z_o - L/2 \text{ and } z_2 = z_d + z_o + L/2$$

because of the oblique incidence, the diffracted 'line' source has been shifted in the z direction a distance z_d. For each edge, there will be a different z_d.

(4) k in $v_B(r,\phi)$ is replaced by k_r. It should be pointed out that the sum and difference patterns are now $E^+(\omega,\theta_1)$ and $E^-(\omega,\theta_1)$ where the spherical coordinates (r,ω,θ_1) are shown in Fig. 7(b) together with (r,ϕ,θ). The relationship between the two coordinate systems is as follows:

$$\phi = \arccos\left(\frac{\sin\theta_1}{(1-\cos^2\theta_1\cos^2\omega)^{1/2}}\right)$$

$$\theta = \arccos(\cos\theta_1 \cos\omega)$$

(ii) Two Apertures.

Expressions for the azimuth on elevation radiation patterns can be obtained from those of the three dimensional normal incidence of two apertures. The modification is basically the same as that of two line sources above. Appropriate z shift due to the oblique incidence for each elemental line source dy should be carefully incorporated into the expression for the total diffracted field $E_t^D(\omega,\theta_1)$ modified from (45). As seen in Appendix D on oblique incidence, the multiplying factor for a two line source case should now be:

$$2\cos\theta_1\cos\omega\int_{z_1}^{z_2} E(z)e^{j(k\cos\theta-k_z)z}\,dz$$

where $z_1 = z_o - L/2$ and $z_2 = z_o + L/2$, the centre of the aperture is at z_o in the z direction.

It can be seen from the above presentation that starting from the diffraction of a line source by a wedge and by using the principle of

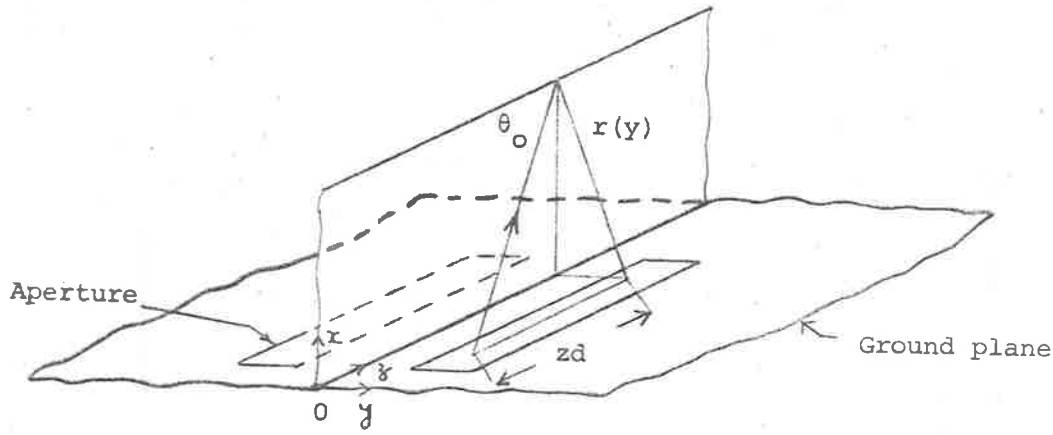

(a) Two travelling wave apertures

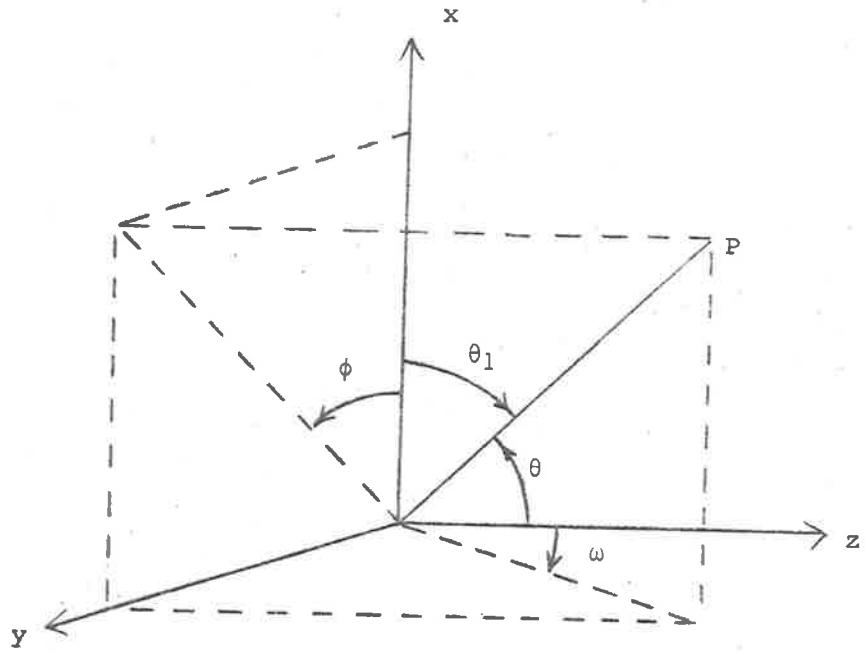

(b) Spherical coordinates

Fig. 10. Diffraction by two finite length apertures (oblique incidence)

superposition, the solution for the diffraction problem described in Chapter One involving the wedge of a partition has been constructed. When the partition is plane, the solution is exact as far as the diffraction expressions are concerned. It is only approximate in the finite line source case as well as the finite length aperture case due to the approximation to the diffraction in the direction parallel to the partition by the radiation pattern of a finite line source or finite length aperture. Expressions for a thick partition or a general wedge will be approximate and will give a good agreement only when the conditions for the asymptotic approximation are met. The above analysis is expected to give a fairly good agreement in the direction of incidence. The partition height must be less than the length of the line source or aperture in the finite length case i.e. three dimensional case to ensure that the cylindrical wave assumption is still valid. The treatment for an E plane partition can be simply extended by using the negative sign in the total diffracted field and the reflected field functions. The line source case has been given a great emphasis because it will prove to be a most useful building block for the analysis of all apertures having a principal polarization. An aperture can be arbitrary and needs not be restricted to a rectangular shape as having been assumed.

When radiation patterns away from the direction of incidence

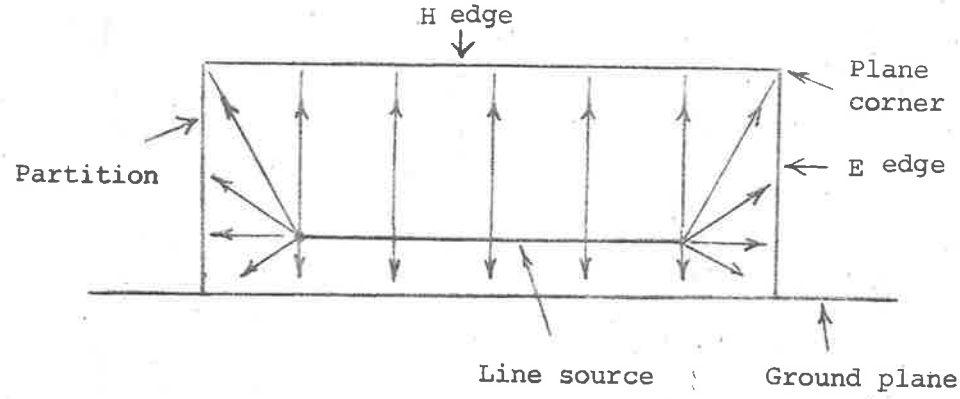

(a) Finite length line source and finite length partition.

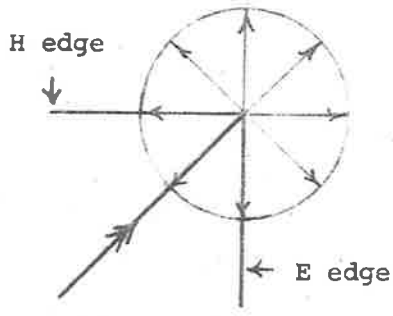

(b) Diffraction by a plane corner (spherical waves)

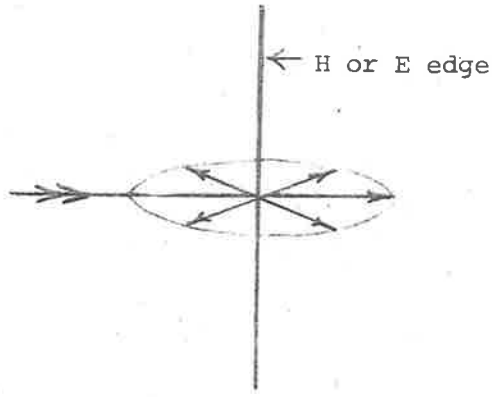

(c) Diffraction by normal incidence (circular cylindrical waves)

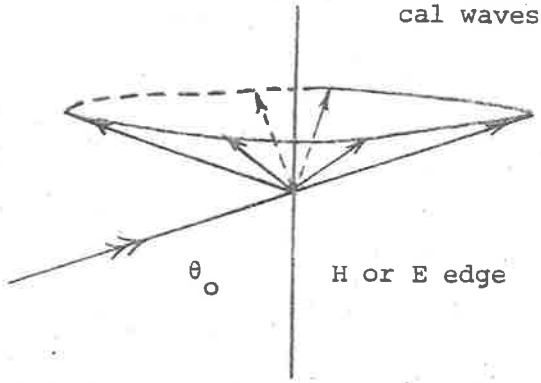

(d) Diffraction by oblique incidence (conical waves)

Fig. 8. Effects of finite length line source and finite length partition.

are required in the finite length case, correction has to be taken for the spreading of the wavefront at either end of the line source. The wavefront in these regions can never be truly cylindrical. To take such an effect into account, the existence of a point source of an appropriate field distribution (i.e. proportional to $\sin\theta$, say) could be assumed and the resulting diffracted field should be added to the above solution for the diffraction by the partition. When the partition is infinite in length, the problem is the diffraction of a point source by a horizontal edge. When the partition is finite in length, the problem is the diffraction of a point source by a plane angular sector consisting of a horizontal edge section, a vertical edge section and a right angle corner. The plane corner diffraction gives rays which emanate from the corner in all directions. This could be serious because the radiation pattern in the region of interest could be adversely affected. An approximate corner diffracted contribution could be included by assuming a spherical wave originating at the plane corner. The exact solution has not been obtained however because the problem of the plane corner diffraction is a very difficult boundary value problem [5].

To verify the above solution for the diffraction off the edge of an H plane partition, the following cases will be considered:

(1) Two slot dipoles in a finite ground plane. The radiation patterns in the principal plane of such an arrangement will be the same as those of two infinite line sources having a normal incidence to the partition.

(2) Two travelling wave slot lines on a ground plane. The azimuth on elevation radiation patterns of such a system have been given in the three dimensional case of two line sources having an oblique incidence.

(3) Two travelling wave apertures. This is the three dimensional case of two apertures having an oblique incidence.

The theory and design for a slot dipole is quite well known. A suitable line source and a suitable aperture will be studied in the next chapter.

CHAPTER THREE

LINE SOURCES AND APERTURES

A suitable line source for use in conjunction with an H plane partition is a new type of long slot leaky wave antenna consisting of a parallel strip transmission line backed by a cavity as shown in Fig. 1. It has been investigated by Willoughby [11] and the author [12]. The properties and characteristics of the antenna will be given in this chapter.

1. A LINE SOURCE

(a) Physical Background

It has been found that when the characteristic impedance of the strip line is designed to be much smaller than that presented by the cavity, the velocity of propagation will be very close to that of light. The antenna when radiating into the whole space, can be considered as the dual of a long wire antenna. By duality, the far field of a magnetic current line source may be obtained from that of an electric current line source by the substitutions:

Electric		Magnetic
$\bar{E}$	$\rightarrow$	$\bar{H}$
μ	$\rightarrow$	ε
I_o^e	$\rightarrow$	I_o^m

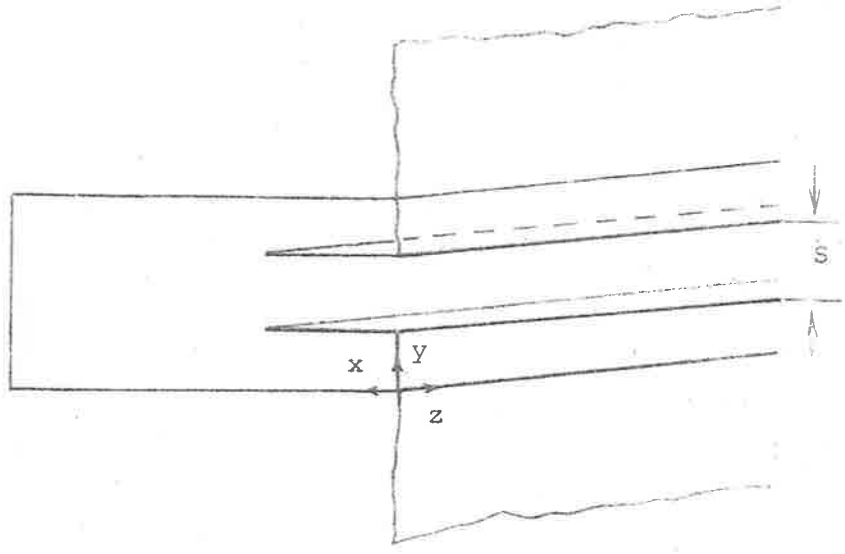

Fig. 1. Leaky wave slot antenna

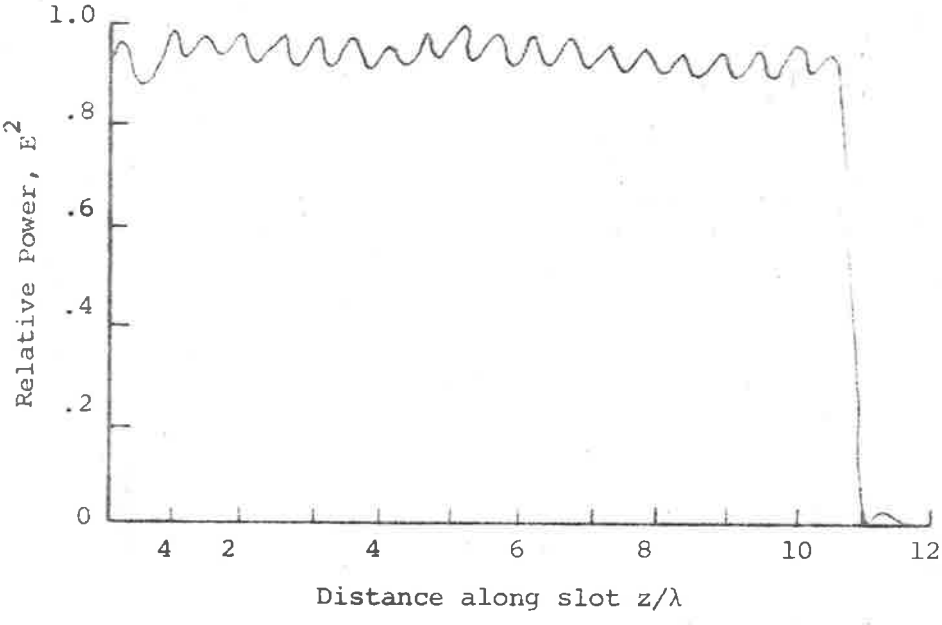

Fig. 2. Field distribution along uniform slot.

If it is properly terminated at one end by a graphite impregnated bakelite wedge (Appendix C), the slot antenna will support a travelling wave and have a wide bandwidth of at least 2:1. The characteristic impedance could be made small by making the strip line impedance small. The directivity of such a line source is comparable to that of a terminated long wire antenna. For instance a slot line of length 11λ, of width .01λ and of depth .083λ has a directivity of 4 dB over the dipole. As the cavity cross sectional area decreases, the velocity ratio, c/v, where c is the velocity of light and v is the velocity of propagation, appears to decrease quite slowly. The field distribution along the slot is given in Fig. 2. The field distributions inside the cavity and along the depth of the slot (i.e. the width of the strip line) have also been studied. The field distribution, in the former case, Fig. 3(b), is measured by inserting a small E probe into holes along the wide side of the cavity. The slot is mounted in a large ground plane. The polarity of the field inside the cavity is established to be as shown in Fig. 3(c). The field distribution in the latter case, Fig. 4(b) is obtained in a similar manner by introducing the E probe into holes in the plane MM' as seen in Fig. 4(a), MM' is the plane of symmetry perpendicular to the electric field. All the holes are tapped so that they can be plugged up when not being used to avoid discontinuity. The plane of symmetry and the ground plane are useful in preventing the active

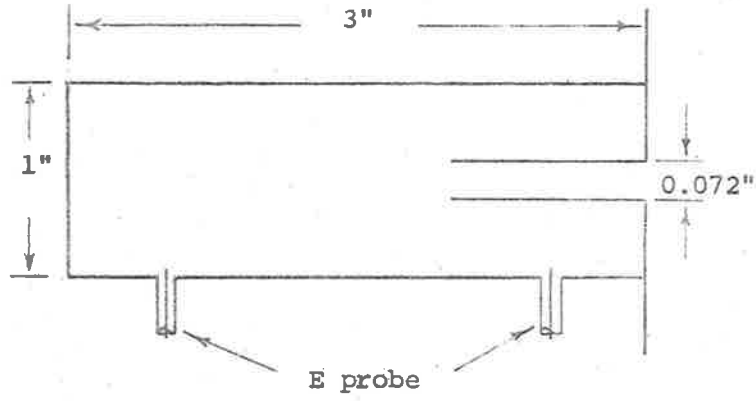

(a)

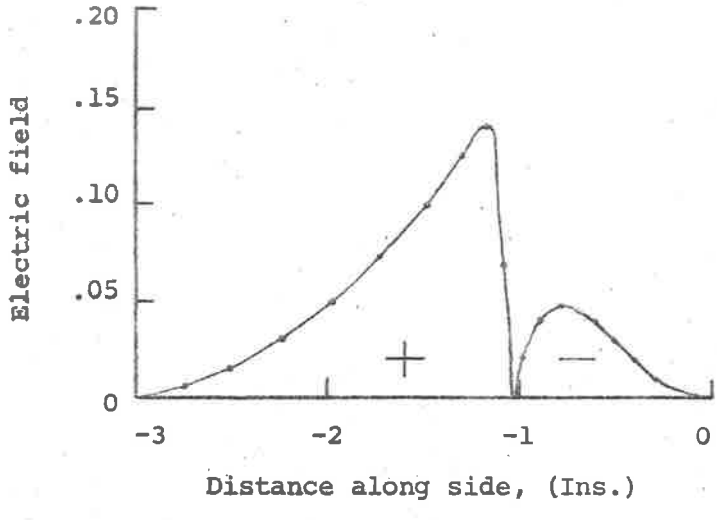

(b)

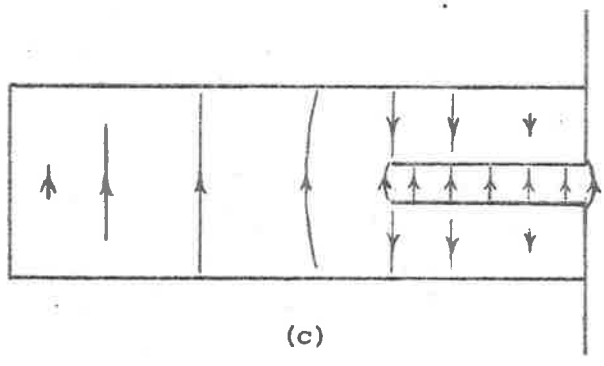

(c)

Fig. 3. Electric field inside cavity (2 GHz)

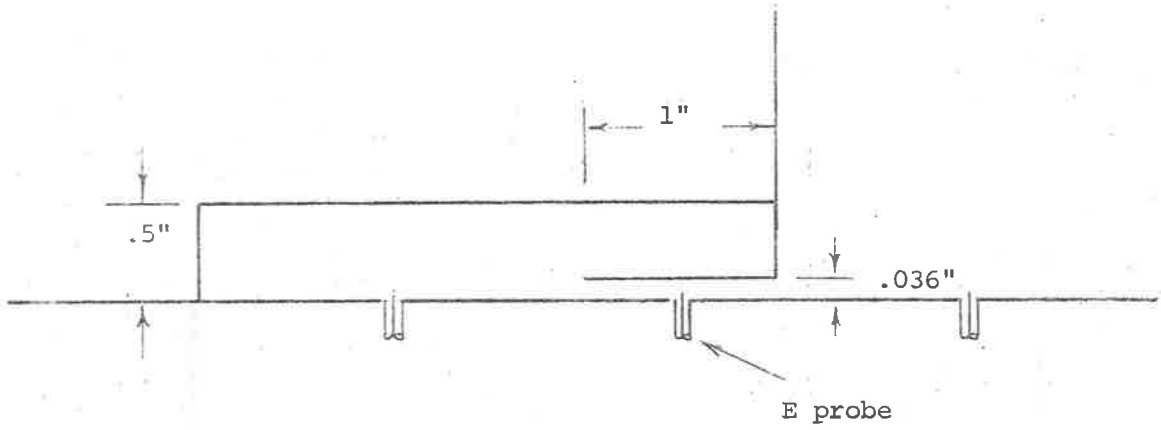

(a)

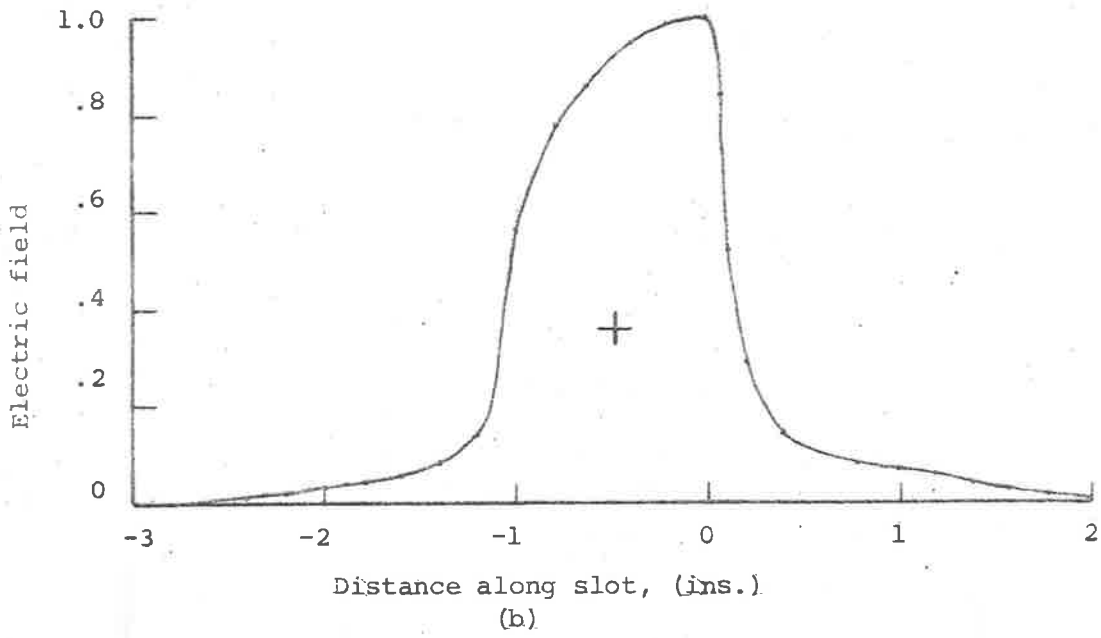

(b)

Fig. 4. Electric field distribution in transverse direction (2 GHz).

field from entering the measuring equipment. The field strength is strongest at the slot and remains fairly constant along the depth of the slot but falls off rapidly to zero towards the bottom side. When the cavity depth is increased, the field strength in the cavity beyond the slot depth appears to take on the shape of a half sine wave. This suggests the existence of a higher order mode, i.e. the TE_{01} mode in this case. Multimode operation for this type of antenna is still being investigated.

(b) Analysis for the New Slot Antenna

The above physical ground work serves as a very useful guide for the analysis of the new slot antenna.

For a travelling wave antenna of this type, the attenuation constant and the velocity ratio, c/v, are some of the most useful information for the designer. There are several analytical methods which could be used here: the differential equation method using Maxwell's equations, the variational method using integral equations or the method of transverse resonance. The last method due to Marcuvitz [13] is favoured since it deals with impedance and admittance which are more in line with many electrical engineering studies. Assuming that the antenna is infinitely long and has a uniform cross section. When the z variation of the antenna is in the form of

$e^{-jk_z z}$ where k_z is the wave number along z, the wave equation becomes separable in z and the remaining transverse wave equation is:

$$[\nabla_t^2 + \kappa^2]\ \underline{H}_z = 0 \qquad \ldots(1)$$

where $\kappa^2 = k^2 - k_z^2$, $k = 2\pi/\lambda$ $\qquad \ldots(2)$

Thus there is a wave propagation in the transverse direction with a wave number κ. From (2) if κ is known then k_z will be known. κ can be obtained by solving the complex transverse resonance equation derived from the transmission line network representing the cross section of the antenna.

Fig. 5 shows a cross section of the slot antenna together with its transverse equivalent network. The transverse resonance equation can be set up by equating the sum of the admittance looking into the cavity and that looking out into the whole space or half space to zero. The inwards admittance normalized to Y_o, the admittance of the section of rectangular waveguide of narrow width b, can be shown to be

$$\frac{Y_B}{Y_o} = -j\,\frac{b(s-(b\tan\kappa a+2b_1\tan\kappa d_1)\tan\kappa d)}{s(b\tan\kappa a+2b_1\tan\kappa d_1+b_1\tan\kappa d)} \qquad \ldots(3)$$

The outwards admittance is given by Marcuvitz [13]:

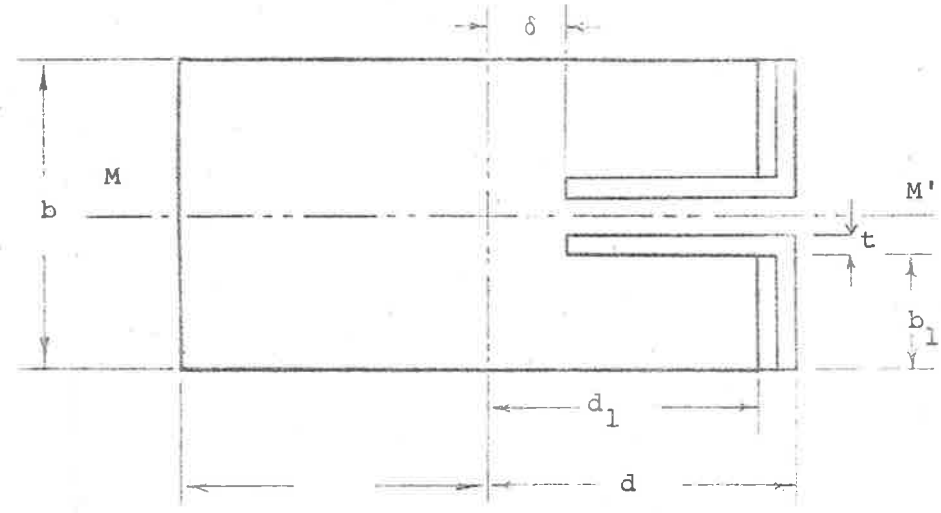

(a)

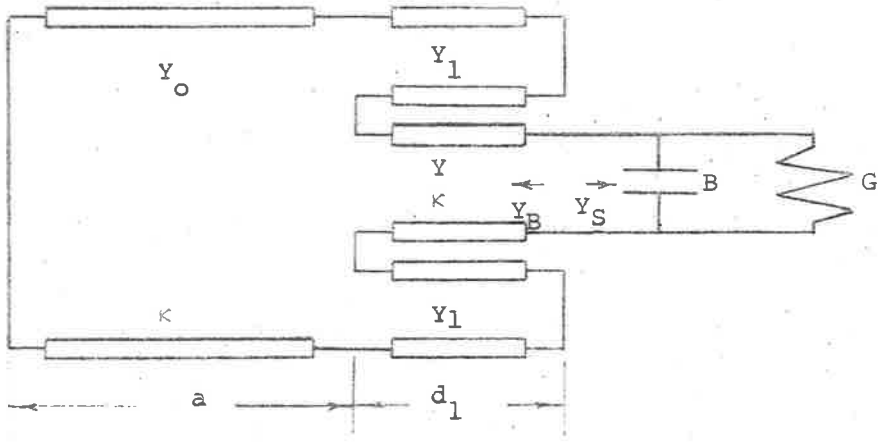

(b)

Fig. 5. Slot antenna cross section and transverse equivalent circuit.

$$\frac{Y_S}{Y_o} = \frac{\kappa b}{2} + j\frac{\kappa b}{\pi}\ln\frac{\pi e}{\gamma s\kappa} \qquad \ldots(4)$$

for a slot radiating into a half space and:

$$\frac{Y_S}{Y_o} = \frac{\kappa b}{4} + j\frac{\kappa b}{2\pi}\ln\frac{4\pi e}{\gamma s\kappa} \qquad \ldots(5)$$

for a slot radiating into the whole space. κ is the transverse propagation constant, e = 2.718, γ=1.781 and other constants are shown in Fig. 5. The transverse resonance equation is given by (3) and (4) or (3) and (5), i.e.

$$F(\kappa) = -j\frac{b(s-(b\tan\kappa a+2b_1\tan\kappa d_1)\tan\kappa d)}{s(b\tan\kappa a+2b_1\tan\kappa d_1+\tan\kappa d)}$$

$$+ \quad \frac{\kappa b}{2} + j\frac{\kappa b}{\pi}\ln\frac{\pi e}{\gamma s\kappa} = 0 \qquad \ldots(6)$$

$$\text{or} \quad \frac{\kappa b}{4} + j\frac{\kappa b}{2\pi}\ln\frac{4\pi e}{\gamma s\kappa}$$

In practice, the antenna finite thickness should be taken into account. For large wavelength, the thickness can normally be assumed to be zero, thus $d_1 \doteq d$ in (6), where d is equal to the width of the parallel strip line plus the fringing effect δ:

$$\delta \doteq \frac{b}{2\pi}\left(\frac{2b_1}{b}\ln\frac{b}{2b_1}+\frac{s}{b}\ln\frac{b}{s}\right) \qquad \ldots(7)$$

When the thickness is not zero, apart from $d_1 \neq d$, a further fringing effect $\Delta\delta$ comes from the thickness t of the strip line, this is given by Rotman [16]

$$\Delta\delta \doteq \frac{2}{\pi}\ln\left|\frac{2-2t/b}{2(1-2t/b)}\right| - \frac{2t}{\pi b}\ln\left|\frac{2t/b(2-2t/b)}{1-2t/b)^2}\right| \qquad \ldots(8)$$

$F(\kappa) = 0$ is a complex transcendental equation which can be solved by numerical analysis using Müller's method [14]. On a CDC 6400 computer the programming is straight forward [15]. Due to the many variables involved, solutions for (6) cannot be expressed in a general form. However a study of a few specific cases will give an insight into the characteristics of the solutions and therefore of behaviour of the slot antenna. A parametric study of the ideal slot line is presented in Appendix A. The only commercially available guides for the frequency of 2 GHz are the aluminium rectangular cylinders of cross sections 3 x 1" and 4 x 1" respectively. Fig. 6 shows the results for the ideal and practical case of a slot having a width .01λ and backed by a 3 x 1" guide, the finite thickness has practically no effect on the velocity ratio, c/v, and only a small effect on the attenuation constant. Fig. 7(a) shows the results for the ideal and the practical

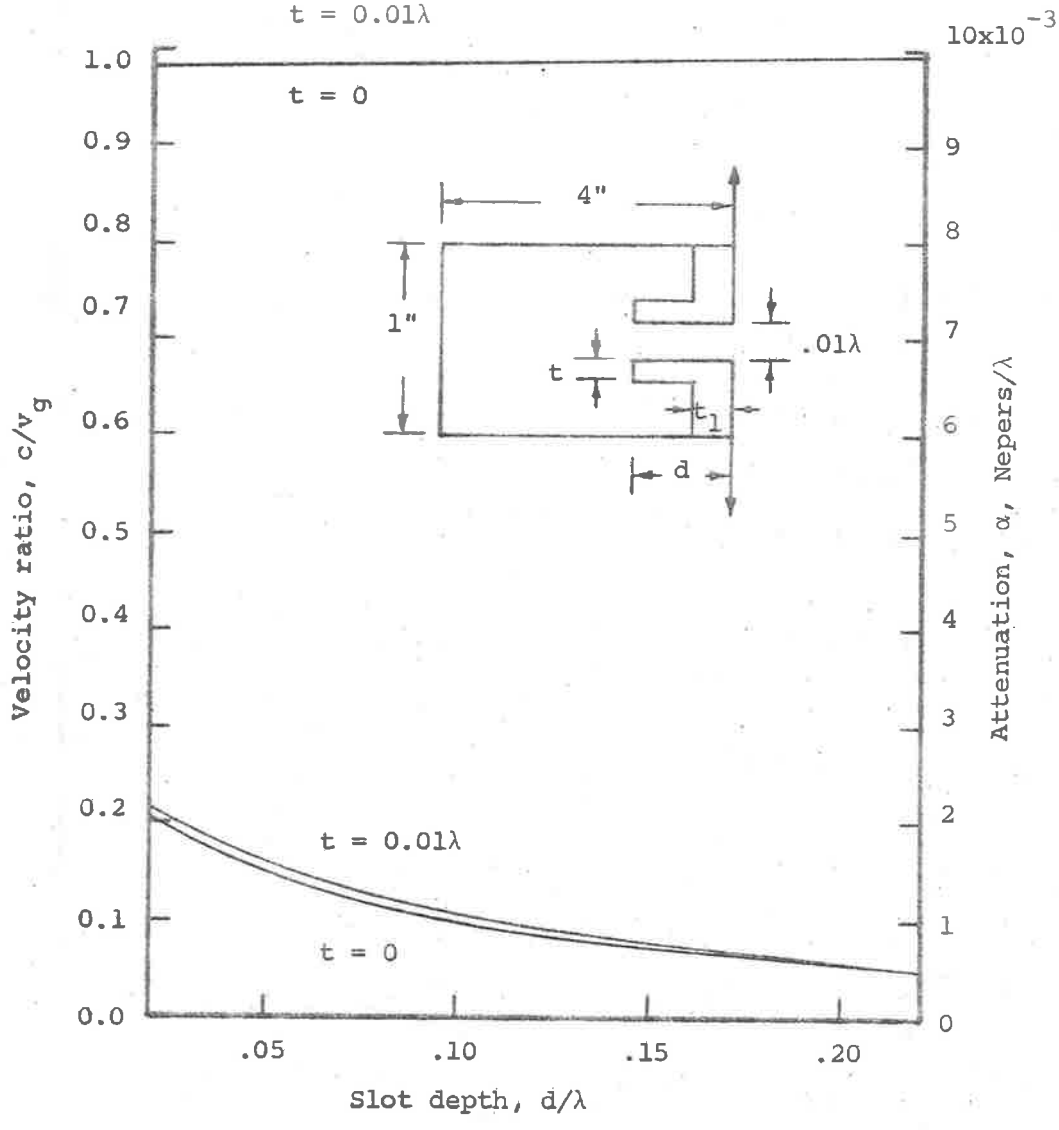

Fig. 7(a). Variation of velocity ratio and attenuation vs slot depth for a 4 x 1" guide. (First set of solutions).

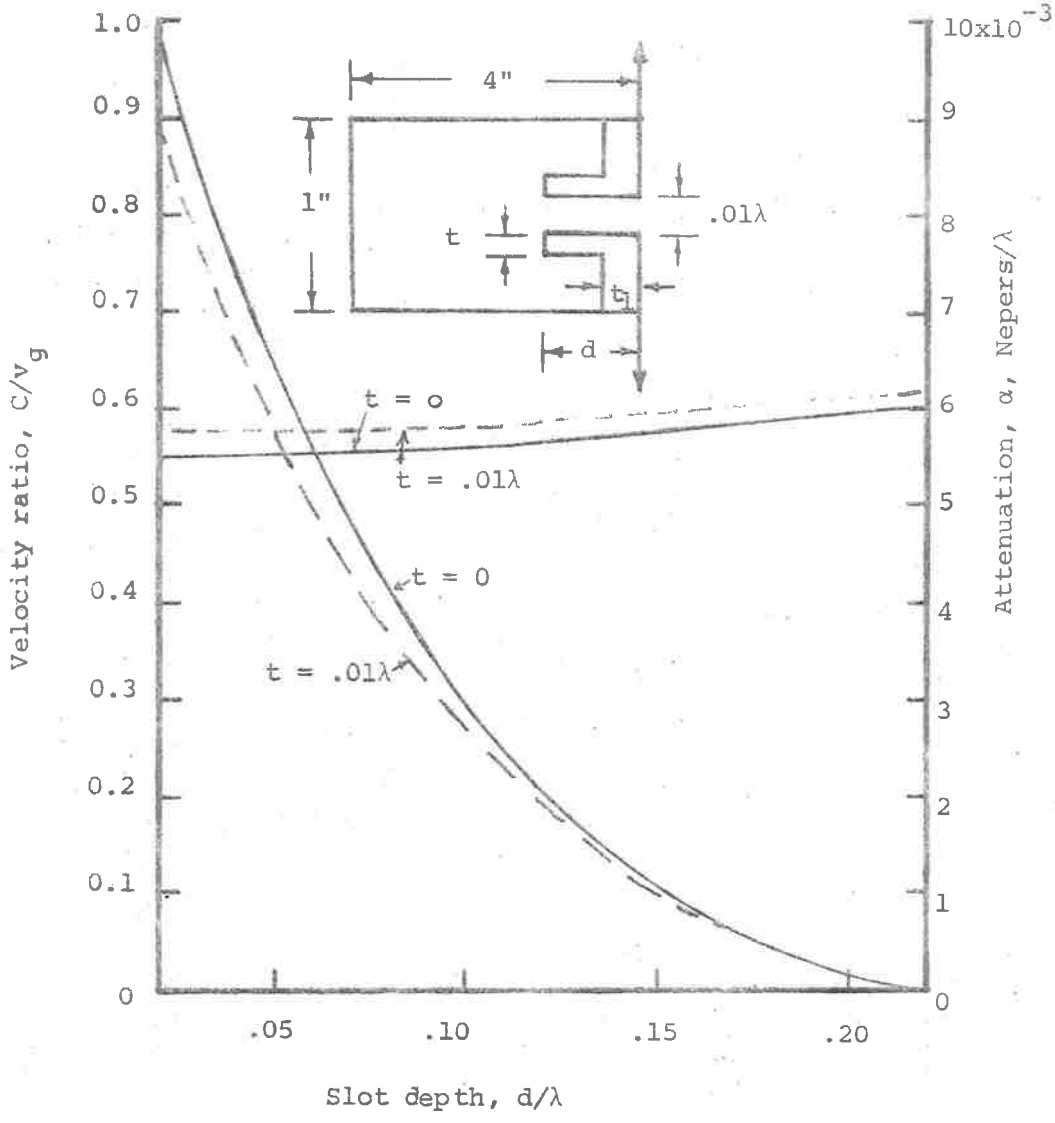

Fig. 7(b). Variation of velocity ratio and attenuation vs slot depth for a 4 x 1" guide. (Second set of solutions).

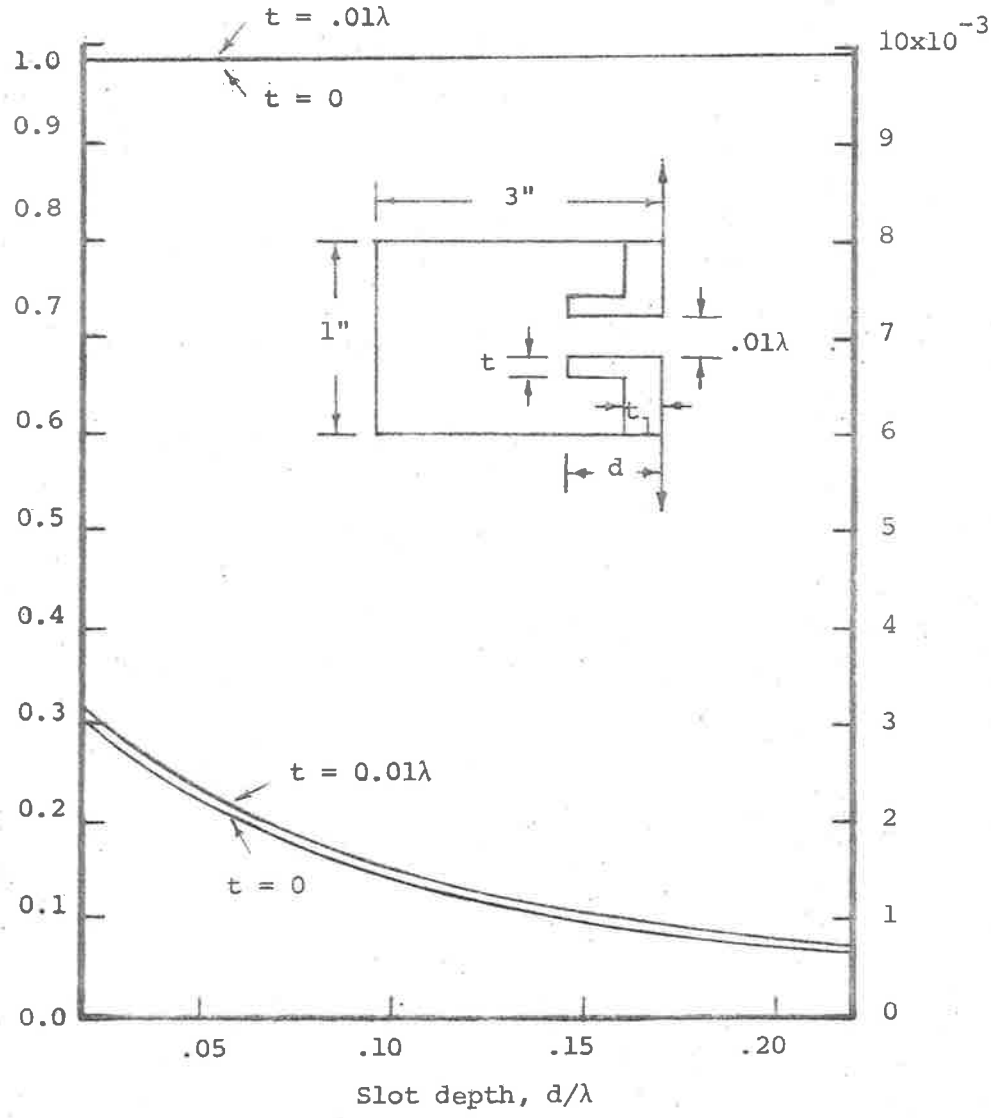

Fig. 6. Variation of velocity ratio and attenuation vs slot depth for a 3 x 1" guide.

case of a slot having a width .01λ and backed by a 4 x 1" guide. $F(\kappa) = 0$ in fact has two sets of solutions. The first set corresponds to the strip line mode and the second set corresponds to the TE_{01} mode. The results from the second set are shown in Fig. 7(b). The antenna with a 4 x 1" cross section when excited will radiate on a multimode basis.

A model at 2 GHz was set up to measure the voltage standing wave ratio along the slot at a short distance from it. The model was a bisected realization of the original structure with a conducting plan through the plane of symmetry MM' as seen in Fig. 4(a). The space between the single strip line and the conducting plane was set at exactly one half of the actual slot width s. The VSWR was plotted by using a small E probe introduced into small holes in the plane MM' The unused holes were plugged up to avoid discontinuity. The wavelength and attenuation were deduced from the VSWR curve. The results shown in Fig. 8 were for the practical slot backed by the 3 x 1" guide. The velocity ratio agreed well with the theoretical values whereas the attenuation constant was too small to be measured accurately. It should be pointed out here that the ohmic loss for aluminium at 2 GHz is quite large compared to the radiation loss and this had complicated the measurement. The results given in Fig. 7 had also been tested. The elevation radiation pattern when such a slot

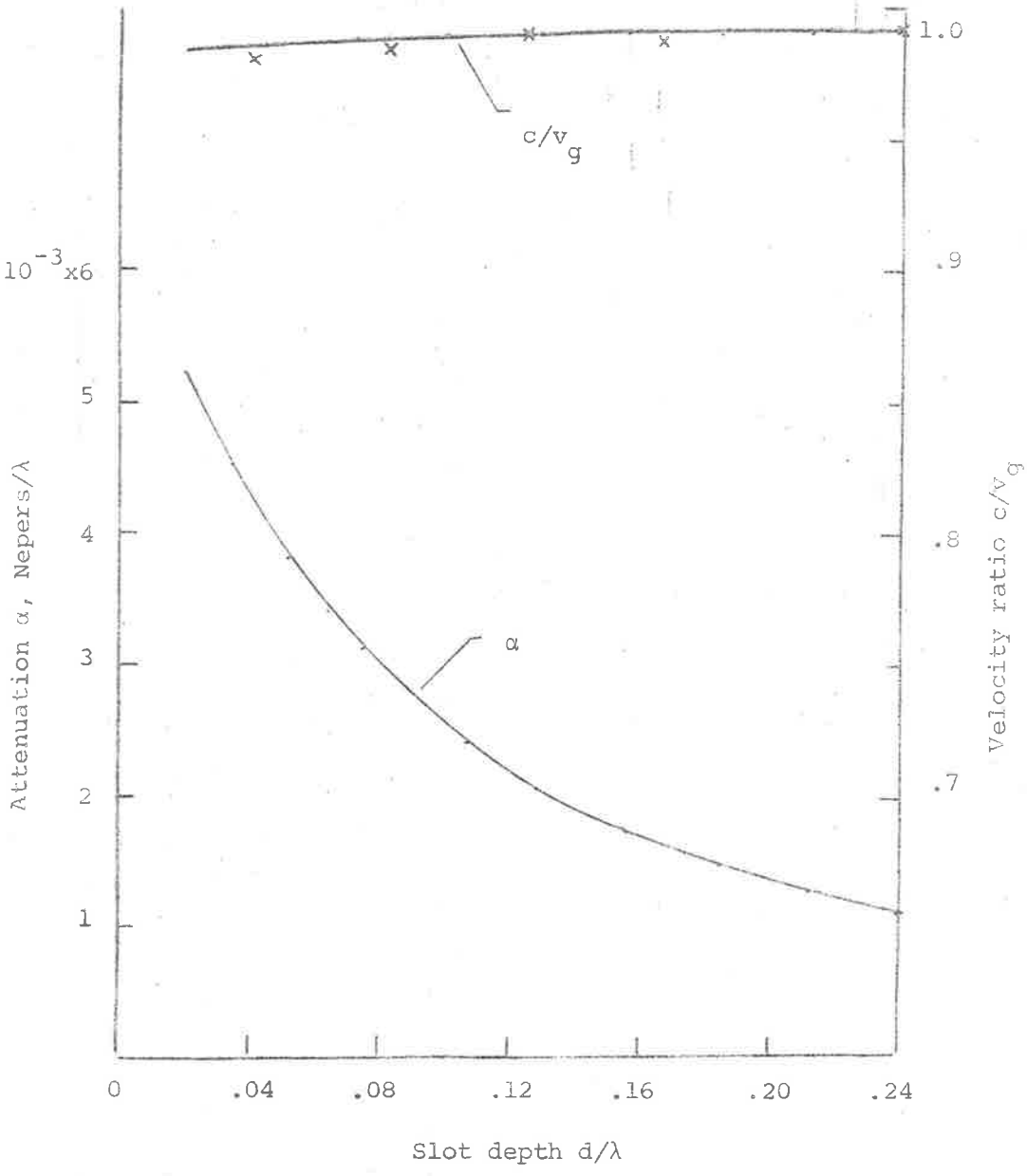

Fig. 8. Variation of c/v_g and attenuation constant against slot depth.

antenna(11λ long) was used as the feed for a parabolic cylinder is given in Fig. 9. The existence of the TE_{01} is clearly shown on the graph. The first maximum at 17° corresponds to the strip line mode and the second maximum at 55° corresponds to the TE_{01} mode. The theoretical angles are expected to be $\simeq 17^{\circ}$ for a line source having $c/v = .985$ and $\simeq 56^{\circ}$ for a line source having $c/v = .56$. The fact that the strip line mode is more dominant than the TE_{01} mode does not contradict the theoretical results shown in Fig. 7. The guide supporting the TE_{01} mode is not matched to the generator.

Even though it was not possible to measure the attenuation constant, its variation with the slot depth suggests that sidelobe suppression and beam shaping can be realised in such a slot antenna. The theory for sidelobe suppression and beam shaping has been given by Dunbar [17]. For sidelobe suppression, the field distribution along the slot must be gaussian and for beam shaping, it must be tapered. Two sets of strip lines were designed to give such distributions and the plots of the near field along the slot are given in Fig. 10(a) and (b). The gaussian distribution was obtained when the slot depth d was shaped approximately proportional to $\exp(-1/2(z/2L)^2)$, where L, the slot length and z, the length from the slot centre, whereas the tapered distribution was produced by a linear depth taper along the slot length. It can be seen in Fig. 19 and Fig. 22 that the amount of sidelobe suppression for the above gaussian distribution is as

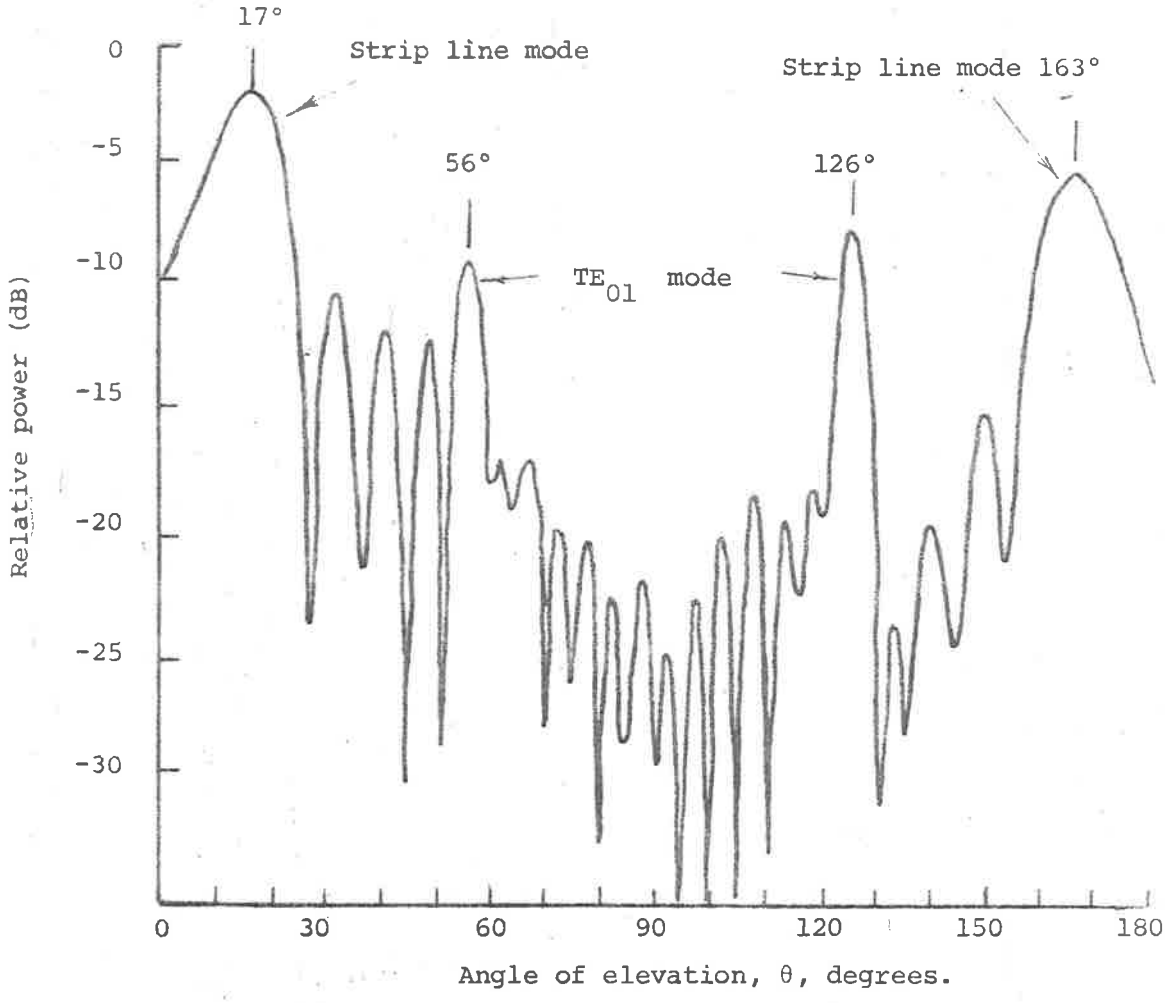

Fig. 9. Elevation radiation pattern at 2 GHz for a uniform slot 11λ long backed by a cavity 4 x 1".
Slot depth = .08λ
Slot width = .01λ

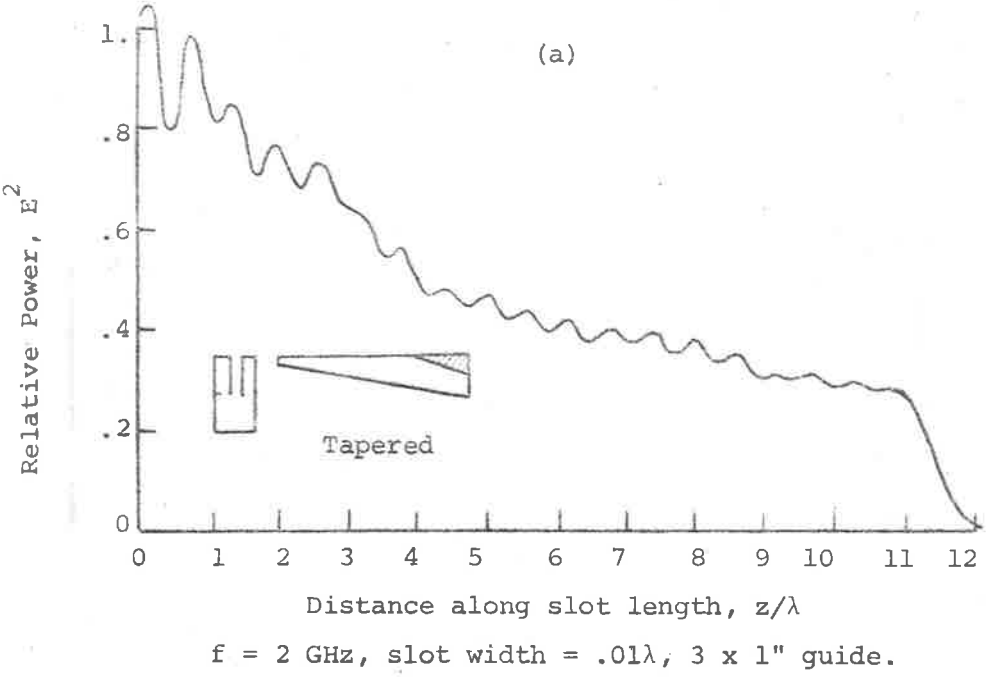

f = 2 GHz, slot width = .01λ, 3 x 1" guide.

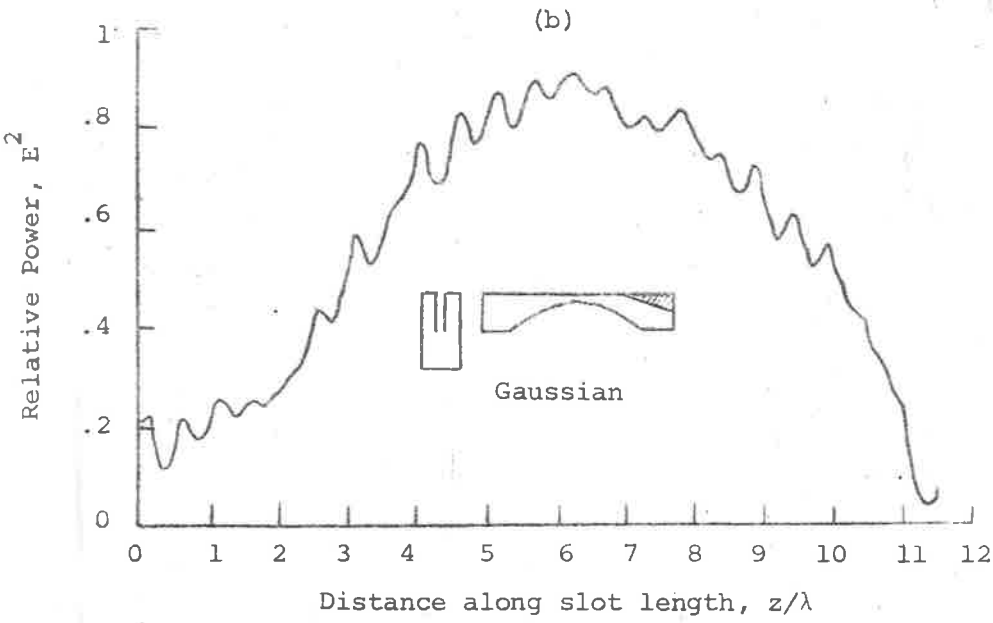

Fig. 10. Tapered and Gaussian field distributions along the slot length.

much as 10 dB compared to the uniform case.

An interesting limiting case is when the strip line thickness extends to the wall of the cavity as shown in Fig. 11. The transverse resonance equation for such a cross section is written as:

$$\frac{-jb}{s}\,\frac{s(B_i-\cot(\kappa a)+b\tan(\kappa d))}{(-b+s(B_i-\cot(\kappa a)\tan(\kappa d))}+$$

$$\frac{\kappa b}{2}+j\frac{\kappa b}{\pi}\ln\frac{\pi e}{\gamma\kappa s}=0 \qquad \ldots(9)$$

where B_i is the internal susceptance given by Marcuvitz [13]. The contribution to the slot susceptance due to the interior region can be ignored when d >> s. When d is comparable to s or smaller (9) becomes [16a]:

$$-j\cot(\kappa a)+\frac{\kappa b}{2}+j\frac{\kappa b}{\pi}\left(\ln\left(\csc\frac{\pi s}{2b}\right)+\ln\frac{\pi e}{\gamma\kappa s}\right)=0 \qquad \ldots(10)$$

The results from (9) are shown in Fig. 12. The velocity ratio and the attenuation constant still have the same characteristic variation as before. When the depth of the cavity becomes large enough, the TE_{01} mode will be excited.

The near field azimuth pattern of the slot antenna is given in

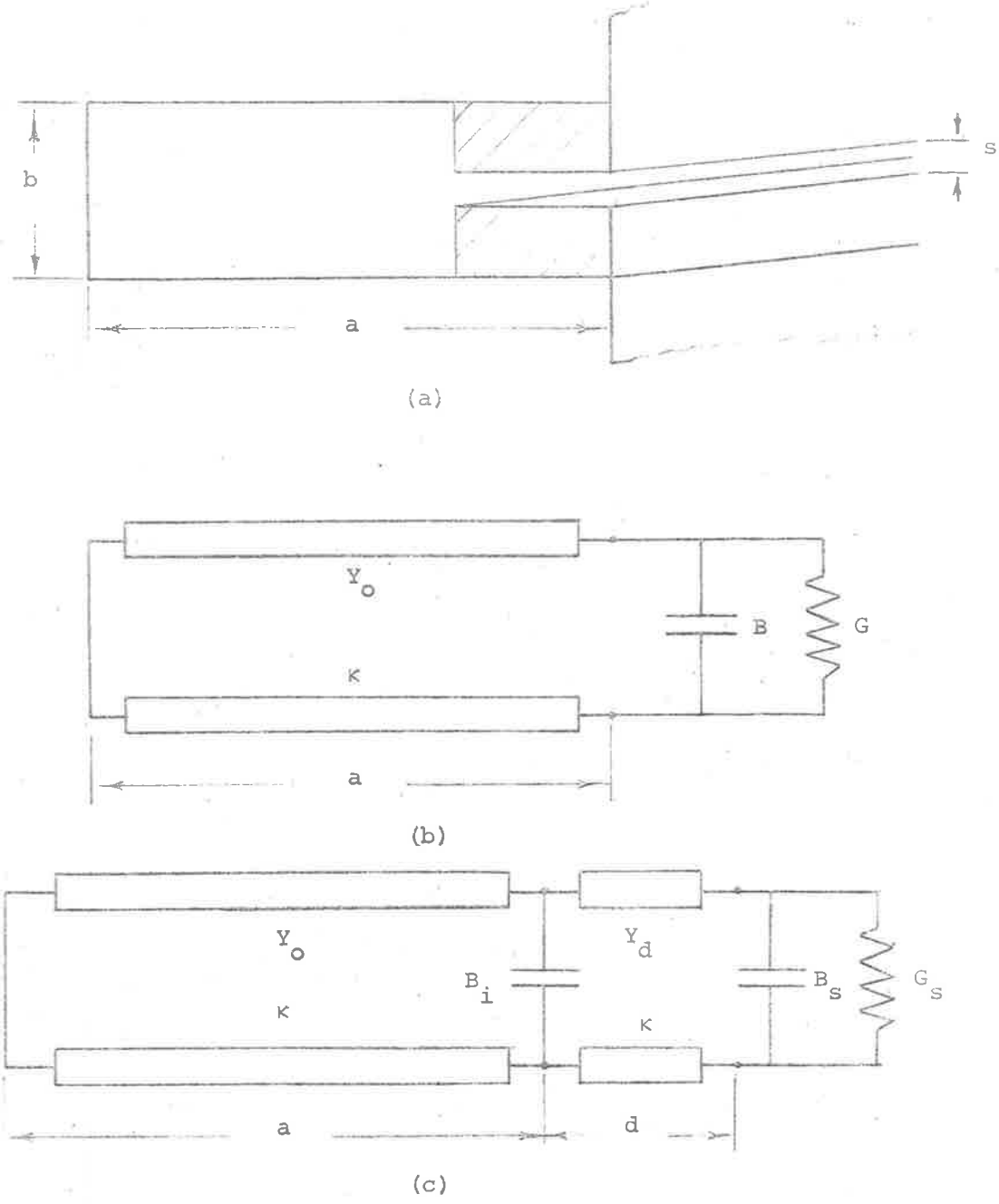

Fig. 11. A limiting case and two transverse equivalent circuits.

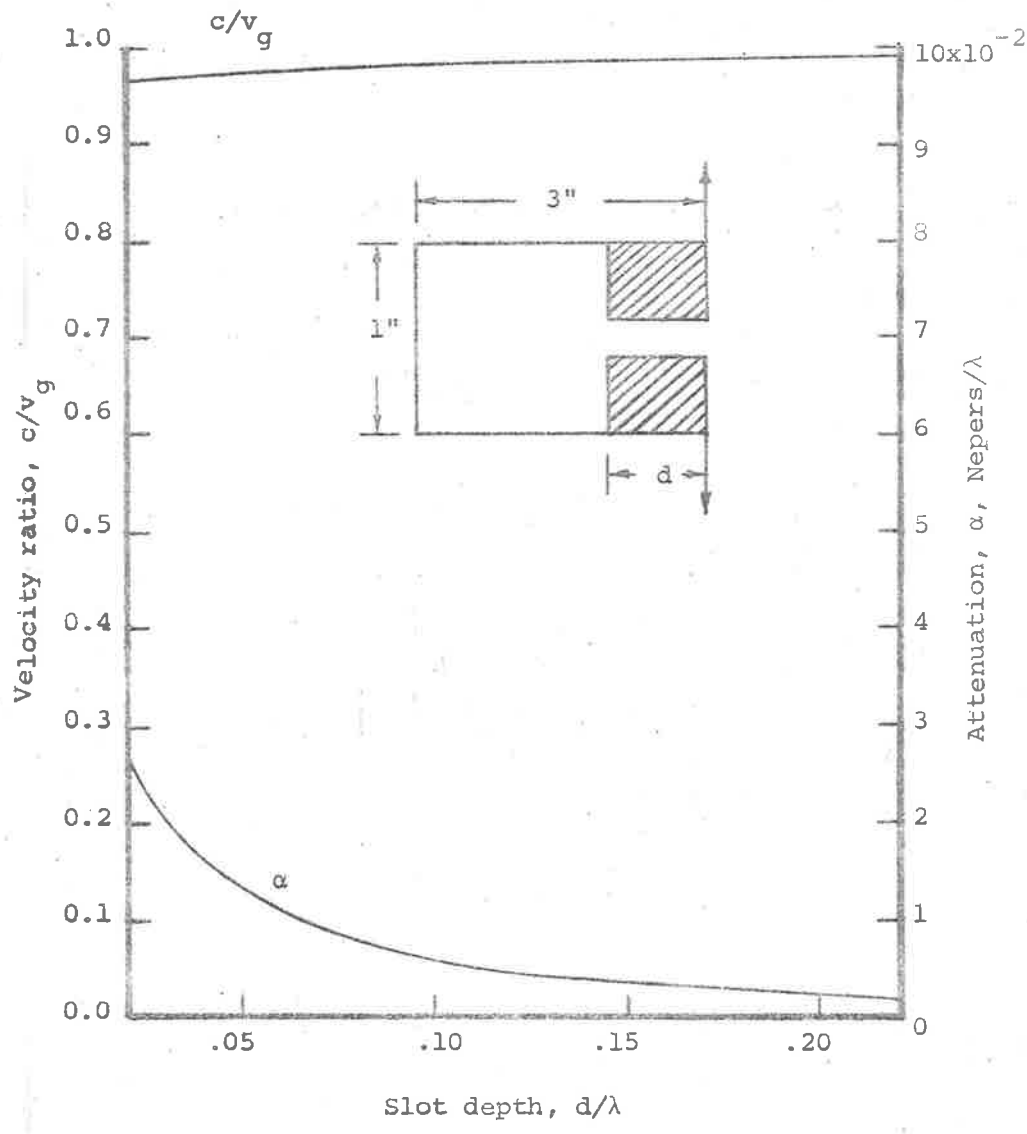

Fig. 12. Variation of velocity ratio and attenuation vs slot depth.

Fig. 13 for the 3 x 1" guide. Since the slot antenna is intended to be used as a feed for a parabolic cylinder, there are at least two ways to avoid the back radiation from affecting the reflected radiation from the aperture adversely:

(i) To select a focal length such that the back radiation and the reflected radiation will add in phase in the desired direction. This will give a narrow bandwidth, or

(ii) To suppress the back radiation.

One way of suppressing the back radiation is to use a pair of small plates on either side of the slot. The plates should not be too large otherwise aperture blocking will become excessive. The azimuth patterns for quite a number of plate arrangements are given in Appendix B. It only needs mention here that some quite interesting patterns have been produced.

It can now be said that the properties of the new slot antenna have been pretty well covered. It could well be justified to say that this slot antenna has as useful a scope of application as its counterpart, the long wire antenna. When a travelling slot is placed at a small distance over a conducting surface, the field from its underside will more or less augment to that of its upperside because of a small phase difference in a similar manner to a long

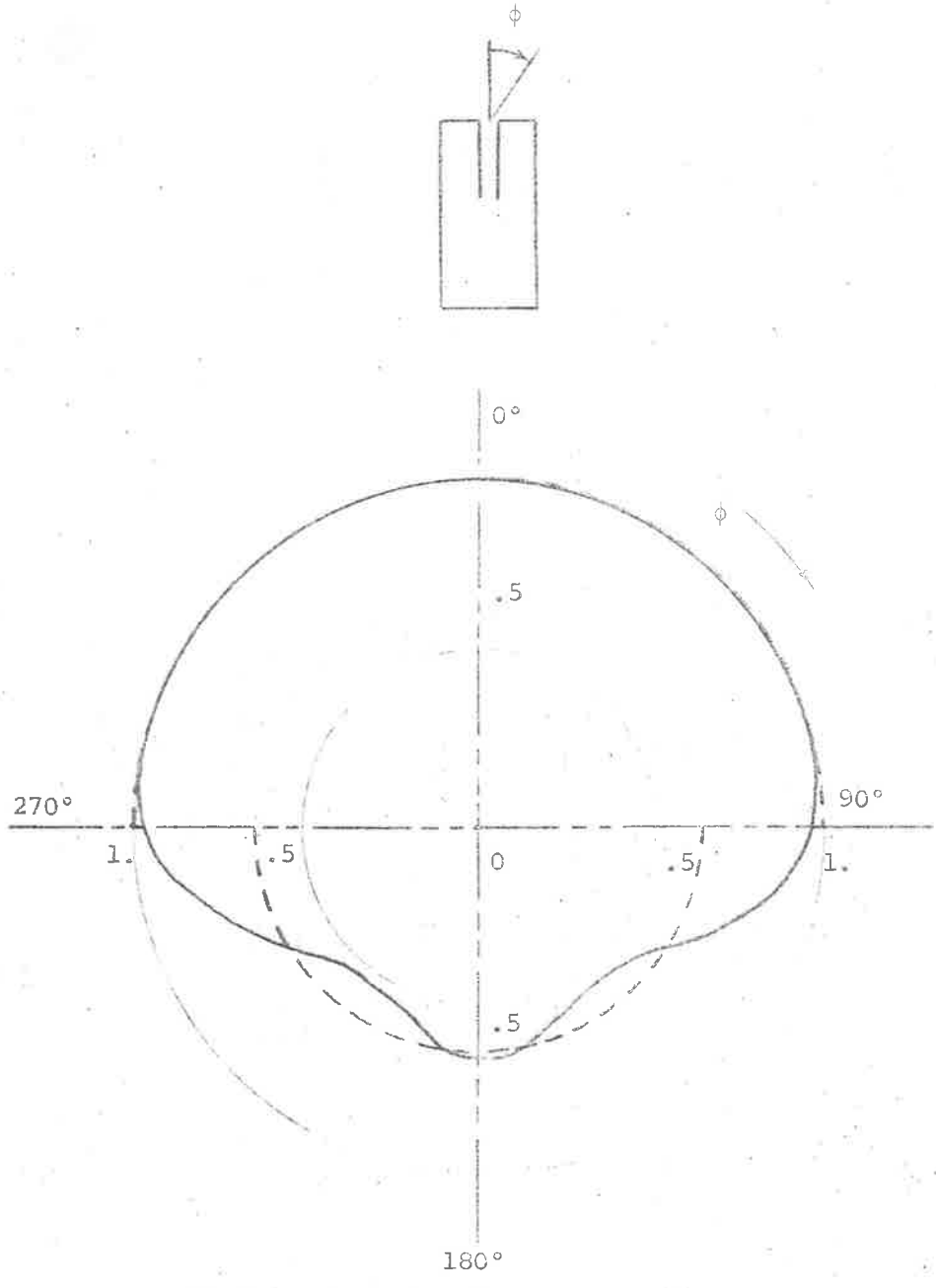

Fig. 13. Electric field around slot.

wire over a magnetic surface or a pure dielectric at grazing incidence.

2. AN APERTURE

The above line source could be used to produce an aperture by placing it along the focal line of a cylindrical parabolic reflector. Such an aperture will be predominantly horizontally polarized, have a higher directivity and lower sidelobe levels. Because of the polarity of the electric field around the slot antenna and the phase reversal after reflection, it can be used much more effectively in conjunction with a reflecting surface at a closer distance than a long wire antenna.

(a) Aperture Field Distribution

The aperture field distribution can be approximated by using ray optics.

It is apparent from treatments of physical optics that a field can be described in terms of rays and wavefronts whenever the phase variation with distance from the source becomes linear. From the cylindrical wave equation, the expression for the potential function of the most general cylindrical wave is given by:

$$\psi_n(\rho,\phi,z) = e^{-jn\phi} H_n^{(2)}(\kappa\rho) e^{-jk_z z} \qquad \ldots(11)$$

and the expression for the electric field is:

$$E\phi = \sum_{-\infty}^{+\infty} A_n \frac{\partial \psi_n(\rho,\phi,z)}{\partial \rho} \qquad \ldots(12)$$

For an azimuth field pattern as shown in Fig. 13, the dominant contribution will be seen later to be the $H_o^{(2)'}(\kappa\rho)$ component. It is interesting to note that the phase variation with distance of $H_o^{(2)'}(\kappa\rho)$ can be assumed to be linear for a distance to the source as close as $.3\lambda$ as seen in Fig. 14. Based on this result it can be said that the field around a typical travelling wave slot line can be described in terms of conical wavefronts whenever the phase variations in both ρ and z directions are linear. For distance very close to the line source the wavefronts become blunted because there is very little phase variation in the transverse direction, Fig. 14(i).

Rays from a travelling wave line source are oblique but beam collimation can still be achieved with oblique incidence by using a parabolic cylinder. The analysis for oblique beam collimation is presented in Appendix E.

To obtain the aperture field distribution by using ray optics, the expression for the electric field around the slot must be known. However it is almost impossible to determine the constants A_n in (12) for a rectangular cross section. Some approximation has to be used.

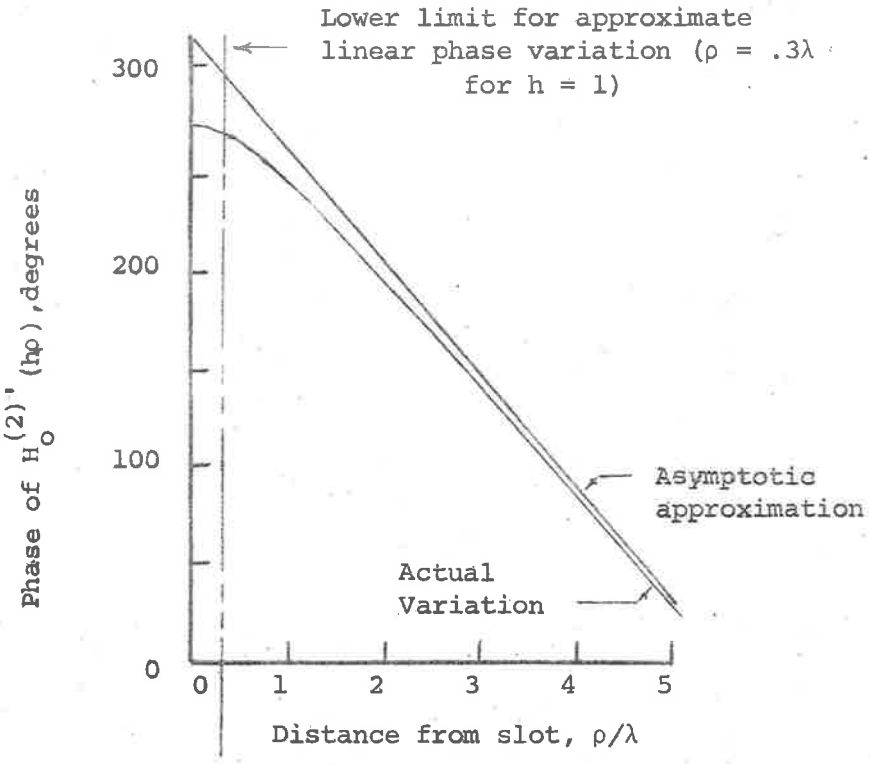

Fig. 14(i). Phase variation with distance from slot.

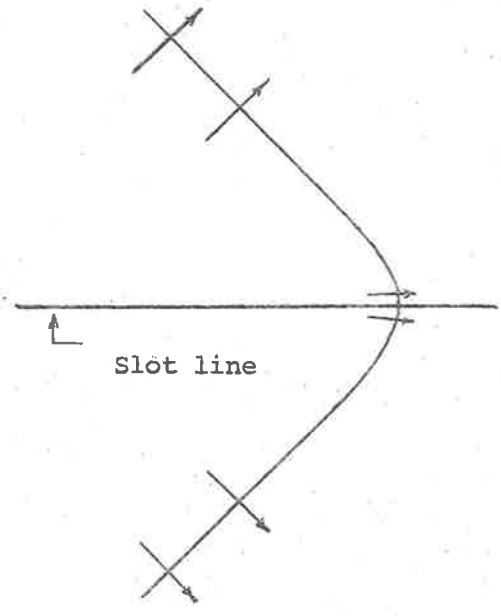

Fig. 14. Blunted conical wavefront around the slot line.

One method of approximation which has proved to be quite useful is to express the measured azimuth electric field pattern as a Fourier series. The leading terms in the Fourier series give a good indication of the dominant terms in the general expression for the electric field given by (12). For instance the Fourier series representation of the azimuth field distribution in Fig. 13 shows that there are only two significant terms and the first term is the most dominant one. Therefore the most dominant contribution to the electric field given by (12) is that due to n = o. The field distribution in Fig. 13 can be approximated by two semi-circles as shown in Fig. 13 and the expression for the electric field in (12) can be reduced to an expression involving only the derivative of the Hankel function of zero order with an appropriate constant of proportionality for the front and back lobe, i.e.

$$E_\phi \propto \frac{\partial}{\partial \rho} H_o^{(2)}(\kappa\rho)\ \exp(-jk_z z) \qquad \ldots(13)$$

It will be seen later that this simple approximation causes very little error.

Using the coordinates indicated in Fig. 15, the emerging rays from the reflector are parallel and the field is assumed to remain constant along the reflected ray. The electric field $E_y(y,z)$ in the aperture plane is given by the value of $E_\phi(\rho,\phi,z)$ at the corresponding point (ρ,ϕ,z), so that the amplitude is:

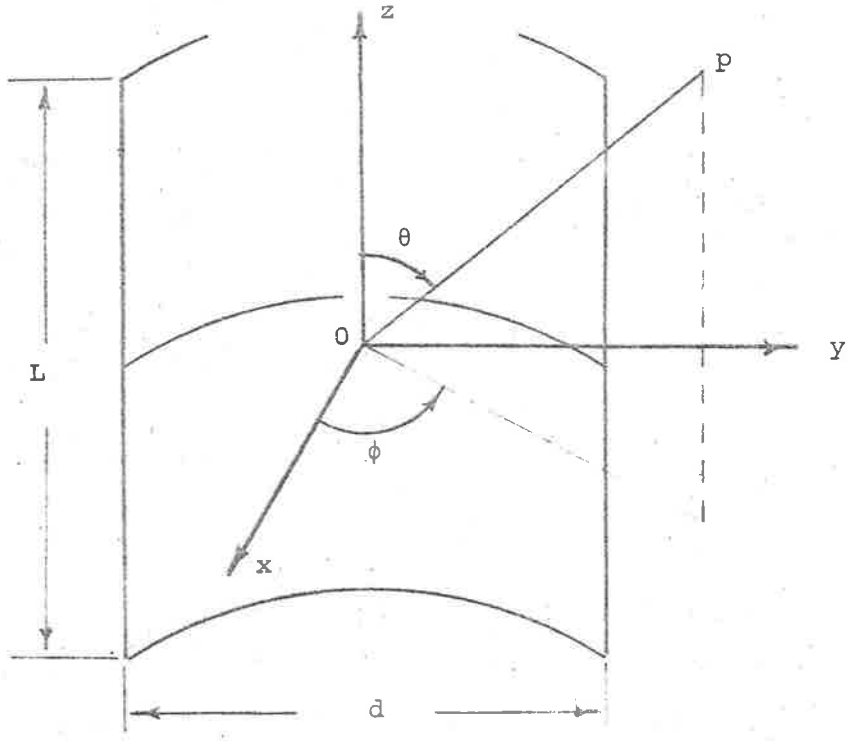

(a) Line source and parabolic cylinder.

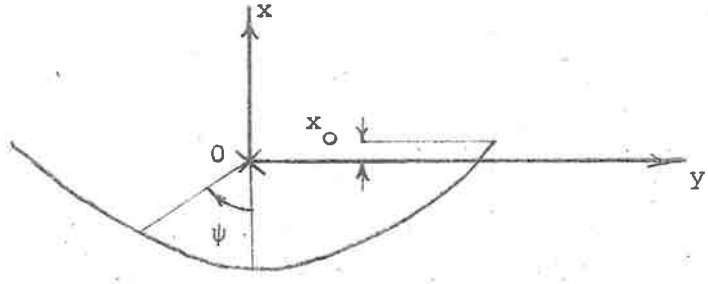

(b) Cross section

Fig. 15. Parabolic cylinder as an aperture.

$$|E_y(y,z)| \propto |f(z) \frac{\partial}{\partial \rho} H_o^{(2)}(\kappa\rho)| \qquad \ldots(14)$$

where $f(z)$ is the field variation along z.

$$\rho = \frac{2f}{1+\cos\psi} = \frac{y^2+4f^2}{4f} \qquad \ldots(15)$$

and the phase is $\exp(-jk\sin\theta\cos\phi(x_o+2f)$ since $\phi = 0$ and $k\sin\theta = h \doteq |\kappa|$ for small attenuation, thus the phase term becomes $\exp(-jh(x_o+2f))$. It should be noted that in the above phase expression, the phase of $H_o^{(2)'}(\kappa\rho)$ has been taken into account.

(b) Aperture Radiation Patterns

The aperture radiation patterns of interest for this type of aperture are the elevation pattern in θ when $\omega = 0$ and the azimuth on elevation pattern in ω when θ_1 is fixed. Such radiation patterns can be obtained from the analysis given in Appendix D for oblique incidence. Let $E(y)$ be the field distribution in y, the general expression for the radiation pattern of the aperture in direction (ω,θ_1) is given by:

$$E^a(\omega,\theta_1) = E_a 2\cos\omega\cos\theta_1 \int\int f(z)\exp(j(k\cos\theta-\kappa z)z)dz.$$

$$\exp(-jh(x_o+2f))E(y)\exp(jky\sin\theta\sin\phi)dy \qquad \ldots(16)$$

If the centre of the aperture is at (x_o, y_o, z_o) instead of $(x_o, 0, 0)$ as being assumed in (16), an extra phase term has to be included i.e. $\exp(jk(y_o \sin\theta \sin\phi + z_o \cos\theta))$. The term $\frac{j}{2\lambda r} \exp(jkr)$ has been suppressed from (16). For a rectangular aperture as seen in Fig. 16, equation (16) becomes:

$$E^a(\omega,\theta_1) = E_a 2\cos\omega\cos\theta_1 \int_{-L/2}^{L/2} f(z)\exp(j(k\cos\theta - \kappa z)z)dz \cdot$$

$$\exp(-jh(x_o+2f)) \int_{-d/2}^{d/2} E(y)\exp(jky\sin\theta\sin\phi)dy \quad \ldots(17)$$

where $f(z)$ can be uniform, tapered, binominal or gaussian. For the 3 x 1" guide with uniform field distribution along the slot, i.e. $f(z) = 1$, $E(y)$ given by (14) is plotted in Fig. 17. The distribution implies a certain amount of sidelobe suppression. In (16) and (17), $E(\omega,\theta_1)$ is expressed in two coordinate systems i.e. (r,ω,θ_1) and (r,ϕ,θ) for clarity and convenience and in actual computation only the (r,ω,θ_1) system is used. The relationship between (r,ϕ,θ) and (r,ω,θ_1) is given by:

$$\cos\theta = \cos\theta_1 \cos\omega \quad \ldots(18a)$$

$$\cos\phi = \frac{\sin\theta_1}{\sqrt{(1-\cos^2\theta)}} \quad \ldots(18b)$$

When $\omega = o$, $E^a(0,\theta_1)$ gives the elevation pattern in θ_1 and when $\theta_1 =$

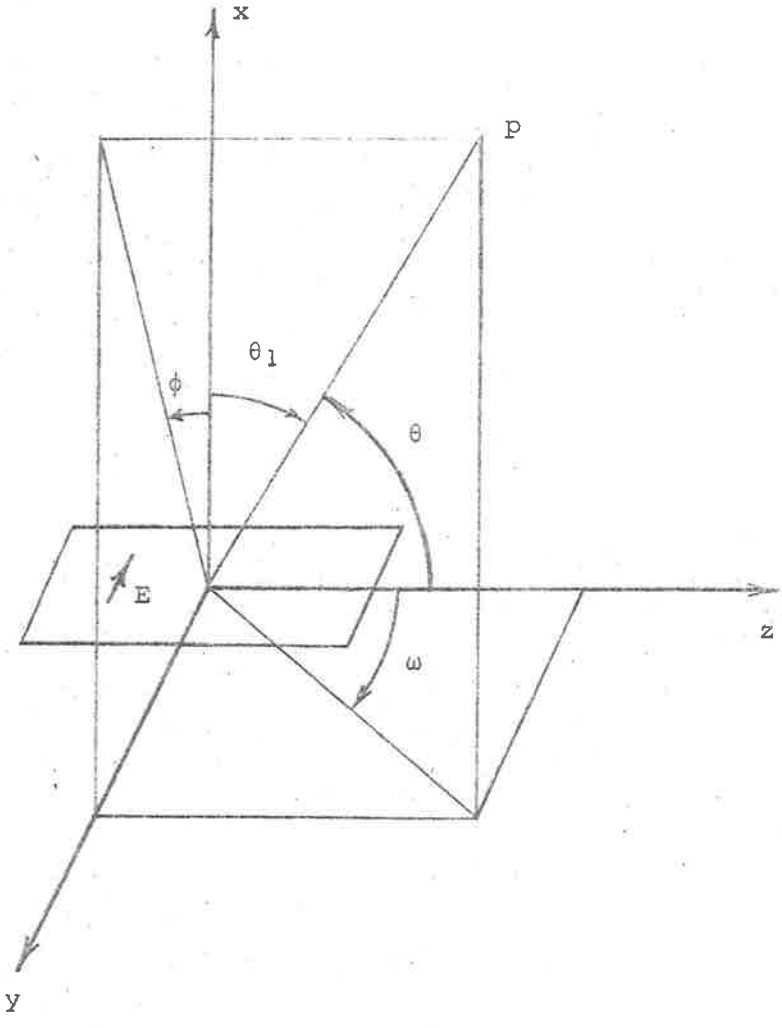

Fig. 16. Spherical coordinates used to evaluate aperture radiation patterns.

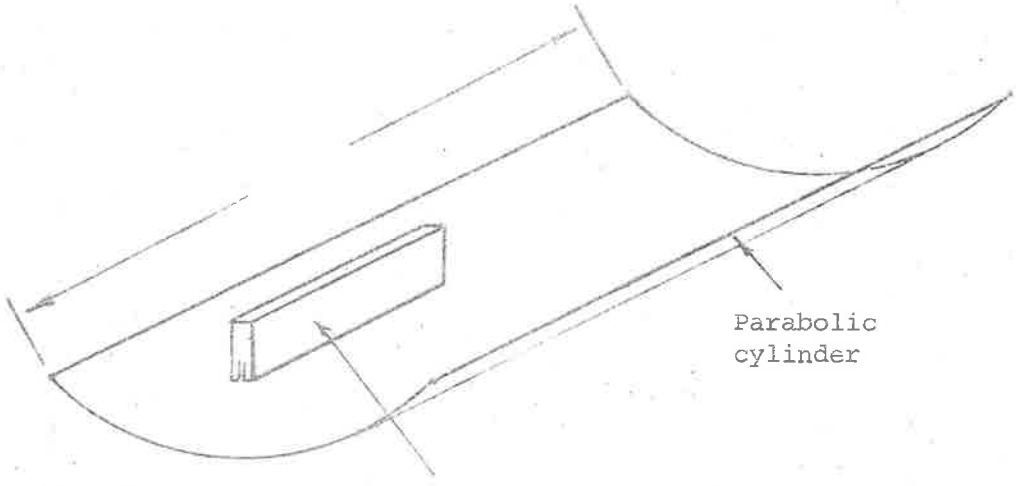

(a)

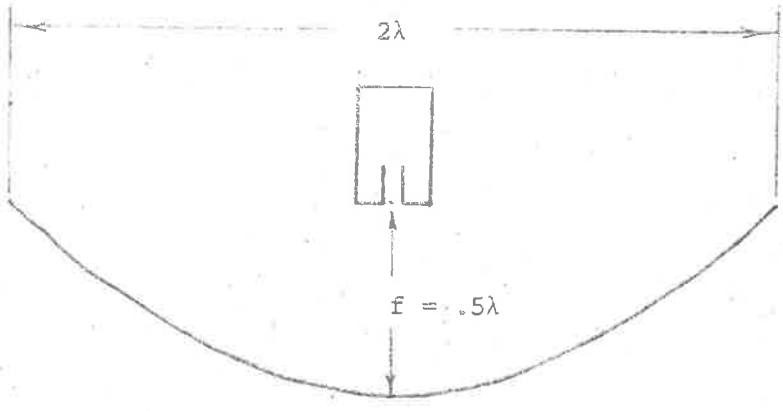

(b) Cross section

Fig. 23. Parabolic cylindrical reflector and travelling wave slot line.

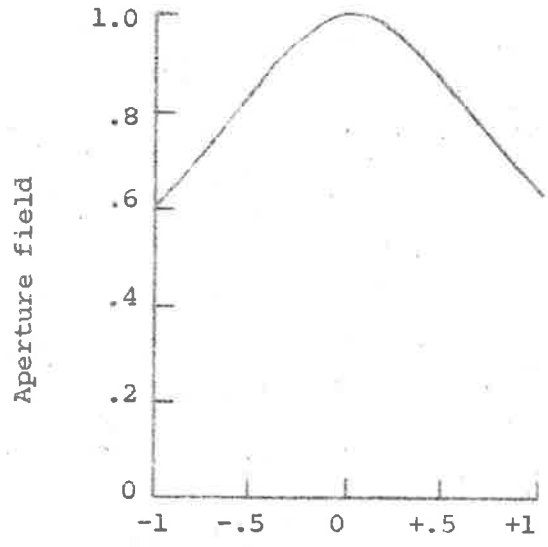

Fig. 17. Field distribution across the aperture for a uniform line source having $c/v_g = .985$.

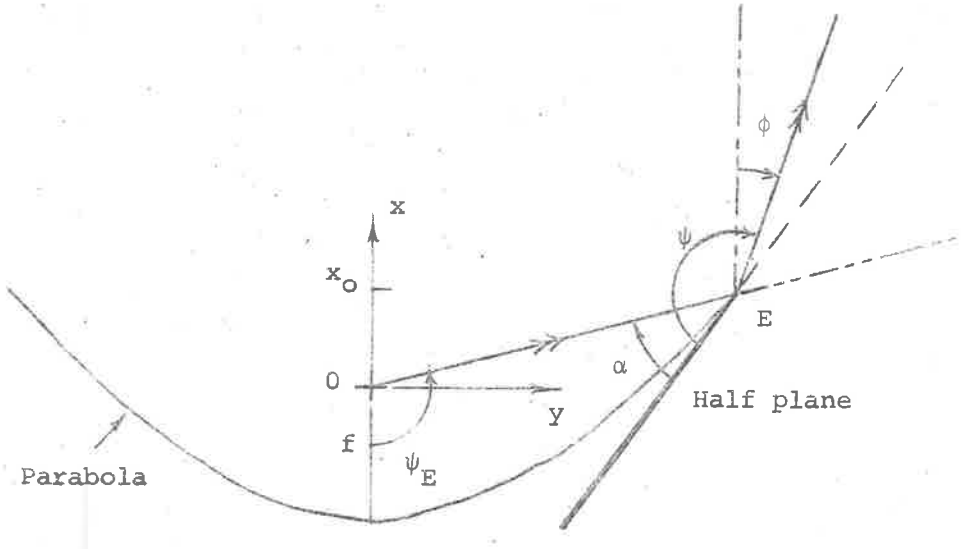

Fig. 18. Edge diffraction for parabolic cylinder.

a constant, α $E^a(\omega,\alpha)$ gives the azimuth on elevation pattern with the elevation angle $90^o - \alpha$.

In practice, the back radiation and aperture blocking have to be taken into account. The back radiation is given by

$$E^b(\omega,\theta_1) = E_b \cos\omega\cos\theta_1 \int_{-L/2}^{L/2} f(z)\exp(j(k\cos\theta-\kappa z)z)dz \qquad ...(18)$$

Due to a 180^o phase change in the azimuth pattern, (18) has the same sign as (17). The aperture blocking is given by:

$$E^{ab}(\omega,\theta_1) = -E_a \cos\omega\cos\theta_1 \int_{-L/2}^{L/2}(...)dz \int_{-\delta/2}^{\delta/2}(...)dy \qquad ...(19)$$

where the terms in the brackets (...) are the same as in (17) and δ is the effective blocking width taken to be 50% more than the actual width as suggested by Cumming et al. [31].

The diffraction off the edge of the parabolic cylinder also plays a dominant role in affecting the sidelobe levels. The first order diffracted field contribution can be obtained by using the analysis presented in Chapter two assuming that the edge is replaced by a tangential half plane. This is a three dimensional case with oblique incidence. For the right hand side edge:

$$E^d(\omega,\theta_1) = [v_B(r,\psi_E+\phi) + v_B(r,\psi_E+2\alpha+\phi)]\ F(\psi_E)\cdot$$

(cont'd next page)

$$\int_{z_1}^{z_2}(....)dz\,\exp(jk(y_o\sin\theta\sin\phi+x_o\sin\theta\cos\phi)) \qquad ...(20)$$

where (...) is as in (18) and $z_1 = z_o - L/2$, $z_1 = z_o + L/2$ and z_o is the z shift due to oblique incidence. $v_B(r,\phi)$ is given in Chapter two, equation (20). The expression for the left hand side edge is obtained from (20) by using $\psi_E - \alpha - \phi$ and $\psi_E + \alpha - \phi$ instea of the existing angles and $F(-\psi_E)$ instead of $F(\psi_E)$.

The final radiation pattern is the sum of all the above expressions.

The above expressions for the radiation pattern have been tested by using a slot antenna 11λ long, having a cross section 3 x 1" for the backing cavity. The slot width is .01λ and slot depth is .083λ. Such a slot antenna has a measured velocity ratio equal to .985 and since the attenuation is very small it can be taken to be zero, h is $k(1-(.985)^2)^{1/2}$ where $k = 2\pi/\lambda$. The parabolic cylinder has a focal length .5λ and a length 18λ. The frequency used is 2 GHz. The elevation and azimuth on elevation patter of the antenna system are shown on Fig. 19(a) and Fig. 20 together with the theoretical results. It can be seen that the agreement between theory and experiment is very good in the vicinity of the main beam. The disagreement in the sidelobe levels in the elevation and azimuth on elevation patterns is due to phase errors and

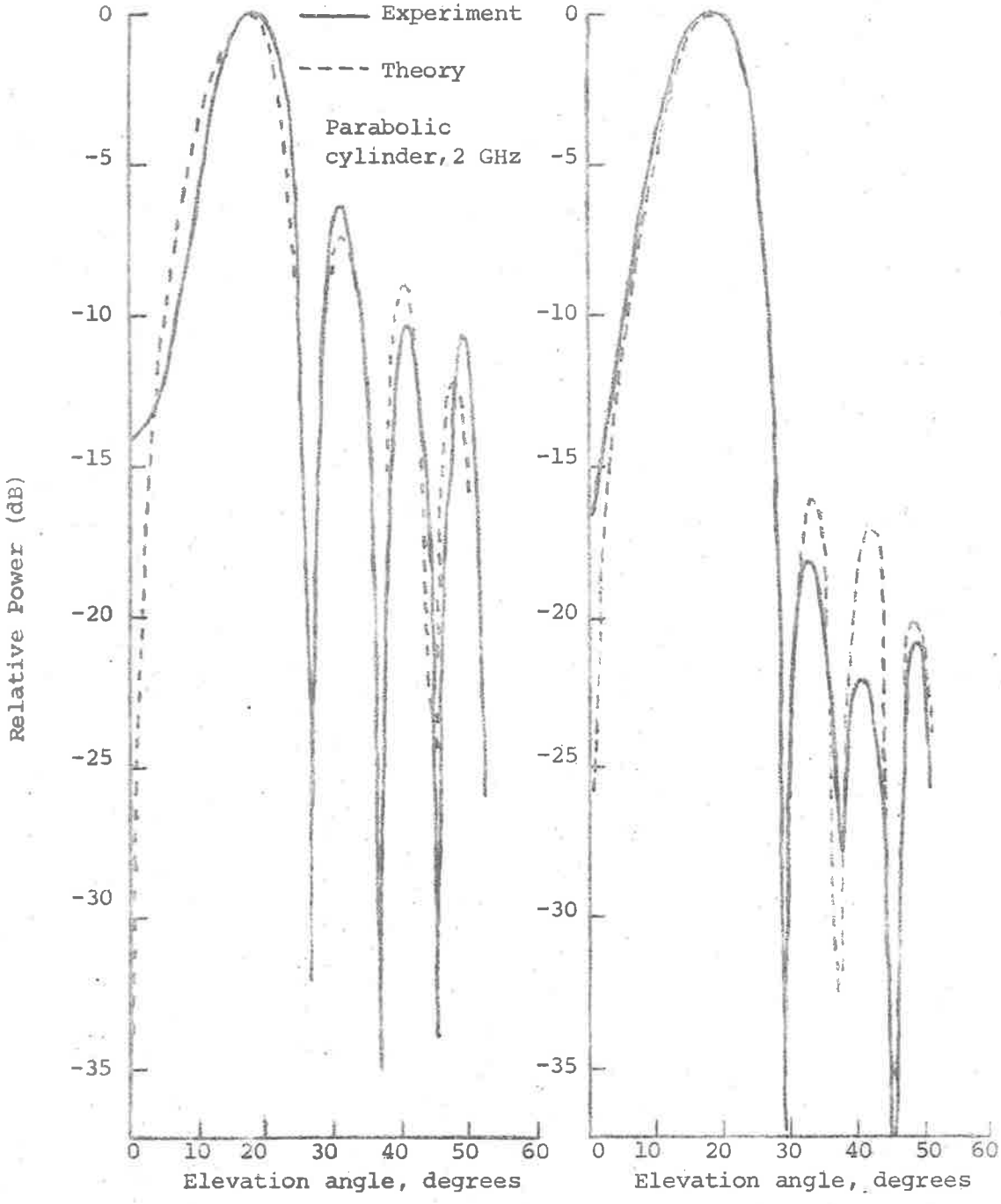

Fig. 19(a). Uniform line feed. Fig. 19(b). Gaussian line feed.

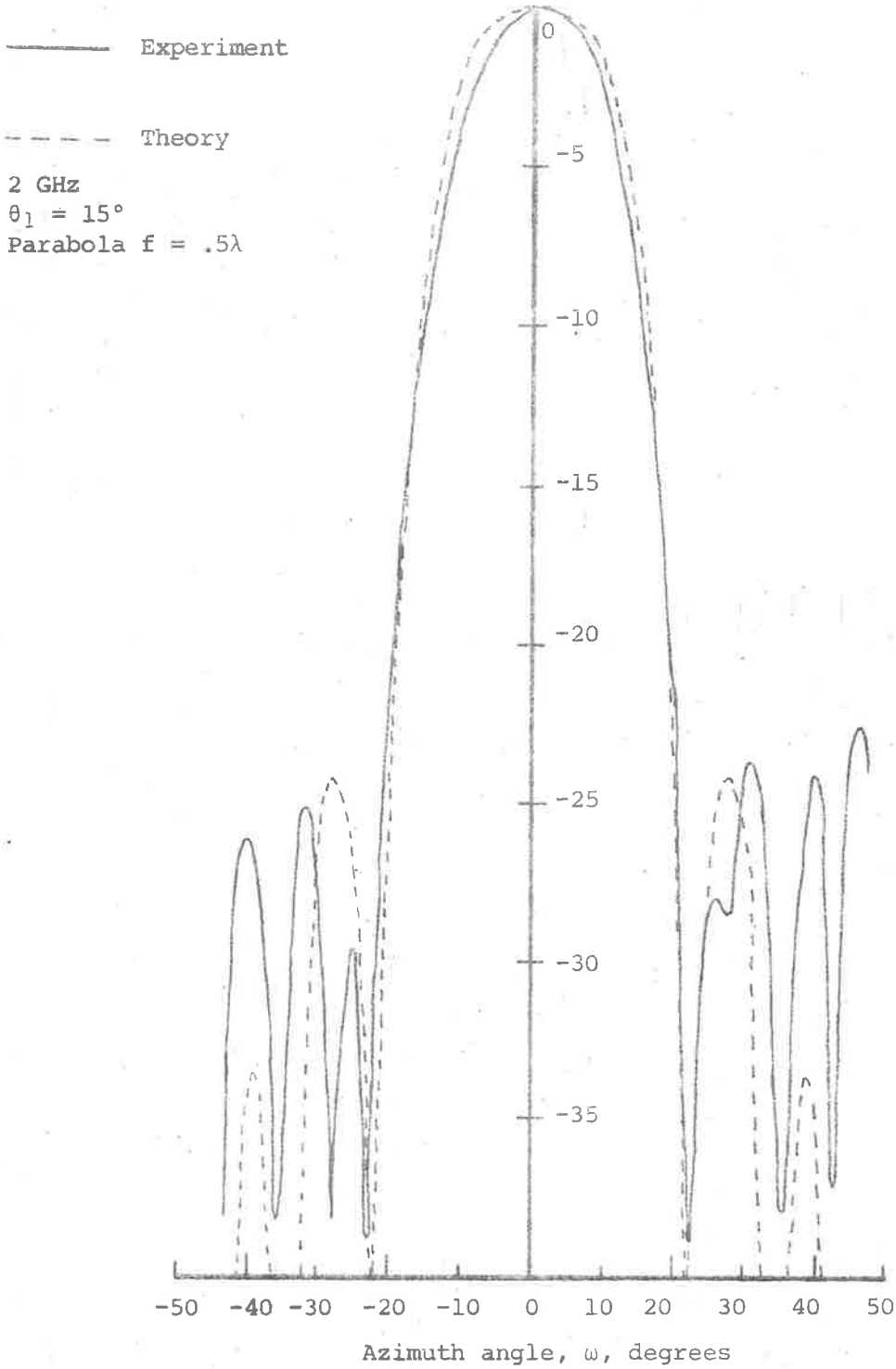

Fig. 20. Azimuth on 15° elevation radiation pattern.

the nature of the approximation given in Fig. 13.

With the line source having a gaussian distribution of Fig. 10(a), the elevation pattern is shown in Fig. 19(b). The experimental results are given in continuous line and the theoretical results are given in dotted line. The agreement is quite good and the sidelobe suppression is as much as 10 dB when compared to the uniform line.

Fig. 20 is the azimuth on elevation radiation pattern for an angle of elevation equal to 15°. The results for the angles of elevation equal to 5° and 2.5° are shown on Fig. 21. Here again the agreement is quite good. The diffraction off the end and the corners of the reflector tends to bring the sidelobe levels up.

The parabolic cylinder can be replaced by a corner cylinder having an angle of 120° without serious deterioration in both the elevation and azimuth on elevation patterns. The beam widths in both patterns are a bit narrower. The measured directivity for the corner reflector is 11.7 dB over a dipole at 2 GHz and that for the parabolic reflector is 12.4 dB. The elevation pattern for the corner reflector is given in Fig. 22. A corner reflector has an advantage over a parabolic cylinder in that it is much easier to construct.

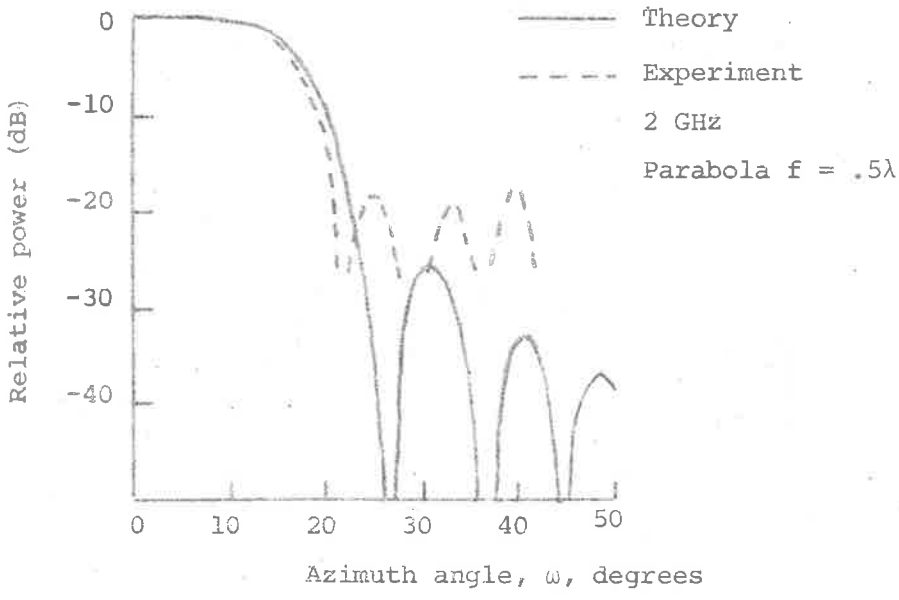

Fig. 21(a). Azimuth on 2.5° elevation radiation pattern (uniform line feed).

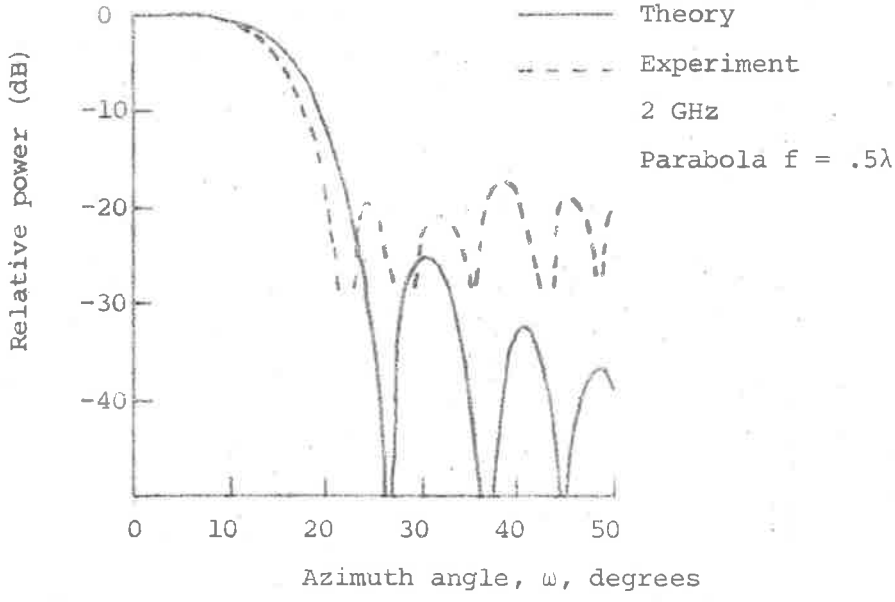

Fig. 21(b). Azimuth on 5° elevation radiation pattern (uniform line feed).

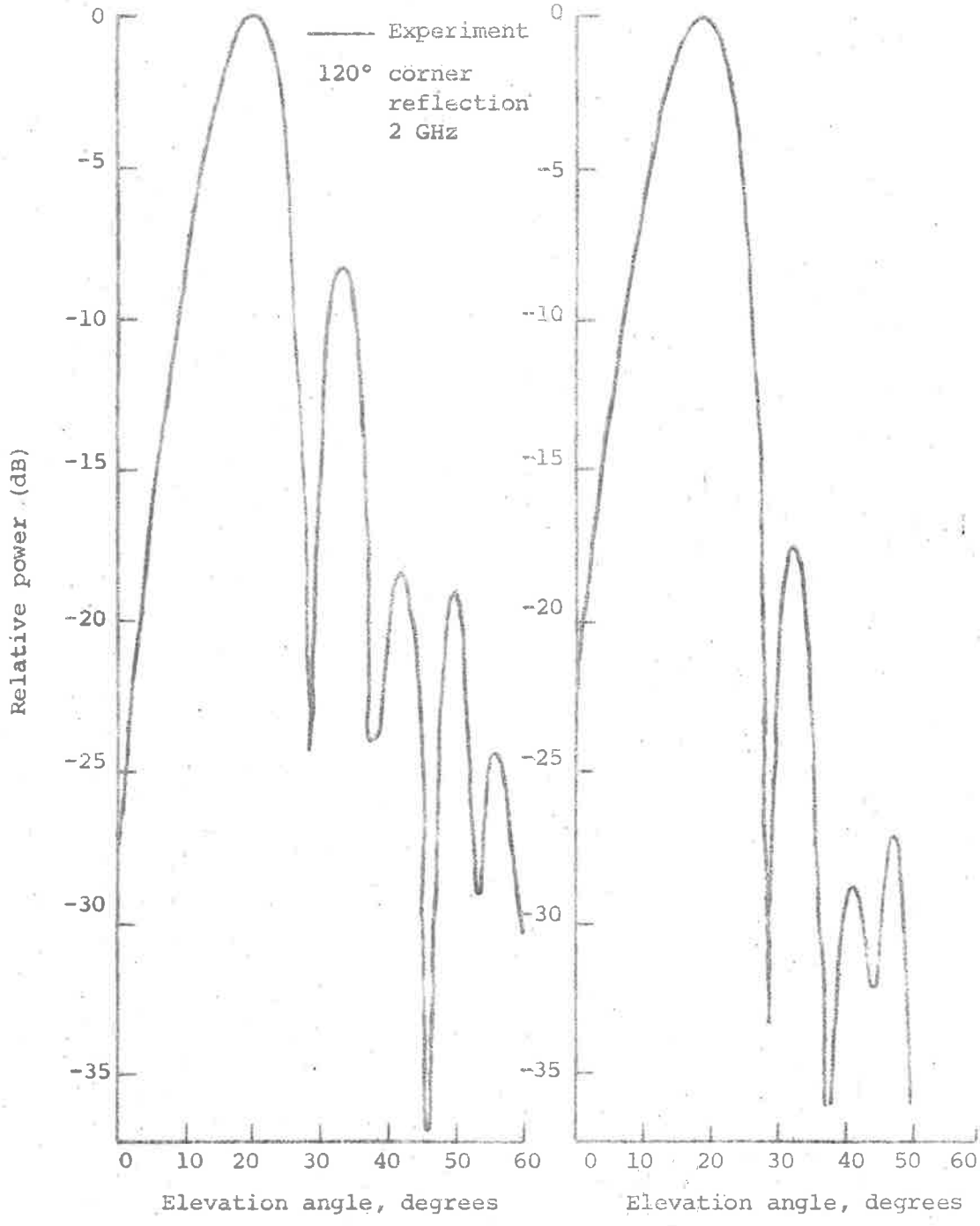

Fig. 22(a). Uniform line feed. Fig. 22(b). Gaussian line feed.

The method of measuring the radiation patterns has been omitted here and will be discussed fully in Chapter four.

The finite length of the parabolic cylinder could be taken into account by solving for the diffraction by a parabolic edge and two plane corners due to the postulated existence of a point source at the end of the line source. A brief discussion on the correction for the finite length partition has already been given in Chapter two. Such an analysis is beyond the scope of this thesis.

In conclusion, it must be said that the above interesting new travelling wave slot antenna can be used as a ground based antenna at close distance to the ground by virtue of the opposite polarity of the electric field on the upper side and lower side of the slot. It can be used in conjunction with a corner reflector or a parabolic reflector to produce azimuth on elevation patterns with very low sidelobe levels. Sidelobe suppression in the elevation pattern together with its capability of beam shaping make the antenna quite versatile and attractive in aircraft navigational systems.

In the following chapter, the antenna will be used as a line source and as a feed for a parabolic cylinder to produce an aperture. A line source and an aperture together with a slot dipole will put the solution for the diffraction off the edge of a partition presented in Chapter two to a good test.

CHAPTER FOUR

EXPERIMENTAL VERIFICATION

The experimental verification of the solution for the diffraction off the edge of a partition is presented in this chapter. Three models have been built for the frequency of 2 GHz.

(i) Two slot dipoles in a finite ground plane.

The equatorial plane radiation pattern of this model is the same as the radiation pattern of two infinite lines having a propagation normal to the partition.

(ii) Two travelling wave slot lines on a large ground plane.

The radiation patterns in azimuth on elevation of such a model are those of two line sources having finite length and a propagation with an oblique incidence to the partition. Since the lines are finite in length, this is a three dimensional case.

(iii) Two travelling wave apertures.

Two parabolic cylinders having each a travelling wave line source feed along its focal line have been used to simulate two apertures. This model does not represent the two ideal apertures in its proper sense in that the direct radiation from the feeds and edge diffraction from the parabolic reflectors are not zero. However

these effects can be easily taken into account. If only the apertur field distribution of the parabolic cylinders is considered, its radiation patterns in azimuth on elevation are those of two aperture having a finite length and a propagation with an oblique incidence to the partition. This is another practical three dimensional case.

The expressions for the radiation patterns of the above three models have been derived and presented in Chapter Two. The theoreti cal results for the three models will be compared with the experimen al ones. Reasonably good agreement has been obtained in all cases.

1. BRIEF DESCRIPTION OF EXPERIMENTAL MODELS

(a) Two Slot Dipoles:

The first model consisted of two parallel slots cut in a groun plate and backed by a rectangular cavity as seen in Fig. 1. Each slot was 0.4λ long, .005λ wide. The two slots were separated by a distance λ/2. The ground plate was 6λ x 3λ. The backing cavity was a guide section 2λ deep and had a cross section .67λ x .17λ. This cross section supported the TE_{01} mode at 2 GHz which in turn excited the slot. The ground plate was bolted onto the backing cavities by a number of screws less than .05λ apart to ensure good electrical contact. Two partitions were used:

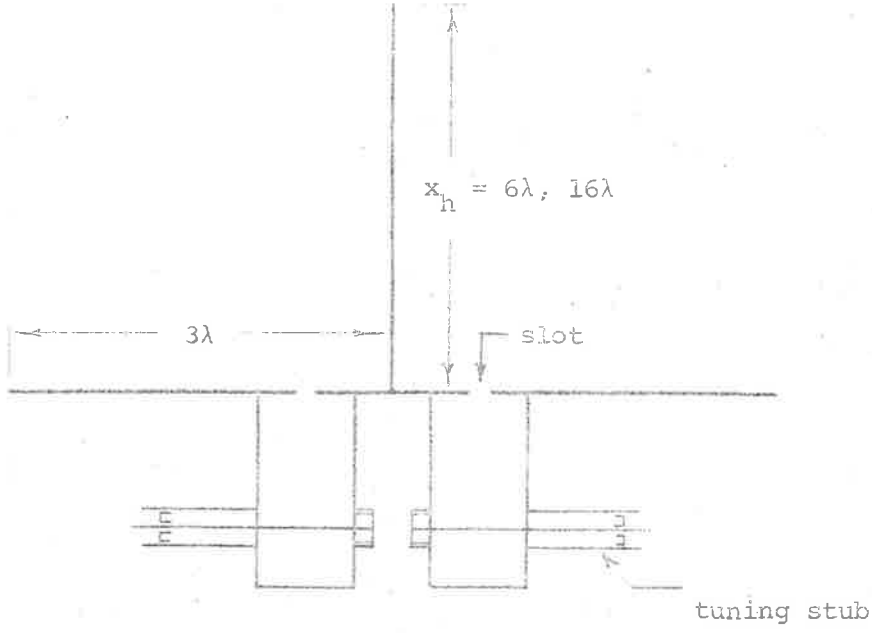

(a)

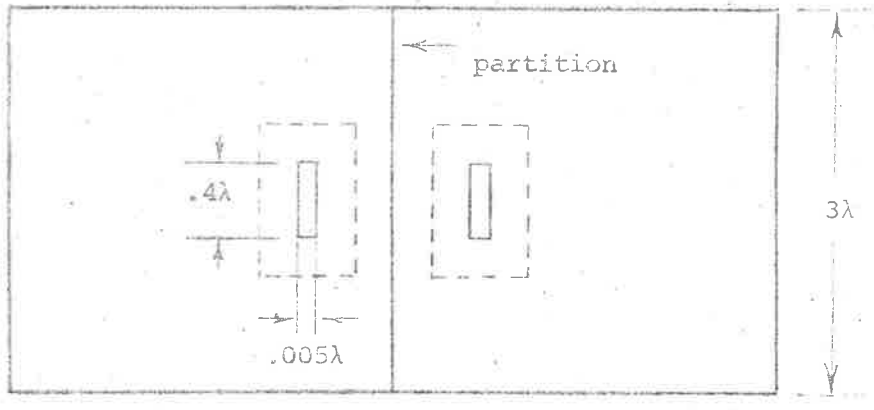

(b)

Fig. 1 Two slot dipoles

(a) 3λ wide and 6λ high

(b) 3λ wide and 16λ high

(b) Two Line Sources:

The second model consisted of two travelling wave slot lines which have been discussed in Chapter Three. The slot was .01λ wide, .083λ deep and 12λ long. When the effective length of the tapered termination was taken into account, the effective slot length was only 11λ. Each slot line was excited at about λg/4 from a short circuited end by a coaxial slit balun inserted through the backing guide as seen in Fig. 2(a). Silver plating was used to enable soldering which would improve the electrical contact. The strip line forming the slot was bolted to the backing guide by a number of screws less than λ/4 apart. The slot lines were mounted parallel to each other at a distance λ/2 apart on a rectangular ground plate 18λ x 16λ (i.e. 9' x 6' at 2 GHz). The ground plate was reinforced by a sheet of 7 ply marine wood to ensure flatness. A partition 18λ long and 3λ high was used.

(c) Two Apertures:

The third model consisted of two parabolic cylinders each having a line source described above as its feed. Each parabolic cylinder had a focal length 0.5λ, a width of 2λ and a length of 18λ. Due to the field distribution around the slot, each was mounted upside down

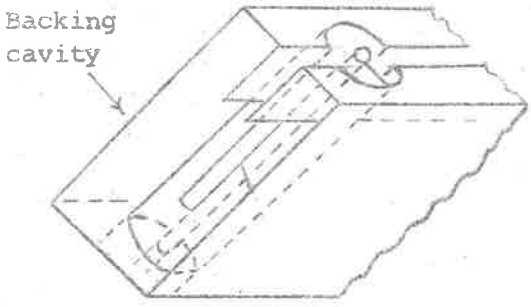

Slit balun

(a) Balun feed

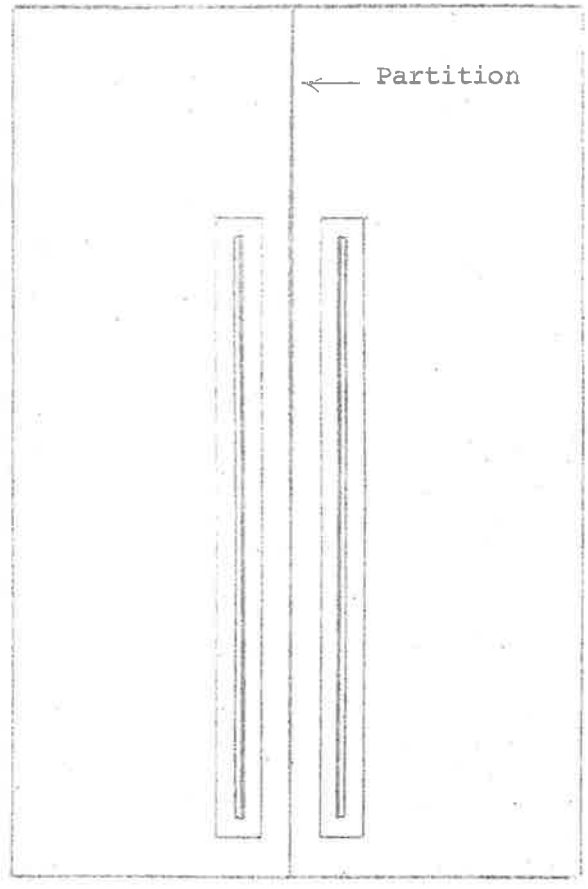

(b)

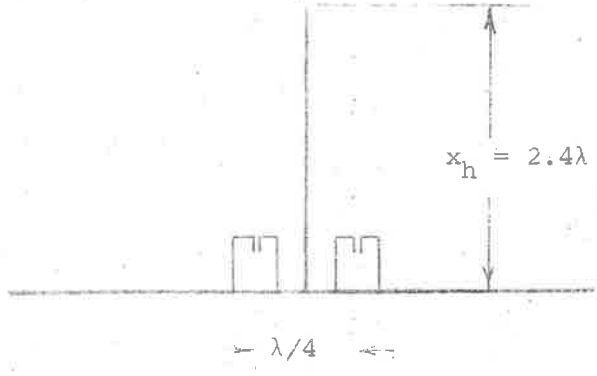

(c)

Line sources above ground plane

Fig. 2

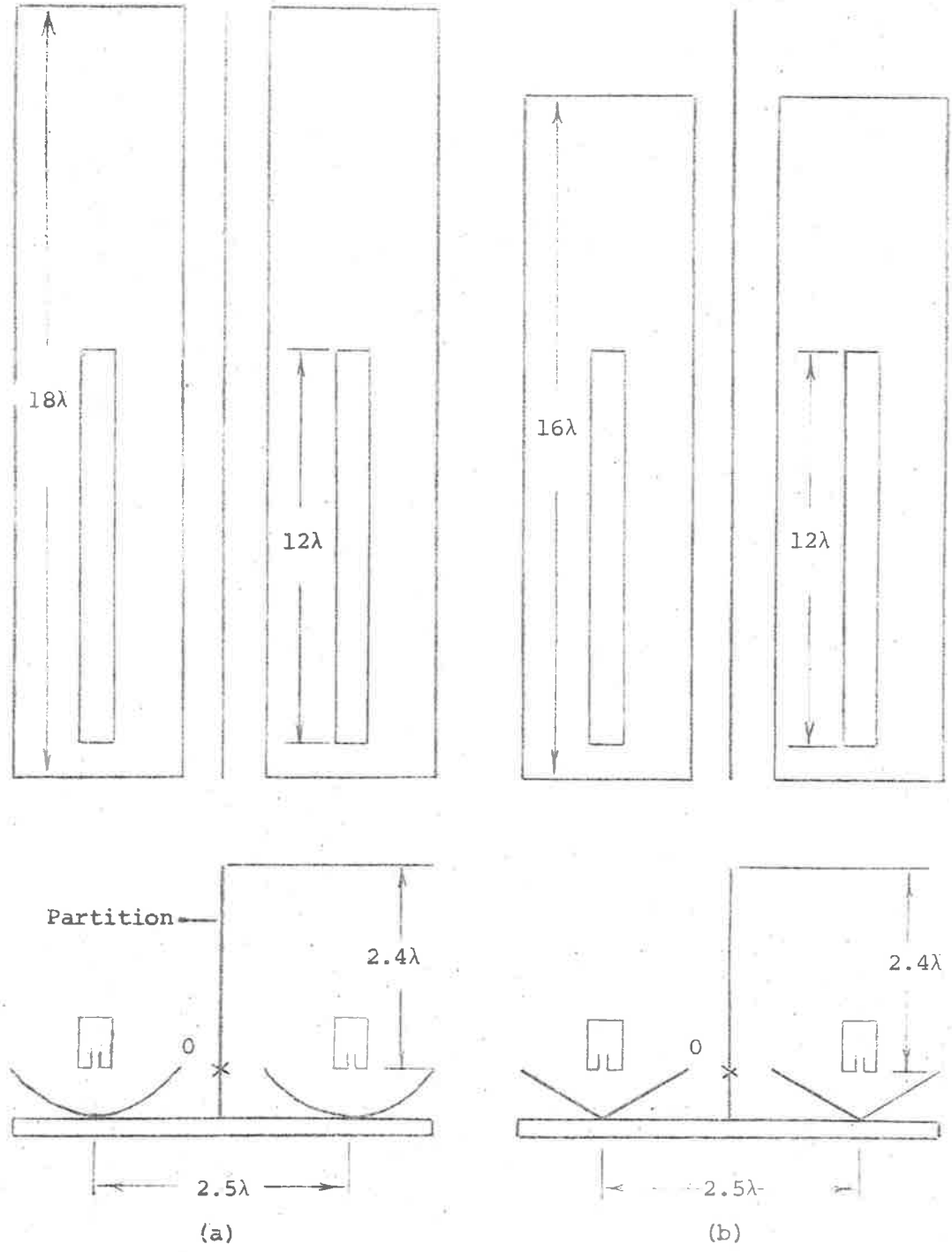

Fig. 3. Parabolic cylinders and approximate 120° corner reflectors.

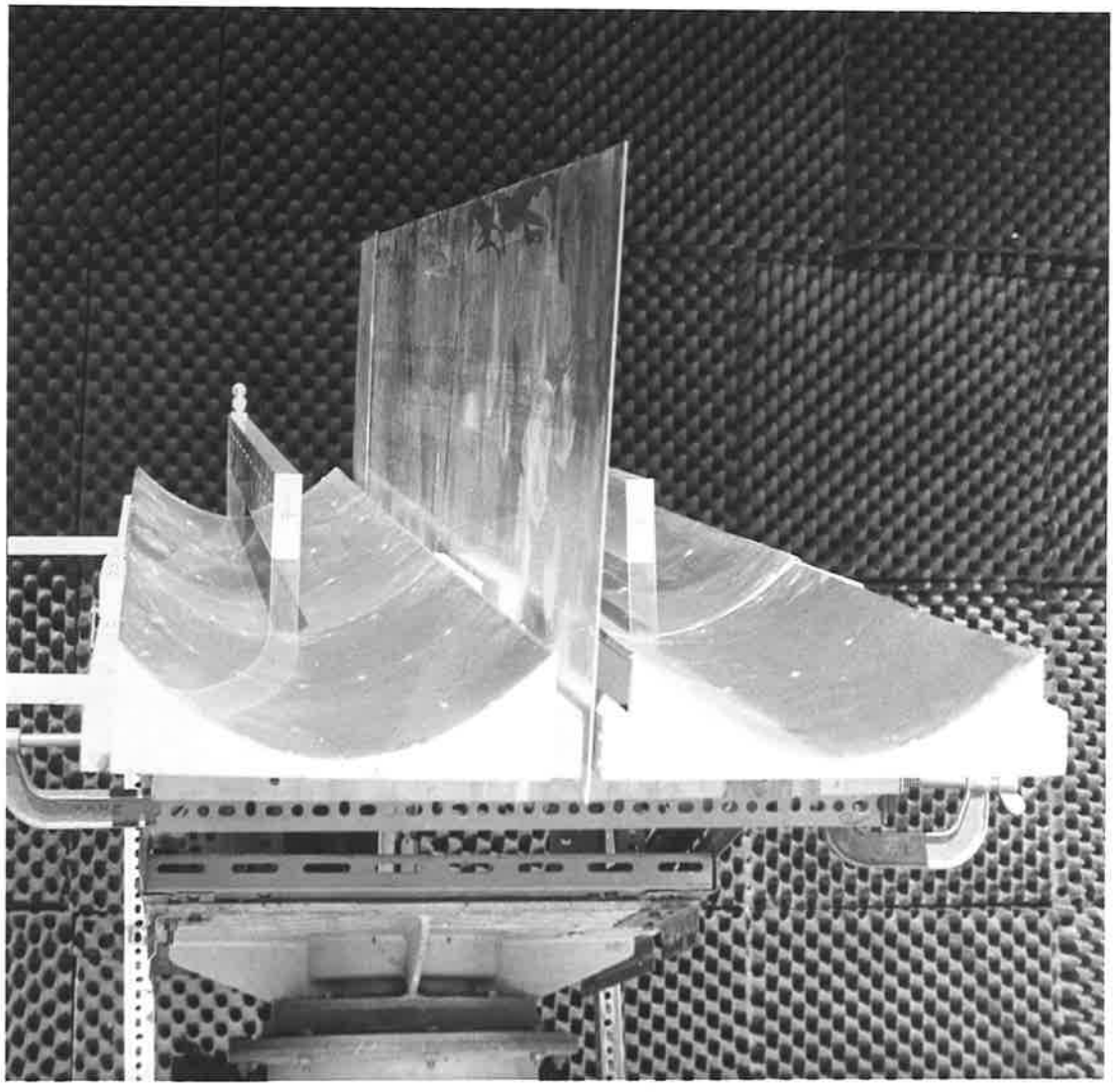

Two parabolic reflectors
and partition.

so that most of the radiation from the slot was intercepted by the parabolic cylinder. The feed cables coming out on top were kept at right angles to the electric field and made as short as possible to reduce loss and also to make tuning less sensitive. Each parabolic cylinder was made of thin aluminium sheets bent according to the parabolic shape of a wooden frame. The parabolic cylinders were mounted on a 7 ply marine board having their foci 2.5λ apart. A partition 18λ long and 3λ high was used.

Two corner reflectors of included angle 120° were also built to approximate the parabolic cylinders. Each had the same width as a parabolic cylinder but a somewhat shorter length of 16λ.

All the above three models despite the strong supports presented many difficult situations in windy conditions.

2. PREPARATORY TUNING AND MATCHING FOR EXPERIMENTS

To obtain the sum and difference patterns from the above models the two aerials need to be fed in phase and 180° out of phase. This could be achieved by using a ring hybrid. The principle of a ring hybrid is quite well known and it can be constructed in the form of a strip line using rexolite, a dielectric material having uniform dielectric constant in all directions. The design and construction

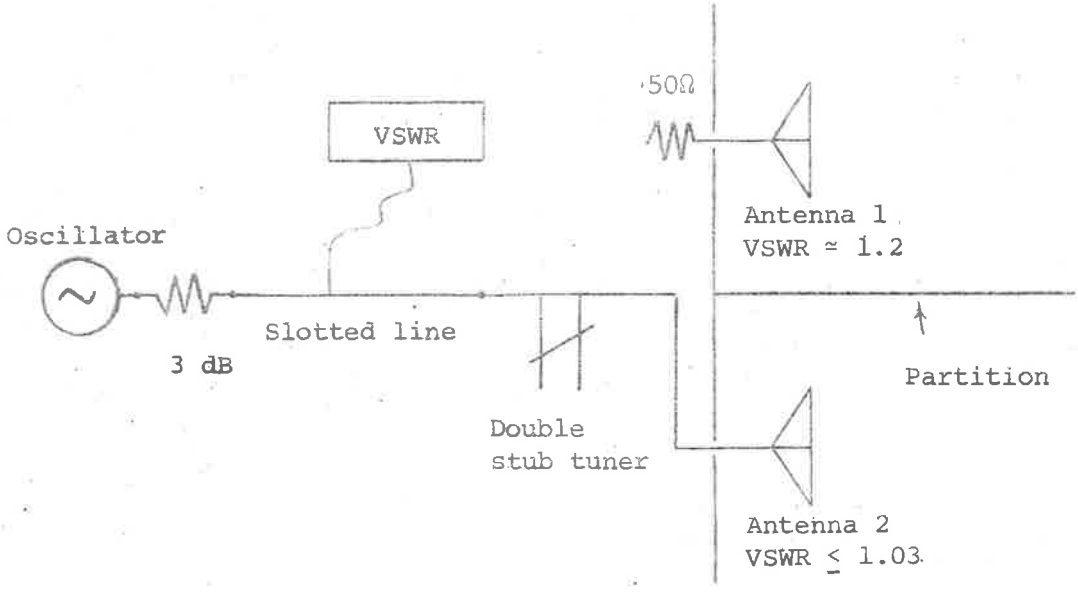

(a) Tuning for each antenna.

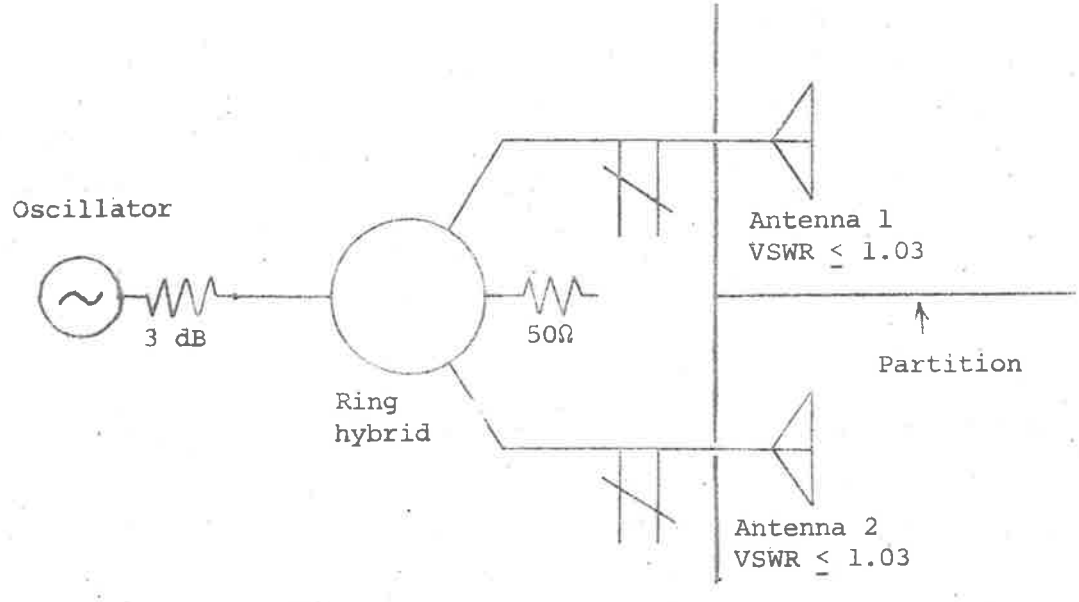

(b) Arrangement for generating sum and difference patterns.

Fig. 4

of a ring hybrid are discussed in Appendix C. To maintain good isolation between the first and third ports, every port must be well matched. This leads to the problem of tuning the above models to a 50 ohms source to obtain a good match.

Tuning for each model was done by using two identical double stub tuners at a conveniently short distance from the antennas. Prior to fine tuning, one antenna was tuned roughly to a VSWR of about 1.2 then the source was disconnected and replaced by a 50 ohms load. This was necessary to eliminate any mismatch reradiation due to coupling when the untuned antenna was being excited for tuning. The source was then connected to the untuned antenna which was properly tuned to a VSWR of better than 1.03. The source was again disconnected from this antenna and a 50 ohms load was put in its place. Proper tuning was carried out on the roughly tuned antenna to obtain a match with a VSWR better than 1.03. The whole process was quite tedious when there was two double stub tuners to tune. In the models involving the two terminated line sources a match of a VSWR of 1.03 or even better was easily achieved. However for the two slot dipole case, the best match achievable had a VSWR somewhat less than 1.1.

Every time a parameter of any one of the models was altered, retuning was carried out to ensure a good match. It was found that the slot dipoles and the slot lines were pretty well isolated when

the partition was about a wavelength high since a further increase in partition height did not alter the VSWR significantly. Each tuned antenna was then connected to an appropriate port on a ring hybrid to generate either a sum or a difference pattern. The VSWR of the model together with the ring hybrid was measured and found to be better than 1.05 for the models involving the slot lines and better than 1.2 for the two slot dipoles model.

The bandwidth of each model was obtained by measuring the 3dB points of the radiated signals as the frequency was altered and was found to be better than 2%.

3. METHOD OF RADIATION PATTERN MEASUREMENTS

(a) Ground Reflection Technique

With an experimental model of dimensions 9 x 6 x 3', it is not practical to make the simulated free space measurement by the usual tall towers technique. Hence the ground reflection technique whereby the ground reflection is combined with the direct signal should be used. The Weapons Research Establishment, Salisbury, S.A. has such a test range together with a turntable and good automatic plotting facilities. This allows convenient and accurate measurements of radiation patterns to be made. Since the ground reflection technique is quite well known, only a brief summary needs be given here.

The technique was studied and reported by Cohen et al. [25] and has been used quite extensively ever since.

Normally to measure the radiation patterns of an antenna in a simulated free space condition involves the use of two tall towers. There are two conditions to be met:

(i) The distance between the antennas, R must be such that

$$R \geq 2D^2/\lambda$$

where λ is the wavelength and D is the largest dimension of the antenna.

(ii) The tower heights must be such that the image of the transmitting antenna with respect to ground does not 'see' the receiving antenna. Under such a condition, no ground reflection will enter the receiving antenna and the radiation pattern is said to be equivalent to that of free space.

The ground reflection technique makes use of the ground reflecte ray and so tall towers are no longer needed. For a grazing incidence of the order of 2° or smaller, the reflection coefficient is 1/180° for both vertical and horizontal polarization, the transmitting antenr and its image can be treated as an array of two oppositely phased

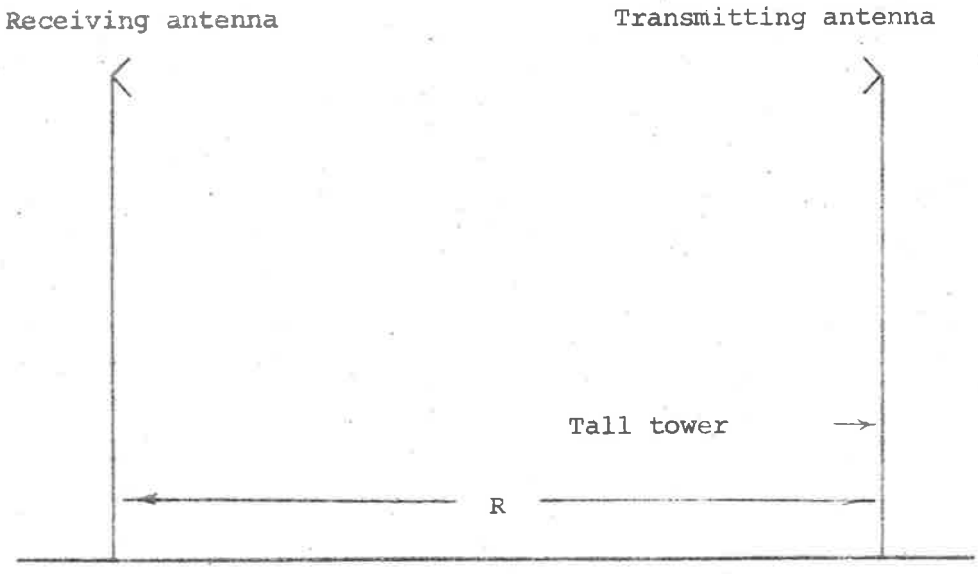

Fig. 5. Simulated free space measurement.

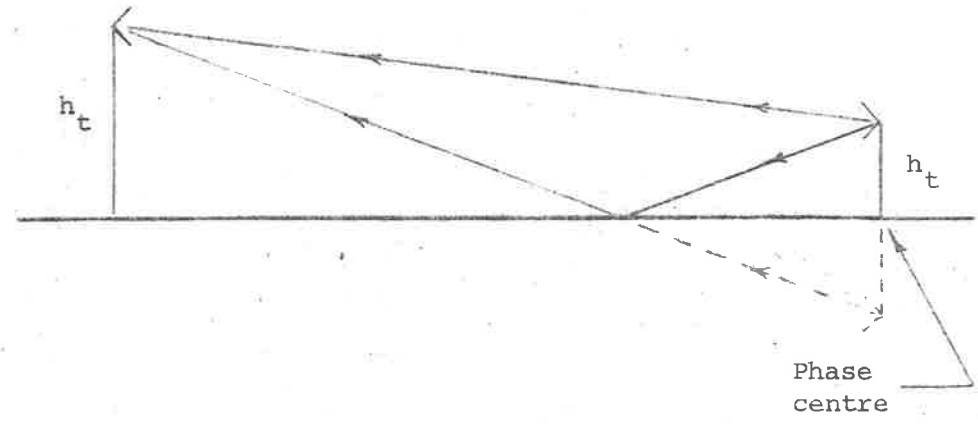

Fig. 6. The ground reflection technique.

antennas in free space (provided that the ground is flat) and the phase centre of the transmitting signal is situated at the foot of the transmitting antenna on the ground.

The field strength of the array in direction θ is given by:

$$E(\theta) \propto F(\theta)\ [\exp(jkh_t\sin\theta)-\exp(-jkh_t\sin\theta)] \quad ...(1)$$

$$\propto F(\theta)\sin(kh_t\sin\theta) \quad ...(2)$$

where $F(\theta)$ is the radiation pattern of the transmitting antenna. Since

$$\theta = \arctan\ (h_r/R) \simeq hr/R \simeq \sin\theta \quad ...(3)$$

Thus

$$E(\theta) \propto F(\theta)\sin(kh_t hr/R) \quad ...(4)$$

The variation of $F(\theta)$ is so slow that it can be considered uniform, therefore (4) implies that the receiving antenna is illuminated by a source placed on the ground at the foot of the transmitting antenna with an elevation beamwidth approximately equal to that of the first lobe of the array and a horizontal beamwidth equal to that of the transmitting antenna. For the condition that the antenna under test be positioned at the peak of the first lobe of the array:

$$\sin(kh_t h_r/R) = 1 \quad ...(5)$$

$$\text{i.e.} \quad kh_t h_r/R = \pi/2 \quad ...(6)$$

$$\text{or } h_t h_r = \frac{\lambda R}{4} \qquad \ldots(7)$$

So the two conditions the ground reflection technique should meet are:

(i) $R \geq 2D^2/\lambda$ as above

(ii) $h_t h_r = \lambda R/4$

To obtain good results, the profile of the field variation at the receiving antenna needs to be probed to establish if there is a uniform plane wave arriving at the receiving antenna at the correct height setting h_r corresponding to h_t given by (7).

The technique does away with tall towers and results in many advantages.

(b) Electrical Equipment and Characteristics

The experimental arrangement is as shown in Fig. 7. Each model was used as a transmitting antenna. The receiving antenna was a parabolic dish having a diameter 4λ and a focal length 1.2λ. The feed was a $\lambda/2$ slit balun dipole with a small circular reflector to reduce the back radiation [26]. The slit balun was selected because it had a broader bandwidth than the choke type, presented no blockage and gave virtually no squint in the radiation patterns of the parabolic dish. The receiving antenna has a gain 12 dB over a dipole and the

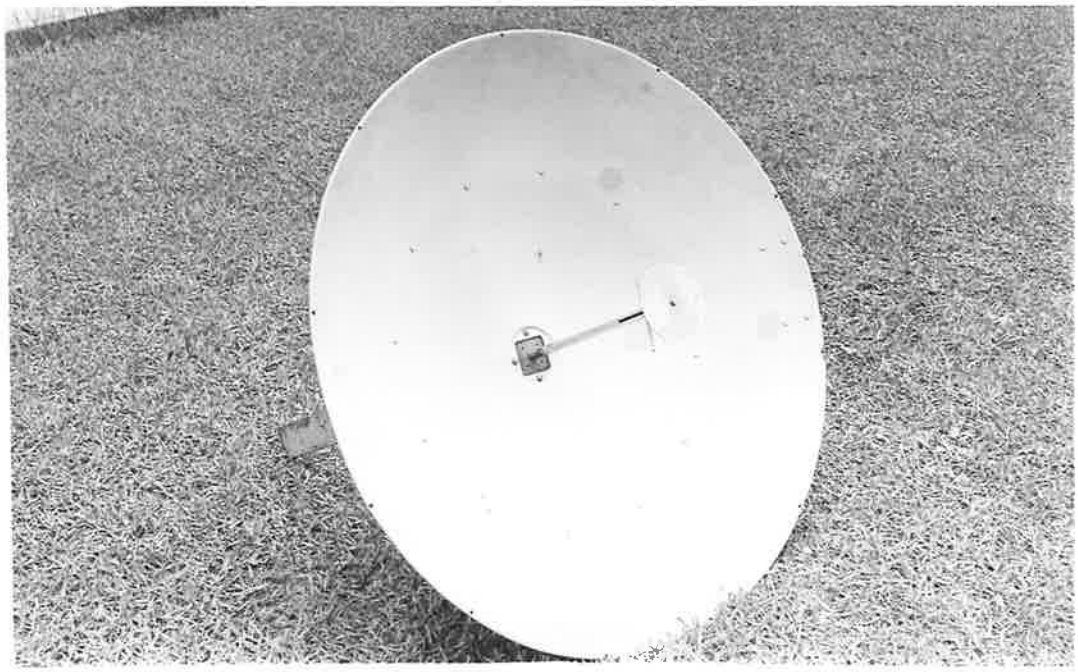

Parabolic dish

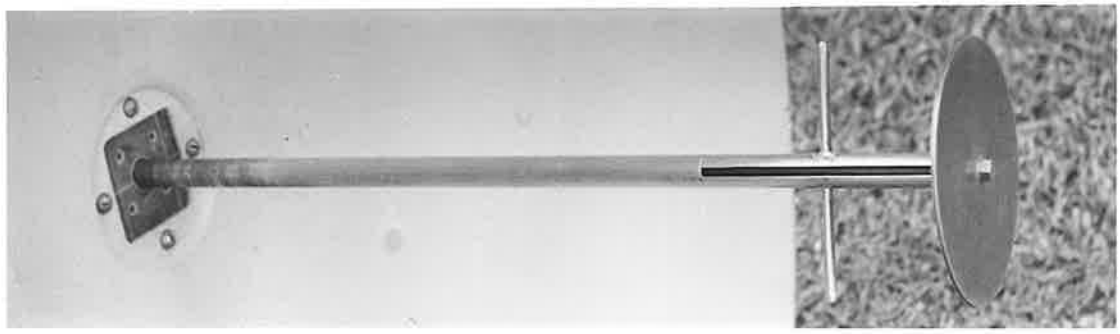

Feed

Slot termination

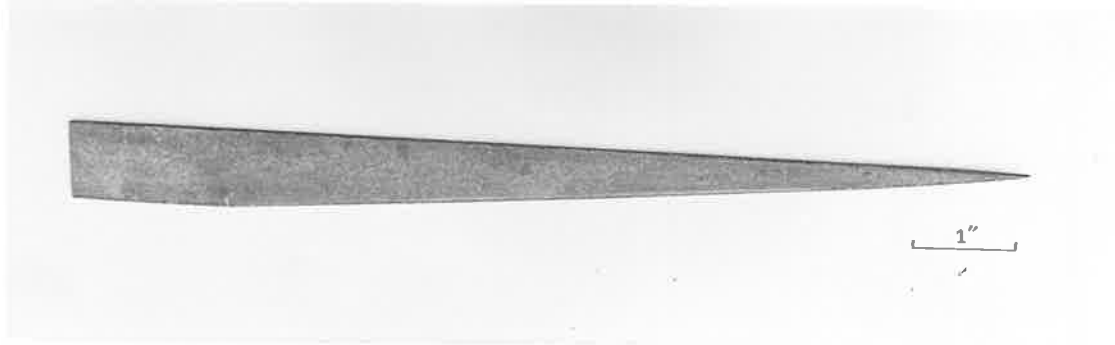

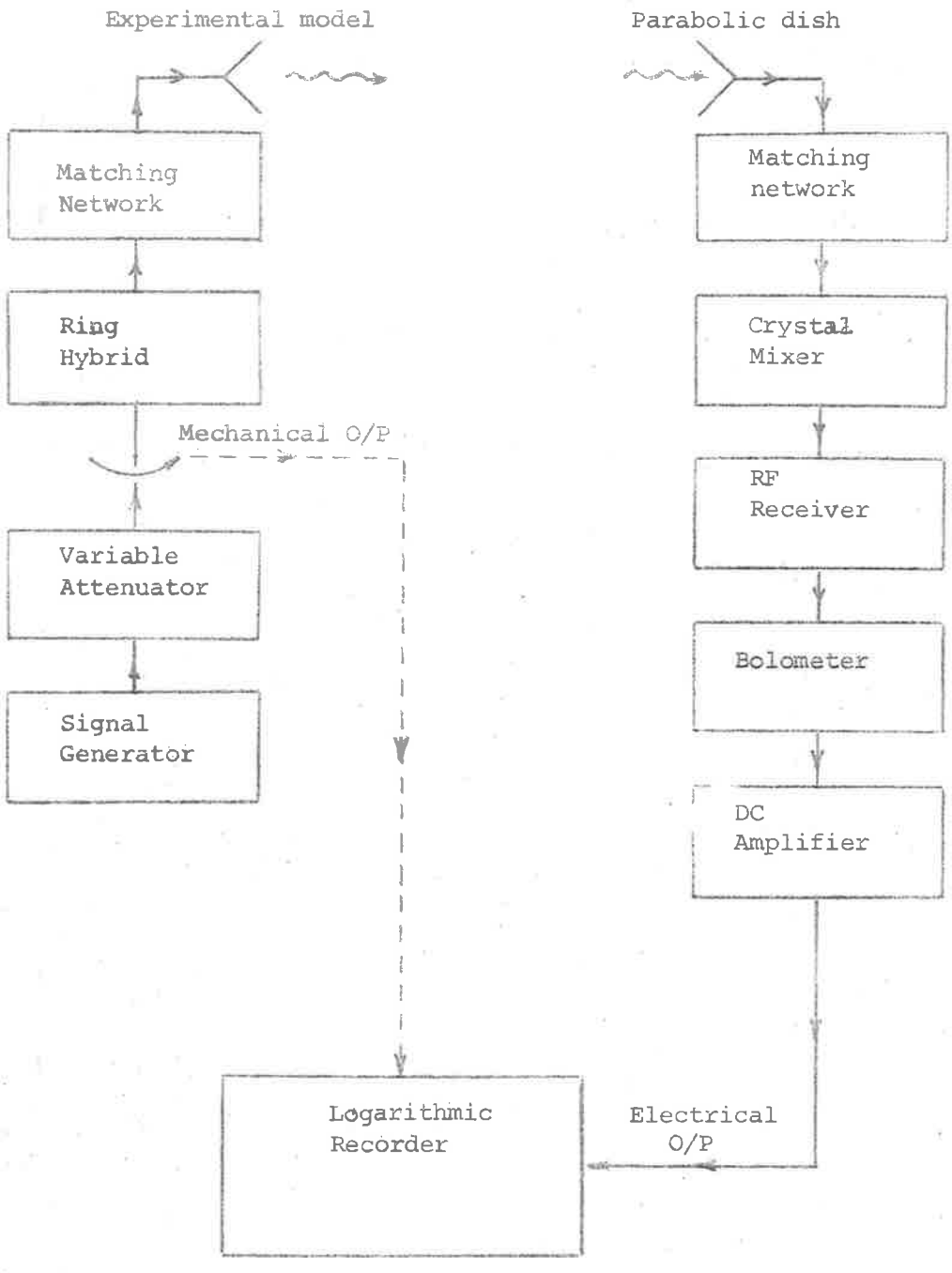

Fig. 7. Arrangement for radiation pattern measurement.

bandwidth was much better than 2%. Such a transmitting gain was ample for a test range of 200 ft. and an RF oscillator having 0 dB_m output.

(i) The Electrical Characteristics:

RF power output: 0 dB_m, CW with internal ALC at 2 GHz.

Bolometer current: 4 mA for square law operation.

Crystal mixer bias: -2mA for square law operation.

Microwave receiver: Gain control with linear range; AFC on lower; bandwidth 0.5 MHz; IF Sweep Width wide; Local oscillator power within linear range and its frequency peaked for maximum response.

Crystal amplifier: gain set at zero for linearity.

The receiving equipment was calibrated before use and the error was found to be about $\pm$ .5 dB.

(ii) The Equipment:

On the transmitting side, there were:

* A turntable with provision for azimuth on elevation rotation.
* Two double stub tuners (Weinschel Engineering Model DS109 and DS 109S).

* A ring hybrid (balanced strip line type, characteristics in Appendix C, made at the University of Adelaide) with better than 30 dB isolation at 2 GHz.
* A 3 dB fixed attenuator (874-G3L General Electric) ± 0.4 dB up to 2 GHz. Signal generator, model 8614A Hewlett-Packard (0.8 - 2.4 GHz) with provision for variable calibrated power output, internal ALC and square wave modulation.

On the receiving side, there were:

* A crystal mixer, Model 14-3 Scientific Atlanta, a broadband coaxial mixer (1.0 - 15. GHz) with a series diode requiring minimum local oscillator power, giving good isolation between local oscillator and signal input.
* A microwave receiver, series 1710 Scientific Atlanta, extremely wide frequency range, high sensitivity, exceptional linearity and good stability. Fast acting electronic AFC circuit and continuous tracking motor AFC correct the 55 MHz local oscillator frequency in the I.F. amplifier unit for changes in the incoming 45 MHz 1st I.F. signal caused by RF signal frequency changes. The end result is a constant 10 MHz 2nd I.F. Dynamic range 40 dB with deviation from linearity less than ± 0.25 dB. I.F. step attenuator. Signal level display permits accurate calibration of R.F. attenuation.

Overall receiver R.F. - I.F. bandwidth selectable at 5 MHz, 0.5 MHz, or 0.1 MHz.

* A crystal-Bolometer Amplifier, model 1554-2 Scientific Atlanta, a sensitive amplifier with wide band (± 1.5% centre frequency) or narrow band (± 3Hz) operations.
* A Rectangular Recorder, Series 1520 Scientific Atlanta for rectangular plot in the three ranges 360°, 180° or 60°.
* A slotted line for tuning, model 874-LV with residual VSWR < 1.035 from 300 MHz to 9 GHz (General Electric) and a 415E SWR meter, tuned amplifier at 1 kHz (Hewlett Packard).

4. THEORETICAL VS EXPERIMENTAL RESULTS

In what follows, the theoretical vs experimental results are presented. Reasonably good agreement has been obtained for all three models.

(a) Two slot Dipoles:

The theoretical expressions for the radiation patterns of two infinitely long line sources separated by a finite height partition of infinite length are also those in the equatorial plane of two slot dipoles in an infinite ground plane separated by the same partition. In practice, the situation is different because the ground plane has

to be finite and the partition can't be infinitely long. Diffraction from the edges of the ground plane can be treated reasonably accurately but that due to various plane corners is still untractable. To reduce such a contribution, the ground plane has been made large and the partition long.

(i) The Case of no Partition

To appreciate the effect of the partition, it is necessary to examine first the sum and difference patterns of an array of two slot dipoles placed at a distance $\lambda/2$ apart and having no partition between them. If the interaction between the two dipoles are eliminated, the sum and difference patterns are as shown in Fig. 9. It can be seen that the maximum of the difference pattern occurs at the same position as the minimum of the sum pattern and the null of the difference pattern is far from being sharp.

(ii) The Case of a Partition of Various Heights

When an H plane partition of a certain height is introduced between the dipoles, the theoretical results show that the sum pattern remains unaltered whereas the difference pattern undergoes three basic changes:

(i) The central null becomes deepened and concentrated near the central plane.

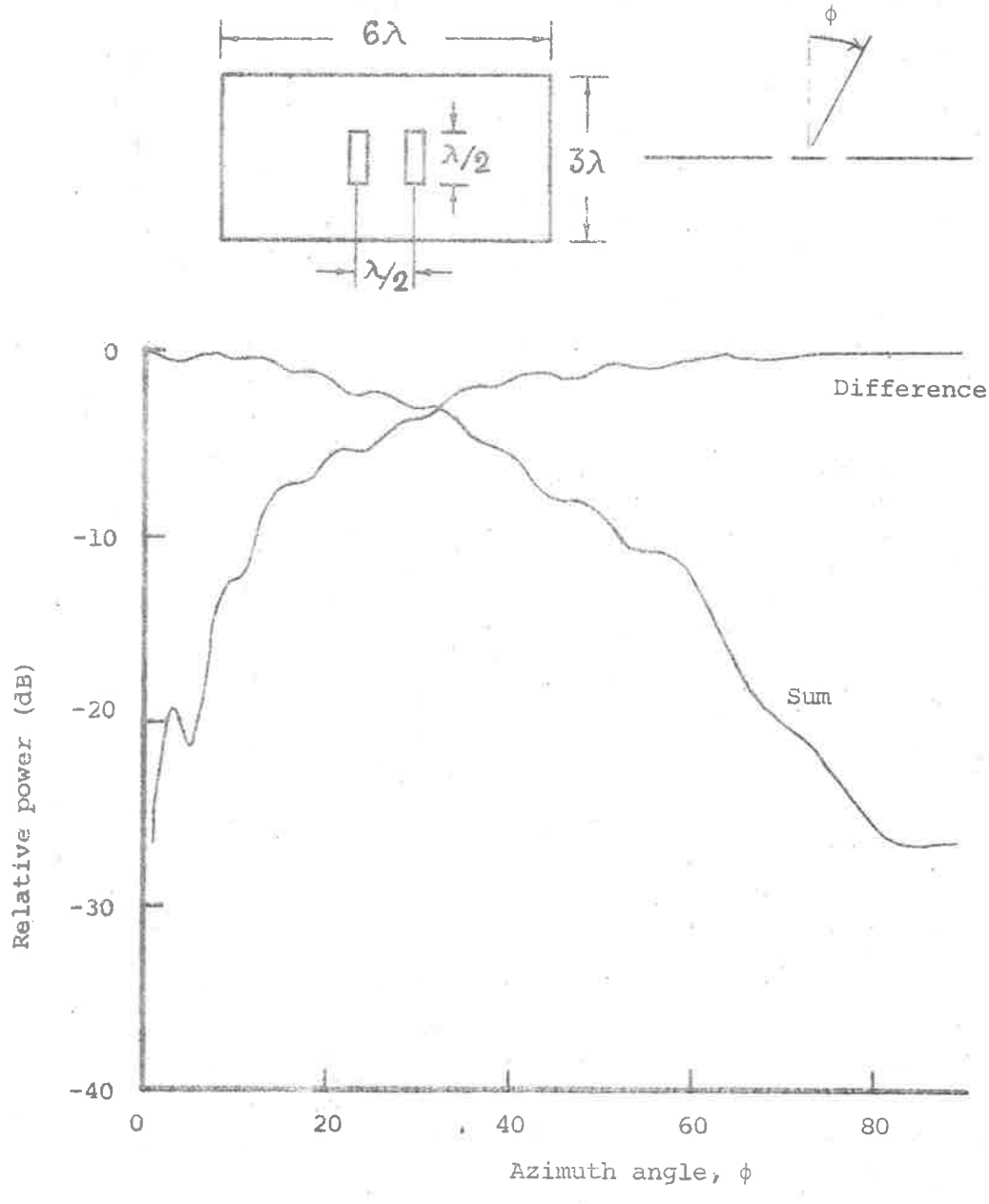

Fig. 9. Sum and difference patterns for two slot dipoles when there is no partition.

(ii) The region outside the central null tends to assume the same shape as the sum pattern.

(iii) Ripples appear on either side of the central null.

The first two characteristics are the desirable characteristics for a navigational system free of false courses but the last one is undesirable and should be reduced or suppressed.

As the partition height increases, the central null gets deeper, the region outside the central null assumes more and more the same shape as the sum pattern and the ripples become more numerous but less pronounced. As the partition height tends to infinity, the sum and difference patterns become coincident with the exception that the latter has opposite polarity on either sides of the central null plane

Two special cases will illustrate the above results more clearly.

(α) For a Partition Height $x_h = 6\lambda$

The theoretical sum pattern is shown in Fig. 10(a) in dotted lines. This is exactly the same as the sum pattern plotted in Fig. 9. The experimental results for the sum pattern are also plotted in continuous lines in Fig. 10(a). The theoretical difference pattern is shown in Fig. 10(b) in dotted lines. The difference between the difference pattern in Fig. 9, and Fig. 10(b) is quite considerable. The experimental results for the

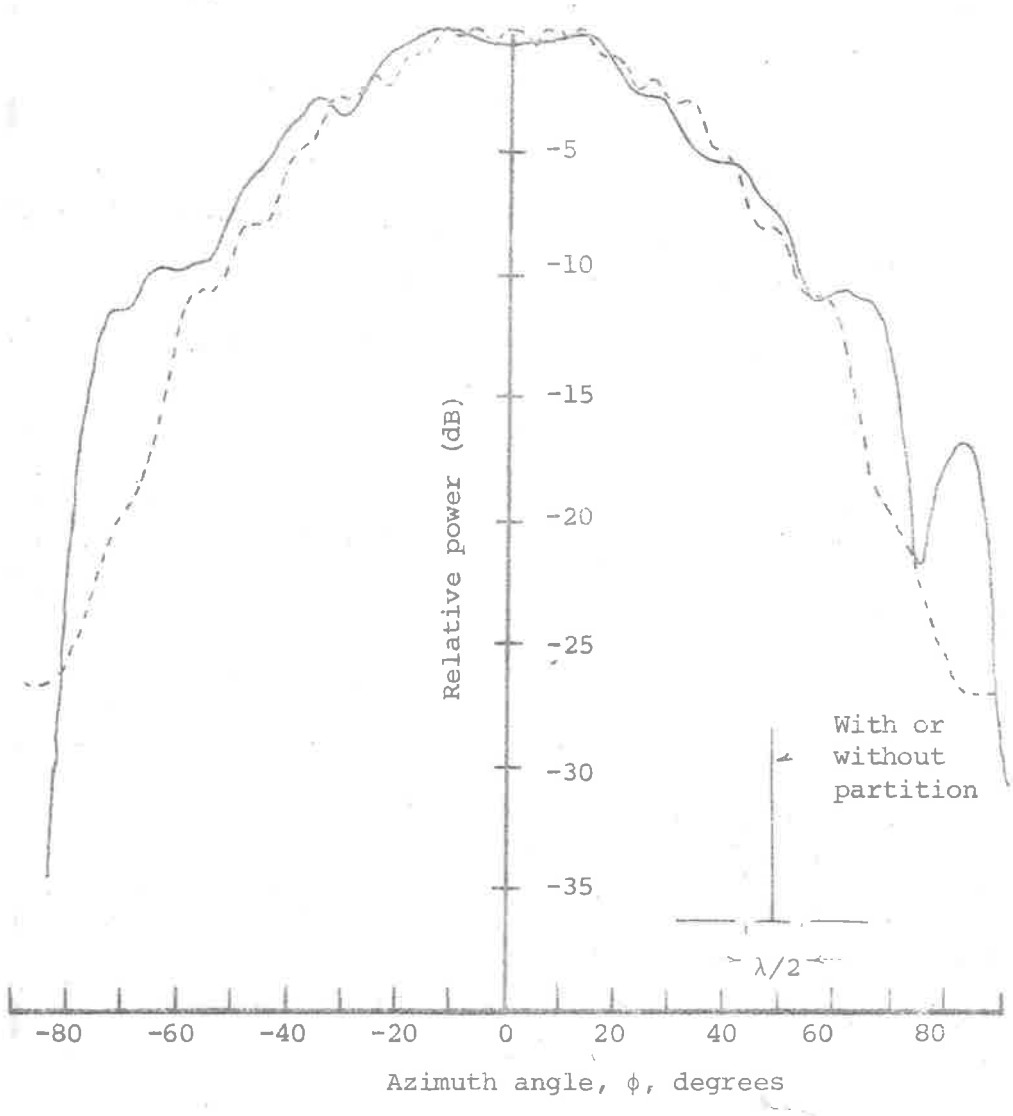

Fig. 10(a) Sum pattern for two slot dipoles

_____ Experiment

- - - Theory

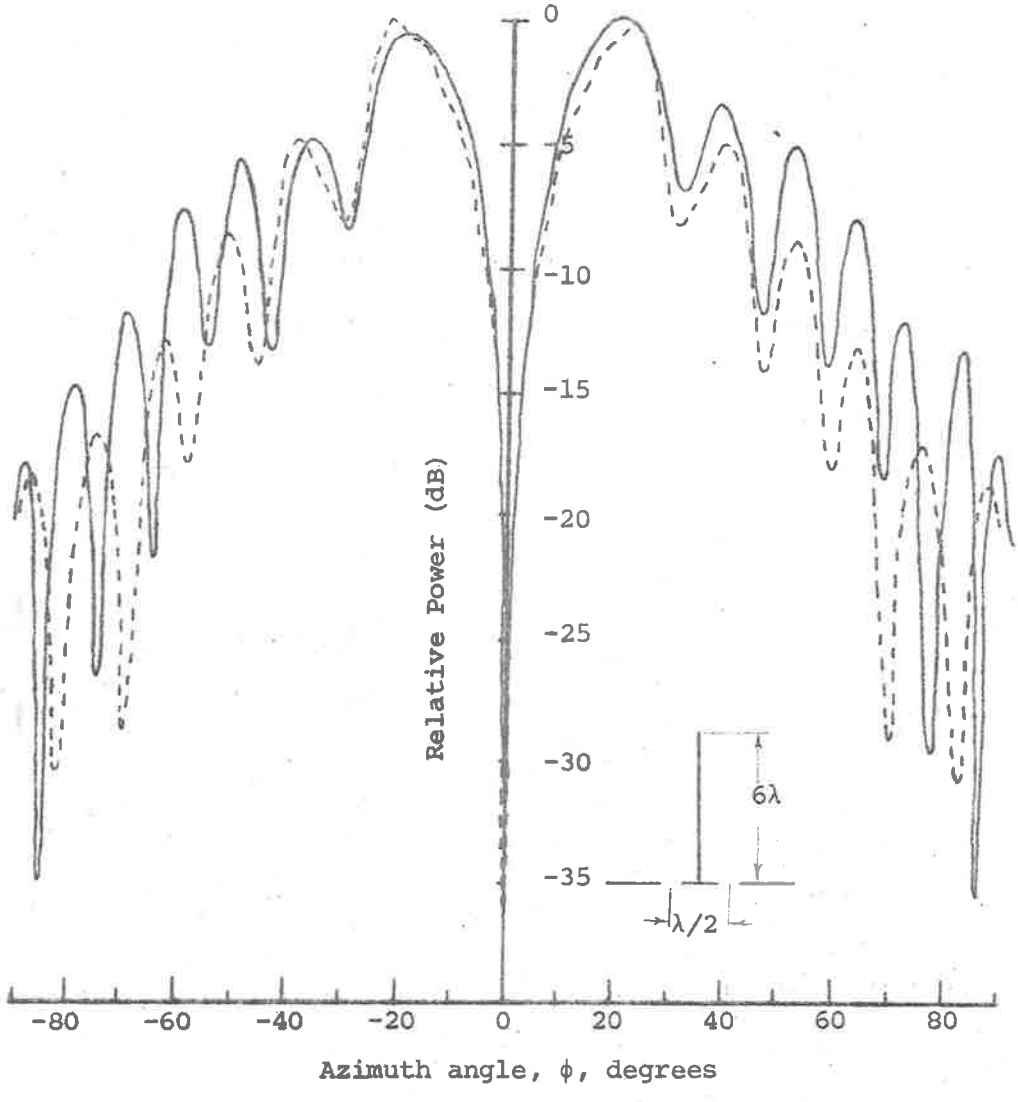

Fig. 10(b). Difference pattern for 2 slot dipoles
Partition height = 6λ

——— Experiment

- - - Theory

difference pattern are also plotted in continuous lines in Fig. 10(b).

(β) For a Partition Height $x_h = 16\lambda$

The sum pattern remains the same as seen in Fig. 10(a), this confirms the characteristics of the diffracted field function discussed in Chapter Two and verifies the physical reasoning that a conducting sheet at right angles to the electric field in a balanced distributed system will have no effect on the radiation patterns of that system. Both the experimental and theoretical results for the difference pattern are shown in Fig. 11 in continuous lines and dotted lines respectively. By comparing this figure with Fig. 9 and Fig. 10(b), the effects of the height of a partition can be readily seen.

It can be seen in Fig. 10(a), Fig. 10(b) and Fig. 11 that the agreement between the theoretical and experimental results is good. The deviation from the symmetrical patterns in the azimuth plane is due mainly to the wind effect on the model, which very often cannot be avoided in an open space test. The theoretical results only include the first and second order effects. To obtain a better agreement higher order terms have to be included together with the contribution due to the diffraction off the plane corners of the partition and the finite ground plane. The effect of a plane corner is to produce spherical diffracted waves having components in the

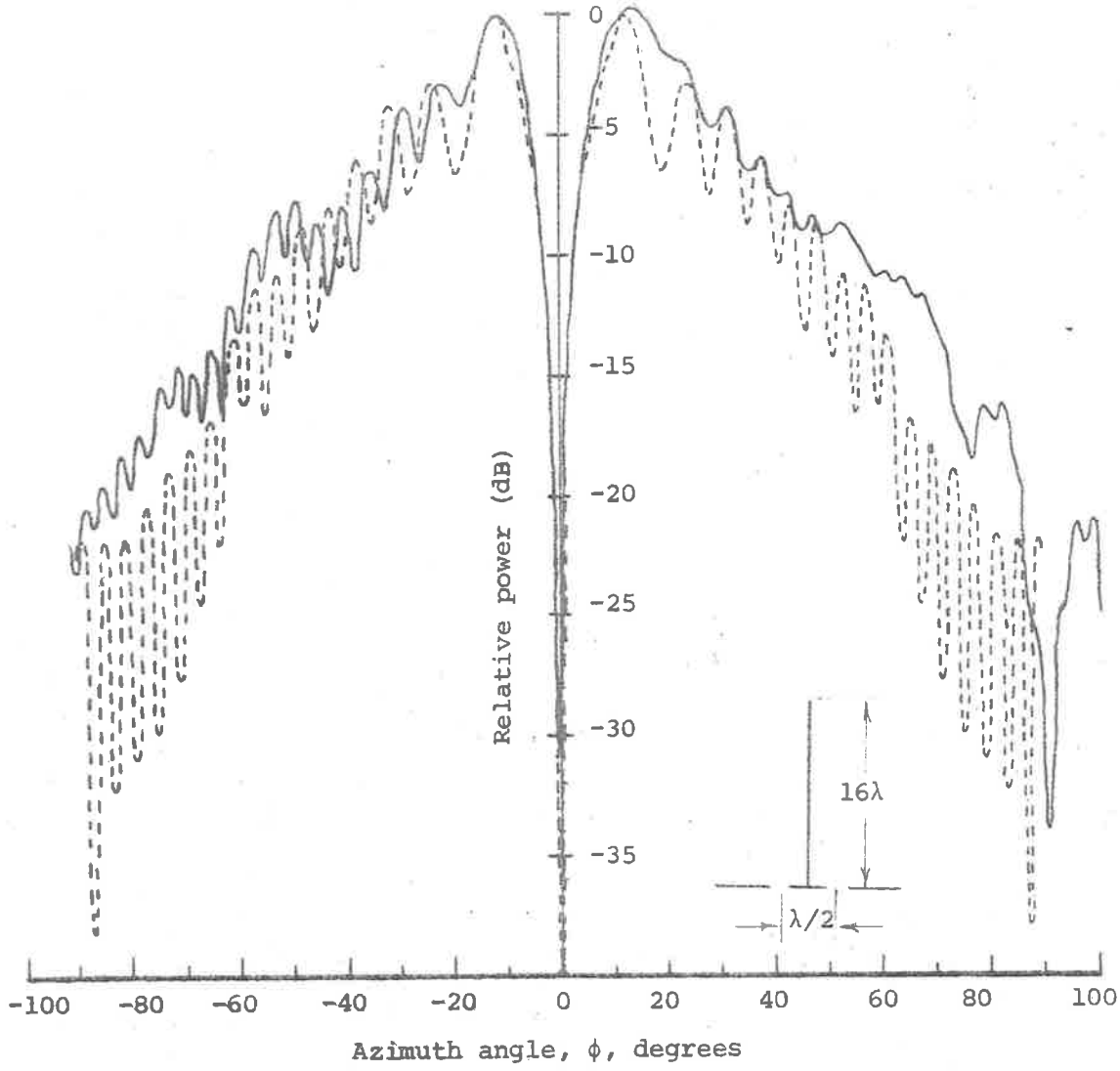

Fig. 11. Difference pattern for 2 slot dipoles
Partition height = 16λ
_____ Experiment
- - - Theory

equatorial H plane. The effect of the finite length partition should also be added. When the partition length is finite, it presents another edge to the incident glancing rays which are then diffracted into a conical wavefront. Rays from this wavefront have components which lie in the equatorial H plane and thus effect the radiation patterns.

No experimental measurement of the phase variation of the sum and didfference patterns was carried out. The theoretical phase variation is shown in Fig. 12 where it can be seen that the sum and difference patterns do not differ much in phase in the immediate regions outside the central null plane. The large phase variation at large ϕ will not cause any concern since the signals in these regions are insignificantly small.

(b) Two Slot Lines:

The theoretical expressions for the radiation patterns of two finite length slot lines separated by a partition and placed above a ground plane are derived and presented in Chapter Two. Each slot line is a travelling wave antenna with a uniform amplitude distribution along the slot. The direction of maximum radiation is dictated by the velocity ratio $c/v_g = .985$ and the slot length. The slot lines are mounted with their feeds towards one side of the ground plane.

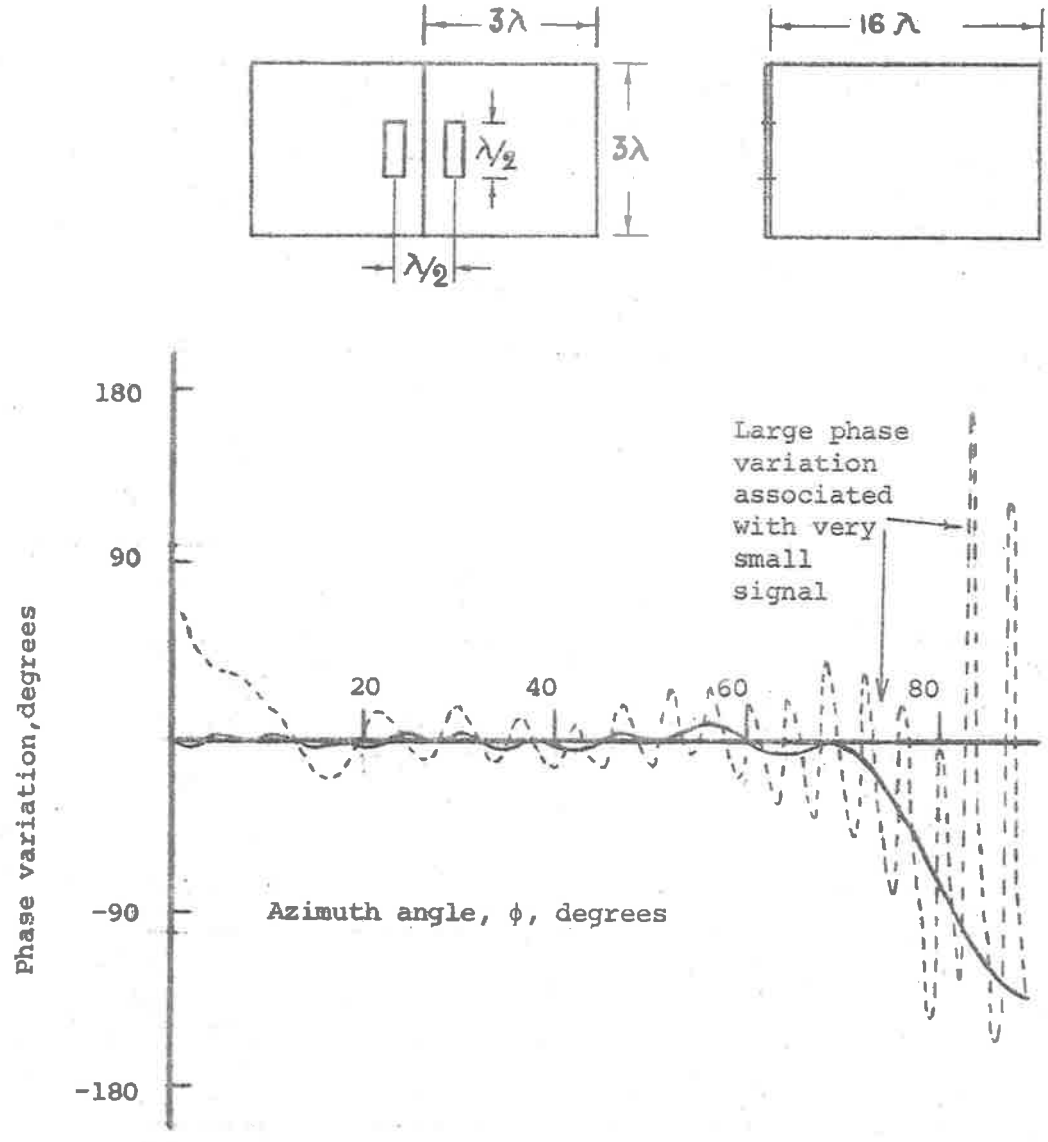

Fig. 12. Phase variation

——— Sum

– – – – Difference

This arrangement will enable the ground plane to capture most of the radiated waves. Because the ground plane has been made quite large, it can be assumed to be infinite. The contribution due to the diffraction off the edge of the finite ground plane has been ignored in the theoretical computation. This is justified because the angle of incidence of the rays from the line source to the edge is almost grazing. The diffracted contribution will have very small effect in the region of the main beam and immediate sidelobes. As seen in Fig. 13, the model is unfortunately large. Probably a smaller model at a higher frequency to be used in an anechoic chamber will be more suitable. Due to continuous windy conditions, many tests had to be abandoned half way through. However the modest results obtained are considered quite sufficient to illustrate the effect of the partition and to give a better physical insight into its behaviour.

Fig. 14(a) and Fig. 14(b) show the theoretical sum and difference patterns in dotted lines. On the same graphs, the experimental results are plotted in continuous lines. The agreement between the theoretical and experimental results are quite good considering the approximations made. Fig. 14(c) shows the experimental sum and difference patterns. From the figure, it can be seen quite clearly that the partition has deepened the null in the central plane considerably and also has caused the alignment of the nulls and the sidelobes. The partition has no effect on the sum pattern. As the partition height

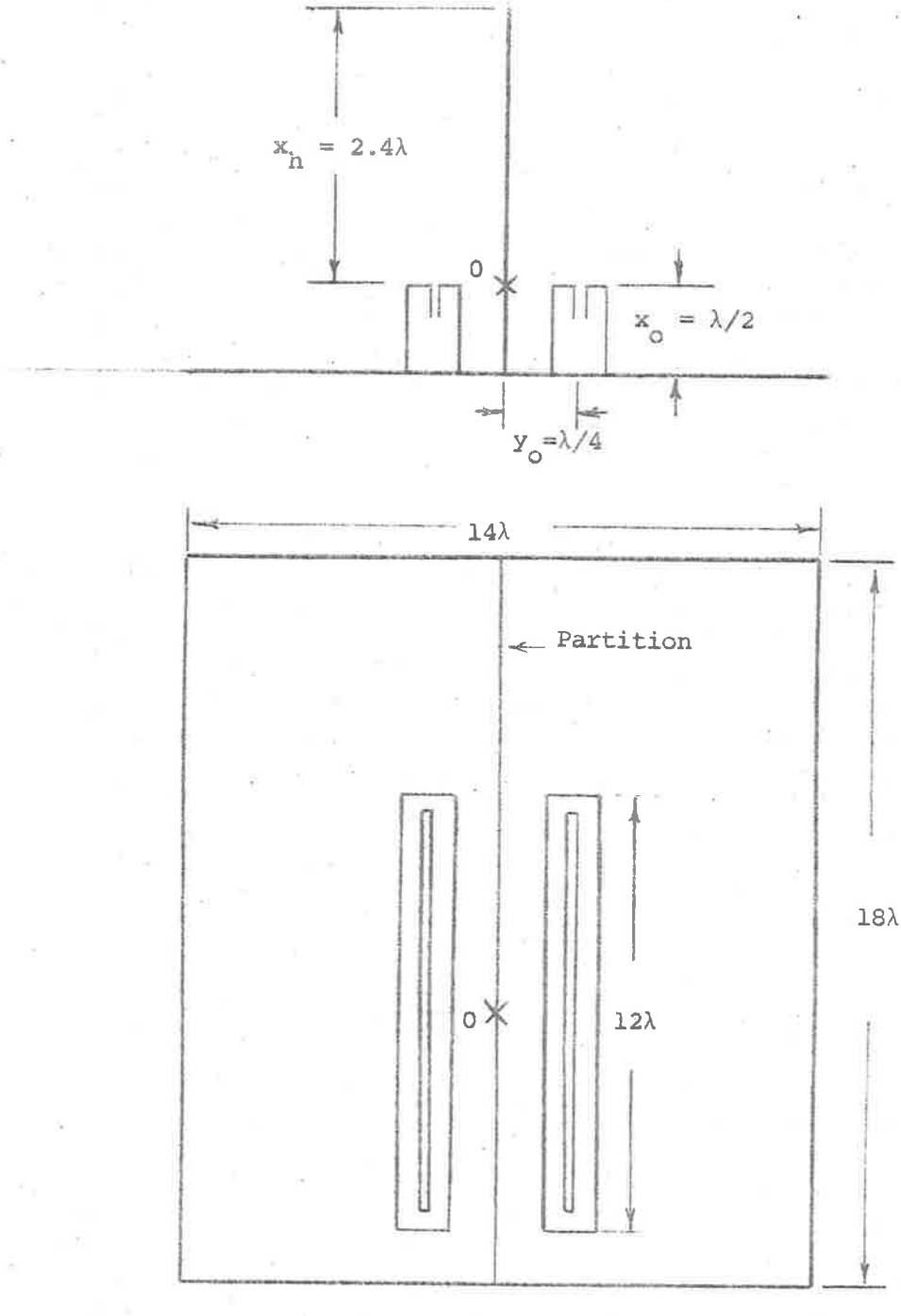

Fig. 13. Two line sources and ground plane.

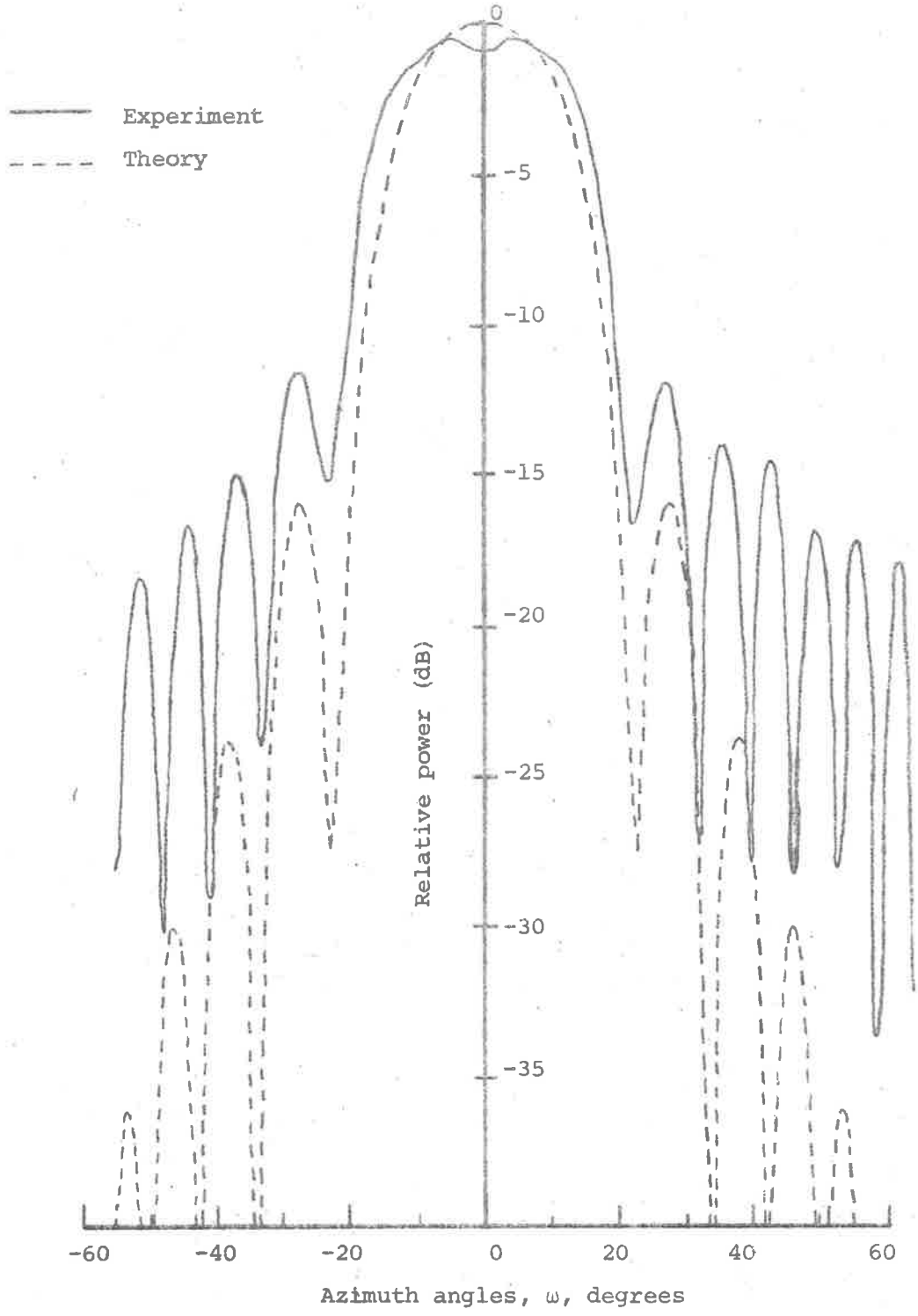

Fig. 14(a). Sum pattern for two travelling wave slot lines. Azimuth on 15° elevation.

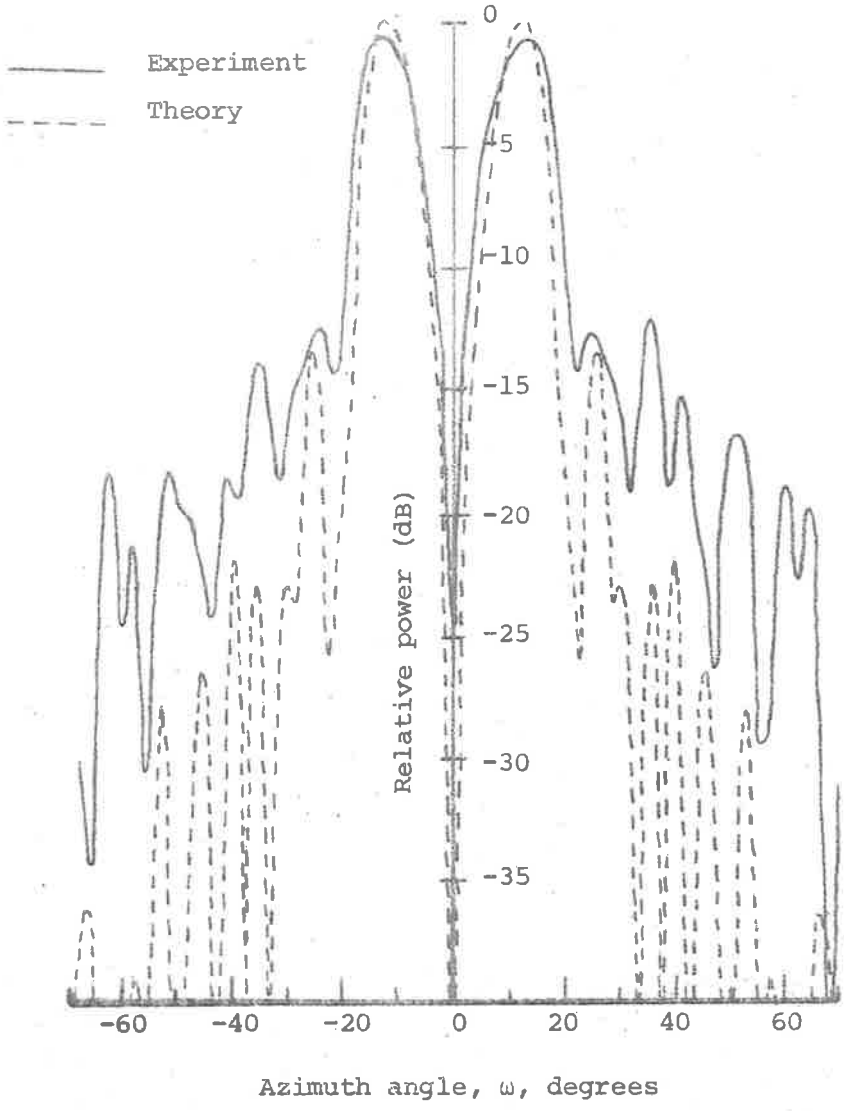

Fig. 14(b). Difference pattern for two travelling wave slot lines.
Azimuth on 15° elevation.

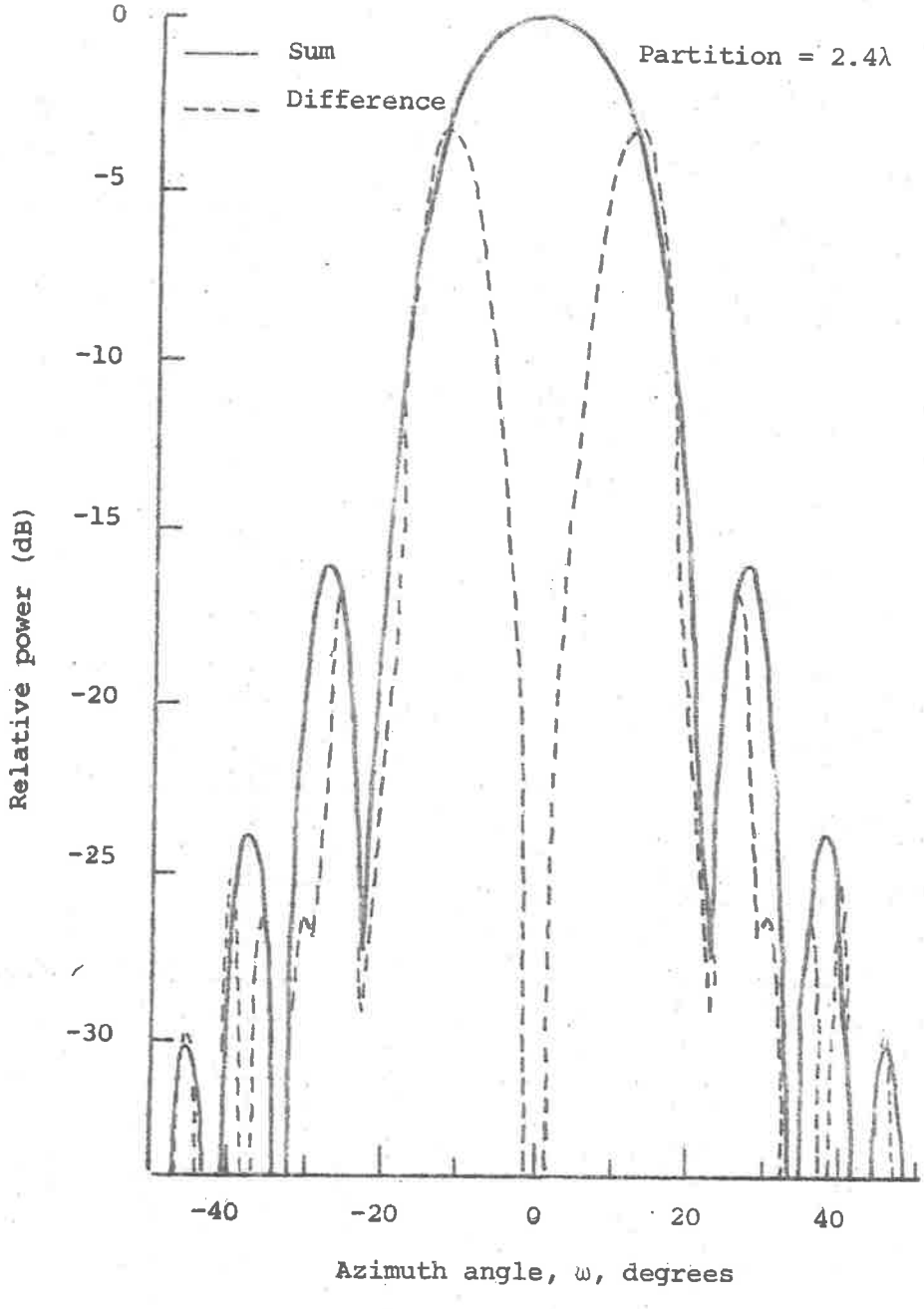

Fig. 14(c). Sum and difference patterns for two slot lines with partition at angle of elevation 15°.

increases, it is expected that the difference pattern will assume the same shape as the sum pattern with an exception that the phases on either sides of the central plane are opposite.

Better agreement between the theoretical and experimental results will be achieved if higher order diffraction terms due to the finite ground plane and finite length partition are included. This slot line model is unlike the slot dipole model in that the slot lines are not cut into the ground plane but are $\lambda/2$ above it. The presence of the backing cavities will complicate the situation somewhat.

(c) Two Apertures:

The theoretical expressions for the sum and difference patterns of two parabolic cylinders can be obtained as follows:

(i) The expressions for two finite length apertures can be applied to the aperture field distributions of the two parabolic cylinders.

(ii) The expressions for the direct radiation from the slot lines are those of two finite line sources separated by a partition.

(iii) The expressions for the diffraction off the edges of each parabolic cylinder have been given in Chapter Three.

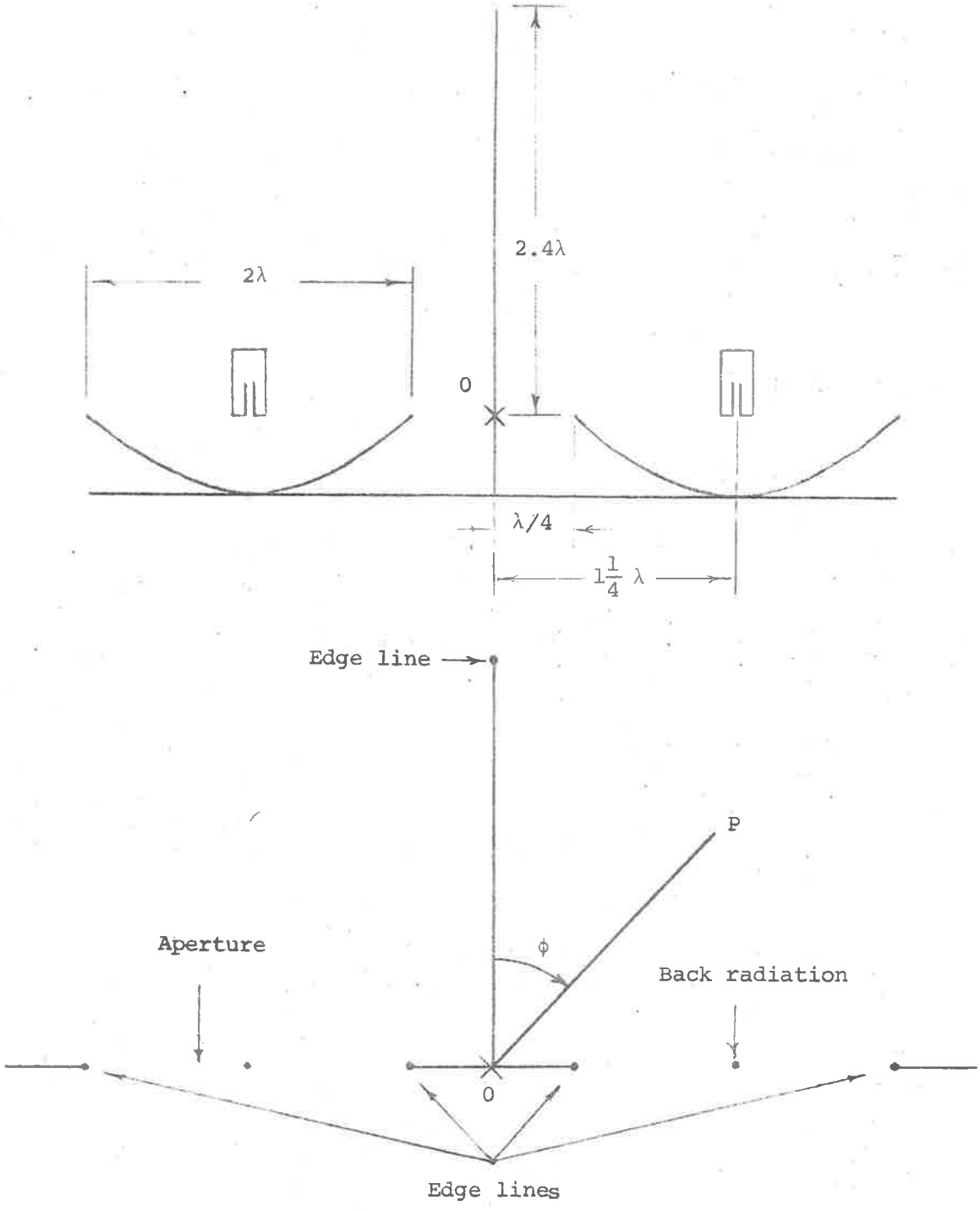

Fig. 15. Parabolic reflectors and equivalent apertures and line sources

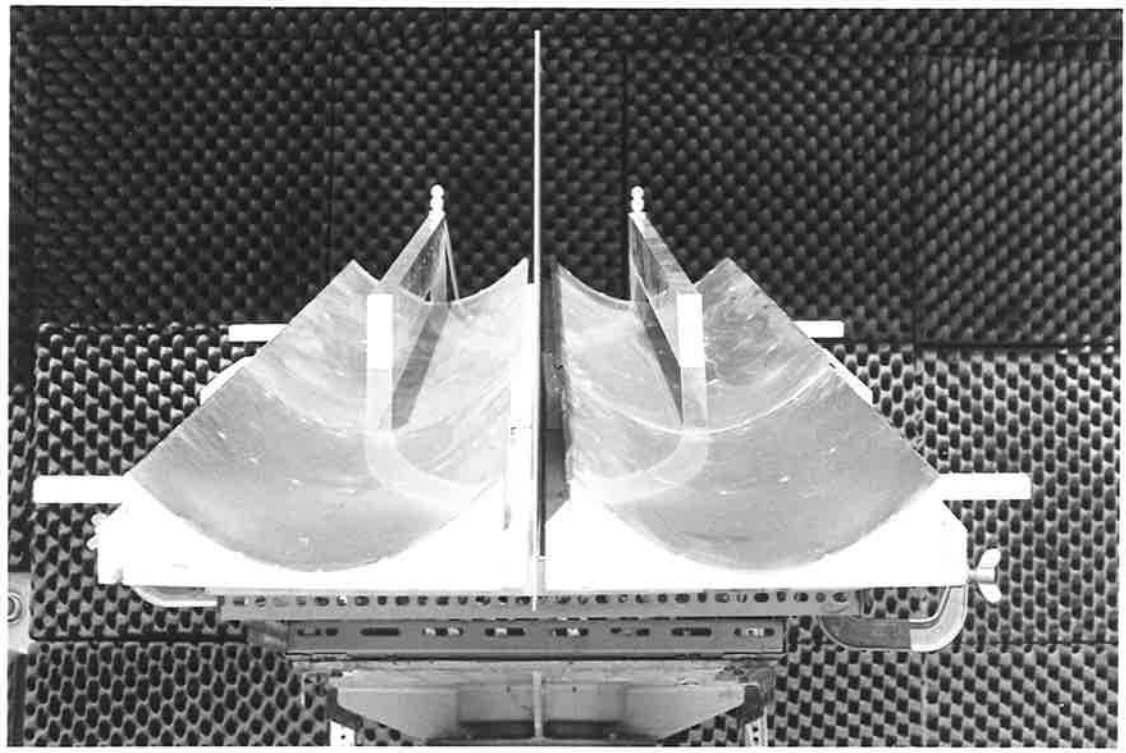

Two parabolic reflectors and partition.

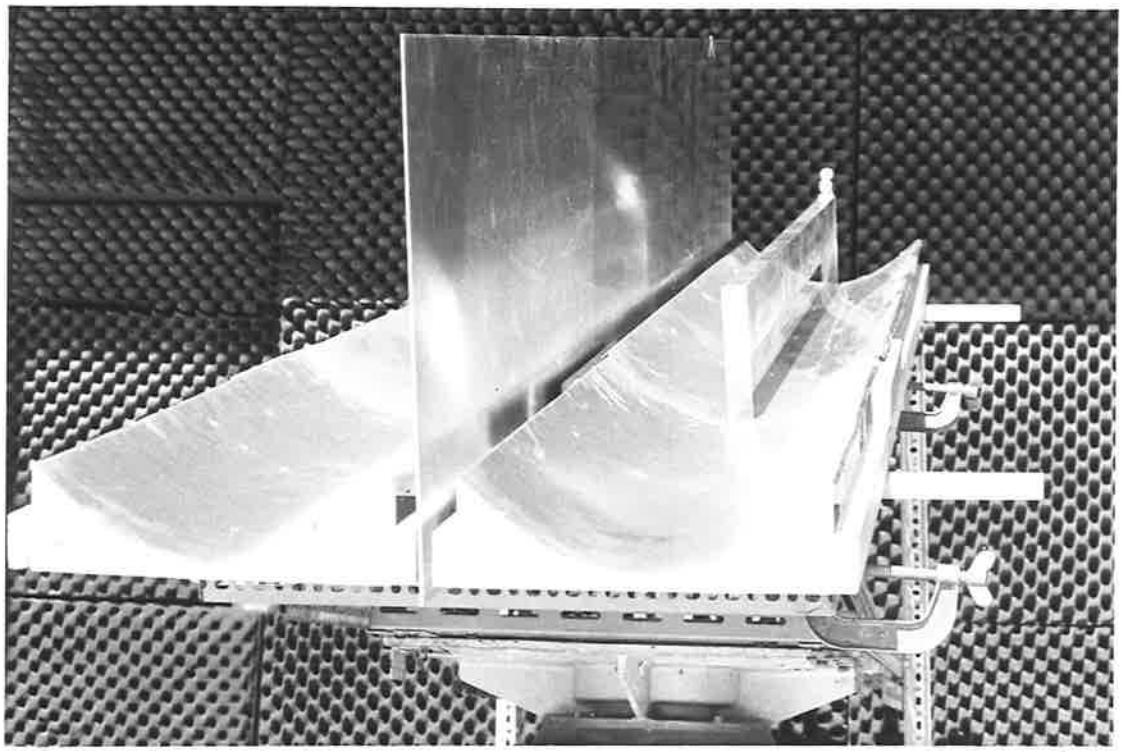

The edge diffraction behaves like a line source thus the edge diffraction contribution can be deduced by applying the expressions for two finite line sources separated by a partition.

To illustrate the effect of the partition, the following cases are considered:

(i) The Case of No Partition:

When the two parabolic cylinders have no partition in between them, the experimental sum and difference patterns are shown in Fig. 16(a). The null in the central plane of the difference pattern is not very sharp and the sidelobes of the sum pattern do not line up with those of the difference pattern. Such sum and difference patterns will contain inherent false courses. Fig. 16(b) and Fig. 16(c) compare the theoretical results with the experimental ones. The agreement is quite good in the regions of the main beam and immediate sidelobes.

(ii) The Case of a Partition 2.4λ High:

When the two parabolic cylinders are separated by a partition 2.4λ high, the experimental sum and difference patterns are as shown in Fig. 17(a). The sum pattern remains unaltered. Once again the theoretical prediction is verified. The null in the central plane of the difference pattern becomes deeper and the sidelobes are brought

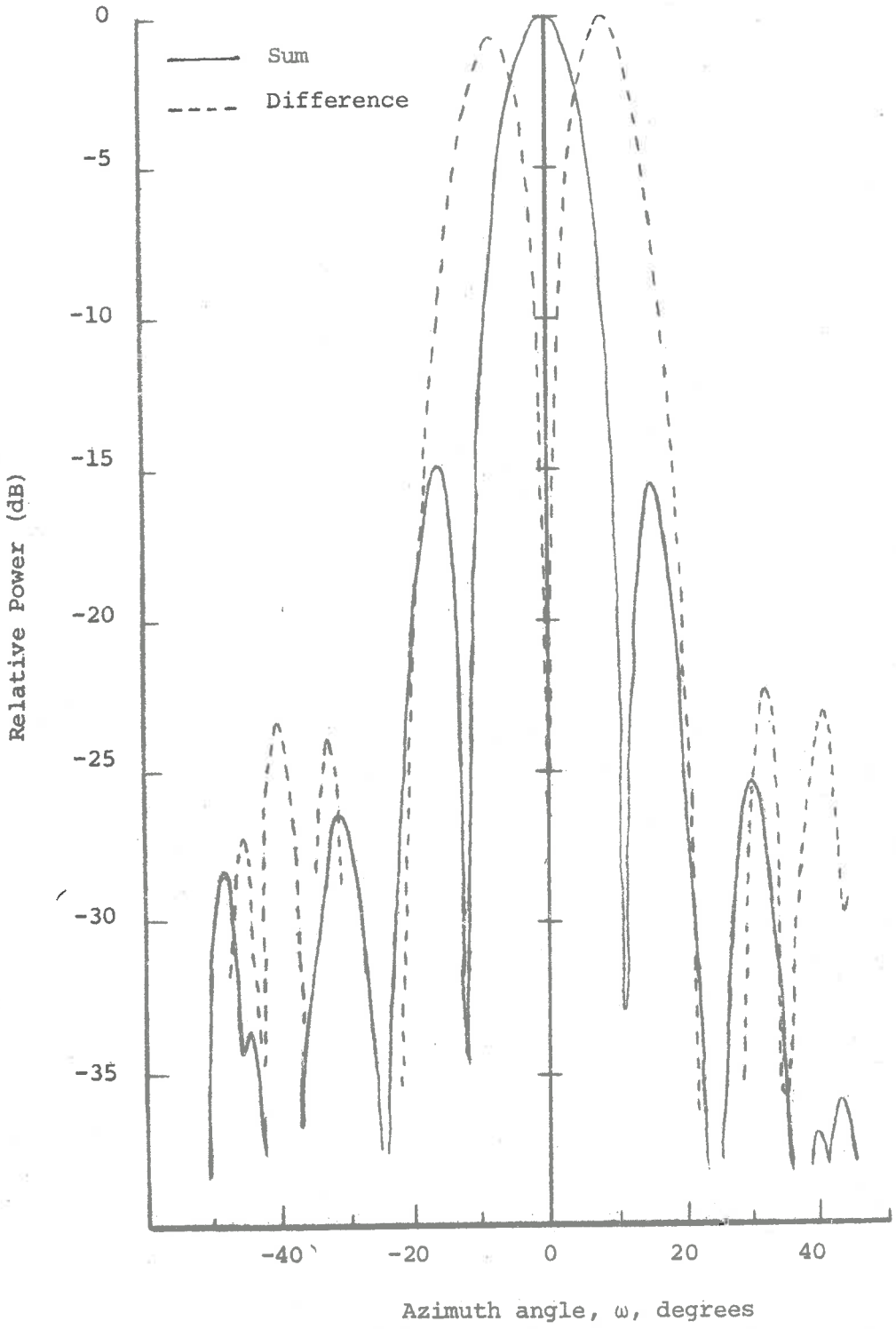

Fig. 16(a). Azimuth on 15° elevation radiation patterns.

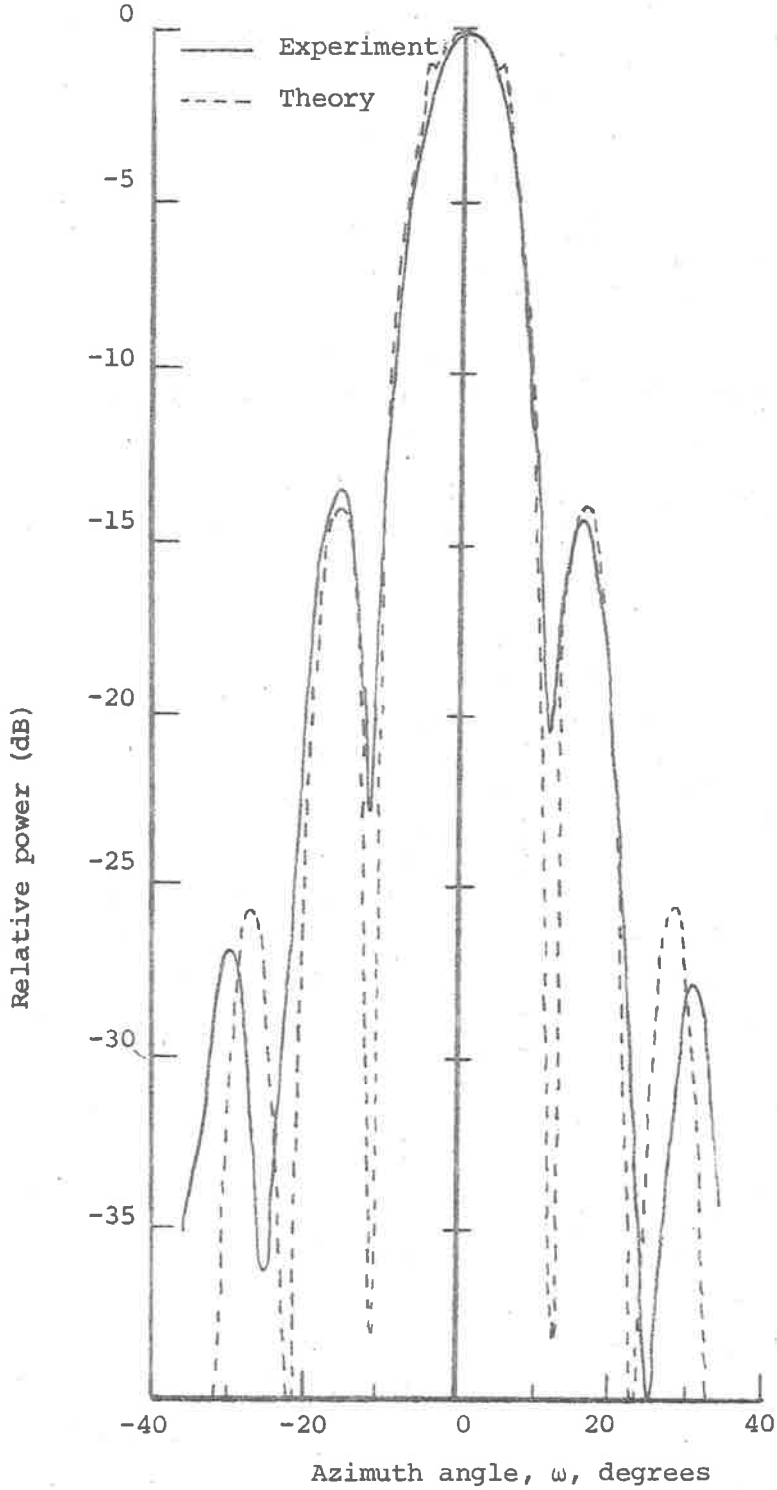

Fig. 16(b). Sum pattern with or without partition for two parabolic cylinders at angle of elevation 15°.

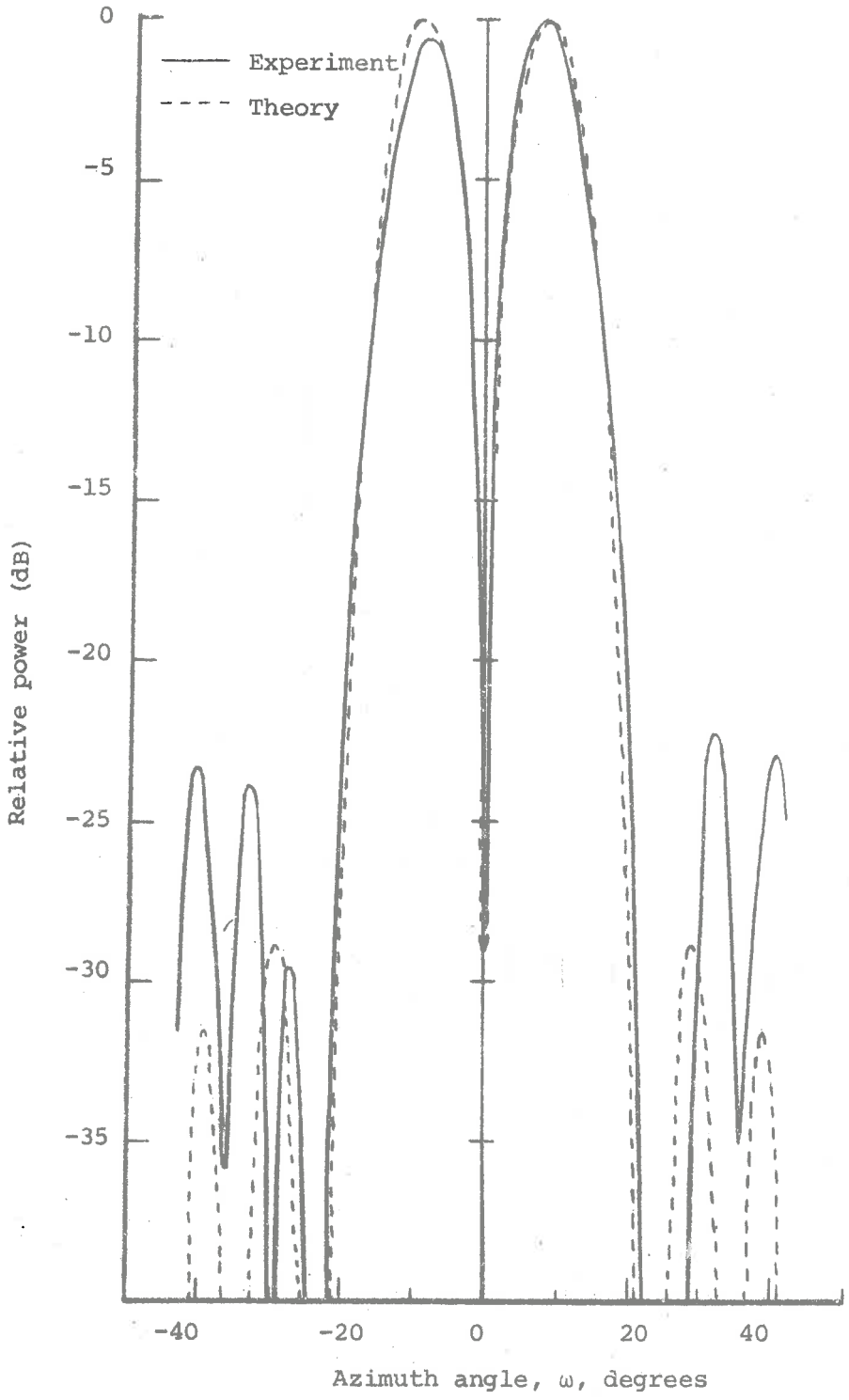

Fig. 16(c). Difference pattern with no partition for two parabolic cylinders at angle of elevation 15°.

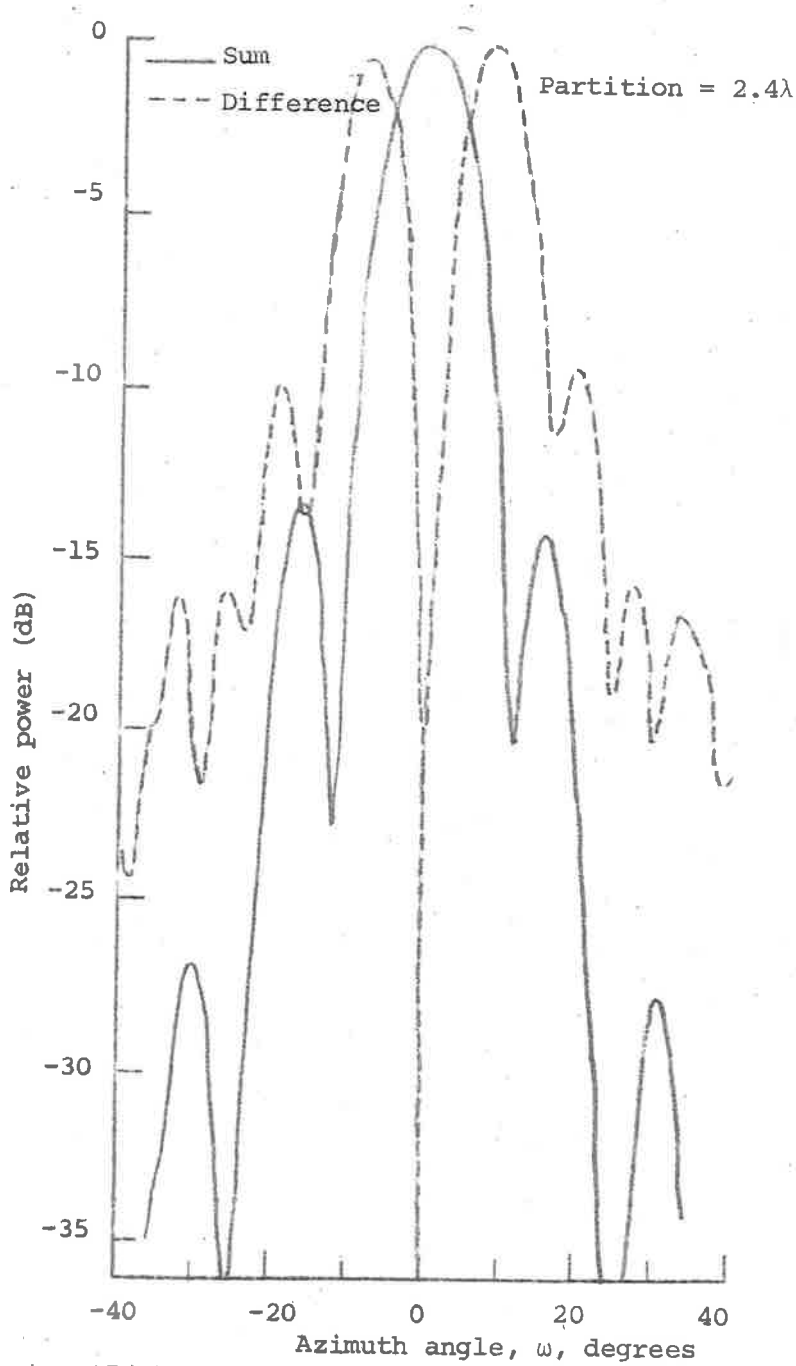

Fig. 17(a). Sum and difference patterns for two parabolic cylinders at angle of elevation 15°.

closer to the central null. It is expected that the difference pattern will resemble the sum pattern more closely when the partition height is increased. Fig. 17(b) compares the theoretical results for the difference pattern with the experimental ones. The agreement is quite good in the vicinity of the null in the central plane but deteriorates rapidly towards the sidelobes. The disagreement is due to the fact that other contributions such as higher order diffraction finite length partition, finite length reflectors and plane corners due to finite length have been omitted. The most significant higher order diffraction contribution is that due to a 'line source' due to diffraction at the edge of the partition illuminating the parabolic reflectors and their edges. The edge diffraction effect can be easily taken into account but it never plays a dominant role in the vicinity of the main beam so it can be safely ignored. However the illumination of the parabolic cylinders by the 'line source' at the edge of the partition will play a dominant role in the main beam but it is too difficult and too involved to analyse. This is so because the partition edge is not the focal line of the parabolic cylinders. Since the length of the partition and the parabolic reflectors has been made as long as practicably possible, the finite length effect has at least been greatly reduced. Depending on whether a plane corner is illuminated by a strong or weak signal, its diffracted contribution could become quite serious. Fig. 18 shows the effect

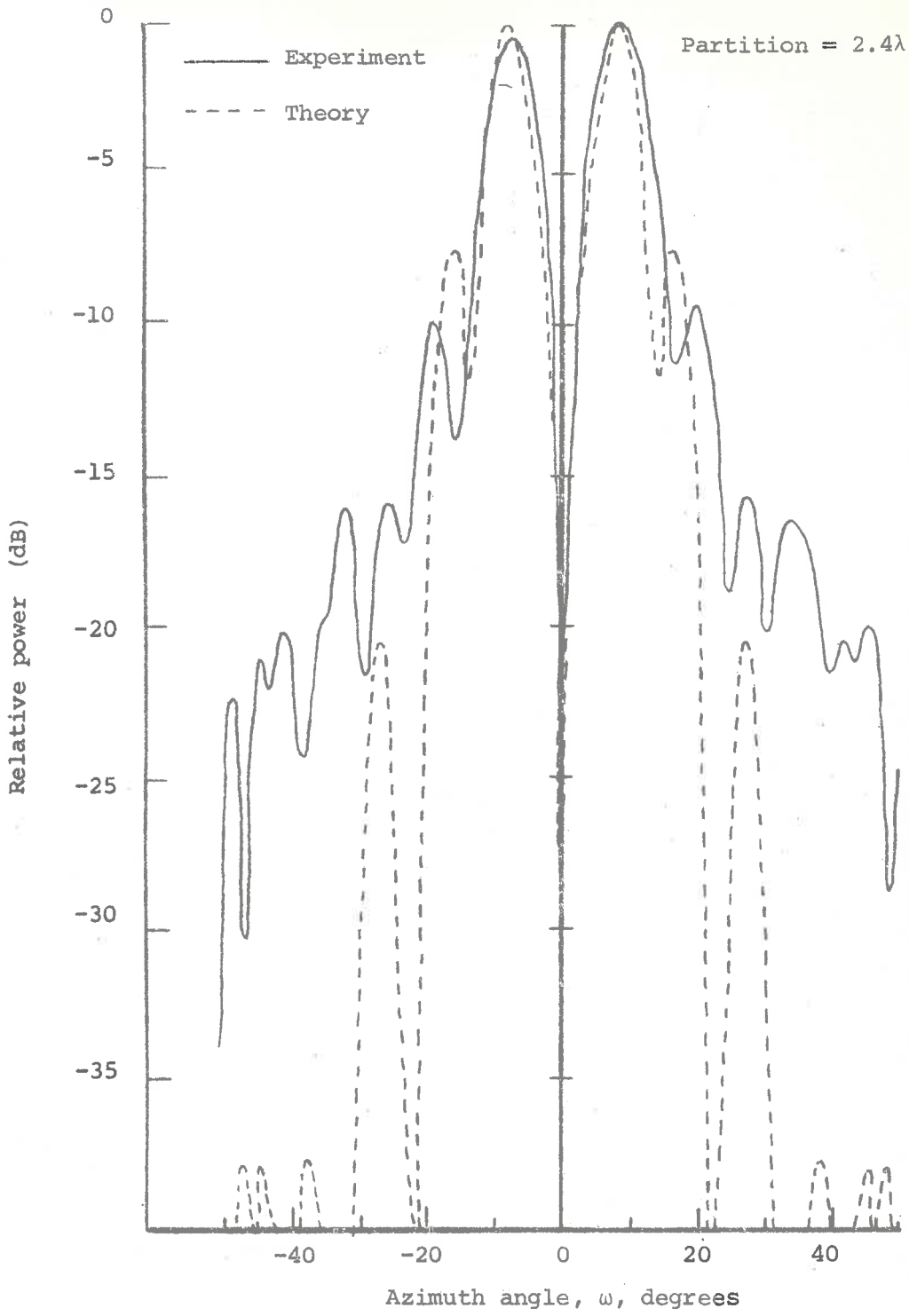

Fig. 17(b). Difference pattern for two parabolic cylinders with partition at angle of elevation 15°.

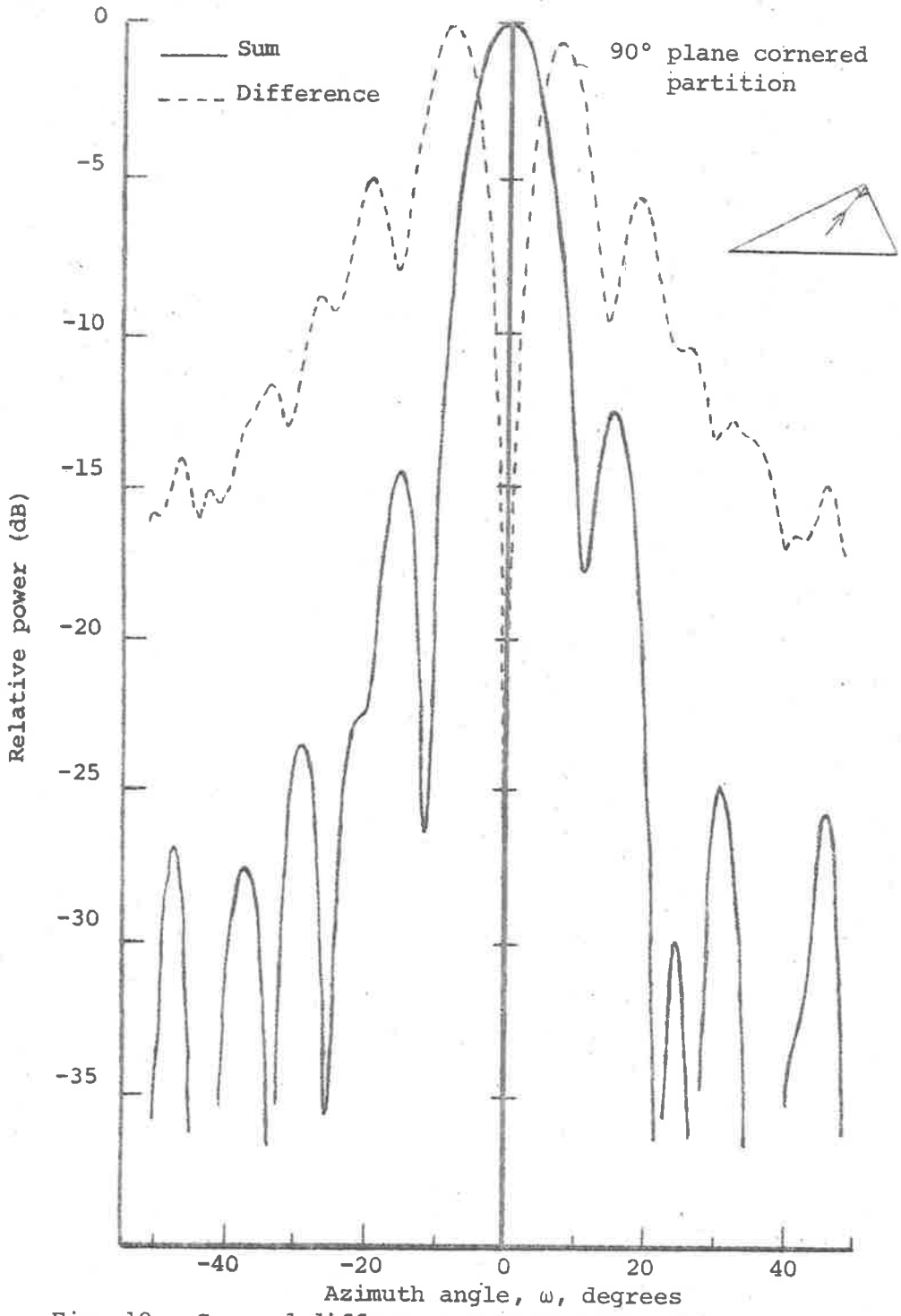

Fig. 18. Sum and difference patterns for two parabolic cylinders at angle of elevation 15°.

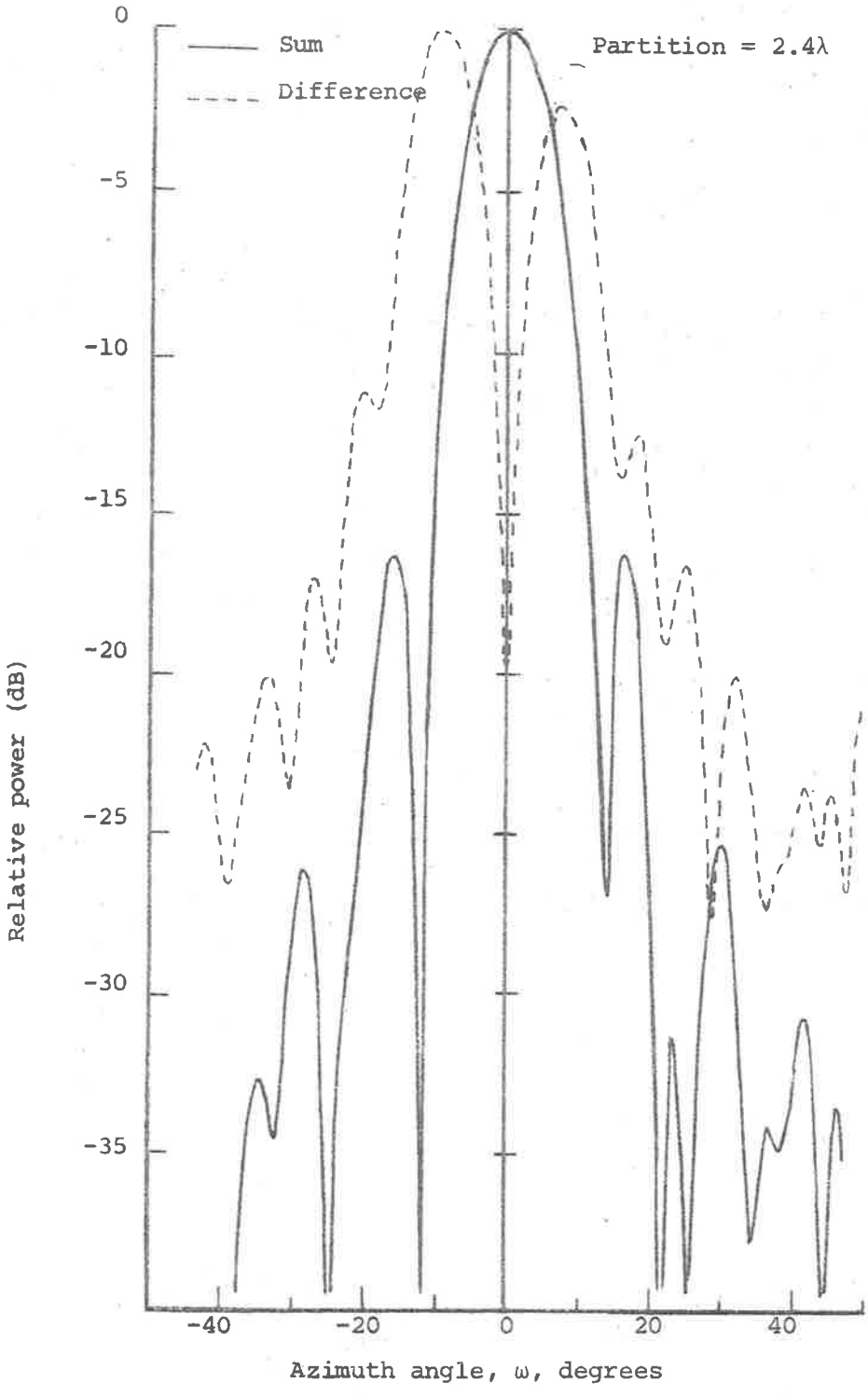

Fig. 19. Sum and difference patterns for two corner reflectors at angle of elevation 15°.

of a partition in the form of a 90° plane corner. The plane corner is 2.4λ high at its highest point, and is illuminated by the main beam of the parabolic cylinders. Predictably, it has no effect on the sum pattern but it raises the sidelobe levels of the difference pattern quite considerably.

The effect of the H plane partition between the two corner reflectors is the same as for the two parabolic cylinders. Fig. 19 shows that the sum and difference patterns of the two corner reflectors do not differ much from those of the two parabolic cylinders. The beamwidth is slightly narrower because of the phase error.

If the measuring equipment accuracy, the manufacturing tolerances of the three models and the errors due to the effects of the test range are taken into consideration, it must be said that the experimental results agree quite well with the first order solutions of the problem of diffraction off the edge of a partition.

The use of an H plane partition in the plane of symmetry of a distributed antenna system tends to create the desirable effects for a navigational system free of false courses. These are:

- the deepening of the null in the central plane of the difference pattern, and

- the lining up of the nulls and sidelobes of the sum and difference patterns.

CONCLUSION

The analysis and experimental verification of the problem of diffraction off the edge of a partition placed along the medial plane of symmetry of a distributed radiating system have confirmed the behaviour of the partition as predicted by physical reasoning.

The geometrical theory of diffraction in its cylindrical wave formulation gives quite an adequate solution to the antenna problem presented in this thesis. It has an advantage in visualization and also the solution is expressed mostly in terms of the well known Fresnel Integrals. The Fresnel Integral representation is exact in the case of thin partitions but only approximate in the case of a partition of any included angle for points well away from a shadow boundary. For points on a shadow boundary, the diffracted field can be taken to be one half of the incident field. When the propagation is at right angles to the edge of a partition, the propagation constant in the Fresnel Integrals should be taken to be $k = 2\pi/\lambda$ where λ is the wavelength. When the propagation is at an angle θ with the edge of a partition, the transverse propagation constant $k_r = \frac{2\pi}{\lambda} \sin\theta$ should be used in the Fresnel Integrals; the diffraction of the component parallel to the edge can be taken to be the radiation pattern of the edge line. Generally for most practical cases, first order diffraction terms are quite adequate. However better results can be

obtained by including higher order diffraction terms. This is done by treating a diffracting edge as a line source.

The partition can be used in the medial plane of symmetry of any distributed antenna system. Its effect, on the radiation patterns depends upon the electric polarization with respect to the edge. This has been discussed in Chapter Two.

The new type of long slot leaky wave antenna described in Chapter Three can be used together with an H plane partition to form a ground based localizer. Because of the opposite polarity of the electric field at the top and bottom of the slot and because of the phase reversal upon reflection, direct and reflected signals are expected to reinforce at angles of elevation of the order of 2° to 5°. This, together with the following characteristics due to a partition:

(i) a sharp null in the difference pattern,

(ii) the lining up of the nulls and sidelobes of the sum and difference patterns,

will make the proposed ground based localizer an attractive system. For broadband operation, the long slot should be terminated and a broadband tapered strip line balun should be used for a coaxial feed line or a tapered waveguide for a waveguide feed line. However the proposed ground based localizer is not perfect. At higher angles of

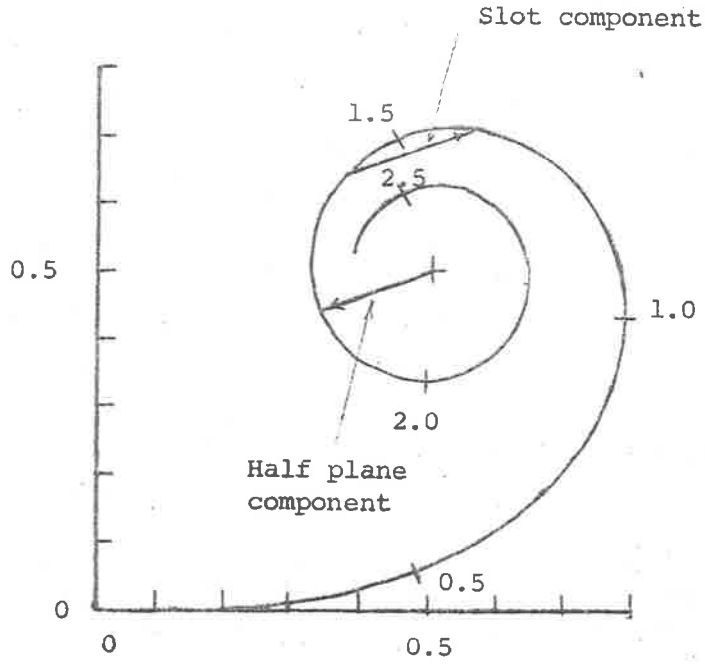

Fig. 1. Cornu spiral and designing concept for slotted partition.

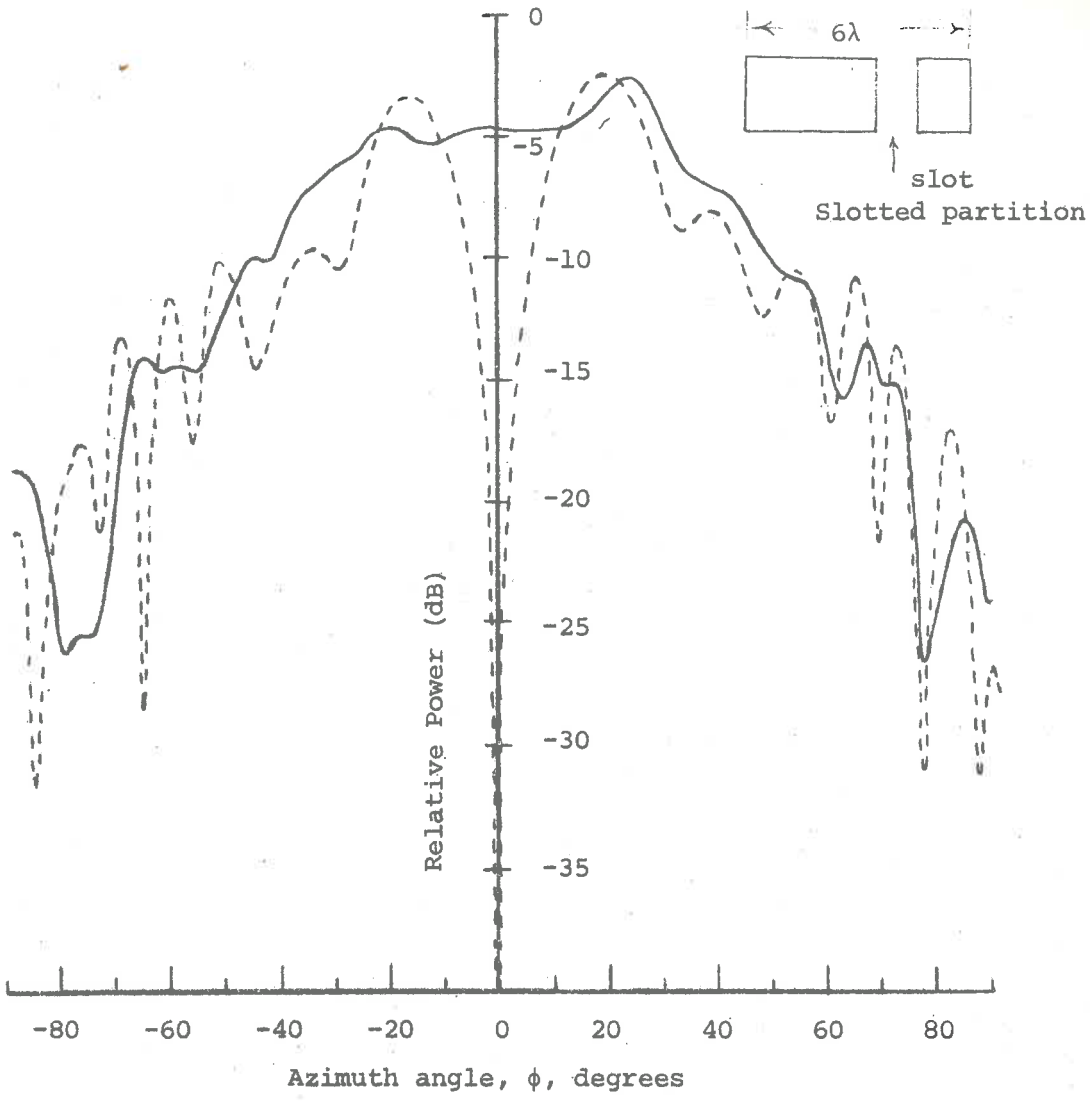

Fig. 2. Effect of a slotted partition on sum and difference patterns of two slot dipoles.

elevation, due to the phase reversal of the sidelobe in the sum pattern, false courses could be set up by the sidelobes of the sum and difference patterns. This is not at all serious because the sidelobes can be suppressed and what is more an aircraft does not often come to land at a steep angle of descent. Low silhouette requirements dictate the height of the partition. For a low partition, diffraction ripples appear in the difference patterns. Thus the proposed ground based localizer appears to be more attractive in microwave systems. One way of reducing the diffraction ripples in the difference patterns is to use a slotted partition. This type of partition will still leave the sum pattern unchanged. While the slot can be designed in such a way that the diffracted contributions from the same side of the partition cancel each other out in the difference pattern. The designing concept [30] is given in Fig. 1 and the results of such a design is seen in Fig. 2. It is demonstrated clearly that the diffracted ripples in the difference pattern are considerably suppressed when the results in Fig. 2 are compared with those in Fig. 10(b), Chapter Four.

The work done in this thesis is by no means complete. The solution to the problem of diffraction off the edge of a partition has been presented in general forms. The use of a partition in a paraboloidal reflector system deserves some serious consideration and the need to suppress the large diffracted ripples due to a low partition in the resulting difference patterns should be studied more thoroug

REFERENCES

[1] Willoughby, E.O.: Navigation Free of False Courses, Electronic Engineering, Dec. 1969, pp. 62-63.

[2] Born, M. and Wolf, E.: Principles of Optics, Pergamon Press, 2nd Edition 1964, pp. 556-589.

[3] Plonsey, R.: Diffraction by Cylindrical Reflectors, Monograph No. 281R, IEE Proc., Jan. 1958, pp. 312-318.

[4] Moullin, E.B.: On the Current Induced in a Conducting Ribbon by a Current Filament Parallel to it, Monograph No. 71R, IEE Proc., 101, Part IV, August 1953, pp. 7-17.

[5] Keller, J.B.: Diffraction by an Aperture, J. of Appl. Physics, 28 April 1957, pp. 426-444.

[6] Rudduck, R.C.: Application of Wedge Diffraction to Antenna Theory, Electrosience Lab., Ohio State Univ. Research Found. Rept. 1691-13, June 30th, 1965 (NASA Rept. CR-372).

[7] Pauli, W.: On Asymptotic Series for Functions in the Theory of Diffraction of Light, Phys. Revue, 54, Dec. 1938, pp. 924-931.

[8] Wait, J.R.: Radiation from a Line Source Adjacent to a Conducting Half Plane, J. of Appl. Physics, 24, 1953, pp. 1528-1529.

[9] Harrington, R.F.: Time Harmonic Electromagnetic Fields, McGraw-Hill Book Co. Inc., New York, 1961, pp. 238-242.

[10] Ohba, Y.: On The Radiation Patterns of a Corner Reflector Finite in Width, I.E.E.E. Trans. on Antennas and Propagation, AP-11, March 1963, pp. 127-132.

[11] Willoughby, E.O.: Travelling Wave Slot Antennas for Low Angle of Fire, Proc. I.R.E.E. (Australia), 30, May 1969, pp. 150-153.

[12] Tran Van Nguyen: Sidelobe Suppression in a Cavity Backed Long Slot Antenna, I.E.E.E. Trans. Sept. 1971 (Communications) pp. 677-678.

[12a] Tran Van Nguyen: Transverse Resonance Solutions for a Long Slot Leaky Wave Antenna, I.E.E.E. Trans., Nov. 1972 (Communications) pp. 776-778.

[13] Marcuvitz, N.: Waveguide Handbook, McGraw-Hill, 1951.

[14] Müller, D.E.: A Method for Solving Algebraic Equations using an Automatic Computer, Math. Comput. Vol. 10-11, pp. 208-215, 1956-1957.

[15] McDonald, A.E.: Zeros of Complex Function by Müller's Method, Comput. Cent. Univ. Texas Austin.

* 7a. Russo P.M. et al., IEEE TRANS. Antenna and Propagation, AP-13, March 1965, pp. 219-224

[16] Rotman, W. and Oliver, A.A.: Asymmetrical Trough Waveguide Antennas, I.E.E.E. Trans. on Antennas and Propagation, April 1959, pp. 153-162.

[16a] Goldstone, L.O. and Oliver, A.A.: Leaky Wave Antennas I: Rectangular Waveguides, I.R.E. Trans. on Antennas and Propagation, Oct. 1959, pp. 307-319.

[17] Dunbar, A.S.: On the Theory of Beam Shaping, J. of Appl. Physics, 1952, 23, pp. 847-853.

[18] Shigesawa, H. et al.: Approximate Pattern Calculation of a Leaky Waveguide, I.E.E.E. Trans. on Antennas and Propagation, Jan. 1969, pp. 36-42.

[19] Peters, L. Jr. et al.: R.F.I. Reduction by Control of Antenna Sidelobes, I.E.E.E. Trans. on Electromagnetic Compatibility, Jan. 1964, pp. 1-11.

[20] Jasik, H.: Antenna Engineering Handbook, pp. 30-16,30-17.

[21] Wind, M. et al.: Handbook of Microwave Measurements, Polytechnic Institute of Brooklyn Microwave Research Institute, 2nd Edition 1955.

[22] Teal, G.K. et al.: Attenuator Materials, Attenuators and Terminations for Microwaves, A.I.E.E. Trans., 1948, 67, pp. 419-428.

[23] Wolff, E.A.: Antenna Analysis, John Wiley and Sons, Inc. 1966 Edition.

[24] Hansen, R.C.: Microwave Scanning Antennas, Volume III, Array Systems, PP.191-194, Academic Press, 1966 Edition.

[25] Cohen, A. et al.: The Lincoln Laboratory Antenna Test Range, Microwave J., Vol. 4, No. 4, April 1961, pp. 57-65.

[26] Silver, S.: Microwave Antenna Theory and Design, Radiation Lab. Ser., No. 12, McGraw-Hill, 1949

[27] Pexton, R.F.: Bessel Functions J_n and Y_n (first and second kind) Berkeley, U.S.A.

[28] I.B.M. Scientific Subroutine Package: Fresnel Integrals.

[29] Harder, D.: Simpson's Rule Integration Los Alamos Scientific Laboratory, U.S.A.

[30] Becker, J.E. et al.: A Double Slot Radar Fence for Increased Clutter Suppression, I.E.E.E. Trans. on Antennas and Propagation, Vol. AP-16, No. 1, Jan. 1968, pp. 103-108.

[31] Cumming, W.A. et al.: Analysis and Reduction of Scattering from the Feed of a Cheese Antenna, I.R.E. Trans. on Antennas and Propagation, July 1959, pp.226-233.

APPENDIX A

A SLOT LINE PARAMETRIC STUDY

As discussed in chapter three, because of the many parameters involved in the equation for the transverse resonance of the long slot leaky wave antenna, viz. slot width (SW), slot depth (SD), narrow side (AN), wide side (AW), strip line thickness (T1) and cavity wall thickness (T2), it is not possible to present the solutions in a general form which will then apply to all cases or at least a majority of cases. However by assuming zero thickness, some physical insight into the behaviour of the slot antenna can be gained by obtaining solutions of the transverse resonance equation for various AW, AN and SW and plotting the results obtained for the attenuation and velocity ratio against SD. Of course there is an infinite number of possible combinations and to obtain all such solutions is impossible

Since multimode operation depends on the dimension of AW, it is therefore considered that AW should have values above and below that of the cut off dimension of the TE_{01} mode i.e. AW = .3λ, .6λ, .9λ.

Sometimes large depth is not practically a good virtue, whereas a wider AN and a shallower AW could do the job better. In such a case AN could be expected to be larger than the cut off dimension

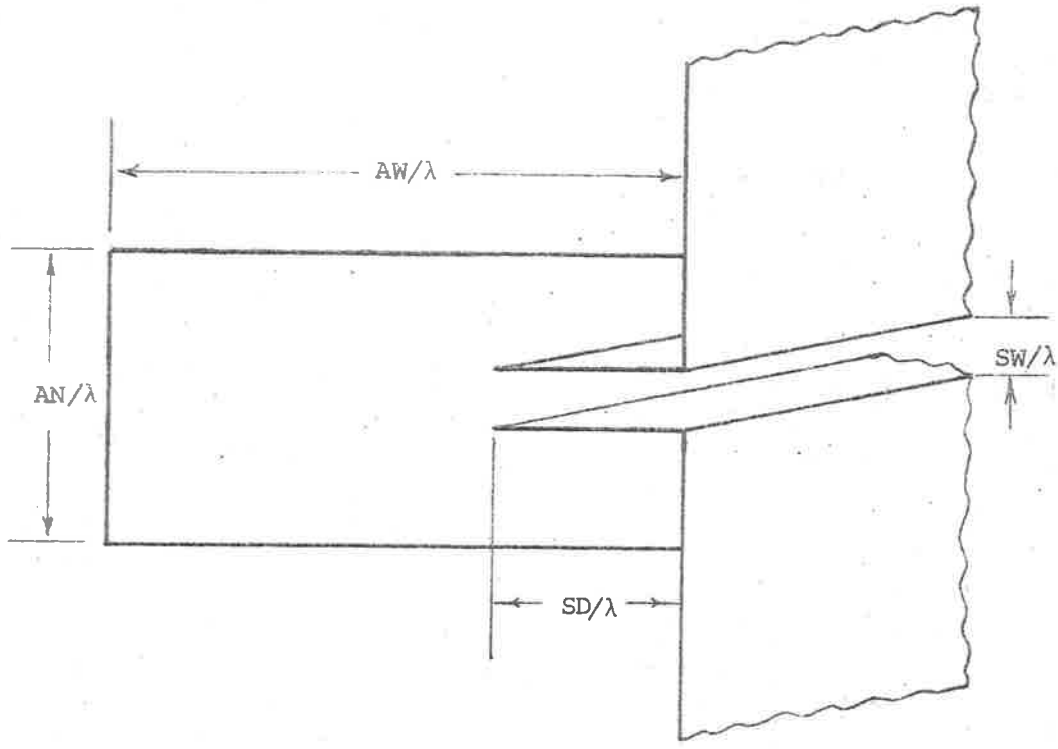

Parameters in slot line parametric investigation.

thus the chosen values for AN are .1λ, .15λ and .6λ.

From the strip line theory, only the TEM exists if the width of the line is made less than λ/4, this puts the limitation on the variation of SD. It can vary from a small value of .25λ. The limitation can be waved if multimode operation involving one more higher order mode is anticipated.

The slot width (SW) is finally selected by taking AN and the characteristic impedance of the line into consideration. Some useful values of SW are 0.005λ, .01λ and .04λ.

The results obtained for the attenuation and velocity ratio can be divided into two types as follows:

Type I includes the following:

(a) AW = .3, AN = .15, SW = .005	(Fig. 1a)	
SW = .01	(Fig. 1b)	
SW = .04	(Fig. 1c)	
(b) AW = .6, AN = .15, SW = .005)	Fig. 2a for 1st solutions	
SW = .01)		
SW = .04)	Fig. 2b for 2nd solutions	
(c) AW = .9, AN = .15, SW = .005)	Fig. 3a for 1st solutions	
SW = .01)		
SW = .04)	Fig. 3b for 2nd solutions	

Type II includes the following:

(a) AW = .3, SW = .01, AN = .1 (Fig. 4)
AN = .6

(b) AW = .6, SW = .01, AN = .1) Fig. 5a for 1st solutions
AN = .6) Fig. 5b for 2nd solutions

(c) AW = .9, SW = .01, AN = .1) Fig. 6a for 1st solutions
AN = .6) Fig. 6b for 2nd solutions

It is interesting to note that for the dimensions in type I(a) and II(a), there is only one acceptable set of solutions to the transverse resonance equation.

From Fig. 1a, 1b and 1c of type I, the velocity ratio is seen to be very close to unity and does not change very much with the slot depth (SD). The attenuation is large when the slot width (SW) is large, which is to be expected from physical consideration. Its change with slot depth (SD) is more rapid as the slot width (SW) decreases.

Fig. 2a presents the first set of solutions for the transverse resonance equation with the characteristics that the velocity ratio is close to unity and the attenuation is large for a large slot width (SW) and decreases as the slot depth (SD) increases. Fig. 2b shows the 2nd set of solutions, the velocity ratio is much less than unity. It is in fact centred around 0.5 and the attenuation is a couple of order of magnitude larger than that given in Fig. 2a. This means that the first higher order mode, the TE_{01} mode, cannot

travel far down the slot before being completely attenuated.

Fig. 3a and 3b represent the first set and 2nd set of solutions respectively. The velocity ratio of the 2nd set of solutions is closer to the first i.e. unity, whereas the attenuation maintains the same trend as described earlier for the type I(a) and I(b) solutions. Since the attenuation is about the same order and velocity ratio is quite close to one another, it is anticipated that a multimode operation could be used here.

The above discussion also applies to the solutions type II(a), (b) and (c). Type II(b) and II(c) have each two sets of solutions like type I(b) and I(c), the second set of solutions as above corresponds to the TE_{01} being excited in the backing cavity.

The approximate constant variation of the velocity ratio together with the variation of the attenuation with the slot width (SW) and more significantly with the slot depth (SD) suggest that distributions other than uniform can be created along the slot. Good gaussian and tapered distributions have been obtained and given in chapter three. The antenna is capable of sidelobe suppression as much as 10 dB and beam shaping.

This modest parametric study of the slot antenna mounted in an infinite ground plane is by no means complete. It is hoped that it

will give a good insight into the behaviour of the slot antenna. The case of the antenna in free space is not much different from the infinite ground plane case as far as the velocity ratio is concerned, but the azimuth directivity is expected to be less due to the spreading of the radiated energy into the whole space.

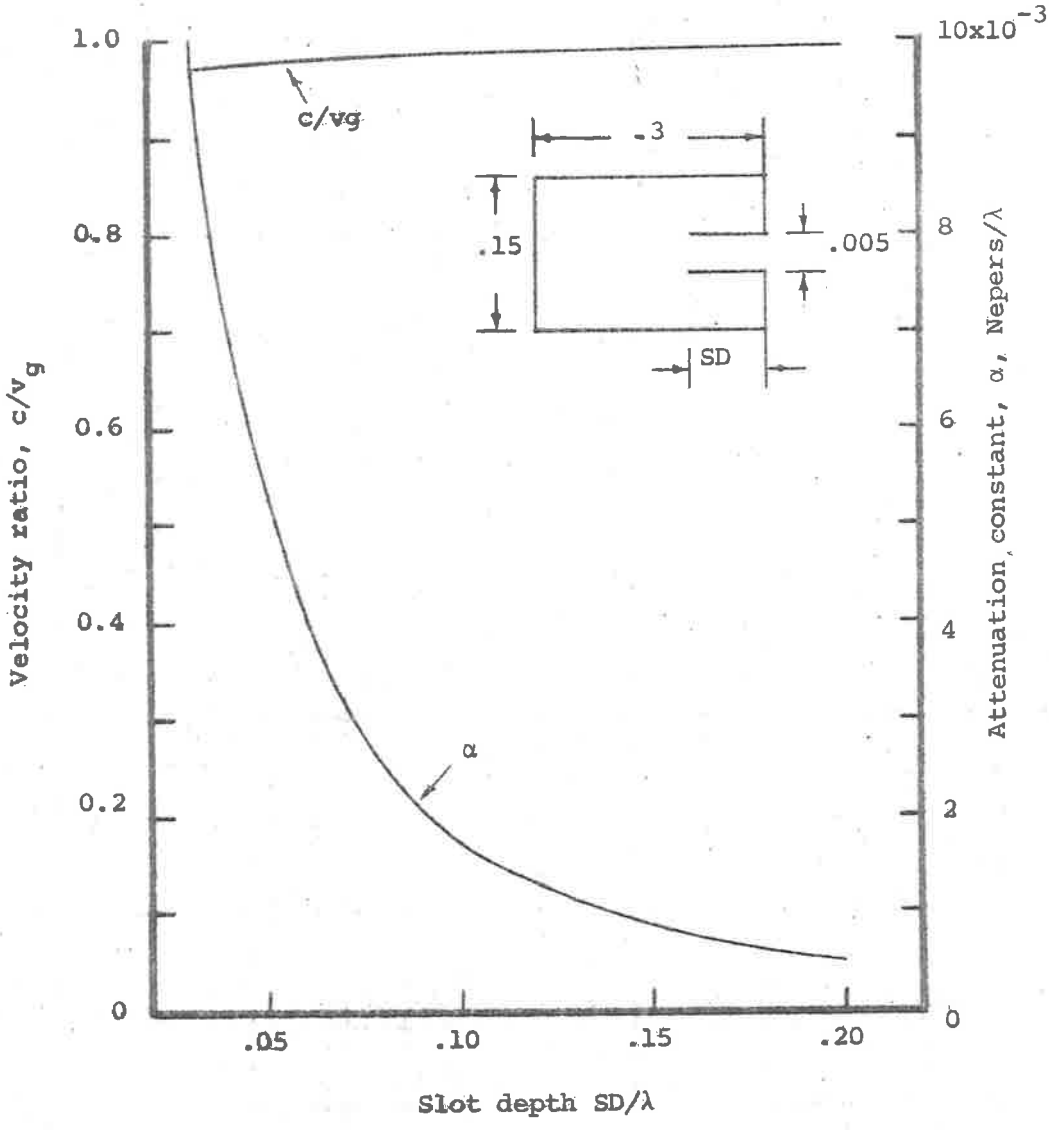

Fig. 1a. Variation of velocity ratio and attenuation constant vs slot depth.

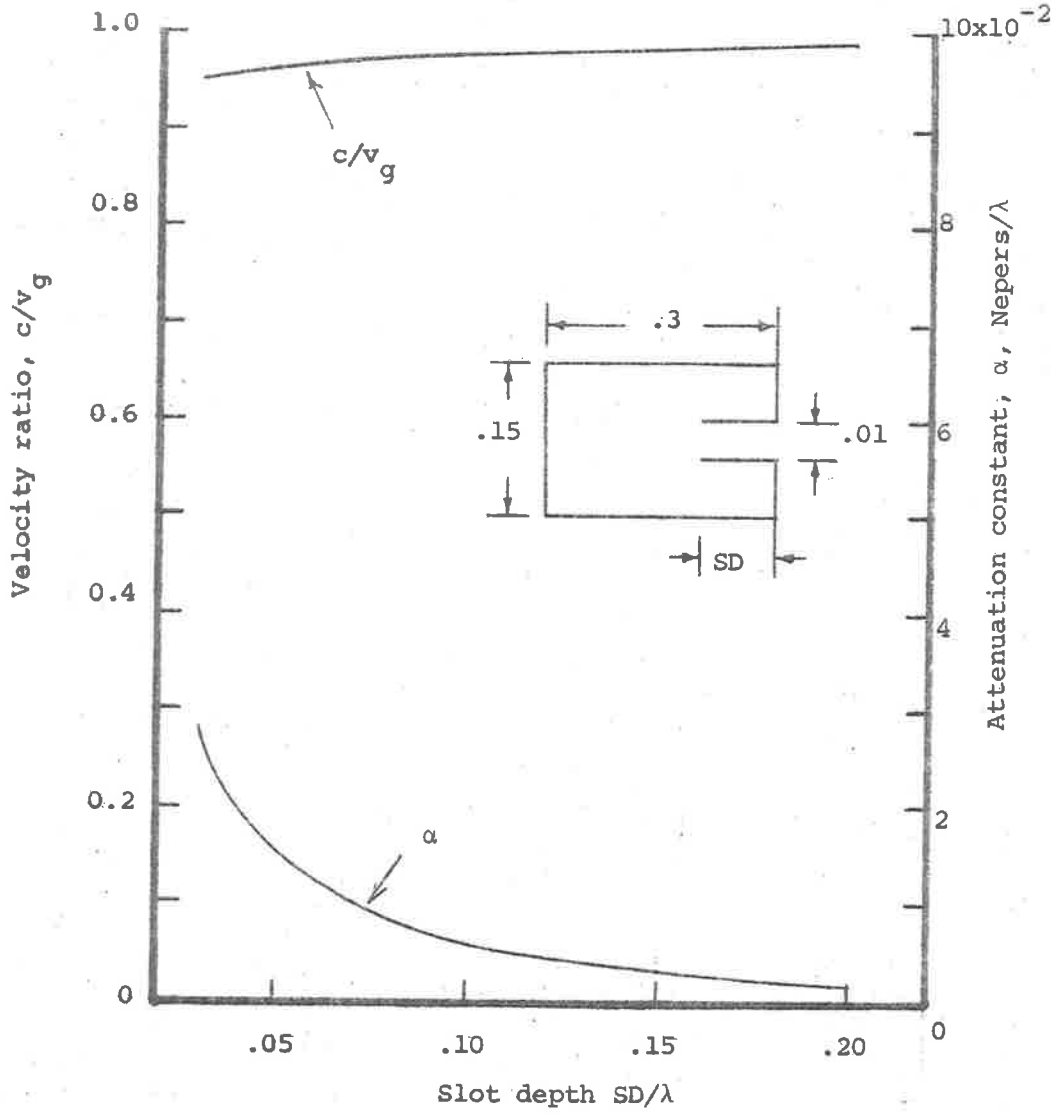

Fig. 1b. Variation of velocity ratio and attenuation constant vs slot depth.

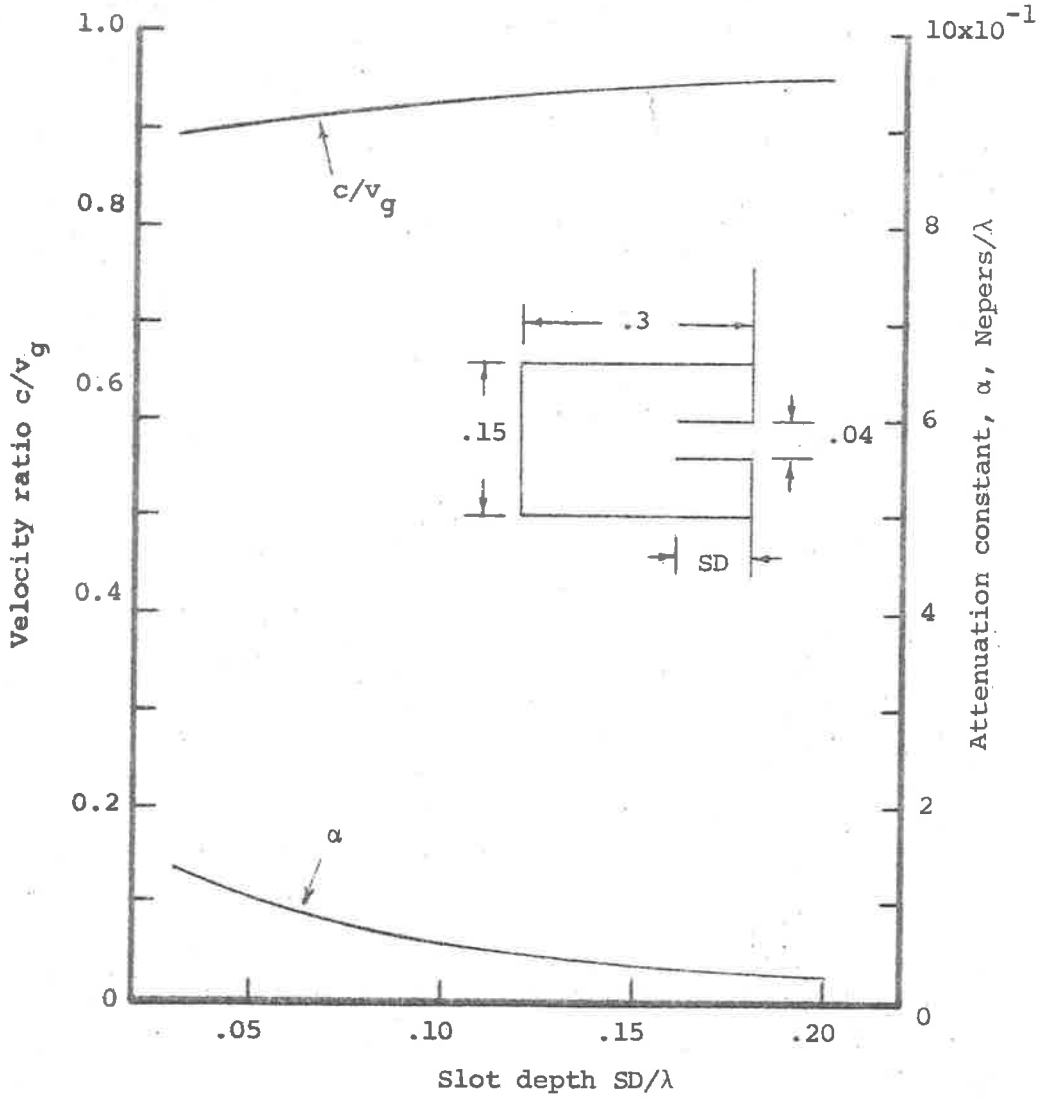

Fig. 1c. Variation of velocity ratio and attenuation constant vs slot depth.

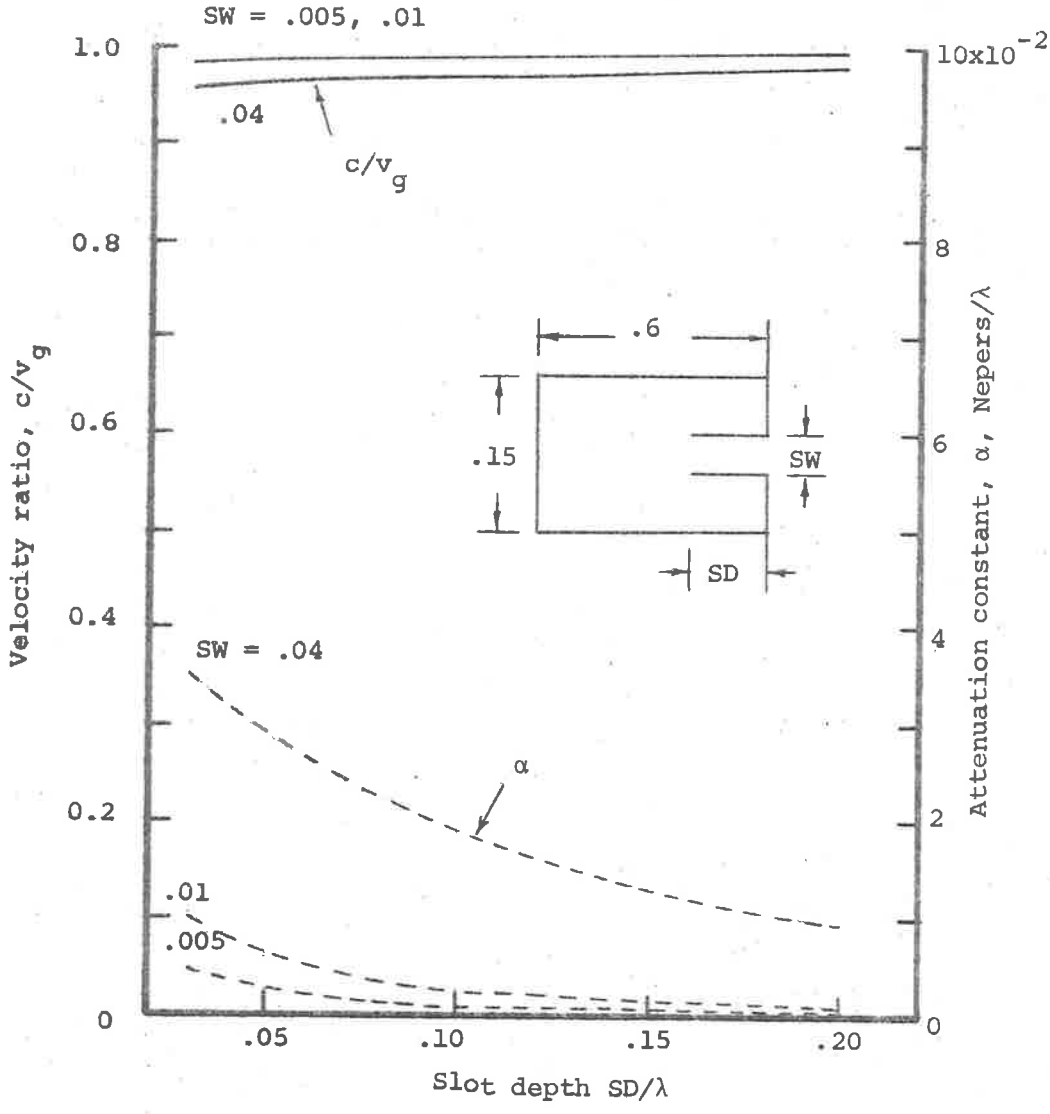

Fig. 2a. Variation of velocity ratio and attenuation constant vs slot depth.

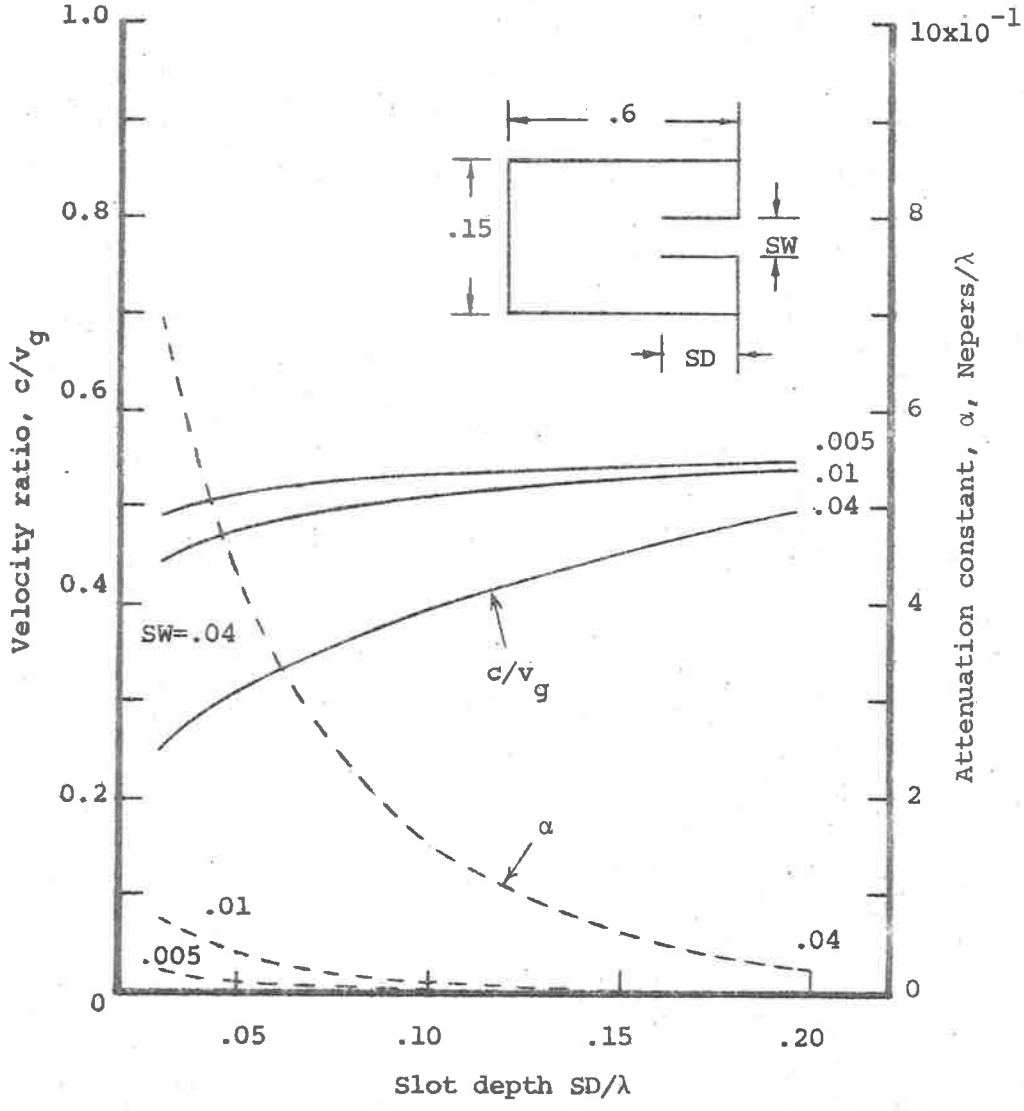

Fig. 2b. Variation of velocity ratio and attenuation constant vs slot depth.

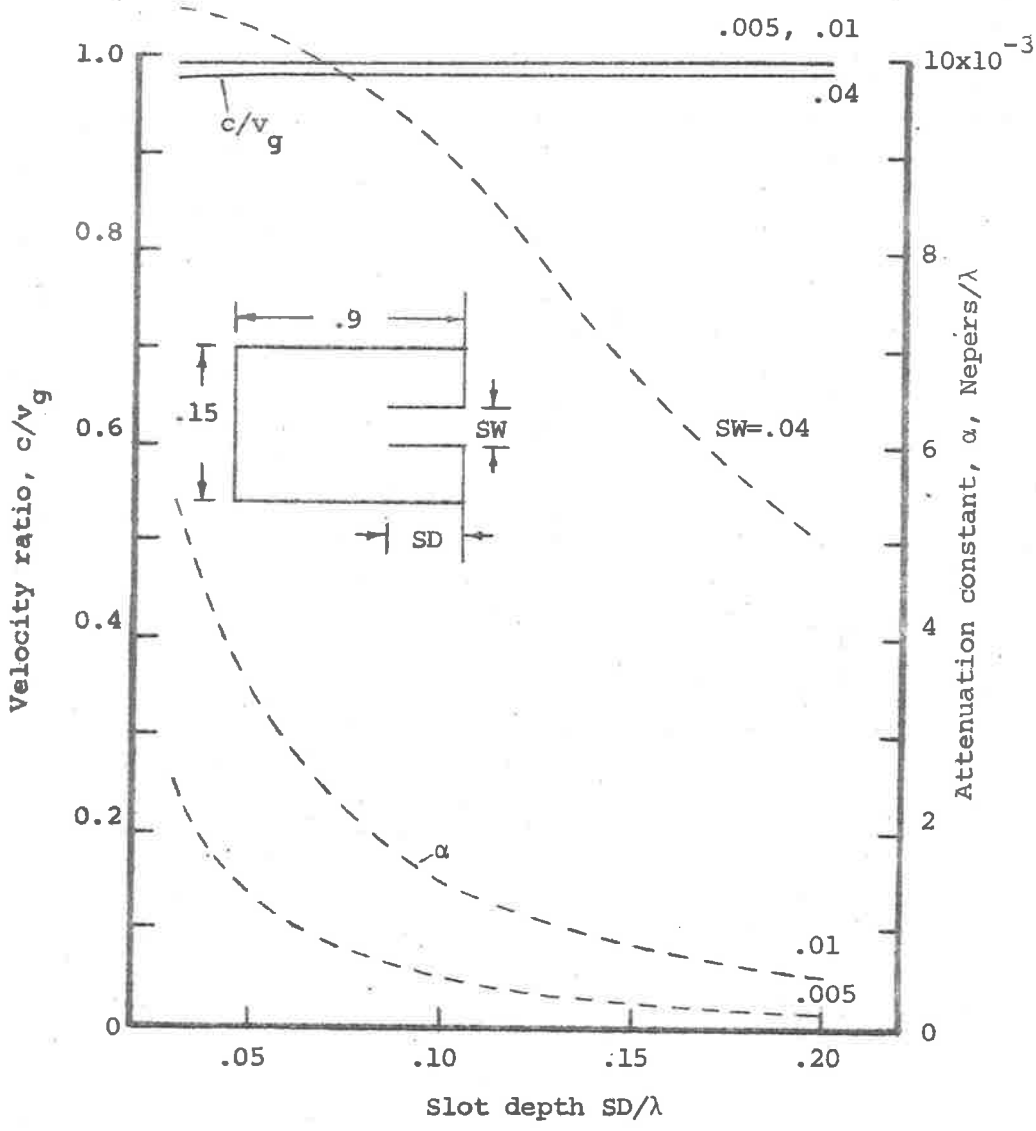

Fig. 3a. Variation of velocity ratio and attenuation constant vs slot depth.

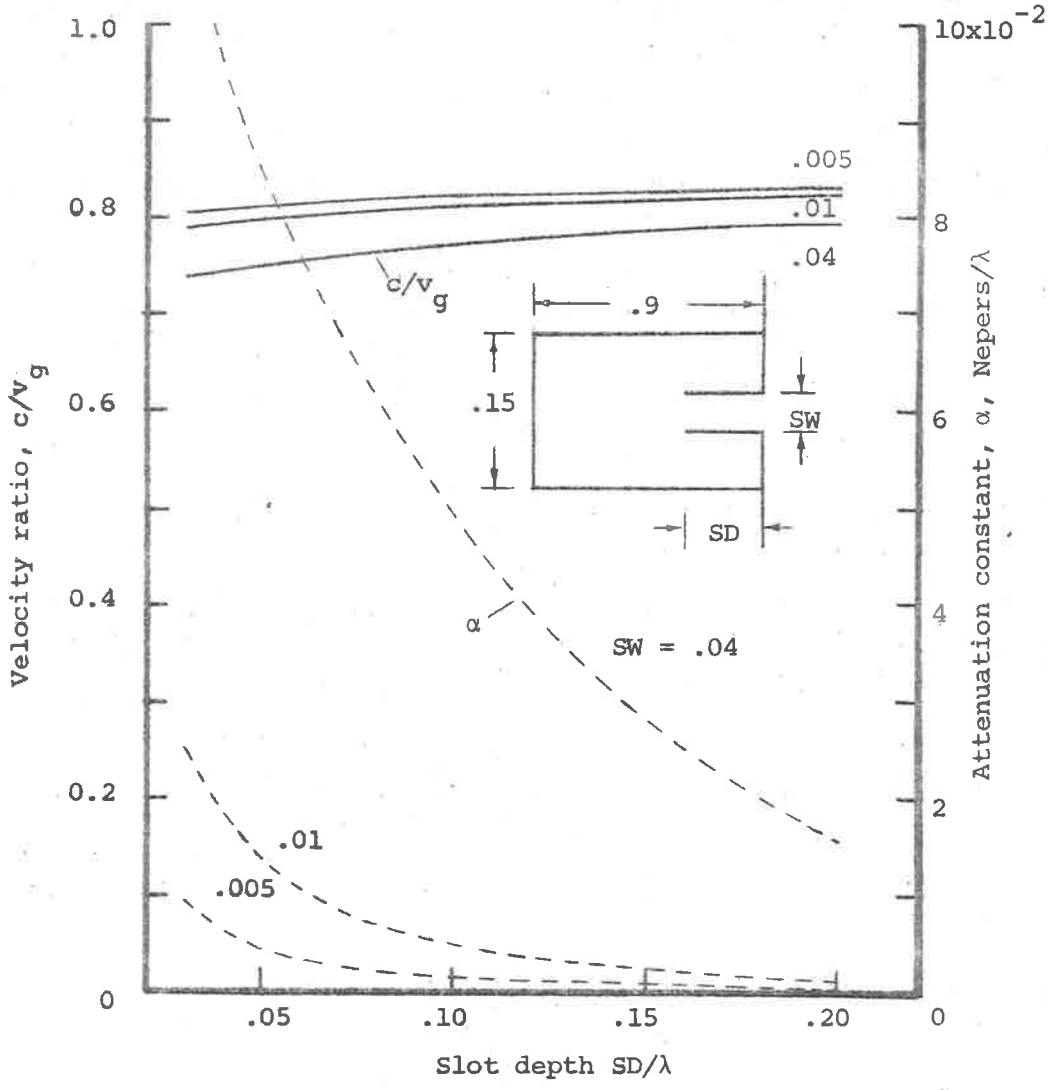

Fig. 3b. Variation of velocity ratio and attenuation constant vs slot depth.

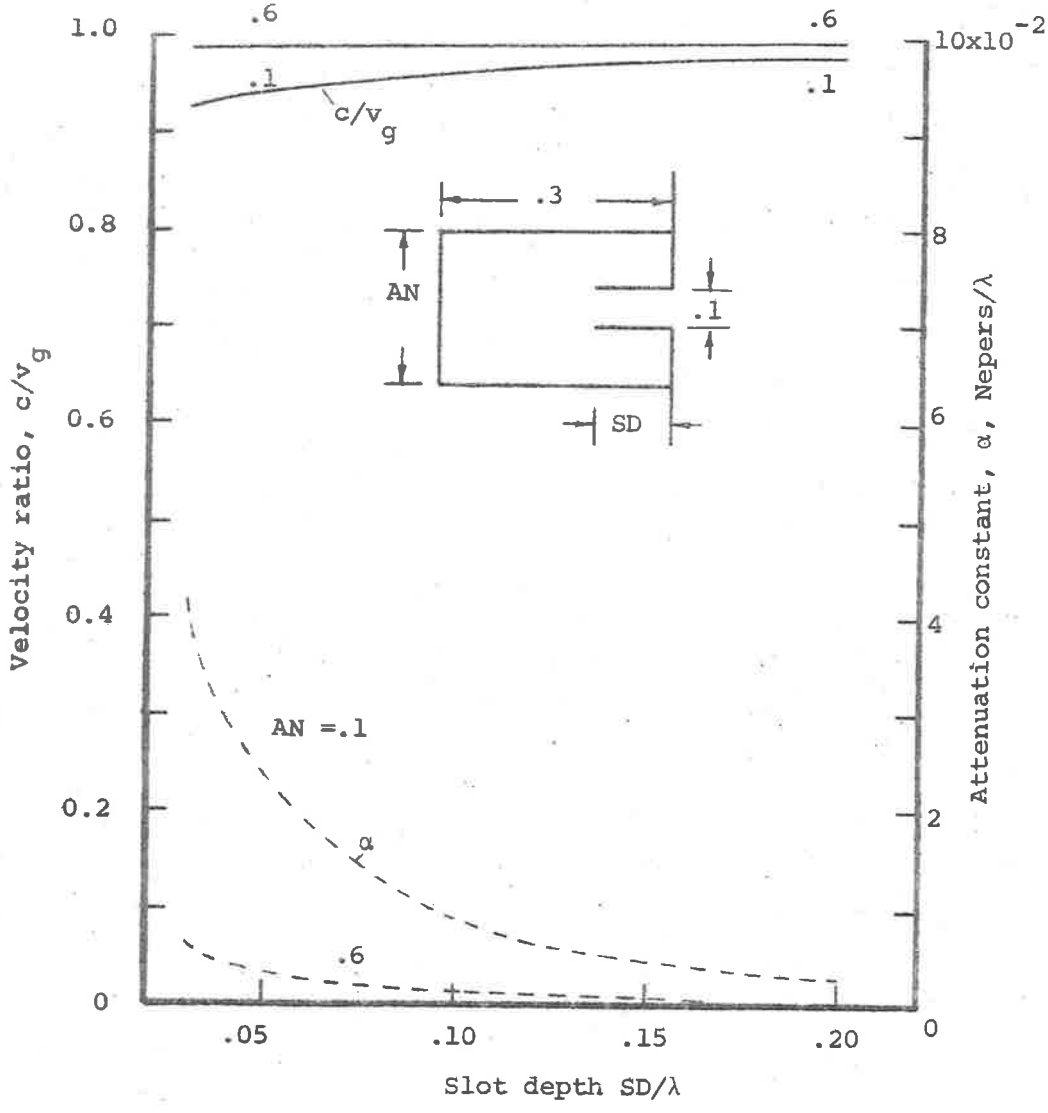

Fig. 4. Variation of velocity ratio and attenuation constant vs slot depth.

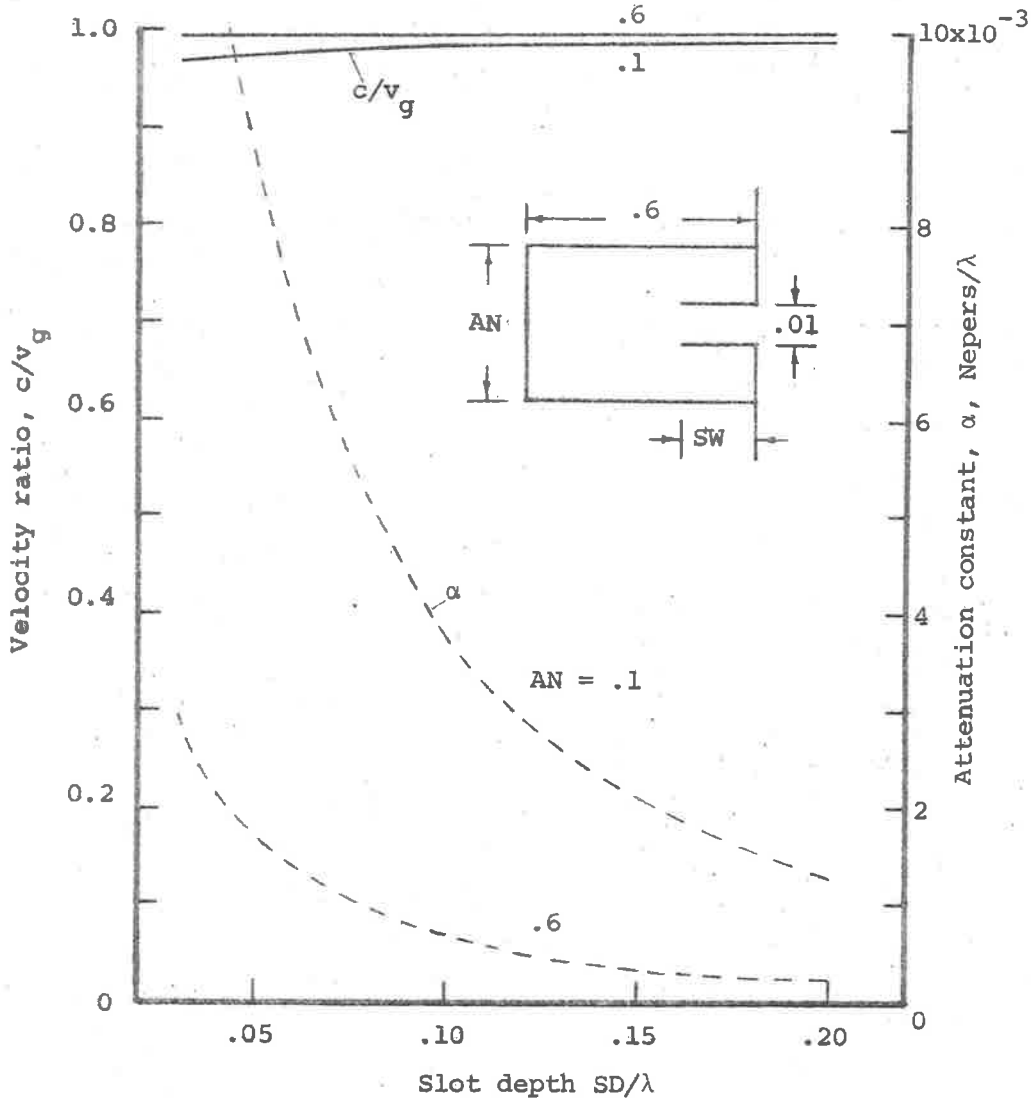

Fig. 5a. Variation of velocity ratio and attenuation constant vs slot depth.

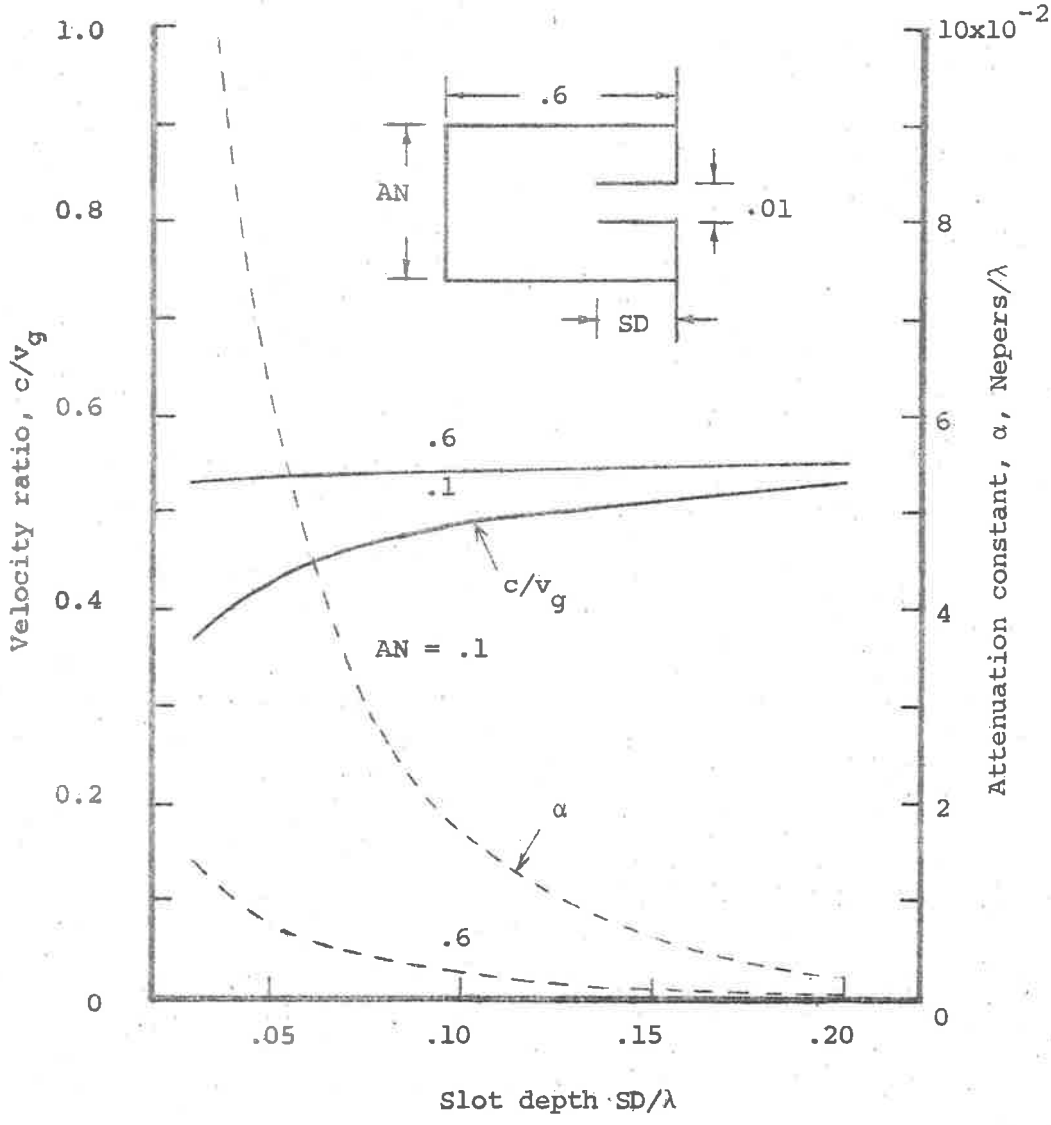

Fig. 5b. Variation of velocity ratio and attenuation constant vs slot depth.

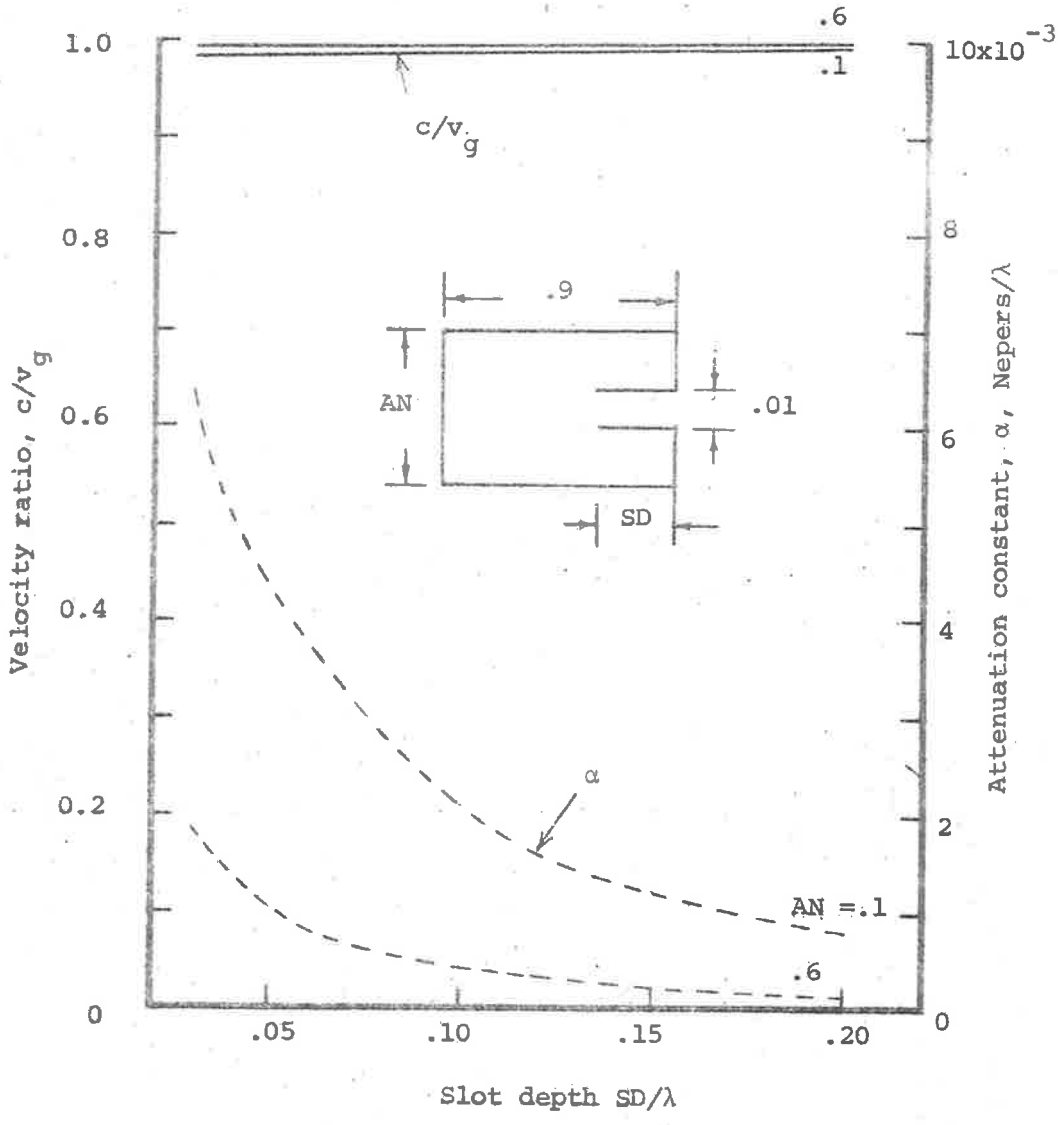

Fig. 6a. Variation of velocity ratio and attenuation constant vs slot depth.

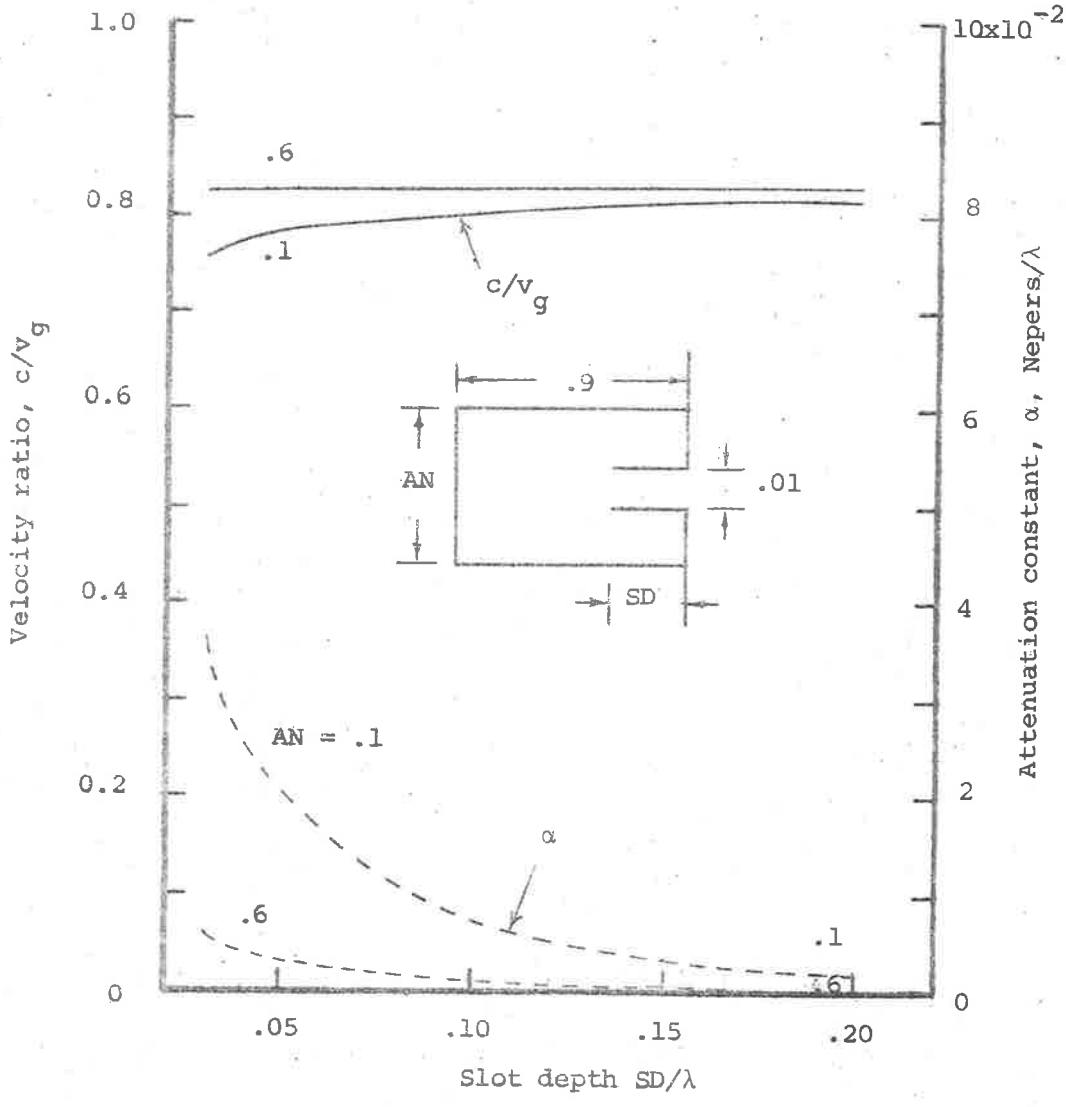

Fig. 6b. Variation of velocity ratio and attenuation constant vs slot depth.

APPENDIX B

SLOT LINE AZIMUTH PATTERNS

The azimuth pattern of a slot line described in chapter three is not necessarily circular. It depends on the geometry of the backing cavity and the depth of the slot i.e. the width of the strip line. The near field azimuth pattern is useful in estimating the amount of direct radiation when such line source is used as a feed for a parabolic reflector, in minimizing the aperture blocking and in suppressing the back lobe due to diffraction by having a steep slope for the field variation along the edge [19]. The control of the azimuth patterns can be achieved by adding narrow strips of metal bent at various angles along the sides bordering the slot.

The method of measurement consists of mounting a terminated slot antenna on a vertical stand well away from the ground with the main beam shooting to the sky, and picking up the signal the slot radiates at various azimuth angles by a small probe. The cable is kept at right angles to the electric field to reduce the current being set up on it to a minimum. The signal received is fed through a variable attenuator and then a crystal detector which in turn drives a tuned amplifier level meter (at 1 KHz). The reading is taken from that of the variable attenuator which brings the

level meter to the same value. Thus the measurement depends on the accuracy of the variable attenuator and no calibration is necessary for the crystal detector.

The figures presented here are self explanatory and the results obtained show that some success has been achieved by using two simple sideplates to shape the azimuth pattern. It should be added here that the azimuth pattern of the slot antenna could be obtained in principle by solving the boundary value problem of the antenna geometry but such an approach is difficult and time consuming. One such example is seen in [18], and therefore the experimental approach has been adopted here.

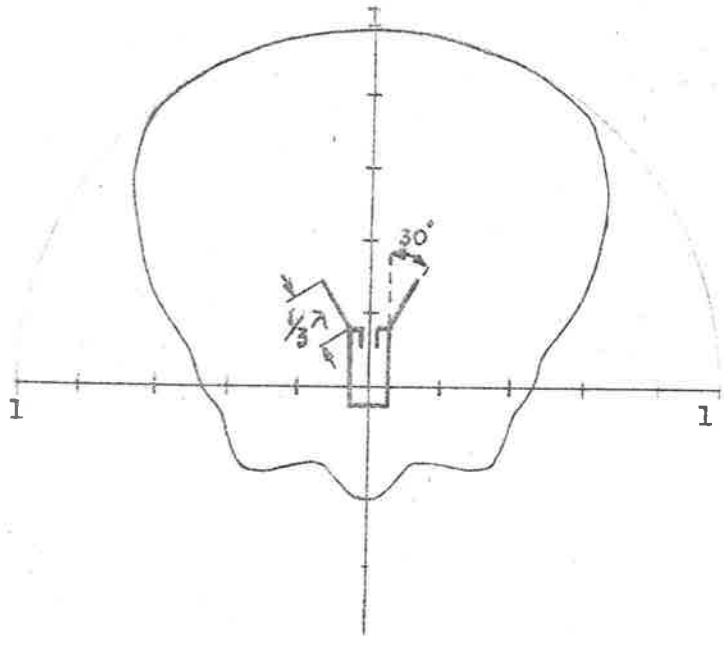

(a)

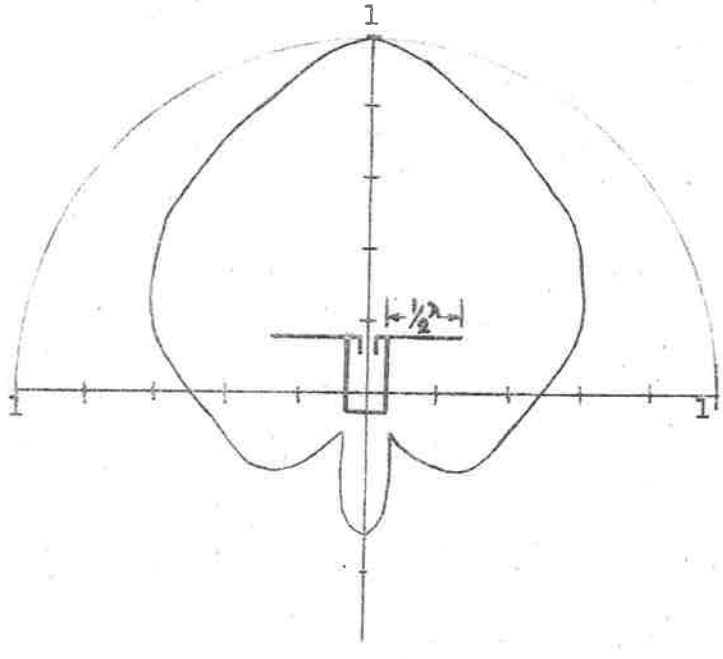

(b)

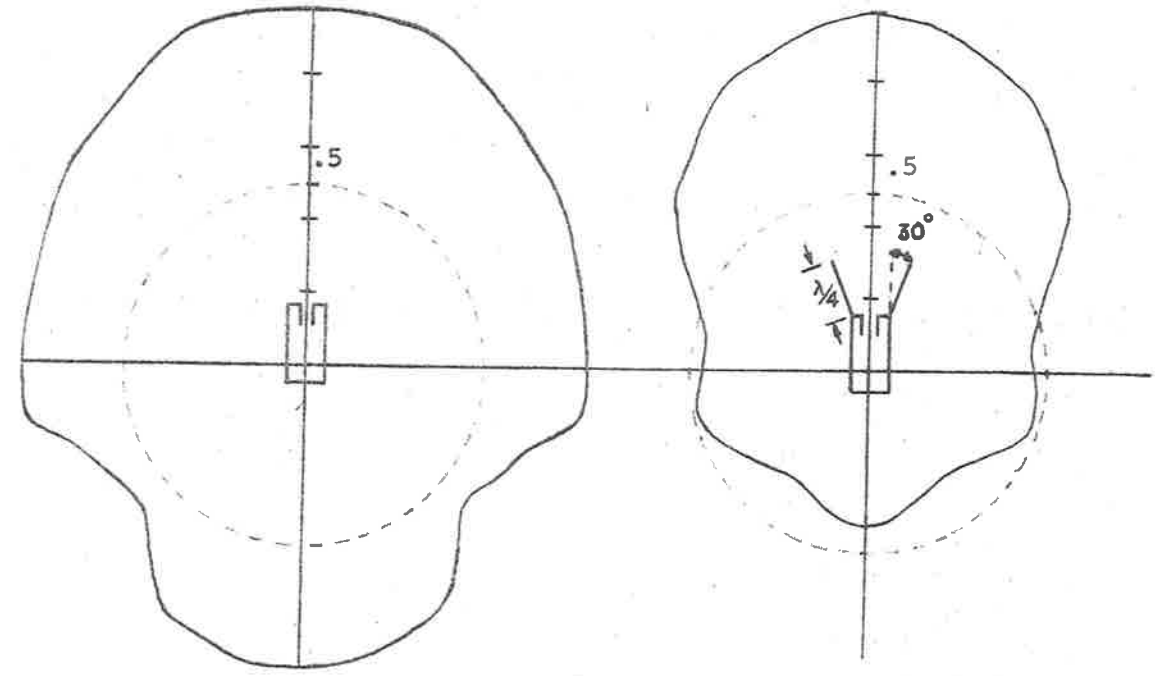

(c) (d)

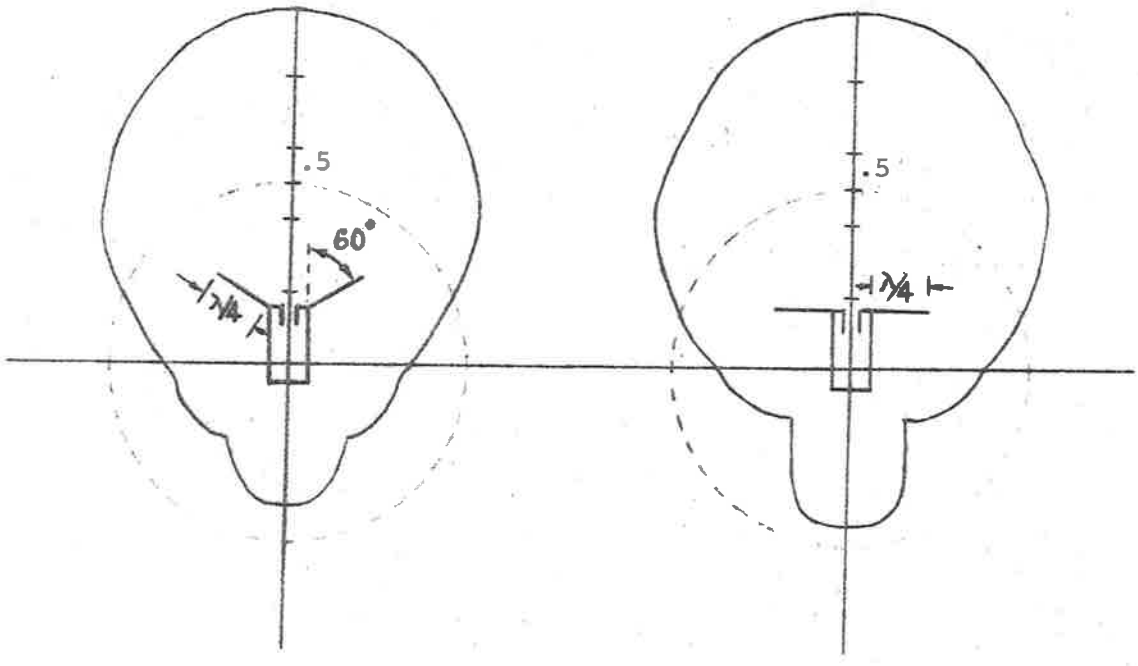

(e) (f)

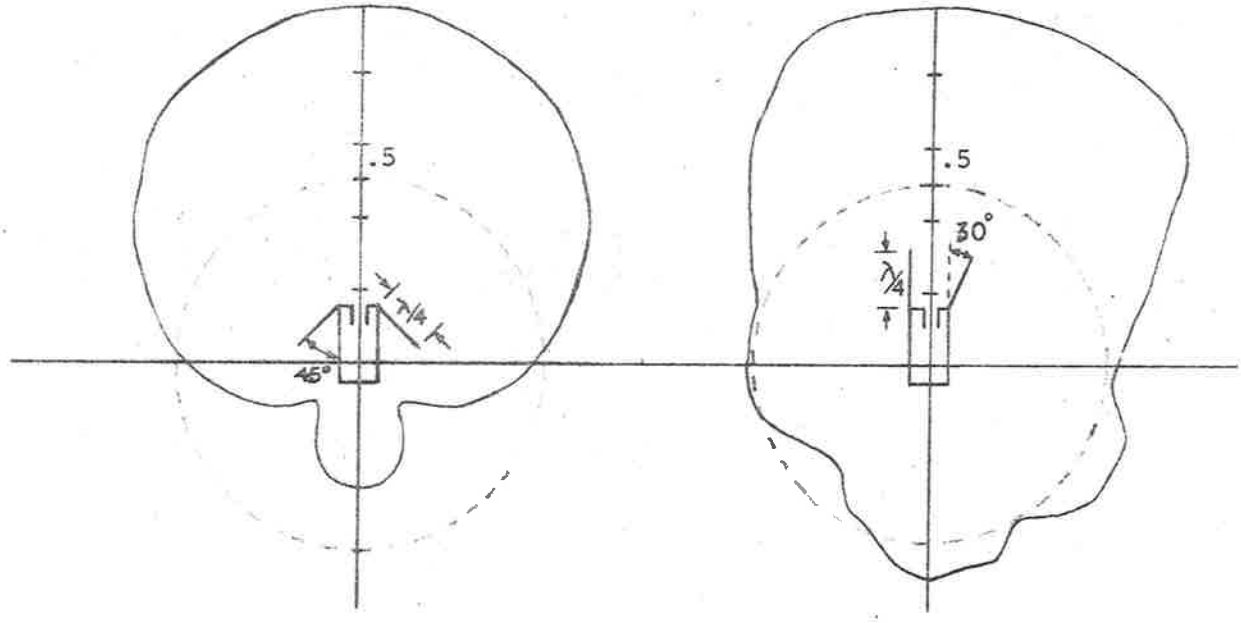

(g)

(h)

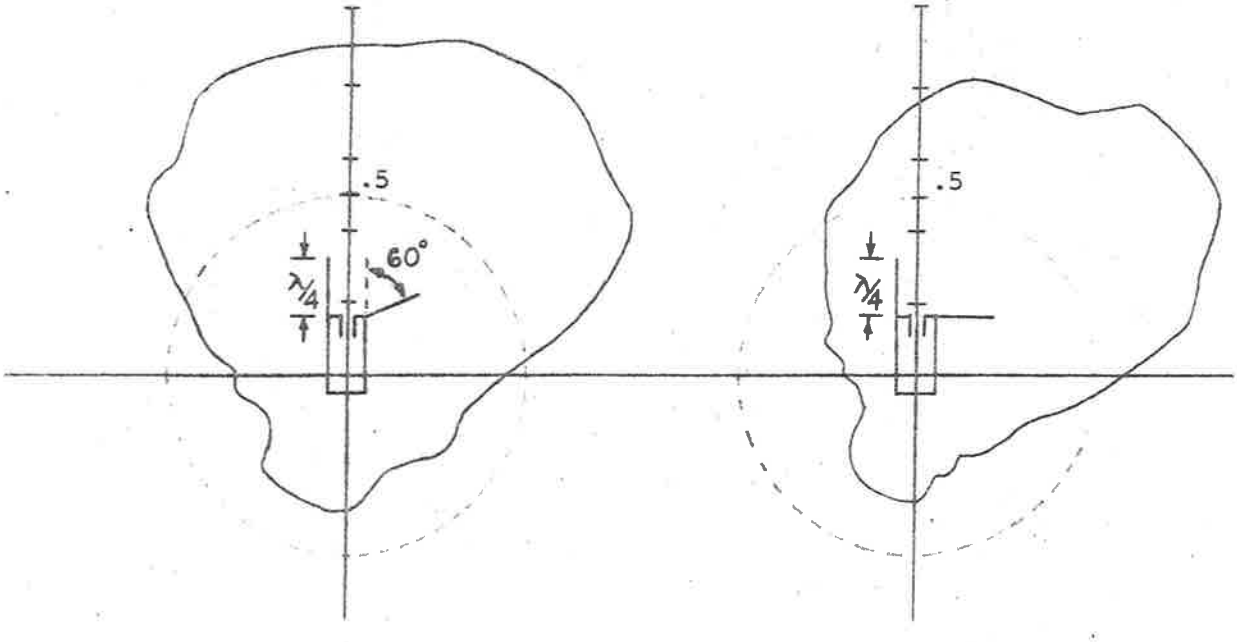

(i)

(j)

APPENDIX C

[A] DESIGN FOR A RING HYBRID

A ring hybrid is used extensively where there is a need for two equal power outputs of the same phase or 180° out of phase to feed two identical loads. Good isolation could be easily realised between a load and the generator and between the two loads. Due to its designed nature, the ring hybrid is frequency sensitive and so narrow-banded.

The Theory

A ring hybrid in parallel form consists of a ring of transmission line of mean circumference of $\frac{6}{4}\lambda$ and four ports as seen in Fig. 1. A signal fed into the ring at port 1, say, will split at the junction into two parts of equal power and set up a pure voltage standing wave within the ring since the ring is assumed to be lossless. The voltages at the various points B, C, D on the ring seen in Fig. 1 are as follows:

(i) at B, a voltage maximum because the two paths $\vec{AB}$ and $\vec{ADCB}$ have the same electrical length.

(ii) at C, a voltage minimum because the two paths $\vec{ABC}$ and $\vec{ADC}$ differ by a half wavelength in electrical length.

(iii) at D, a voltage maximum because the two paths $\overrightarrow{ABCD}$ and $\overrightarrow{AD}$ differ by one whole wavelength in electrical length.

Thus the positions of voltage maximum and minimum will alternate every $\lambda/4$ on the ring. A matched load placed at a position of voltage maximum will derive maximum power output whereas at a voltage minimum will derive no output. It is essential that each arm should be terminated by a matched load to preserve the balance of the ring.

Using the above characteristics of the ring, two signals of the same phase or 180° out of phase can be easily achieved. For instance an input fed into port 1 will give an output each at port 2 and 4 of equal power and opposite phase and no power output at port 3. Similarly, an input fed into port 2 will give an output each at port 1 and 3 of equal power and same phase and no power output at port 4. For an input at 2, say, any small mismatch from the load at 1 will tend to cancel out at 3 and vice versa, and any mismatches from the two identical loads at 1 and 3 will cancel one another out at 2. Thus good isolation is obtained between the two loads themselves and between them and the generator. Port 4 is usually terminated in a dummy matched load.

By using the reciprocity theorem, any two signals may be added

to or subtracted from one another. The signals when fed into ports 1 and 3 will give the sum at port 2 and the difference at port 4, if the fourth port is terminated in a matched dummy load.

The Design

The equivalent circuit for a ring hybrid in parallel form is given in Fig. 2. Assuming $Z_s = Z_o$, the impedance presented at A by each load Z_L at B and D must be $2Z_o$, thus the characteristic impedance of the quarter wave transformer Z_1 must be:

$$Z_1 = \sqrt{2Z_o Z_L} \qquad \ldots(1)$$

if $Z_L = Z_o$ then

$$Z_1 = \sqrt{2xZ_o} \qquad \ldots(2)$$

Thus the characteristic impedance of a ring arc is $\sqrt{2}$ times the characteristic impedance of a sidearm.

Since the ring hybrid is intended for use with 50Ω loads and source impedance, the characteristic impedance of the ring will be:

$$Z_1 = \sqrt{2} \times 50 = 70.7\Omega \qquad \ldots(3)$$

Such a ring hybrid could be made out of strip transmission line and there is available on the market a dielectric material called Rexolite 2200 of dielectric constant 2.62 (this remains unchanged

over a wide bandwidth from 3 cm to 20 cm) and of thickness 1/8".

The characteristic impedance of a parallel plate transmission line is given by H. Jasik [20]:

$$Z_o = \frac{94}{\sqrt{\varepsilon_r}} \frac{1 - t/d}{\frac{W}{D} + 0.47 + 0.65\ t/D - 1.12(t/D)^2} \qquad \ldots(4)$$

for $t \leq 0.5D$ and $W \geq .35\ (D-t)$.

For Rexolite 2200, t = 0.001", D = 1/4" and $\varepsilon_r = 2.62$.

For $Z_o = 70.7\Omega$ $W_1 = 0.0867"$

$Z_o = 50.\ \Omega$ $W = 0.170995"$

and for f = 2GHz

$$\lambda g_{TEM} = \frac{\lambda_o}{\sqrt{\varepsilon_r}} = 3.628"$$

The Construction

The hybrid was drawn up in indian ink at five times its full size for accuracy with calibrated dimension markings for reducing purposes. The drawing was photographed and reduced to the correct size. A 'positive' negative was then made and etched onto the rexolite in the normal fashion. The resulting hybrid was gold

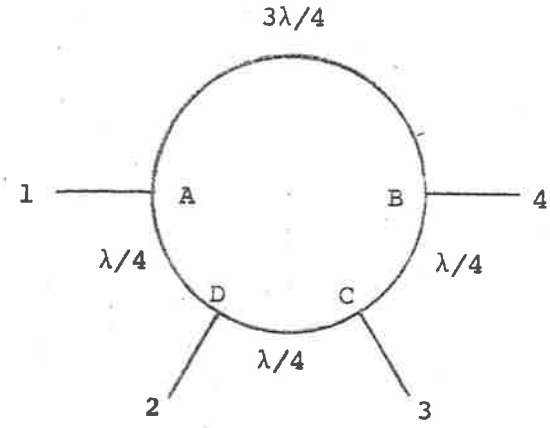

Fig. 1. Ring Hybrid.

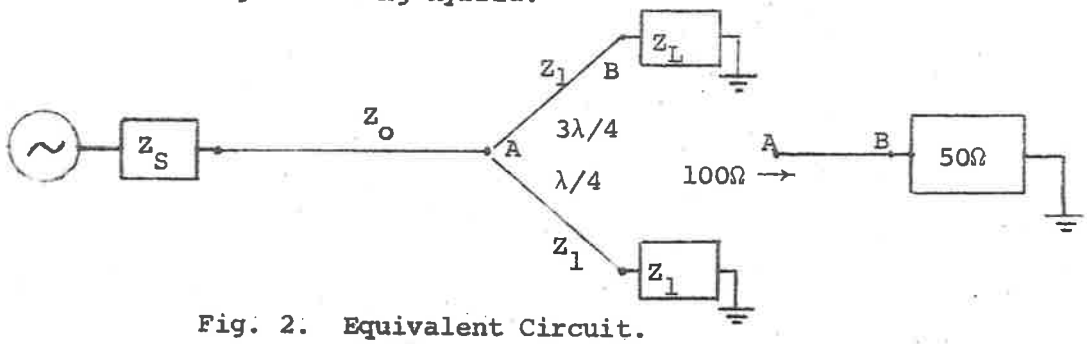

Fig. 2. Equivalent Circuit.

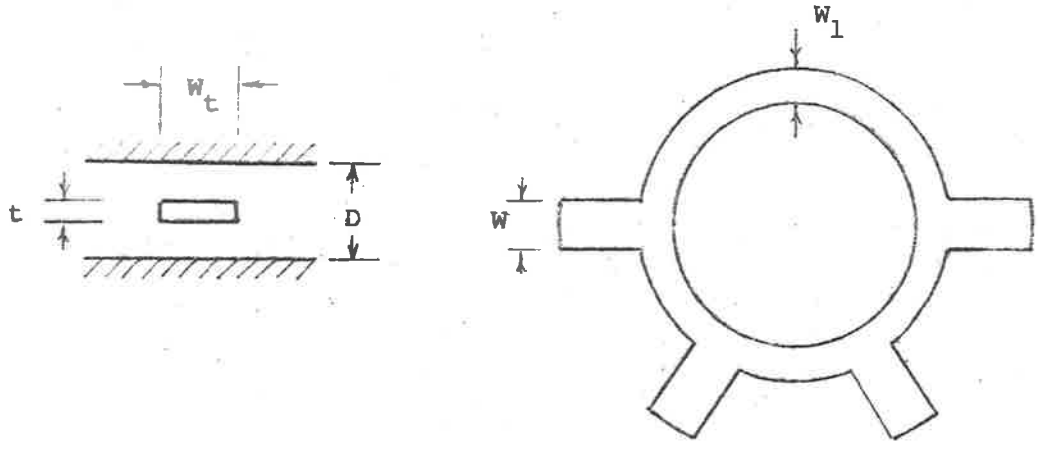

Fig. 3. Strip line ring hybrid.

plated before being assembled and held together by a series of screws not more than $\lambda/4$ apart well away from the ring. Female N-type connectors were then carefully mounted and the whole set up was bolted onto a solid bakelite plate for support.

The Performance

The performance of a ring hybrid is measured in terms of the equal power division and the dB isolation between an input port and the third port. The bandwidth must also be known. The performance of a typical ring hybrid designed for the frequency of 2GHz is shown in the following table:

TABLE I

	Frequency (GHz) →								
Relative Power (dB) →	1.92	1.94	1.96	1.98	2.00	2.02	2.04	2.06	2.0
Port 2	0	0	0	0	0	0	0	0	0
Port 4	0.7	0.2	0.3	0	0.1	0.3	0.05	0.1	0.1
Port 3	-23.0	-28.8	-25.1	-30.1	-32.9	-29.7	-25.2	-28.8	-27.1

The results in Table I were some typical ones obtained by feeding a signal kept at a predetermined constant level into port 1. Signal was also fed into the other ports and the measurements indicated that the order of magnitude was the same as that given in

Table I. The method of measuring the performance of a ring hybrid is set out in Microwave Measurements by Wind and Rappaport [21].

Thus from the above table, it can be said that the ring hybrid have a practically equal power division and an isolation between port 1 and 3 better than 30 dB in a bandwidth of approximately 2%. The VSWR of such a ring hybrid at the centre frequency is better than 1.02.

[B] MAKING A LOSSY TERMINATION

As mentioned in chapter three, there is a need for a lossy termination for the long slot leaky wave antenna to make it a travelling antenna. There is no commercially available lossy terminations which could be used for a slot of width of the order of 1/16" wide and 1/2" to 1" deep. G.K. Teal et al. [22] made an intensive study of the lossy materials and apart from others, came up with the idea of using graphite and silica dispersed in phenol formaldehyde (bakelite) as a microwave absorber. The basic requirements of a good microwave absorber are:

(i) The loss tangent ($\tan\delta$) must be of the order of 0.1 to 1 or even larger,

(ii) or else the dielectric constant value of the material

must be greater than 40.

The dielectric constant of bakelite at 3 GHz increases from 3 to about 70 at 45% graphite by weight. The loss tangent increases in a similar manner and reaches 1.1 at 45% graphite by weight. This data indicate a loss range from .9 to 219 dB per wavelength. For practical reasons,a lossy termination for the slot should be as short as possible or else the length of the antenna will become prohibitively long. Thus the length of the lossy termination was fixed at 1.5λ or less. To reduce the amount of reflection the determination must have a gradual taper. To achieve a VSWR ratio near 1, there was no option but to experiment with various compositions of silica, graphite and bakelite. The following compositions appeared to give the best result:

(24%C + 76% Bakelite) + 16% (fine Si)

84%

All the above ingredients were commercially available. After having been thoroughly mixed, they were poured into a mould of a desired tapered shape and subjected to a pressure of 10,000 lbs/in^2. The mould was heated slowly from room temperature up to 200^{o}C and kept there for 4-6 mins in an oven. It was then taken out and a bakelite tapered termination was obtained. It took up to half a year to

achieve some success with the above experiments. An ambitious program of analysing and measuring the dielectric constant of the various compositions was abandoned for lack of time and immediate relevency to the present work.

Moulded bakelite with dispersed silica and graphite particles is capable of high power applications.

APPENDIX D

APERTURE FAR FIELD DERIVATION

A comprehensive analysis of aperture radiation fields has been given by E.A. Wolff [23]. The radiation fields from a two dimensional aperture can be determined when the fields and geometry of the aperture are specified. This appendix applies the radiation from an elemental area to a rectangular aperture with normal and oblique plane wave 'incidence'.

An Elemental Area

Considering an elemental area of an arbitrary aperture lying in the plane x = o. Such an elemental area in general can be excited by both electric and magnetic fields. Let $\underline{J}$ and $\underline{M}$ be the electric and magnetic surface current densities and $\underline{n}$ be the unit vector normal to the elemental area, then

$$\underline{J} = \underline{n} \times \underline{H} \text{ and } \underline{M} = -\underline{n} \times \underline{E} \qquad \ldots(1)$$

The electric and magnetic vector potentials are then given by:

$$\underline{A} = \frac{\mu}{4\pi} \int_S \underline{J} \frac{e^{-jkR}}{R} ds \qquad \ldots(2)$$

$$\underline{F} = \frac{\varepsilon}{4\pi} \int_S \underline{M} \frac{e^{-jkR}}{R} \, ds \qquad \ldots(3)$$

where S is the area of the aperture,

ds is the elemental area.

From Fig. 1, $R = r - r' \cos\psi$, and for far field condition:

$$\underline{A} = \frac{\mu e^{-jkr}}{4\pi r} \underline{N} \qquad \ldots(4)$$

$$\underline{F} = \frac{\varepsilon e^{-jkr}}{4\pi r} \underline{L} \qquad \ldots(5)$$

where $$\underline{N} = \int_S \underline{J} \, e^{jkr'\cos\psi} \, ds \qquad \ldots(6)$$

$$\underline{L} = \int_S \underline{M} \, e^{jkr'\cos\psi} \, ds \qquad \ldots(7)$$

if the vector potentials are known, the electric and magnetic fields are given by,

$$\underline{E} = -j\omega\underline{A} - \frac{j\omega}{k^2} \nabla(\nabla.\underline{A}) - \frac{1}{\varepsilon} \nabla \times \underline{F} \qquad \ldots(8)$$

$$\underline{H} = -j\omega\underline{F} - \frac{j\omega}{k^2} \nabla(\nabla.\underline{F}) + \frac{1}{\mu} \nabla \times \underline{A} \qquad \ldots(9)$$

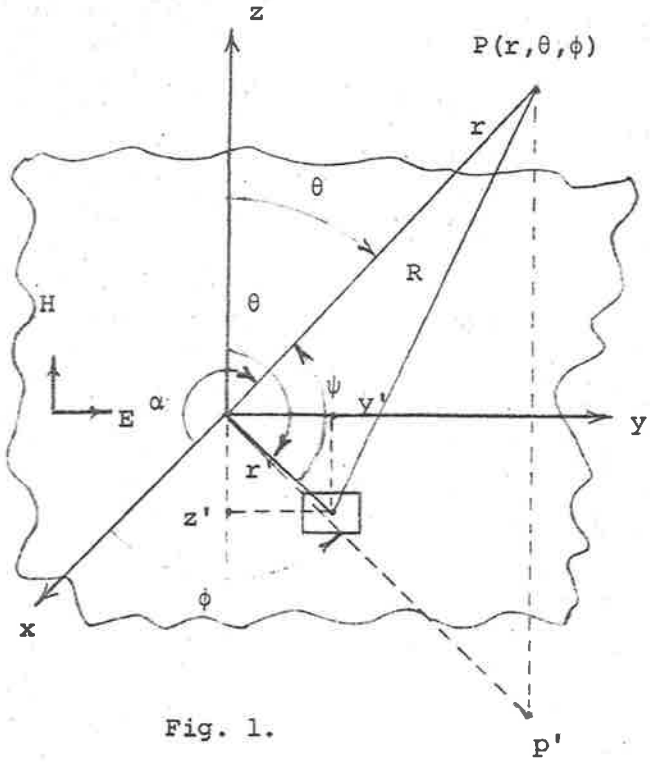

Fig. 1.

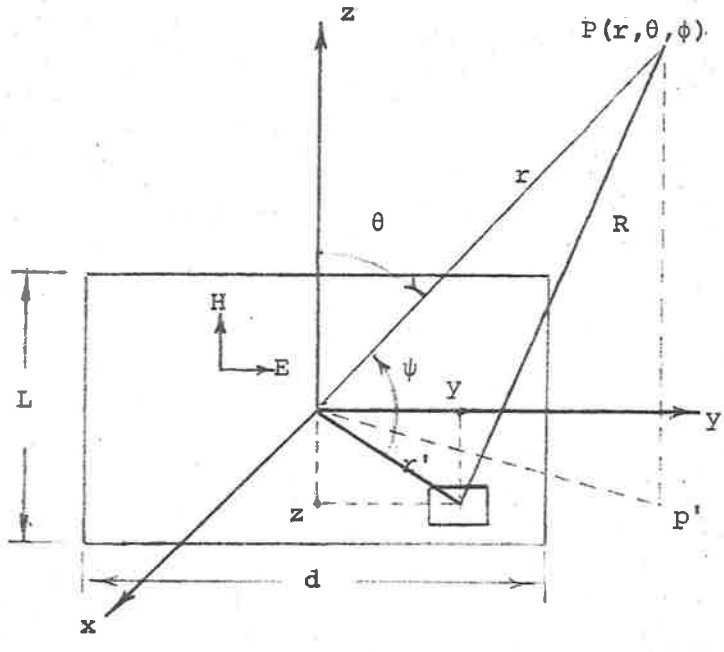

Fig. 2.

Each expression contains the far field contributions from the electric and magnetic vector potentials, i.e.

$$\underline{E} = \underline{E}_A + \underline{E}_F \text{ and } \underline{H} = \underline{H}_A + \underline{H}_F \qquad \ldots(10)$$

where $\underline{H}_A = \frac{1}{\mu} \nabla \times \underline{A}$

$$\left.\begin{aligned} \underline{H}_F &= -j\omega \left[\underline{F} + \frac{1}{k^2} \nabla (\nabla \cdot \underline{F})\right] \\ \underline{E}_A &= -j\omega \left[\underline{A} + \frac{1}{k^2} \nabla (\nabla \cdot \underline{A})\right] \\ \underline{E}_F &= -\frac{1}{\varepsilon} \nabla \times \underline{F} \end{aligned}\right\} \qquad \ldots(11)$$

The field components in the directions θ or ϕ can be obtained by expressing $\nabla \times \underline{V}$ in spherical coordinates:

$$\nabla \times \underline{V} = \frac{\underline{a}_r}{r\sin\theta} \left\{ \frac{\partial}{\partial\theta} (\sin\theta V_\phi) - \frac{\partial V\theta}{\partial\phi} \right\} + \frac{\underline{a}_\theta}{r} \left[\frac{1}{\sin\theta} \frac{\partial Vr}{\partial\phi} \right.$$

$$\left. - \frac{\partial}{\partial r} (rV_\phi) \right\} + \frac{\underline{a}_\phi}{r} \left\{ \frac{\partial}{\partial r} (rV_\theta) - \frac{\partial Vr}{\partial\theta} \right\} \qquad \ldots(12)$$

where $\underline{V}$ is either $\underline{A}$ or $\underline{F}$.

When r is very large, (12) becomes:

$$\nabla \times \underline{V} = -\underline{a}_\theta \frac{\partial V\phi}{\partial r} + \underline{a}_\phi \frac{\partial V\theta}{\partial r} \qquad \ldots(13)$$

Applying (13) to the magnetic vector potential:

$$H_{A\theta} = \frac{jke^{-jkr}}{4\pi r} N_\phi \qquad \ldots(14a)$$

$$H_{A\phi} = \frac{-jke^{-jkr}}{4\pi r} N_\theta \qquad \ldots(14b)$$

and plane waves can be assumed for the far fields, thus:

$$E_{A\theta} = \frac{-jke^{-jkr}}{4\pi r} Z_o N_\theta \qquad \ldots(15a)$$

$$E_{A\phi} = \frac{-jke^{-jkr}}{4\pi r} Z_o N_\phi \qquad \ldots(15b)$$

Similarly, by applying (13) to the electric vector potential together with the plane wave assumption:

$$E_{F\theta} = \frac{-jke^{-jkr}}{4\pi r} L_\phi \qquad \ldots(16a)$$

$$E_{F\phi} = \frac{jke^{-jkr}}{4\pi r} L_\theta \qquad \ldots(16b)$$

and

$$H_{F\theta} = \frac{-jke^{-jkr}}{4\pi r} \frac{L_\theta}{Z_o} \qquad \ldots(17a)$$

$$H_{F\phi} = \frac{-jke^{-jkr}}{4\pi r} \frac{L_\phi}{Z_o} \qquad \ldots(17b)$$

The electric field components of the far field are given by:

$$E_\theta = E_{A\theta} + E_{F\theta} = \frac{-jke^{-jkr}}{4\pi r} (L_\phi + Z_o N_\theta) \qquad \ldots(18a)$$

$$E_\phi = E_{A\phi} + E_{F\phi} = \frac{jke^{-jkr}}{4\pi r} (L_\theta - Z_o N_\phi) \qquad \ldots(18b)$$

and the magnetic field components are:

$$H_\theta = H_{A\theta} + H_{F\theta} = \frac{-je^{-jkr}}{2\lambda r Z_o} (L_\theta - Z_o N_\phi) \qquad \ldots(19a)$$

$$H_\phi = H_{A\phi} + H_{F\phi} = \frac{-je^{-jkr}}{2\lambda r Z_o} (L_\phi + Z_o N_\theta) \qquad \ldots(19b)$$

An Aperture with Normal Plane Wave

Considering a rectangular aperture in the plane x = o as shown in Fig. 2. The electric field is parallel to y axis and the magnetic field is parallel to the z axis. Thus the plane wave is travelling in the direction normal to the aperture, the x axis. Since

$$\underline{J} = \underline{n} \times \underline{H} = \underline{a}_x \times \underline{a}_z H_o = -\underline{a}_y H_o = -\underline{a}_y \frac{E_o}{Z_o} \qquad \ldots(20)$$

$$\underline{M} = -\underline{n} \times \underline{E} = -\underline{a}_x \times \underline{a}_y E_o = -\underline{a}_z E_o \qquad \ldots(21)$$

Hence

$$d\underline{N} = \underline{J}ds = -\underline{a}_y \frac{E_o ds}{Z_o} \qquad \ldots(22)$$

$$d\underline{L} = \underline{M}ds = -\underline{a}_z E_o ds \qquad \ldots(23)$$

The θ and ϕ components of $\underline{N}$ or $\underline{L}$ are given by the rectangular components as follows:

$$N_\theta = (N_x \cos\phi + N_y \sin\phi) \cos\theta - N_z \sin\theta \qquad \ldots(24)$$

$$N_\phi = -N_x \sin\phi + N_y \cos\phi \qquad \ldots(25)$$

Therefore:

$$dN_\theta = dN_y \sin\phi\cos\theta = \frac{-E_o ds \sin\phi\cos\theta}{Z_o} \qquad \ldots(26)$$

$$dN_\phi = dN_y \cos\phi = \frac{-E_o ds \cos\phi}{Z_o} \qquad \ldots(27)$$

$$dL_\theta = -dL_z \sin\theta = E_o ds \sin\theta \qquad \ldots(28)$$

$$dL_\phi = 0 \qquad \ldots(29)$$

The component of the far field which is of interest here is that in the direction ϕ, given by:

$$dE_\phi = \frac{je^{-jkR}}{2\lambda R}(dL_\theta - Z_o dN\phi)$$

$$\text{or} \quad dE_\phi = \frac{je^{-jkR}}{2\lambda R} ds(\sin\theta + \cos\phi) \qquad \ldots(30)$$

Hence

$$E_\phi = \frac{jE_o e^{-jkr(\sin\theta+\cos\phi)}}{2\lambda r} \iint e^{jkr'\cos\psi} dydz \qquad \ldots(31)$$

It can be shown that

$$r'\cos\psi = \underline{a}_r . r' = y'\sin\theta\sin\phi + z\cos\theta \qquad \ldots(32)$$

Thus (31) becomes:

$$E_\phi = \frac{jE_o e^{-jkr(\sin\theta+\cos\phi)}}{2\lambda r} \int_{-d/2}^{d/2} \int_{-L/2}^{L/2} \exp[jk(y\sin\theta\sin\phi + z\cos\theta)]dydz \qquad \ldots(33)$$

An Aperture with Oblique Plane Wave

Now considering the same rectangular aperture with the plane wave travelling in a plane which passes through the y axis and makes an angle θ with the z axis. This is the oblique 'incidence' case. The electric field is again parallel to the y axis and the magnetic field makes an angle $90^\circ - \theta$ with the z axis. The far field component of interest for such an aperture is the ω component of the

electric field on a cone of half angle $90^{o} - \theta = \theta_1$ as shown in Fig. 3.

Using the spherical coordinates (r, θ_1, ω)

$$\nabla = \underline{V} = -\underline{a}_{\theta_1} \frac{\partial V\omega}{\partial r} + \underline{a}_{\omega} \frac{\partial V\theta_1}{\partial r} \qquad \ldots(34)$$

from (12).

Since

$$\underline{J} = \underline{n} \times \underline{H} = \underline{a}_x \times \underline{a}_z \cos\theta_1 H_o = -\underline{a}_y \cos\theta_1 \frac{E_o}{Z_o} \qquad \ldots(35)$$

$$\underline{M} = -\underline{n} \times \underline{E} = -\underline{a}_x \times \underline{a}_y E_o = -a_z E_o \qquad \ldots(36)$$

Hence

$$d\underline{N} = \underline{J}ds = -\underline{a}_y \cos\theta_1 \frac{E_o}{Z_o} ds \qquad \ldots(37)$$

$$d\underline{L} = \underline{M}ds = -\underline{a}_z E_o ds \qquad \ldots(38)$$

The θ_1 and ω components of $\underline{N}$ and $\underline{L}$ are given by

$$N_{\theta_1} = -N_2 \sin\theta_1 + (N_y \sin\omega + N_z \cos\omega) \cos\theta_1 \qquad \ldots(39)$$

$$N_{\omega} = -N_y \cos\omega + N_z \sin\omega \qquad \ldots(40)$$

Therefore:

$$dL_{\theta_1} = -\cos\omega\cos\theta_1 E_o ds \qquad \ldots(41)$$

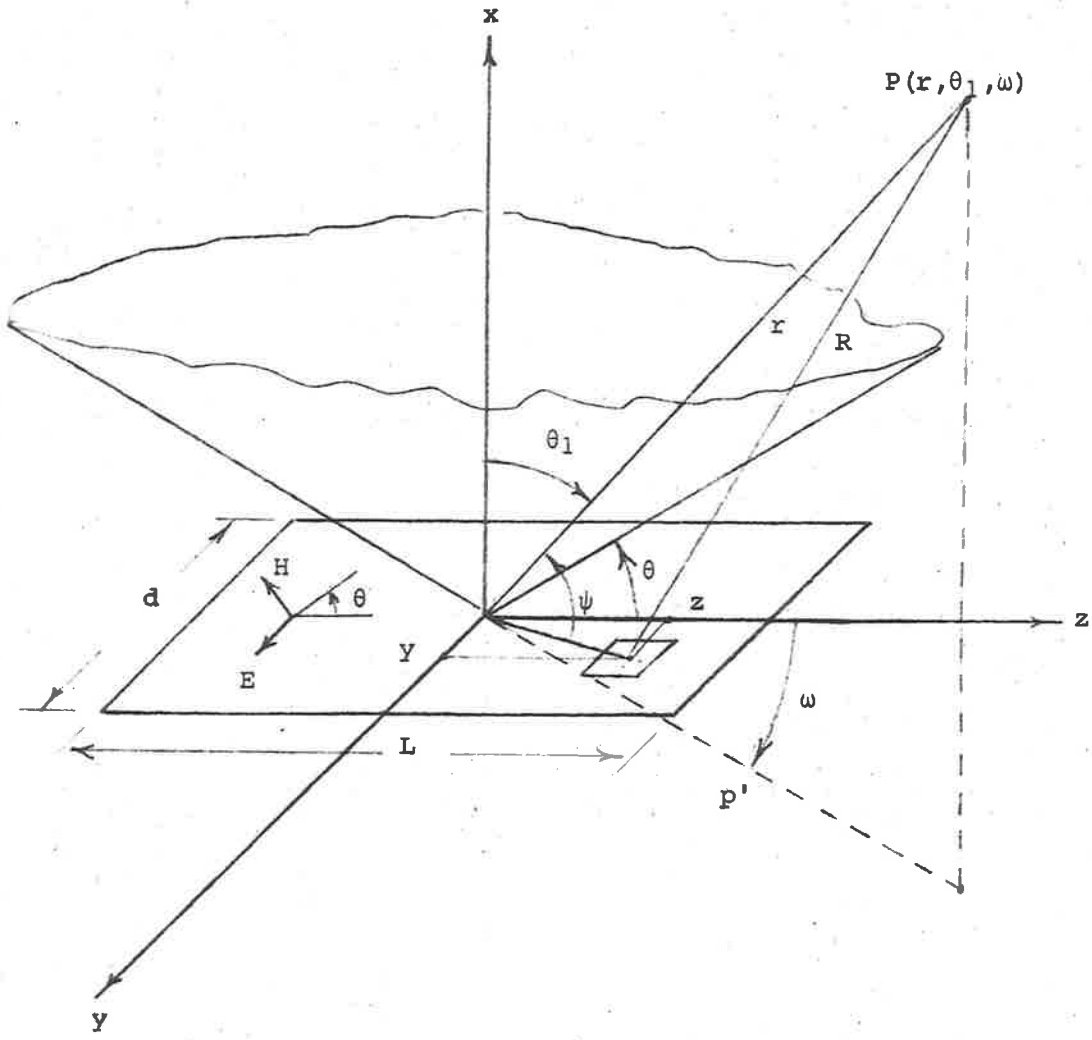

Fig. 3.

$$dN_\omega = -\cos\omega\cos\theta_1 E_o ds \qquad \ldots(42)$$

The component of the electric far field in the direction ω on a cone of half angle θ_1 is:

$$dE_\omega = -\frac{je^{-jkR}}{2\lambda R}(dL_{\theta_1} - Z_o dN_\omega)$$

$$= -\frac{je^{-jkR}}{2\lambda R} 2\cos\omega\cos\theta_1 ds \qquad \ldots(43)$$

$$E_\omega = \frac{jE_o e^{-jkr} 2\cos\omega\cos\theta_1}{2\lambda r}\iint e^{jkr'\cos\psi} dydz \qquad \ldots(44)$$

Using (32) in (44):

$$E_\omega = \frac{jE_o e^{-jkr}}{2\lambda r} 2\cos\omega\cos\theta_1 \int_{-d/2}^{d/2}\int_{-L/2}^{L/2} \exp[jk(y\sin\theta\sin\phi) + z\cos\theta)]\, dydz \qquad \ldots(45)$$

It should be pointed out that the results obtained in (33) and (45) are for aperture field of uniform amplitude. If the amplitude is not constant but dependent upon y and z then function like E(y) and E(z) should be inserted into (33) and (45). This is the case for many applications especially the aperture distribution mentioned in chapters three and four.

APPENDIX E

BEAM COLLIMATION FOR OBLIQUE INCIDENCE

The analysis of beam collimation for a scanning line source feeding a parabolic cylinder is given by N.A. Begovich [24]. If a line source feed illuminating a parabolic cylinder radiates at broadside, then the rays reflected from the cylinder are collimated to a plane wavefront. The reflected rays from the parabolic cylinder will still be collimated if the line source radiates off broadside.

Let the rays leaving a point 0 on the line source shown in Fig. 1 form a cone of half angle θ with the axis of the line source. The path length of one of such rays being bounced off the reflector to a plane P making an angle $90^{\circ} - \theta$ with the line source is constant. This can be proved by considering the contributions to the path length. The equation of the plane P is

$$z - sx + k = 0 \qquad \ldots(1)$$

where $s = -\tan\theta$ and k is a constant. Let (x_1, y_1, z_1) be the point on the reflector hit by a ray from 0, then the distance d_1 from 0 to the reflector is given by:

$$d_1 = (x_1^2 + y_1^2 + z_1^2)^{1/2} \qquad \ldots(2)$$

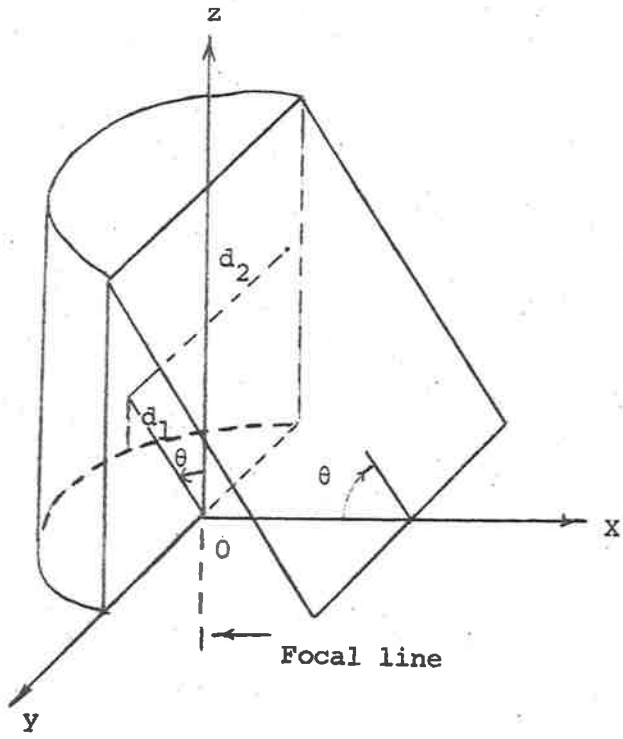

Fig. 1. Parabolic cylinder with travelling wave line source feed.

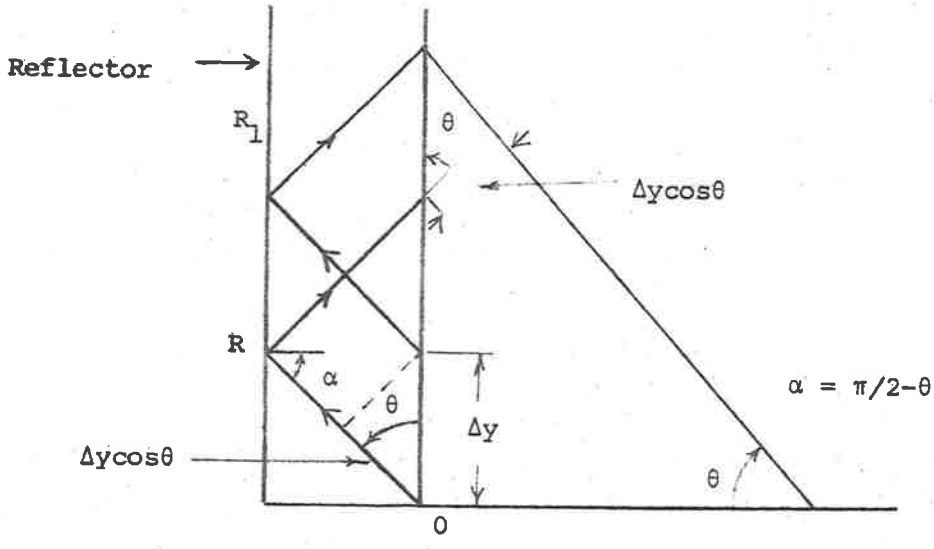

Fig. 2.

where $z_1 = (x_I^2 + y_I^2)^{1/2} \cot\theta$ ...(3)

and $y_I^2 = 4f(x_1 + f)$ ...(4)

By adding x_I^2:

$$x_I^2 + y_I^2 = 4f(x_1 + f) + x_I^2$$

$$x_I^2 + y_I^2 = (x_1 + 2f)^2 \quad \text{...(5)}$$

Using (5) in (3):

$$z_1 = (x_1 + 2f) \cot\theta \quad \text{...(6)}$$

d_1 can now be written as:

$$d_1 = (x_1 + 2f) \csc\theta \quad \text{...(7)}$$

A line parallel to x axis passing through (x_1, y_1, z_1) will meet P at (x_2, y_1, z_1) where x_2 is given by (1):

$$x_2 = (z_1 + k)/s \quad \text{...(8)}$$

The distance from (x_1, y_1, z_2) to the plane P is therefore:

$$d_2 = (x_2 - x_1) \sin\theta \quad \text{...(9)}$$

From (3),

$$d_3 = -(x_1 \csc\theta + 2f\cos^2\theta \csc\theta + k\cos\theta) \quad \text{...(10)}$$

Thus the path length of a ray from O to the plane P after being

reflected off the reflector is:

$$d = d_1 + d_2 = 2f\sin\theta = k\cos\theta \qquad \ldots(11)$$

Since f and k are constant, d is a constant if θ is constant. It can be seen from (11) that all rays from O to the plane P off the reflector have the same path length.

It now remains to be proved that P is a wavefront of all rays coming from the line source and being bounced off the parabolic reflector. As seen from Fig. 2, the progressive phase delay between any two elements is $\frac{2\pi}{\lambda}\Delta y\cos\theta$. The phase of a ray leaving o' lags that of a ray leaving O by $\frac{2\pi}{\lambda}\Delta y\cos\theta$ but it reaches P ahead in phase by $\frac{2\pi}{\lambda}\Delta y\cos\theta$. Hence, the rays from O and O' arrive at P in phase.

Thus it can be concluded that all rays leaving the line source placed at the focus of a parabolic cylinder will collimate for any angle of scan.

APPENDIX F

COMPUTER PROGRAMS

To obtain the theoretical results for the work presented in the thesis, extensive automatic computation has been performed on a CDC 6400 computer. Generally speaking, all computer programs used consist of:

(i) Main Programs

The main program defines the problem, supplies data, performs the computation and displays the results in appropriate forms.

(ii) Functions Subprograms

The expressions to be processed are entered in the form of EXTERNAL FUNCTIONS.

(iii) Subroutines

Several subroutines are used. Each performs a certain specific computation. Some are written whereas others are made available through the University of Adelaide Computing Centre. Some useful subprograms are:

(a) Bessel functions J_n and Y_n (first and second kind) [27].

This routine evaluates tables of Bessel functions $J_n(x)$ and $Y_n(x)$ for $n = 0, 1, 2...$ If $n < 0$ only $J_n(x)$ is calculated. A recursive procedure is used to obtain the Bessel functions $J_n(x)$, $Y_n(x)$ is then

computed through a summation involving the lower order of $J_n(x)$.

(b) Fresnel integrals [28].

This routine computes the Fresnel integrals of $C(x) = \int_0^x \cos(t)/\sqrt{2\pi t}\, dt$ and $S(x) = \int_0^x \sin(t)\sqrt{2\pi t}\, dt$. Evaluation using different approximations for $x < 4$ and $n > 4$.

(c) Complex roots of a complex equation [15].

This subroutine MULROOT uses Müllers algorithm and complex arithmetic to compute a zero of an arbitrary complex function f(x). It compares the moduli of $F(x_{k-2})$, $F(x_{R-1})$, $F(x_k)$ at each step and discards the point $(xj, f(xj))$ for which $|f(xj)|$ is maximal (j=k, k-1, k-2). That point is replaced by the latest iterate, x_{k+1}. This device often provides a sense of direction to the search phase.

(d) Simpson's rule integration [29].

This routine obtains the quadrature by adaptive Simpson method subdividing the range of integration non-uniformly as required to obtain the desired accuracy.

(e) Simpson's rule integration for a complex integrand.

This routine obtains the complex quadrature when the integrand is complex. The limits of integration are real.